DISSERTATION

In Partial Fulfillment of the Requirements
for the Degree of Doctor of Philosophy
from TELECOM ParisTech

Specialization: Communication and Electronics

Shakti Prasad Shenoy

Efficient Communication over Wireless Channels: New Results in Equalization, Diversity and Interference Alignment

Thesis defended on the 25th of June 2010 before a committee composed of:

President	Prof. Luc Deneire, Université de Nice, France
Reporters	Prof. Joakim Jalden, Royal Institute of Technology (KTH), Stockholm
	Prof. Marc Moonen, K. U. Leuven, Belgium
Examiners	Prof. Angel Lozano, Universitat Pompeu Fabra (UPF), Barcelona
	Dr. Bertram Gunzelmann, Infineon Technologies, Munich
	Prof. David Gesbert, EURECOM
	Dr. Irfan Ghauri, Infineon Technologies, France
Thesis supervisor	Prof. Dirk T. M. Slock, EURECOM

THESE

présentée pour obtenir le grade de

Docteur de TELECOM ParisTech

Spécialité: Communication et Electronique

Shakti Prasad Shenoy

Communications efficaces sur des canaux sans fil: Nouveaux résultats sur légalisation, la diversité et l'alignement des interférences

Soutenance le 25 juin 2010 devant le jury composé de :

Président	Prof. Luc Deneire, Université de Nice, France
Rapporteurs	Prof. Joakim Jalden, Royal Institute of Technology (KTH), Stockholm
	Prof. Marc Moonen, K. U. Leuven, Belgium
Examinateurs	Prof. Angel Lozano, Universitat Pompeu Fabra (UPF), Barcelona
	Dr. Bertram Gunzelmann, Infineon Technologies, Munich
	Prof. David Gesbert, EURECOM
	Dr. Irfan Ghauri, Infineon Technologies, France
Directeur de thèse	Prof. Dirk T. M. Slock, EURECOM

To my parents Kapu Yekanath Shenoy and Kapu Sugandha Shenoy.

Abstract

When data is transmitted over the wireless communication channel, the transmit signal experiences distortion depending on the channel's fading characteristics. On the one hand, this calls for efficient processing at the receiver to mitigate the detrimental effects of the channel and maximize data throughput. On the other hand, the diversity inherently present in these channels can be leveraged with appropriate transmit processing in order to increase the reliability of the transmission link. Recently, in [1] it was shown that the channel characteristics can be exploited to maximize the total data throughput in the interference channel where multiple user pairs rely on the same resource to communicate among themselves. In this PhD dissertation, we first propose novel equalizer designs for frequency selective channels. We then present new results on the diversity gain of equalizers in fading channels when appropriate precoding is applied at the transmitter. Toward the end of the thesis we provide some new insights into interference alignment [1], where the aim is to maximize network throughput in interference channels with joint transmit and receive processing. A summary of the three parts of this dissertation is given below.

The first part of the thesis studies receiver designs that maximize the data throughput in the high speed downlink packet access (HSDPA). We propose two-stage equalization for both single antenna (SISO) and multiple antenna (MIMO) frequency selective channels. The first stage consists of chip-level processing and the second stage of processing takes place at the symbol level. In principle, the presence of the aperiodic scrambler at the transmitter renders the symbol level channel time-variant and affects the achievable throughput at the receiver. We analyze the performance of these receivers when the scrambler used at the transmitter is modeled as a random sequence and compare it with the results of the deterministic treatment of the scrambler. In MIMO HSDPA where the receiver is required to choose the precoding matrix that maximizes its aggregate transport block

size, we derive analytical expressions for the choice of the optimum precoding matrix that maximizes the sum-capacity of the receiver when it is based on MMSE designs. Finally we extend the current single-user MIMO scenarios in HSDPA to the multiuser case. These extensions require minimal changes to existing standards. When multiple users are to be simultaneously serviced in the downlink, we suggest practical multi-user scheduling strategies that can be employed at the base station so as to maximize the downlink throughput.

The second part of the thesis is devoted mainly to theoretical analysis of the diversity order of linear equalization (LE) for transmission in fading channels. It is known that zero-padded block transmission allows LE to achieve full multipath diversity present in frequency selective channels. We first show here that, in a dual fashion, LE can achieve full Doppler diversity in time-selective channels when guard bands are inserted in the transmit signal. We then analyze the performance of LE in time-and-frequency (doubly) selective channels. In [2], a two-dimensional generalization of the zero-padding precoder was shown to enable maximum likelihood equalizers (MLE) to achieve the full joint multipath-Doppler diversity offered by doubly selective channels. We show here that the same precoder also allows linear, decision feedback and “hybrid" equalization schemes to achieve the same diversity gains as that of MLE. We also devote our attention to low-complexity implementations of these full diversity equalizers. It also appears that a redundancy proportional to channel delay spread is largely enough to allow MLE to collect full channel diversity. We present simulation results that support this observation.

In the final part of the thesis we study communication over flat fading multiple input multiple output (MIMO) interference channels (IFC). We consider the K-link constant MIMO IFC where inter-link interference is treated as Gaussian noise (Noisy MIMO IFC). Starting from Interference Alignment (IA) constraints [1], analytical conditions that need to be satisfied in order to admit an IA solution for such a MIMO IFC are derived. For a given degrees of freedom allocation, these conditions, along with a recursive algorithm to check its validity in a given K-link MIMO IFC, allow an analytical evaluation of the existence of IA solutions (or lack thereof). Such an attempt has been made recently for several interesting special cases in the published literature, however we address here the most general case of the MIMO IFC and are able to show that, when an IA solution exists, these conditions are satisfied at every step of the proposed recursive algo-

rithm and that an IA solution does not exist when these conditions are not satisfied.

Résumé

Lorsque des données sont transmises sur le canal de communication sans fil, la transmission subit une distorsion du signal qui dépend des caractéristiques de l'évanouissement du canal. D'une part, ceci exige un traitement efficace au niveau du récepteur pour atténuer les effets néfastes du canal et maximiser le débit de données àtravers le canal. D'autre part, la diversité intrinsèquement présente dans ces canaux peut être exploitée avec un traitement approprié en émission en vue d'accroître la fiabilité de la communication. Plus récemment, il a été démontré que les caractéristiques du canal peuvent être exploitées afin de maximiser le débit total dans un canal àinterférence dans lequel plusieurs paires d'utilisateurs exploitent les mêmes ressources pour communiquer entre eux. Dans cette thèse nous proposons, dans un premier temps, de nouveaux types d'égaliseurs pour canaux sélectifs en fréquence. Nous présentons ensuite de nouveaux résultats de gains en diversité pour des égaliseurs de canaux à évanouissement lorsqu'un précodage adéquat est mis en place en émission. Vers la fin de la thèse, nous donnons quelques nouveaux et intéressants aperçus concernant l'alignement d'interférence dans le cas de canaux à interférence. Ce principe nécessite un traitement mixte àla transmission et la réception. Un résumé des trois parties de la thèse est présenté ci-après.

La première partie de la thèse traite la conception de récepteurs maximisant le débit des données dans un accès à haut débit par paquets en liaison descendante (HSDPA). Nous proposons dans le cas de canaux sélectifs en fréquence une égalisation en deux étapes aussi bien pour les systèmes à antenne unique (SISO) que pour ceux à antennes multiples (MIMO). La première étape consiste en un traitement au niveau des chips alors que la seconde est réalisée au niveau des symboles. Nous effectuons, dans cette partie une analyse des performances des récepteurs basés sur ce traitement en deux étapes.

La deuxième partie de la thèse est consacrée essentiellement à l'analyse théorique des gains en diversité des égalisations linéaires (LE) pour une

transmission dans des canaux à évanouissements. Il est connu que les précodeurs basés sur l'ajout de zéros ("zero-padding") permettent aux égaliseurs à maximum de vraisemblance (MLE) d'exploiter pleinement la diversité disponible dans les canaux à évanouissements. Nous montrons ici que cette même classe de précodeurs, couplée avec des égaliseurs linéaires, avec retour de décision ou encore "hybride", permettent d'obtenir le même gain en diversité que MLE. Nous avons également étudié des réalisations à faible complexité de ces égaliseurs à diversité pleine. Dans le cas d'une double sélectivité du canal de transmission (temporelle et fréquentielle), il semble qu'une redondance des symboles proportionnelle à l'étalement temporel du canal est suffisante pour permettre au MLE de recouvrir la totalité de la diversité du canal. Nous présentons des résultats de simulation qui confirment cette observation.

Dans la dernière partie de cette thèse, nous étudions la communication sur un canal MIMO non dispersif en fréquence à K liens interférents (flat fading MIMO interference channels) appelé MIMO IFC. Considérant l'interférence comme du bruit gaussien, nous abordons le problème d'évaluer de façon analytique la faisabilité des solutions d'alignement d'interférences (IA). Cette étude est effectuée pour une distribution donnée des antennes de transmission et de réception et une répartition des degrés de liberté entre les K paires d'utilisateurs (DoF allocation). Nous obtenons un ensemble de conditions qui, moyennant un algorithme récursif, permettent de réaliser une évaluation analytique de l'existence de solutions IA.

Acknowledgements

Get real! There are no Gods. Just parents and teachers

Foremost, I would like to express my deepest gratitude to my advisor Prof. Dirk T. M. Slock. To him I owe all the knowledge that I have gained during the course of this research. The perpetual energy, superhuman patience, immense knowledge and analytical skills that he deploys in tackling difficult research problems sets a very high standard for his students. I fondly recall the numerous lengthy discussions we had when I walked in at 6 PM into his office (oftentimes without an appointment, luring him with a “Just a quick question" preamble). Sessions that ended only several hours later, that too after repeated phone calls to him from home. I would leave exhausted and tired while he would not have the slightest trace of fatigue on his face. I find it difficult to imagine having a better advisor and mentor for my Ph.D study. Indeed, I was extraordinarily fortunate to have him as my thesis advisor.

I gratefully acknowledge the guidance and help of Irfan Ghauri, Jean-Xavier Canonicci and all my colleagues at Infineon Technologies France. Irfan’s constant support, invaluable guidance and critical eye for detail was instrumental in the successful completion of this thesis.

Sincere thanks are due to Prof. Joakim Jalden and Prof. Marc Moonen for reviewing the thesis and offering valuable comments. I would also like to thank Prof. Angel Lozano, Prof. David Gesbert, Prof. Luc Deneire and Dr. Bertram Gunzelmann for kindly agreeing to be a part of the jury.

I shall forever be indebted to my family. My father Yekanath Shenoy who is no longer with us but shall forever be fondly remembered, my mother Sugandha Shenoy for her unconditional love, sister Vaishali Pai for her unflagging support, brother-in-law Rajesh Pai for being a close friend

and confidant and my dearest nephew Balaram Pai for his love and affection. This thesis would not have been possible without them. In many ways, this thesis is as much a result of their effort as mine.

I would like to warmly thank all my friends at Infineon Technologies France and EURECOM for making my “off-thesis" time ever so pleasant and interesting. Rizwan Ghaffar and his family, Umer Salim, Praveen Chandrashekarappa, Vikram Sharma, Usman Saeed, Francesco Negro, Xiao Lei, Erick Amador, Pranav Pandey, Anoop Mantena, Barkha Khatri, Ruchna Nigam, Himanshu, Shishir and Shaifali Gupta, Kiran Chitriki, Supriya, Achin Grover and Sheenu Chawla deserve special mention.

Special thanks to Nancy Bertin, presently at INRIA, Rennes for offering to help a total stranger with the French translation. Thanks are also due to Mustafa Amara for his timely help in translating the abstract in French at a very cruical time.

Finally, the financial support of Infineon Technologies France during the thesis period is gratefully acknowledged.

Contents

List of Figures

Acronyms

All the acronyms used throughout this thesis are listed here. In some cases, multiple appended acronyms are used (e.g., MIMO IFC to mean multiple-input multiple-output interference channel), although this usage is kept at a minimum. These acronyms are also applicable in the French summary.

3GPP	3rd Generation Partnership Program
AWGN	Additive White Gaussian Noise
BER	Bit Error Rate
BTS/BS	Base Station
CDMA	Code Division Multiple Access
CP	Cyclic Prefix
CSI	Channel State Information
DS	Doubly Selective
DFE	Decision Feedback Equalizer
DMT	Diversity-Multiplexing Tradeoff
D-TxAA	Dual Stream Transmit Adaptive Array
EVD	Eigen Value Decomposition
FDD	Frequency Division Duplex
FDMA	Frequency Division Multiple Access
FIR	Finite Impulse Response
FS	Frequency Slective
HARQ	Hybrid Automatic Repeat Request
HSDPA	High Speed Downlink Packet Access
IBI	Inter Block Interference
ICI	Inter Carrier Interference
IFC	Interference Channel
ISI	Inter Symbol Interference
LE	Linear Equalizer
LHS	Left Hand Side

(L)MMSE	(Linear) Minimum Mean Squared Error
MCS	Modulation and Coding Scheme
MFB	Matched Filter Bound
ML	Maximum Likelihood
MLE	Maximum Likelihood Equalization
MMSE-ZF	Minimum Mean Squared Error Zero Forcing
MRC	Maximum Ratio Combining
MSE	Mean Squared Error
MIMO	Multiple-Input Multiple-Output
MISO	Multiple-Input Single-Output
MU	Multiple User
OVSF	Orthogonal Variable Spreading Factor
PARC	Per-Antenna Rate Control
PE	Polynomial Exapansion
PEP	Pairwise Error Probability
PER	Packet Error Rate
QAM	Quadrature Amplitude Modulation
OFDM	Orthogonal Frequency Division Multiplexing
QPSK	Quadrature Phase-Shift Keying
RHS	Right Hand Side
RX	Receiver
SC	Single Carrier
SIC	Successive Interference Cancelation
SIMO	Single-Input Multiple-Output
SINR	Signal-to-Interference-Noise Ratio
SISO	Single-Input Single-Output
SNR	Signal to Noise Ratio
SU	Single User
SVD	Singular Value Decomposition
TDD	Time Division Duplex
TS	Time Selective
TX	Transmitter
Tx-AA	Transmit Adaptive Array
UE	User Equipment
UMTS	Universal Mobile Telecommunication System
WCDMA	Wideband CDMA
w.l.o.g	without loss of generality
ZF	Zero Forcing
ZP	Zero Padding

Notations

Boldface/italics upper-case letters denote matrices, boldface/italics lower case letters denote column vectors and lower-case italics denote scalars. Calligraphic upper case letters denote sets (unless stated otherwise).

$\mathbb{E}$	Expectation operator
$\lfloor x \rfloor$	Floor operation, rounds the elements of x to the nearest integers towards minus infinity
$\lceil x \rceil$	Ceil operation, rounds the elements of x to the nearest integers towards infinity
$\otimes$	Kronecker product of matrices
$\oplus$	Diagonal composition
$\mathbb{C}^n$	The set of $n \times 1$ vectors with complex-valued entries.
$[\mathbf{X}]_{i,j}$	The (i, j)th element of the matrix $\mathbf{X}$, if the latter is defined
x_i	The ith element of vector $\mathbf{x}$, if the latter is defined
$\mathrm{tr}(\mathbf{X})$	trace of the matrix $\mathbf{X}$
$\det(\mathbf{X})$	Determinant of the matrix $\mathbf{X}$
$\|\mathbf{x}\|^2$	Squared Euclidean norm of vector $\mathbf{x}$
$\|\mathbf{X}\|^2$	Squared Frobenius norm of a matrix $\mathbf{X}$
$\|x\|$	Absolute value of x
$\mathbf{X}^*$	The complex conjugate of matrix $\mathbf{X}$
$\mathbf{X}^H$	The complex conjugate transpose (Hermitian) of matrix $\mathbf{X}$
$\mathbf{X}^{\mathrm{T}}$	The transpose of matrix $\mathbf{X}$
$\mathbf{X}^{-1}$	The inverse of the (square) matrix $\mathbf{X}$
$\mathrm{diag}\,(\mathbf{X})$	The diagonal entries of the matrix $\mathbf{X}$
$\mathbf{X}^{1/2}$	Hermitian square root of the positive semidefinite matrix $\mathbf{X}$
$\mathbf{I}_N$	Identity matrix of dimension N
$\Pr$	Probability
$\sim$	Distributed according to
$\|\mathcal{A}\|$	Cardinality of set $\mathcal{A}$

Chapter 1

Thesis summary

1.1 Opening comments

The overarching theme of this thesis is efficient communication over wireless channels. A slightly greater emphasis is laid on linear processing techniques applied at the receiver and transmitter. The topics addressed in this thesis span communication over flat fading, frequency or time selective only, as well as frequency and time selective channels. Moreover, we also consider single (SISO) and multiple antenna (MIMO) communications. When considering communications over such a wide range of channels, *efficiency* takes on different meanings depending on the context.
The first part of this thesis deals with communication over frequency selective channels in the context of UMTS HSDPA downlink. Since most of the processing at the transmitter is standardized, we study equalization at the receiver and propose new equalization techniques that improve the achievable data rates at the receiver. In this context, a receiver is more efficient than the other when, under the same channel conditions, it can achieve a higher downlink throughput. In this part, we propose and analyze receiver designs for HSDPA in SISO and MIMO frequency selective channels.
While the work in the first part is closer to the wireless standards, the second part is more exploratory in nature. In this part of the thesis we study the diversity gain of equalizers other than maximum likelihood equalizers (MLE) in time/frequency as well as time and frequency selective channels.

The diversity gain of an equalizer is a measure of its efficiency in reducing the BER in the high-SNR regime. In particular, the higher the diversity gain, steeper is the drop in BER as SNR increases. Our quest in this part is to theoretically analyze the diversity gain of lower complexity linear as well as non-ML equalizers and compare their diversity gains against the optimal MLE. In fact, for transmission over a class of wireless channels that can be modeled by the complex-exponential basis expansion models, we are able to show the diversity gains of non-maximum likelihood and maximum likelihood equalizers are the same. Here, we also concern ourselves with low complexity implementation of these full diversity equalizers.

The third and final part of the thesis moves further down the exploratory path and studies communications over the MIMO interference channel (IFC). However, in this part we limit out scope to frequency-flat or the so-called constant coefficient MIMO IFC. It was recently shown that in the MIMO IFC, the concept of interference alignment (IA) can be used to increase the total number of interference-free streams that can be communicated among the different users comprising the interference channel. However, there are numerous problems in the MIMO IFC that remain open. The last part of this thesis addresses one such problem, that of feasibility of IA in the constant coefficient MIMO IFC

1.2 Thesis layout

Each part of this thesis begins with a short introduction to the problem that is being addressed, and its context. This is followed by the signal model to be used therein. Any new notation that is particular to the part of thesis is also introduced here. This introductory section is then followed by the chapters that address the problem in a systematic fashion. Wherever required, each chapter ends with numerical examples or simulations. A brief outline of each of the chapters in the thesis follows: Chapter 3 is introductory in nature and provides a quick review of the HSDPA standard. Chapter 4 introduces the key ideas of deterministic treatment of scramblers and combined chip-level and symbol level equalization in the context of SISO HSDPA. In the process we propose and evaluate a novel equalization scheme based on channel sparsification at chip-level and equalization at symbol level. In chapter 5 we extend the two-step equalizer design to MIMO HSDPA. We first investigate optimum precoder selection in MIMO HSDPA and then propose several receiver designs based on joint chip-level

and symbol level processing both with and without the deterministic treatment of the scrambler. In chapter 6 we investigate some possible extensions of HSDPA to the MU scenario. This is the concluding chapter of the first part. At the end of chapters 4, 5 and 6 simulation results are provided to compare the performance of the proposed receivers. Chapter 7 is the introductory chapter of the second part of this thesis and furnishes the background material for diversity analysis of equalizers in selective channels. Chapter 8 is devoted to theoretical analysis of diversity gains of the linear and non-maximum likelihood equalizers for selective channels. In chapter 9 we concern ourselves with low complexity implementations of the equalizers discussed in chapter 8. Chapters 10 and 11 form the third and the final part of this thesis where we discuss interference alignment in constant coefficient MIMO interference channels. Chapter 10 introduces the concept of interference alignment and chapter 11 addresses the problem of analytically evaluating the feasibility of interference alignment in a given MIMO IFC.

1.3 Research contributions

We summarize here the original contributions of this thesis.

1.3.1 Chapter 4

The focus of this chapter is equalization for SISO HSDPA downlink. This chapter also introduces the key idea of combined chip-level and symbol level processing that we shall use throughout the first part. It also introduces the deterministic treatment The original contributions of this chapter are.

- The idea of deterministic treatment of the scrambler and its consequence on the receiver bias for MMSE chip equalization based receivers
- A novel equalizer design based on joint chip level and symbol level processing. In particular we propose a chip level channel sparsifier followed by reduced dimension non-linear processing at the symbol level.

These results were published in the following papers

- Irfan Ghauri, Shakti Prasad Shenoy and Dirk T. M. Slock, “On LMMSE bias in CDMA SIMO/MIMO receivers", *IEEE International Conference on Acoustics, Speech, and Signal Processing (ICASSP 2008), March 30 - April 4, 2008, Las Vegas, Nevada, USA*

- Shakti Prasad Shenoy, Irfan Ghauri and Dirk T. M. Slock, “Chip-sparsification and symbol-equalization for WCDMA downlink", *IEEE International Symposium on Personal, Indoor and Mobile Radio Communications (PIMRC 2008), 15-18 September 2008, Cannes, France*

1.3.2 Chapter 5

This chapter addresses equalization for MIMO HSDPA. A key innovation that led to the high spectral efficiency and downlink throughput in HSDPA is the fast channel feedback that effectively leverages multi-user diversity to enhance the spectral efficiency and throughput of the HSDPA network. In the HSDPA standard, the receiver is required to feedback the PCI or the precoder channel information that indicates the appropriate precoding matrix (from a pre-specified codebook) to be applied at the transmitter. In fact, this approach has also been adopted for the 3G Long Term Evolution (LTE) standards. One of the contributions of this chapter is an analytical solution for the optimal choice of this precoder matrix when the receiver is based on MMSE designs. The research contributions of this chapter are

- Analytical solution for the choice of optimum precoder to be applied at the transmitter to maximize the sum rate in MIMO HSDPA

- Receiver designs for MIMO HSDPA based on joint chip level and symbol level equalizers treating scrambler as a random/deterministic sequence

The publications associated with this chapter are

- Shakti Prasad Shenoy, Irfan Ghauri and Dirk T. M. Slock, “Optimal precoding and MMSE receiver designs for MIMO WCDMA", *IEEE 67th Vehicular Technology Conference (VTC-Spring 2008), May 11Ű14, Singapore*

- Shakti Prasad Shenoy, Irfan Ghauri and Dirk T. M. Slock, “ Receiver designs for MIMO HSDPA", *IEEE International Conference on Communications (ICC-2008), May 19-23, Beijing, China*

1.3.3 Chapter 6

The current HSDPA standards support only a single user in the downlink in the MIMO mode. In this chapter we explore multiuser extensions to MIMO HSDPA that require minimal changes in the present standards. These proposals were published in the following paper:
Shakti Prasad Shenoy, Irfan Ghauri and Dirk T. M. Slock, "Multiuser extensions for closed loop transmit diversity in HSDPA", *International Conference on Communications (ICC-2009), June 14-18, Dresden, Germany*

1.3.4 Chapter 8

It is known that maximum-likelihood equalizers are able to exploit the full diversity gains available in time/frequency and time-frequency selective channels with appropriate precoding at the transmitter. This was shown for a class of wireless channels that can be modeled using the complex exponential basis expansion model in [2]. Subsequently it was shown that the same precoders also enable linear equalizers to achieve full diversity gain in the case of frequency selective channels. The main contribution of this chapter is the analytical proof that the precoders in [2] allow linear and other equalizers of lower complexity than maximum likelihood equalizers to achieve full diversity present in doubly selective channels. The original contributions in this chapter are

- Proof that linear equalization can achieve full Doppler diversity in time-selective channels
- Proof that linear equalization can achieve full channel diversity in doubly-selective channels and that decision feedback equalizers can achieve full channel diversity in time/frequency/doubly-selective channels

A part of the proof of full diversity gain using DFE uses the proof technique of [3]. However [3] addresses frequency-selective channels and we address frequency/time selective and doubly selective channels. The associated publications are

- Shakti Prasad Shenoy, Irfan Ghauri and Dirk T. M. Slock, "Diversity order of linear equalizers for block transmission in fading channels", *42nd Asilomar Conference on Signals Systems and Computers (Asilomar 2008), October 26-29, Asilomar, California, USA*

- Shakti Prasad Shenoy, Irfan Ghauri and Dirk T. M. Slock, "Diversity order of linear equalizers for doubly selective channels"', *10th IEEE International Workshop on Signal Processing Advances in Wireless Communications (SPAWC 2009), June 21-24, Perugia, Italy*

1.3.5 Chapter 9

In this chapter we are concerned with implementation aspects of the full diversity equalizers. In this chapter we show that approximate equalizers based on polynomial expansion do not seem to impact the diversity gains of these equalizers. The key contributions of this chapter are

- A method to derive diversity gains with linear equalization in cyclic prefixed systems
- Approximate, full diversity equalizers for doubly selective channels
- Low complexity full diversity hybrid equalization for doubly selective channels

The associated publications are

- Shakti Prasad Shenoy, Francesco Negro, Irfan Ghauri and Dirk T. M. Slock, "Low-complexity linear equalization for block transmission in multipath channels", *IEEE Wireless Communications and Networking Conference (WCNC 2009), April 5-8, Budapest, Hungary*
- Shakti Prasad Shenoy, Irfan Ghauri and Dirk T. M. Slock, "Approximate full diversity equalizers for doubly selective channels", *17th European Signal Processing Conference(Eusipco 2009), August 24-28, Glasgow, Scotland*
- Shakti Prasad Shenoy, Irfan Ghauri and Dirk T. M. Slock, "On full diversity equalization for precoded block transmission systems", *43rd Asilomar Conference on Signals Systems and Computers (Asilomar 2009), November 1-4, Asilomar, California, USA*

1.3.6 Chapter 11

In this chapter we address the following problem. Consider a MIMO interference channel characterized by K users each having M_k transmit and N_k receive antennas. Assume further that each transmit-receive pair intends to communicate d_k independent data streams between themselves.

If transmit and receive processing is constrained to be linear. It is known that using the concept of interference alignment (IA), the total number of interference free streams that can be transmitted in this network of K users can be maximized. However, for a given network characterized by the set K, M_k, N_k the maximum $d_{tot} = \sum_k d_k$ achievable is not known and remains an open problem. It is also not known if there is an analytical method for evaluating the existence of IA solutions even if the set d_k is given. Some solutions for special cases have been given for the single stream case in [4] and numerical solutions were provided, for example in [5]. In this chapter we provide new insights to the existence of IA solutions for a given MIMO interference channel and the set d_k. While we do not yet have a concrete proof, we believe that the recursive algorithm we present in this chapter constitutes sufficient conditions for the existence of IA solutions. In this part of the thesis, we therefore claim the following contributions:

- New insights into the existence of feasibility of interference alignment solutions for a given MIMO interference channel and stream allocation among different users
- A recursive algorithm to analytically evaluate the existence of interference alignment solutions for a given MIMO interference channel

The results presented in this chapter were published in:
Francesco Negro, Shakti Prasad Shenoy, Irfan Ghauri and Dirk T. M. Slock, "Interference Alignment Feasibility in Constant Coefficient MIMO Interference Channels", *11th IEEE International Workshop on Signal Processing Advances in Wireless Communications (SPAWC 2010), June 20-23, Marrakech, Morocco*

Chapter 2

Résumé Etendu

2.1 Remarques préliminaires

Le thème principal de cette thèse est la communication efficace sur canaux sans fil. La thèse traite de la communication sur les canaux dits «à évanouissements uniformes»(en anglais *flat fading*), qu'il s'agisse de canaux sélectifs en fréquence, en temps, ou les deux. Nous considérons des schémas de communication à une (en abrégé SISO, pour l'anglais *single input single output*) ou plusieurs (resp. MIMO, *multiple input multiple output*) entrées/sorties. Sur une telle variété de canaux possibles, le sens donné au concept d'*efficacité* varie suivant le contexte.

La première partie de cette thèse traite de la communication sur des canaux sélectifs en fréquence dans UMTS HSDPA. Ici, nous proposons des techniques d'égalisation en vue d'améliorer le débit de données que l'on peut atteindre au niveau du récepteur. Dans ce contexte, un récepteur est plus efficace qu'un autre lorsque, à canal identique, il peut atteindre un débit supérieur. Dans cette partie, nous proposons et analysons la conception de récepteurs pour le protocole HSDPA, pour des systèmes SISO et MIMO, les canaux étant sélectifs en fréquence.

La deuxième partie de la thèse est de nature plus exploratoire. Dans cette partie, nous étudions le gain de diversité d'égaliseurs différant des

égaliseurs réalisant le maximum de vraisemblance (MLE pour l'anglais *maximum likelihood equalizer*), les canaux étant sélectifs à la fois en fréquence et en temps. Le gain de diversité d'un égaliseur mesure sa capacité à réduire le taux d'erreur (en abrégé BER pour *bit error rate*) dans les régimes de haut rapport signal sur bruit (SNR pour *signal-to-noise ratio*). L'objectif principal de cette partie est d'analyser théoriquement le gain de diversité d'égaliseurs linéaires de faible complexité, et d'égaliseurs non-MLE, et de comparer leurs gains de diversité à celui du MLE optimal. Nous verrons que, pour la transmission sur des canaux sans fil qui pouvant étre modélisés par les modèles CE-BEM, nous pouvons montrer que la diversité des gains non-ML et MLE est la mémes.

La troisième et dernière partie de la thèse s'avance encore davantage dans la voie exploratoire. Nous étudions ici les communications sur des canaux MIMO avec l'interférence entre utilisateurs (MIMO IFC). Nous nous limitons dans cette partie à l'étude ommunication sur les canaux de la «à évanouissements uniformes»ou la MIMO IFC à coefficients constants. Il a été récemment demontré que, en MIMO IFC, le concept de l'alignement des interférences (IA) peut étre utilisé pour augmenter le nombre total de flux sans interférence qui peuvent étre communiqués entre les différents utilisateurs dans le canal. De nombreux problèmes restent en suspens en MIMO IFC. La dernière partie de cette thèse étudie le problème, non résolu, de la possibilité d'IA pour les MIMO IFC.

2.2 Résumé des contributions

Nous résumons ici les contributions originales de cette thèse.

2.2.1 Partie I: Égalisation

Dans le chapitre 4, nous étudions les récepteurs SISO HSDPA linéaires qui minimisent l'erreur quadratique moyenne (LMMSE), et les biais en sortie de l'égaliseur. Nous introduisons l'idée d'examiner l'embrouilleur (en anglais *scrambler*) comme déterministe, ainsi que l'idée de combiner une égalisation au niveau des symboles et au niveau des bribes (*chip*) en HSDPA.

En conséquence de ce choix, la contribution attendue du signal à la sortie du corrélateur n'est pas seulement présente dans un seul robinet du

canal-égaliseur cascade, donc, dans un canal LTI ce biais est constant à la sortie de chip-equalizer, mais évolue au fil du temps à la sortie du corrélateur.

Cela a des conséquences sur le SINR obtenu avec de tels récepteurs. Nous décrivons la relation entre l'égaliseur LMMSE et la sortie du corrélateur (variable dans le temps). Nous obtenons l'expression analytique de la SINR. Nous montrons que, en principe, ce biais doit étre pris en compte dans le traitement du récepteur.

Ensuite, nous proposons un nouvel égaliseur basé sur un "sparsifieur" de canal (*channel sparsifier*). Le sparsification est contrôlée par un critère de conception approprié. Parce que l'on considère le scrambler comme déterministe, le modèle résultant est variant dans le temps. Cette mise en cascade débouche sur un problème réduit en nombre de paramètres, dont la dimension peut étre contrôlée par la conception du sparsifieur. Tandis que l'égaliseur MMSE classique est très efficace pour atténuer les effets de la dispersion temporelle et pour restaurer l'orthogonalité des codes, il fonctionne sur le principe d'une combinaison optimale de l'énergie dans un seul robinet, qui correspond au délai-cible pour l'égaliseur. Ceci exclut toute possibilité de recourir à un traitement de type Viterbi à un quelconque étage ultérieur. Dans la thèse, nous montrons que des récepteurs HSDPA améliorés peuvent étre connus, en s'appuyant simultanément sur une sparsification contrôlée, un traitement déterministe du scrambler et une détection non-linéaire.

Le paragraphe suivant présente les résultats de simulation et une comparaison des performances des différentes structures de récepteurs proposées dans le chapitre.

Nous appelons RX-1 le récepteur classique MMSE-CE/Correlator, et RX-2 le récepteur qui effectue PIC suivie par une égalisation MLE après sparsification. RX-3 est le récepteur MLE et nous appelons RX-4 l'égaliseur qui effectue une simple MRC après sparsification. La figure 2.1, illustre le SINR pour les récepteurs 1, 2 et 3. Le SINR à la sortie du récepteur avec "chip-equalizer" et corrélateur est calculé en considérant l'embrouilleur comme aléatoire, et comparé à la distribution du SINR à la sortie des deux autres récepteurs, où le scrambler est cette fois considéré comme déterministe. En fait, le traitement déterministe implique que le canal est variable dans le temps à l'échelle des symboles ; cependant, ici, nous utilisons la valeur moyenne du gain de canal (variable dans le temps) pour tracer les SINR.

Nous voyons ici que RX-2 est bien meilleur que le récepteur classique

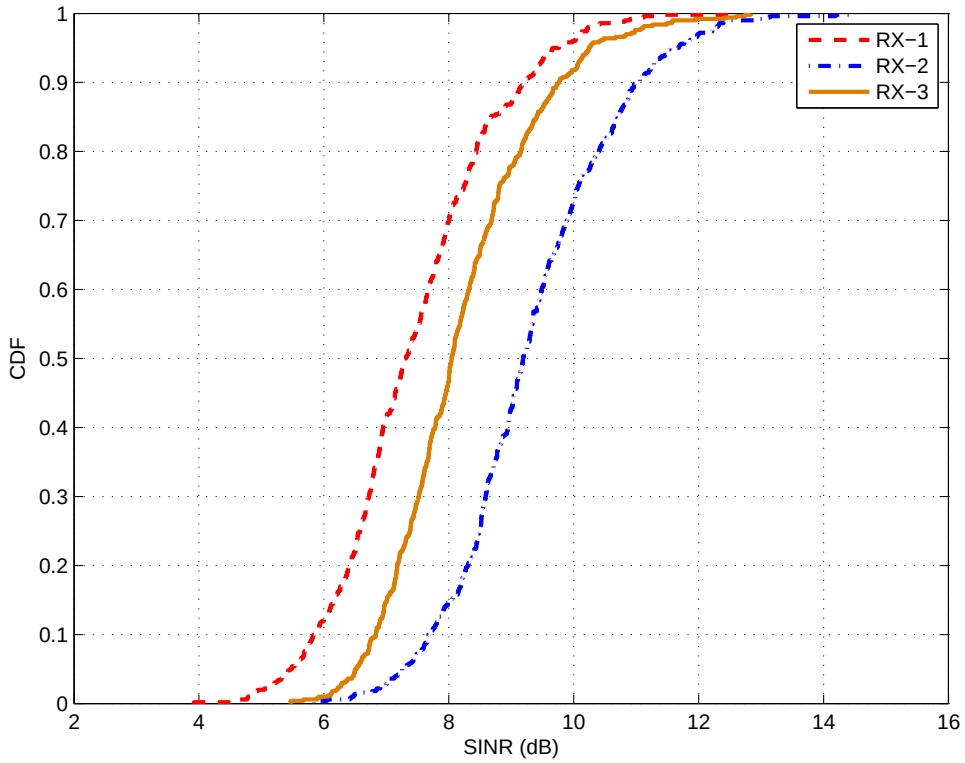

Figure 2.1: SINR comparison of RX 1, RX 2 and RX 3.

chip-equalizer. La complexité de RX-3 est significativement réduite en raison de l'absence de l'étape d'interférence entre les codes d'annulation, supposés présents dans RX-2 ; cependant RX-3 surpasse encore RX-1.

Sur la figure 2.2, nous comparons les performances du récepteur MRC avec notre récepteur de référence. Ici aussi, nous trouvons que d'un récepteur qui rend d'abord le canal parcimonieux puis qui considère l'embrouilleur comme déterministe surpasse le récepteur de référence. Enfin, dans la figure 2.3, nous comparons les performances de tous les récepteurs en fonction du SINR moyen, pour différentes valeurs de SNR.

Ces résultats ont été publiés dans les articles suivants :

- Irfan Ghauri, Shakti Prasad Shenoy and Dirk T. M. Slock, "On LMMSE bias in CDMA SIMO/MIMO receivers", *IEEE International Conference*

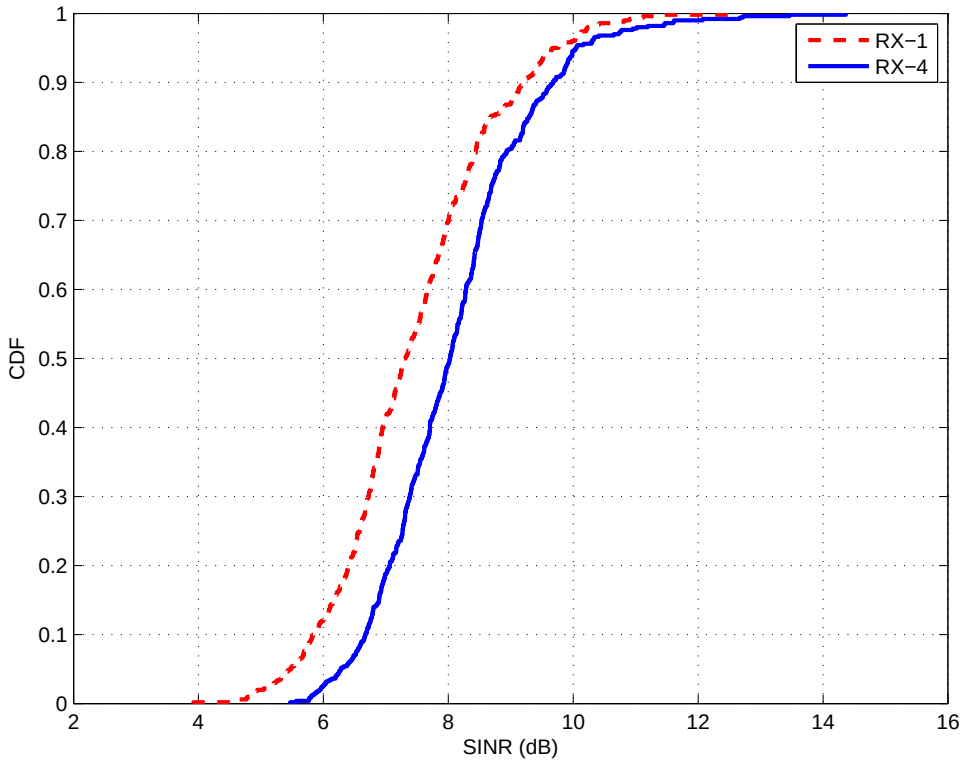

Figure 2.2: SINR comparison of RX 1 and RX 4.

on Acoustics, Speech, and Signal Processing (ICASSP 2008), March 30 - April 4, 2008, Las Vegas, Nevada, USA

- Shakti Prasad Shenoy, Irfan Ghauri and Dirk T. M. Slock, "Chip-sparsification and symbol-equalization for WCDMA downlink", *IEEE International Symposium on Personal, Indoor and Mobile Radio Communications (PIMRC 2008), 15-18 September 2008, Cannes, France*

Le chapitre 5 traite de l'égalisation pour MIMO HSDPA. L'une des contributions de ce chapitre est l'établissement d'une solution analytique pour le choix optimal du précodeur unitaire, à appliquer à l'émetteur lorsque le récepteur est basé sur une conception MMSE. Ici, nous étendons également les résultats obtenus dans le chapitre précédent au cas MIMO de l'UMTS HSDPA.
Les contributions à la recherche de ce chapitre sont :

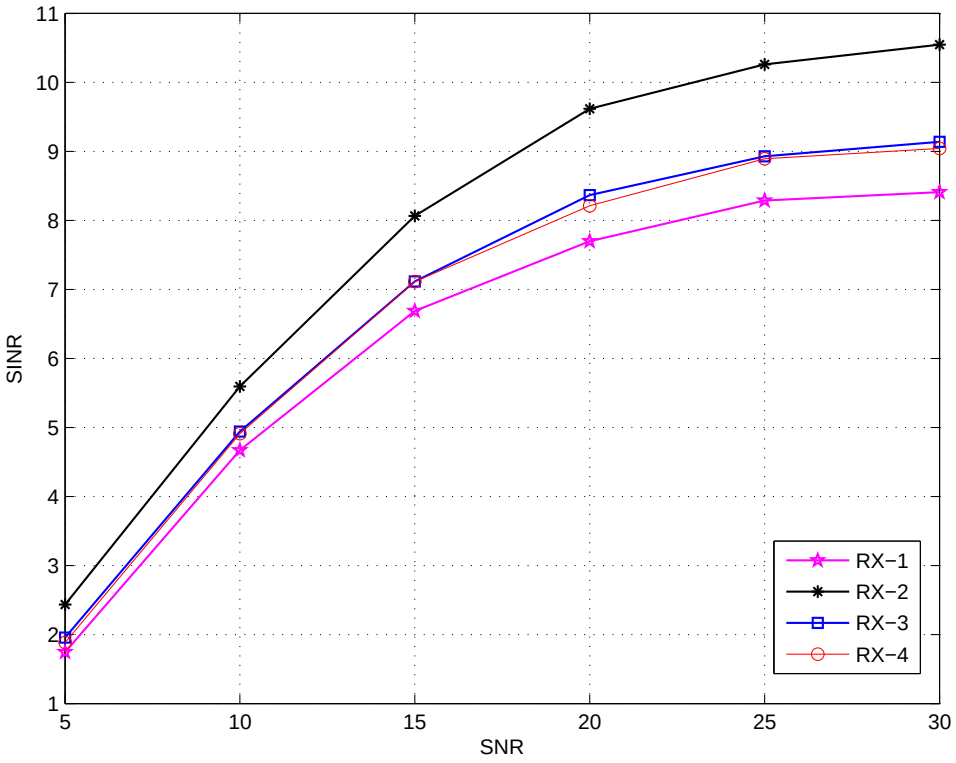

Figure 2.3: SNR vs. average SINR comparison of all receivers.

- Une solution analytique pour le choix du précodeur optimal à appliquer à l'émetteur afin de maximiser le débit de données en MIMO HSDPA ;
- La conception de récepteurs MIMO HSDPA fondée sur la combinaison d'égaliseurs à la fois au niveau de la chip et des symboles, tout en tenant compte du scrambler en tant que séquence aléatoire/déterministe;

Les publications associées à ce chapitre sont :

- Shakti Prasad Shenoy, Irfan Ghauri and Dirk T. M. Slock, "Optimal precoding and MMSE receiver designs for MIMO WCDMA", *IEEE 67th Vehicular Technology Conference (VTC-Spring 2008), May 11?14, Singapore*

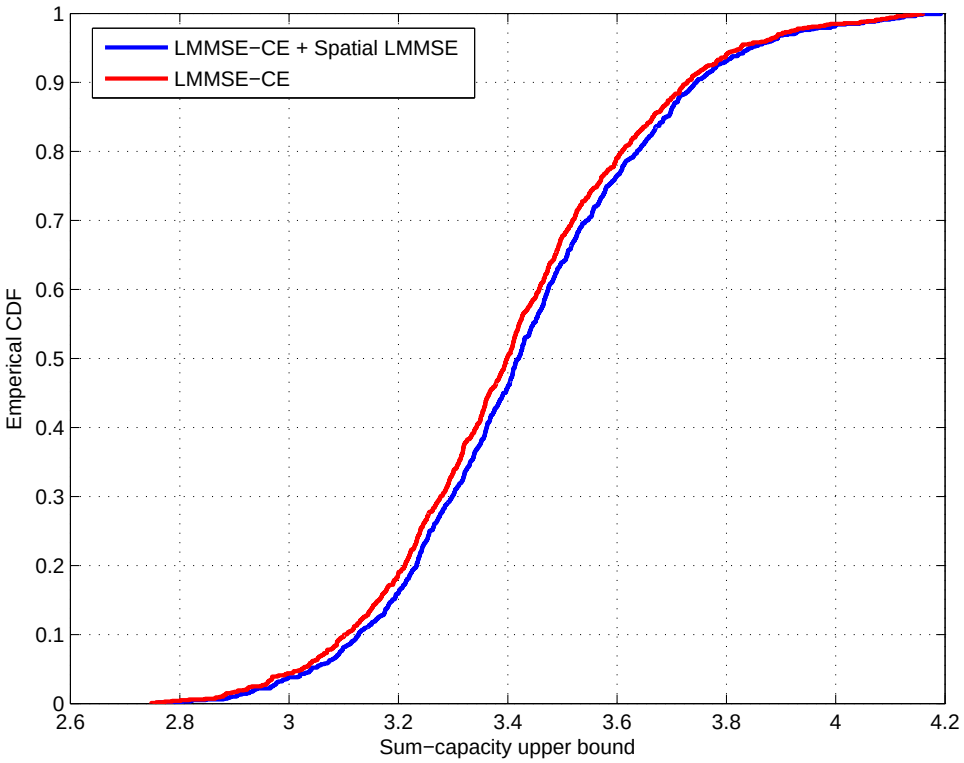

Figure 2.4: Performance of LMMSE chip-equalizer/correlator receiver and LMMSE chip-equalizer and spatial MMSE receiver.

- Shakti Prasad Shenoy, Irfan Ghauri and Dirk T. M. Slock, " Receiver designs for MIMO HSDPA", *IEEE International Conference on Communications (ICC-2008), May 19-23, Beijing, China*

Nous présentons ici quelques résultats de simulation pour comparer les performances des différentes structures de récepteurs proposés dans ces articles. La figure 2.4 montre la distribution de capacité totale à la sortie du récepteur égalisé MMSE au niveau du chip, et celle du récepteur MMSE spatial proposé. Avec une étape de traitement supplémentaire d'une complexité très faible, nous sommes en mesure d'observer un gain modeste mais réel dans le débit au récepteur. Dans la figure 2.5 nous comparons les performances du récepteur égalisé par LMMSE au niveau du chip, avec le récepteur qui effectue non seulement l'égalisation spatiale MMSE spa-

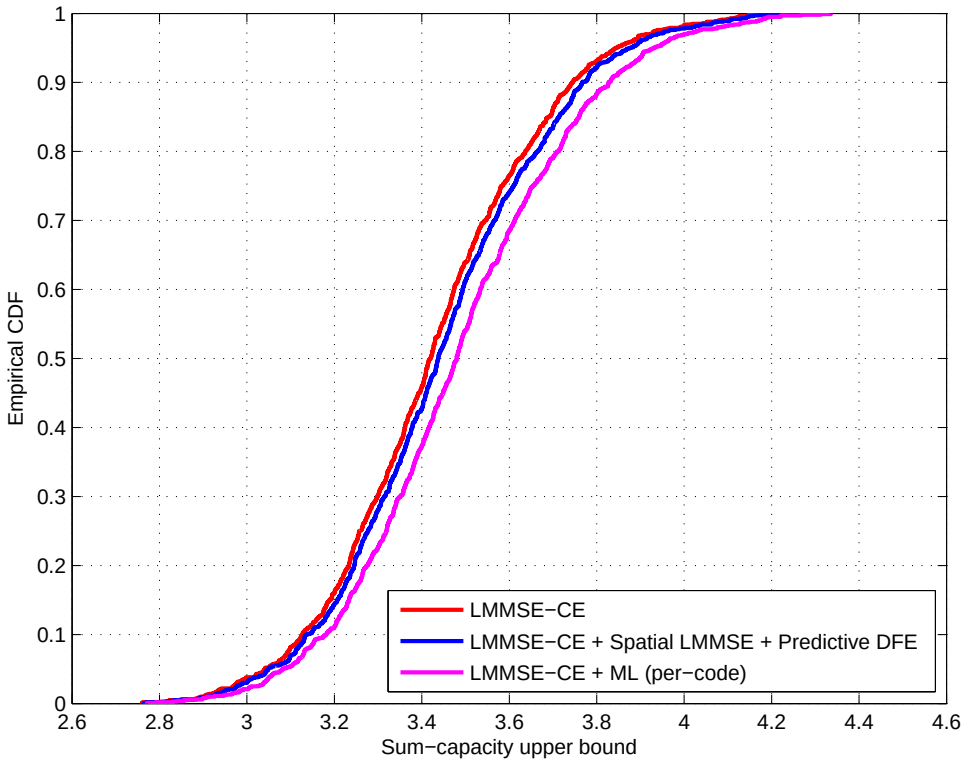

Figure 2.5: Comparison of sum-capacity upper bounds for different receiver structures.

tiale mais aussi une “prédictive-DFE", et avec le récepteur maximisant la vraisemblance des codes. Comme précédemment, les matrices de précodage optimal sont utilisées à la station de base (BS).

Le récepteur qui effectue une LMMSE spatiale et une DFE bénéficient légèrement du traitement spatial supplémentaire des deux flux ainsi que de l'étape d'égalisation non-linéaire du flux 2. La performance de ce récepteur est limitée par les performances du flux 1. En effectuant la détection spatiale ML nous pouvons obtenir une performance bien meilleure. Ensuite, dans la figure 2.6, nous traitons les limites de capacité pour les deux cas. Dans le premier cas, nous considérons le scrambler comme aléatoire. L'énergie de symbole pour le code k est donc donnée par la variance du symbole pour ce code, modifié par un facteur multiplicatif arbitraire et in-

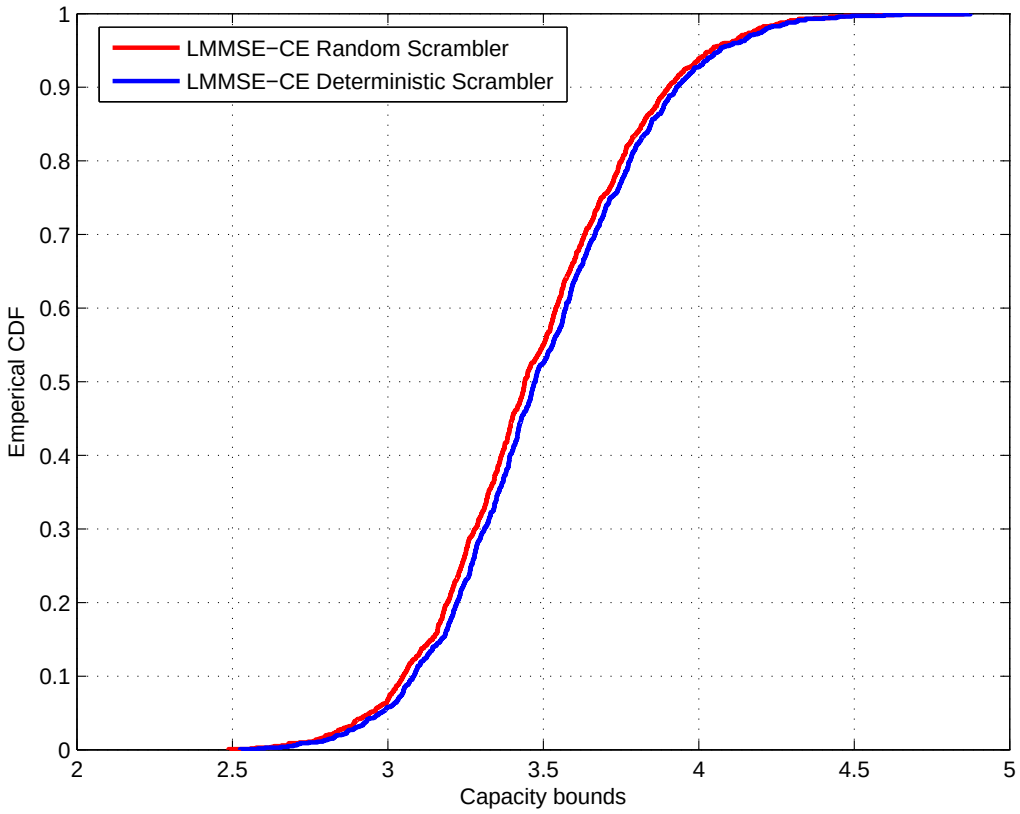

Figure 2.6: Performance of LMMSE chip-equalizer correlator with random and deterministic scrambler.

variant dans le temps. Dans le second cas, nous considérons le scramber comme une séquence connue.

Dans ce cas, d'une part, l'énergie du signal varie comme le débit de symboles. Cette énergie de signal variable dans le temps peut être considéré comme la somme d'une contribution «moyenne égale à l'énergie du signal lorsque le scrambler est considérée comme aléatoire, et d'une contribution variant dans le temps, due au traitement déterministe du scrambler.

Actuellement, HSDPA supporte un seul utilisateur en mode MIMO. Dans le chapitre 6, nous explorons les extensions multi-utilisateur de MIMO

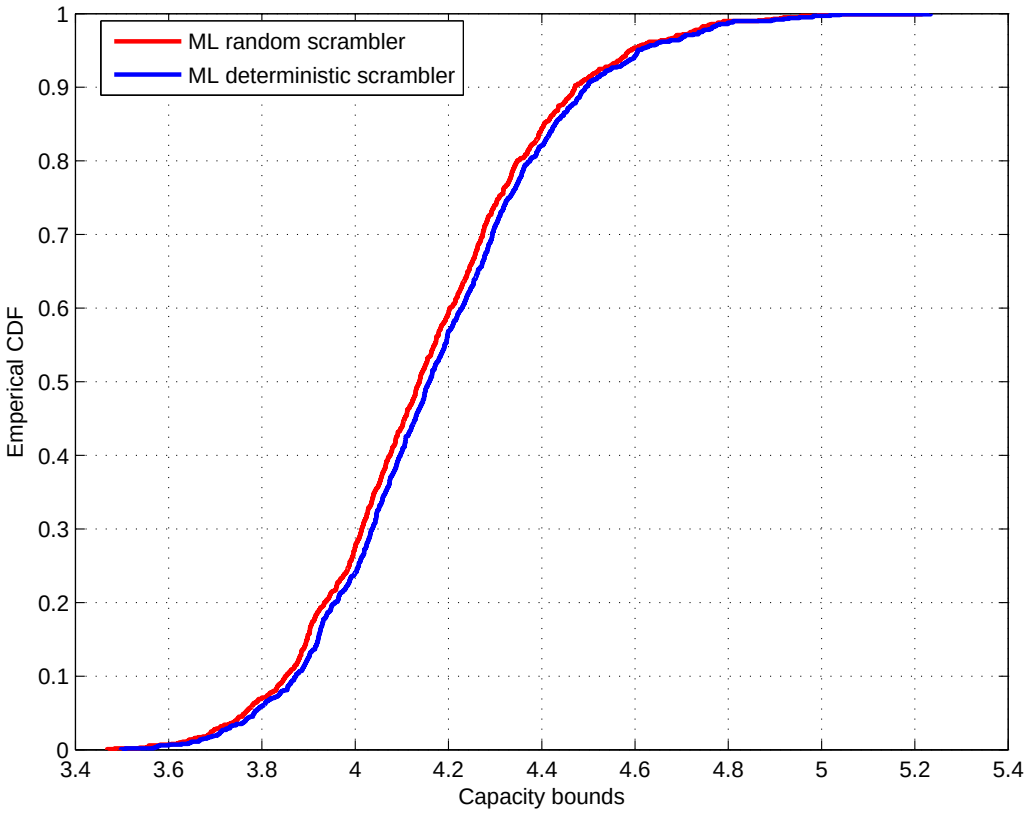

Figure 2.7: Sum-capacity at the output of spatial-ML receiver with deterministic and random scrambler.

HSDPA qui nécessitent des changements minimes dans le standard actuel. Ici, pour le TX-AA, nous suggérons diverses stratégies de formation de voies multi-utilisateurs, et proposons de comparer leurs performances à l'aide de simulations de Monte Carlo.

Pour le D-TxAA, nous montrons qu'en MIMO HSDPA, le débit de données sur la liaison descendante est maximisé en utilisant le canal MIMO pour desservir de multiples utilisateurs du flux, au lieu d'utiliser un multiplexage spatial des utilisateurs uniques, qui est la solution actuellement prise en charge dans les standards. Ces propositions et leurs résultats ont été publiés dans le document suivant:

- Shakti Prasad Shenoy, Irfan Ghauri and Dirk T. M. Slock, “Multiuser extensions for closed loop transmit diversity in HSDPA", *International Conference on Communications (ICC-2009), June 14-18, Dresden, Germany*

2.2.2 Partie II: Diversité

Nous savons que les égaliseurs ML sont en mesure d’exploiter toute la diversité disponibles sur les canaux sélectifs en temps-fréquence ou en temps, si le précodage approprié est réalisé au niveau de l’émetteur. Ceci a été démontré pour les canaux sans fil modélisés à l’aide de la CE-BEM dans [2]. En outre, il a été montré que ces précodeurs permettent également aux égaliseurs linéaires de bénéficier de toute la diversité de canaux sélectifs en fréquence. La principale contribution du chapitre 8 est la preuve analytique que les précodeurs proposés dans [2] permettent également aux égaliseurs linéaires et et aux égaliseurs ne réalisant pas le ML de bénéficier de la méme diversité des canaux doublement sélectifs. Les contributions originales dans ce chapitre sont :

- La preuve que l’égalisation linéaire permet d’obtenir toute la diversité Doppler dans les canaux sélectifs en temps
- La preuve que l’égalisation linéaire permet d’obtenir toute la diversité dans les canaux doublement sélectifs, et que l’égalisation DFE permet d’obtenir toute la diversité dans les canaux des trois types (sélectifs en temps et/ou en fréquence)

Les preuves et les lemmes associés peuvent étre trouvées dans le chapitre 8. Une partie de la preuve concernant le gain de diversité en utilisant DFE repose sur la preuve exposée dans [3]. Cependant, [3] résout seulement le cas des canaux sélectifs en fréquence tandis que nous traitons les canaux sélectifs en temps et/ou en fréquence.
Les publications associées sont :

- Shakti Prasad Shenoy, Irfan Ghauri and Dirk T. M. Slock, “Diversity order of linear equalizers for block transmission in fading channels", *42nd Asilomar Conference on Signals Systems and Computers (Asilomar 2008), October 26-29, Asilomar, California, USA*
- Shakti Prasad Shenoy, Irfan Ghauri and Dirk T. M. Slock, “Diversity order of linear equalizers for doubly selective channels"', *10th IEEE*

International Workshop on Signal Processing Advances in Wireless Communications (SPAWC 2009), June 21-24, Perugia, Italy

Dans le chapitre 9 nous nous intéressons aux aspects pratiques de la mise en œuvre de ces égaliseurs. Dans ce chapitre, nous montrons que les égaliseurs approchés, fondés sur un développement pôlynomial, ne semblent pas avoir d'impact sur le gain de diversité de ces égaliseurs. Les principales contributions de ce chapitre sont :

- Une méthode pour calculer les gains de diversité des égaliseurs linéaires dans des systèmes cycliques prédéterminés ;
- Des égaliseurs approchés obtenant toute la diversité dans les canaux doublement sélectifs ;
- Des égaliseurs hybrides, obtenant toute la diversité dans les canaux doublement sélectifs, de faible complexité.

Les publications associés sont :

- Shakti Prasad Shenoy, Francesco Negro, Irfan Ghauri and Dirk T. M. Slock, "Low-complexity linear equalization for block transmission in multipath channels", *IEEE Wireless Communications and Networking Conference (WCNC 2009), April 5-8, Budapest, Hungary*
- Shakti Prasad Shenoy, Irfan Ghauri and Dirk T. M. Slock, "Approximate full diversity equalizers for doubly selective channels", *17th European Signal Processing Conference(Eusipco 2009), August 24-28, Glasgow, Scotland*
- Shakti Prasad Shenoy, Irfan Ghauri and Dirk T. M. Slock, "On full diversity equalization for precoded block transmission systems", *43rd Asilomar Conference on Signals Systems and Computers (Asilomar 2009), November 1-4, Asilomar, California, USA*

Nous donnons ici quelques résultats numériques pour montrer la diversité des égaliseurs présentés dans ce chapitre. Dans la figure 2.8, nous notons que la diversité des ZP-OFDM est supérieure à celle du système de CP-OFDM. Cela n'est pas surprenant, car le système CP-OFDM n'est pas en mesure de bénéficier de la diversité des chemins multiples présents dans le canal sans précodage.

La performance de ZP-OFDM avec préfixe cyclique, et avec égalisation linéaire de faible complexité pour trois valeurs différentes de e_t, montre clairement que e_t approche L,et que la diversité des système approche

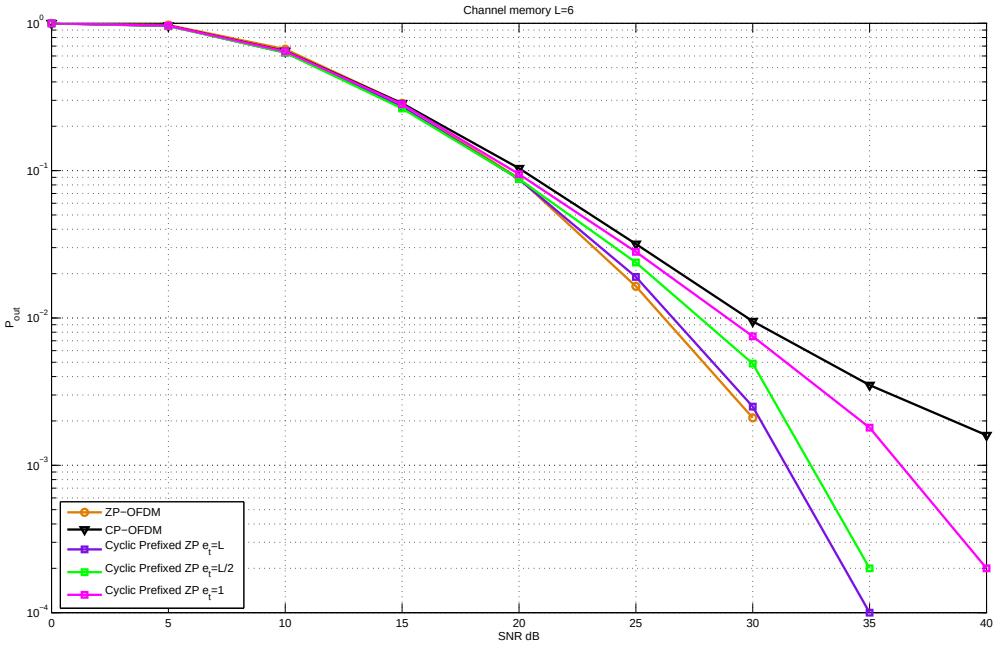

Figure 2.8: Outage Probability results for frequency selective channels.

également L. Autrement dit, le système est capable d'exploiter le temps disponible en excès pour fournir un gain additionnel de diversité de l à l'égalisation linéaire.

La figure 2.9 illustre l'évolution de la pente de l'ordre de diversité atteinte, en fonction de l'ordre du polynôme utilisé pour approché l'égaliseur dans l'équation (9.17). Nous voyons que la pente s'aplatit de la courbe que les mesures aplatit la diversité à des niveaux inférieurs d'approximations. C'est à cause de la erreurs d'approximation grande à ces niveaux. Mais les résultats sont meilleurs aux niveaux supérieurs de rapprochement de l'égaliseur.

La figure. 2.10 montre la comparaison de l'ordre de diversité lorsque l'on met en œuvre l'égaliseur MMSE-ZF par la méthode de la force brute et pour des canaux doublement sélectifs. Le SNR de l'égaliseur de l'expansion polynomiale se situe à un décalage constant par rapport à la force brute, ce qui était à prévoir, puisque l'égaliseur est une approximation du récepteur MMSE-ZF. Cependant, il parvient à recueillir toute la diversité of-

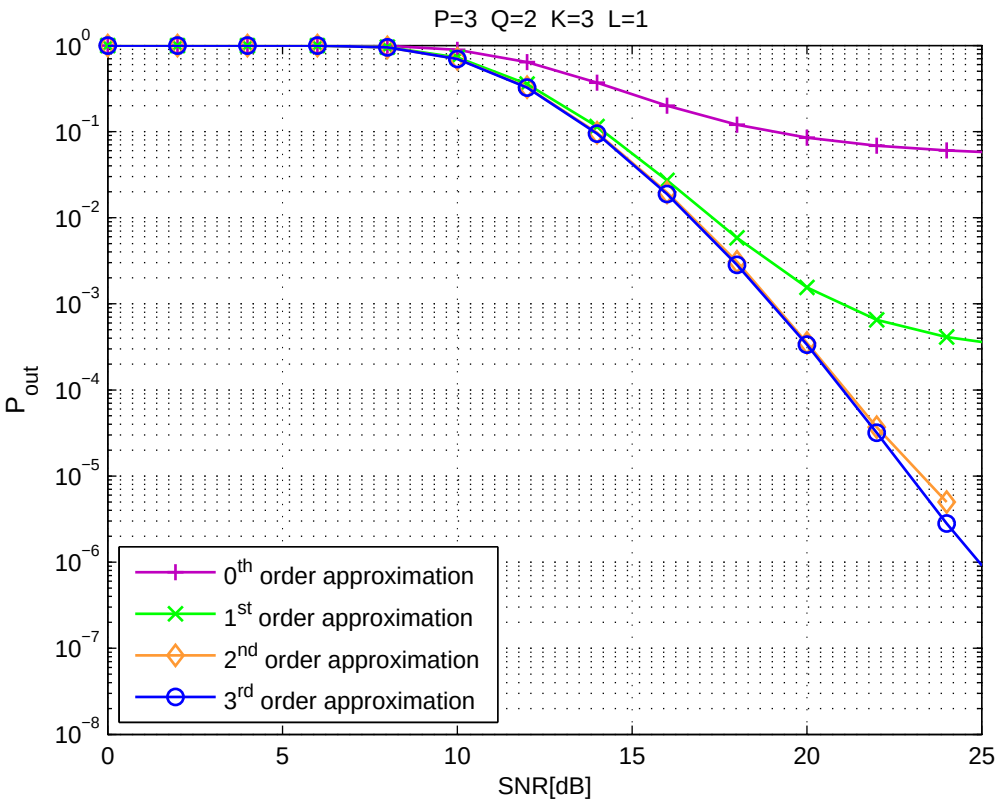

Figure 2.9: Evolution of diversity order for different iterations.

ferte par le canal doublement sélectif, à un ordre d'approximation relativement faible. La performance de l'approximation polynômiale qui minimise l'EQM au niveau du récepteur (9.19) est représentée sur la figure 2.11. Nous voyons une amélioration notable des performances au premier ordre d'approximation, par rapport à l'approximation par expansion polynômiale dans (9.17). L'expansion polynômiale provoque un effet de saturation sur la probabilité d'interruption. Le seuil de saturation s'abaisse lorsque l'ordre d'approximation augmente. Cependant, pour des SNR faibles, avant que ce seuil ne soit atteint, la probabilité d'interruption bénéficie pleinement du gain de diversité, et le seul effet de la PE est une perte constante de SNR. À ordre d'approximation fixé, l'utilisation de coefficients de combinaison MMSE diagonaux dans la PE conduit à une chute significative de la valeur plancher de l'erreur, comparée à de simples ZF PE. Dans les simu-

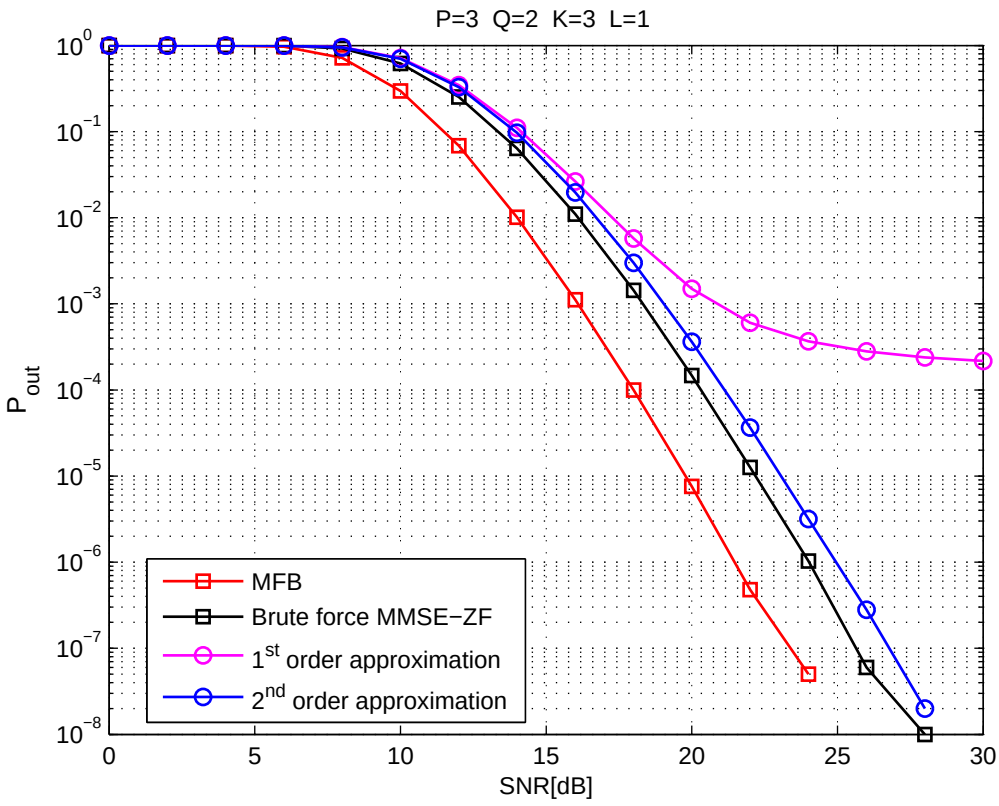

Figure 2.10: Diversity order of LE approximated by PE.

lations, il apparaît que la sous-optimalité du PE de premier ordre avec coefficients de combinaison MMSE diagonaux est négligeable par rapport à la mise en œuvre simple du récepteur MMSE-ZF linéaire, dans toutes les situations d'intérêt pratique en terme de valeur de la probabilité d'interruption de service. Dans la figure 2.12, nous comparons les performances de l'égaliseur hybride dans le cas de précodeurs de taille carrée. Le récepteur MMSE-ZF ne recueille pas toute la diversité, alors que la diversité obtenue par l'égaliseur hybride est la méme que celle de MLE, qui a une complexité de calcul beaucoup plus élevée par rapport à l'égaliseur hybride. Enfin dans la figure 2.13, on compare l'ordre de diversité des précodeurs "square-tall" avec celui des précodeurs "square-square", quand MLE est appliqué au niveau du récepteur. Nous voyons que les deux précodeurs permettre à MLE d'exploiter toute la diversité du canal. Toutefois, le précodeur

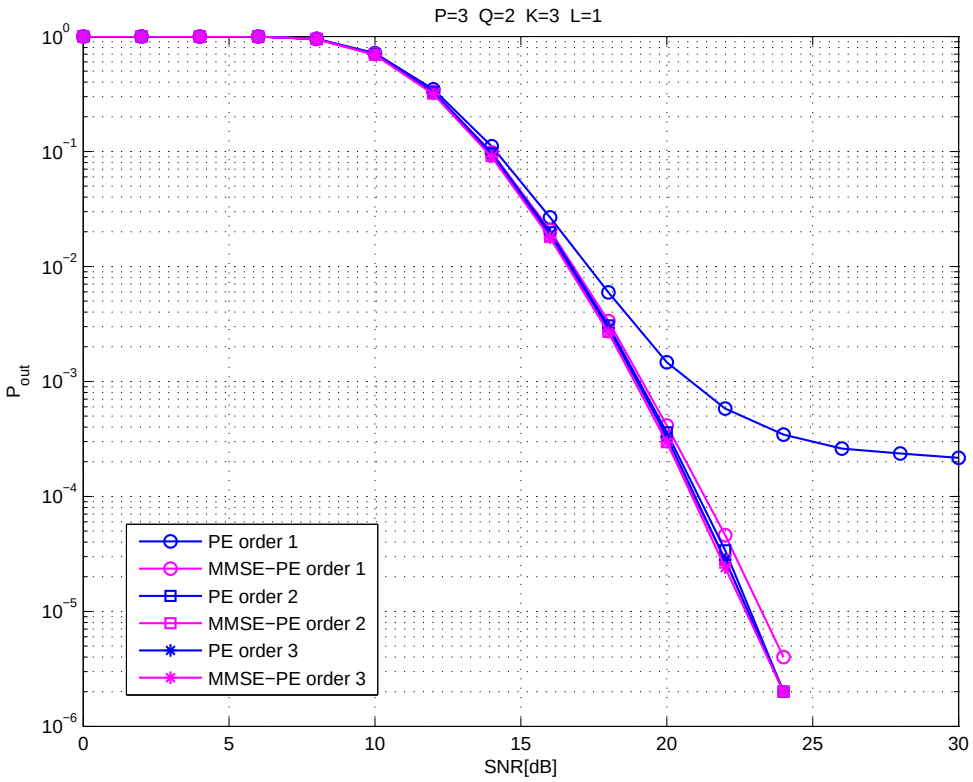

Figure 2.11: Comparison of performance of the two PE approximations.

“square-square" précodeurs a une meilleure efficacité en bande passante, mais le précodeur “square-tall" possède un meilleur gain de codage.

Ainsi, les principales contributions de la deuxième partie de la thèse peut étre résumées comme suit :

- Pour les canaux sélectifs en temps, les égaliseurs linéaires peuvent obtenir la pleine diversité Doppler, lorsque des bandes de gardes appropriées sont insérées dans les symboles à transmettre, de la méme manière qu’on ajouterait des symboles zéro en transmission ZP pour atteindre la pleine diversité dans des canaux à trajets multiples.

- LE et DFE atteignent la diversité maximale offerte par le canal doublement sélectif, avec un précodeur à deux niveaux, permettant au MLE d’obtenir de la diversité multiplicative Doppler à trajets multi-

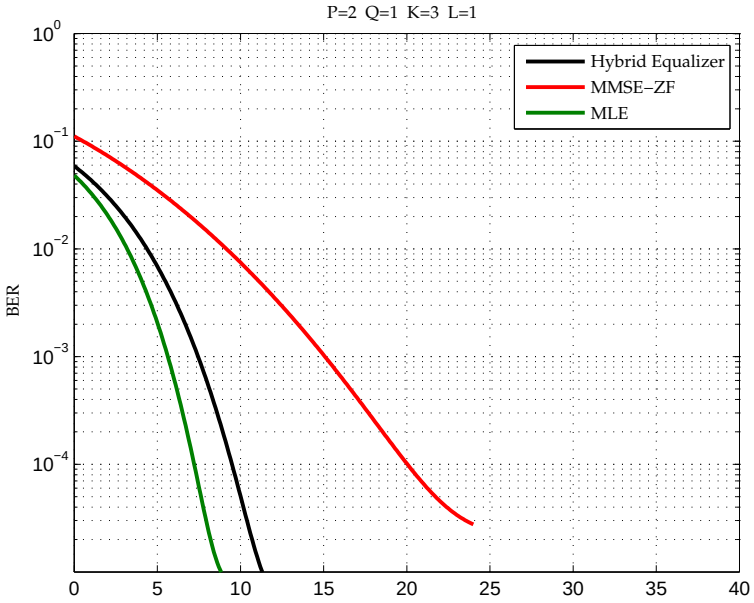

Figure 2.12: Performance of hybrid equalizer with square-tall precoder.

ples.

- Avec un précodeur à un niveau, n'introduisant de la redondance que dans le domaine temporel, il est possible d'obtenir le gain de diversité maximal en employant une technique d'égalisation hybride dont la complexité est inférieure à celle du MLE.

Nous présentons également quelques résultats qui suggèrent qu'une quantité importante de la redondance introduite par le précodeurs 2-D n'est pas nécessaire pour MLE, et que la redondance de l'ordre de la propagation de dispersion du canal est suffisante pour permettre une réception de diversité maximale avec l'égaliseur ML dans les canaux doublement sélectifs. Les tableaux suivants servir de référence rapide pour les contributions et les cas traités dans cette thèse.

En dehors de ces principales contributions, nous avons également étudié en détail la question de la mise en ouvre de ces récepteurs avec une complexité de calcul réduite. Conséquemment à notre étude, nous remarquons que le précodage à l'émetteur peut aider à la réduction de la complexité de l'égalisation du récepteur, tout en permettant la pleine exploitation de la diversité. Nous avons montré ce résultat dans le cas des canaux sélectifs en fréquence. Une autre observation intéressante est que, pour des canaux simulés, il semble que la sous-optimalité d'un récepteur approché

	η	Résultats connus	Nos contributions
tall	$\frac{N}{M}$	ML [MG] BLE (MMSE) [CT] BLE (MMSE-ZF) [CT]	BLE (MMSE) BLE (MMSE-ZF) BDFE (MMSE) BDFE (MMSE-ZF)

[MG]:- [2] [CT]:- [6]
BDFE:- Block DFE, BLE:- Block Linear Equalizer, MMSE-ZF:- Minimum Mean Squared Error-Zero Forcing

	η	[MG]	cette thèse
tall-tall	$\frac{Q'L'}{(Q'+Q)(L'+L)}$	ML	ML-BLE BDFE (MMSE) BDFE (MMSE-ZF) BLE (MMSE) BLE (MMSE-ZF)
square-tall	$\frac{L'}{L'+L}$	ML	ML-BLE

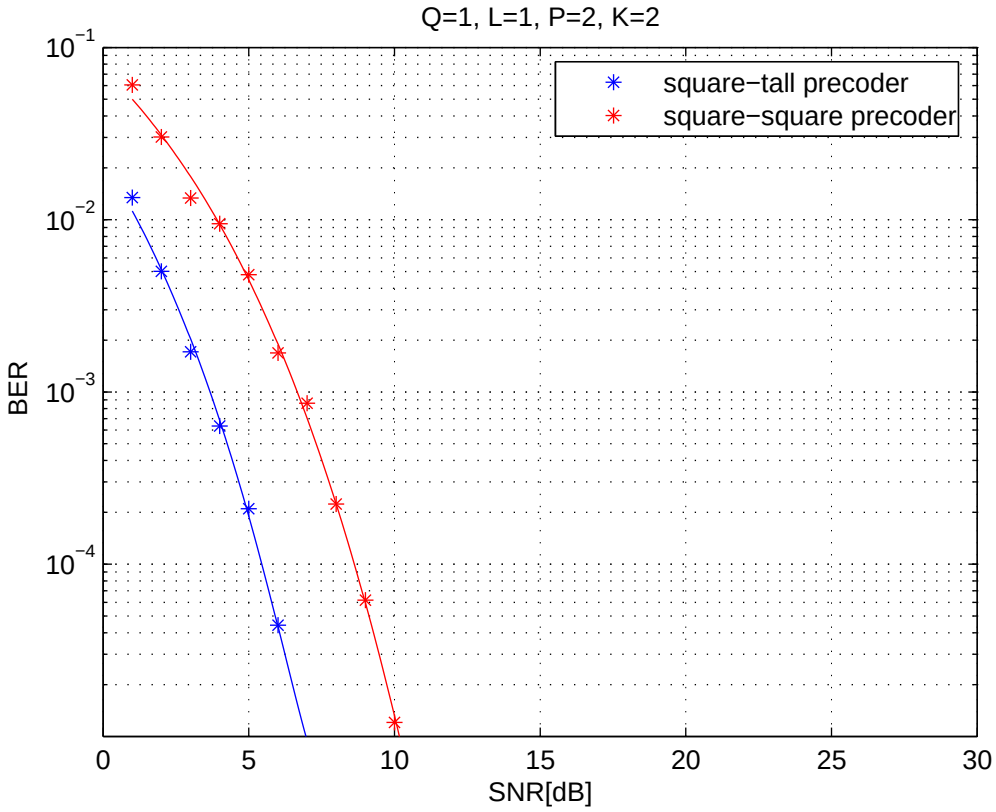

Figure 2.13: Comparison of diversity order with square-tall and square-square precoders.

(à savoir, une expansion polynomiale de premier ordre (PE) avec des coefficients MMSE d'égalisation diagonaux) est négligeable, comparée au récepteur linéaire MMSE-ZF de force brute, sur n'importe quelle plage de probabilité d'interruption de service ayant un intérêt pratique.

2.2.3 Partie III: L'alignement des interférences

Le chapitre 11 étudie le problème suivant. Considérons un MIMO IFC caractérisé par K utilisateurs, chacun d'entre eux ayant M_k antennes de transmission et N_k antennes de réception. Supposons également que chaque paire d'émission-réception a l'intention de communiquer d_k flux de données mutuellement indépendants. Si le traitement à l'émetteur et au récepteur est contraint à être linéaire, il est connu que si l'on utilise le con-

cept d'alignement des interférences (IA), le nombre total de flux sans interférence pouvant étre transmis dans ce réseau de K utilisateurs peut étre maximisé. Toutefois, pour un réseau caractérisé par l'ensemble K, M_k, N_k, le maximum $d_{tot} = \sum_k d_k$ réalisable n'est pas connu et demeure un problème ouvert. Nous ne savons pas non plus s'il existe une méthode analytique pour évaluer l'existence de solutions IA, méme si l'ensemble d_k est connu. Quelques solutions pour des cas particuliers ont été donnés, dans le cas d'un flux unique, dans [4], et des solutions numériques ont été établies, par exemple dans [5]. Dans ce chapitre, nous fournissons de nouvelles perspectives à l'existence de solutions IA pour un MIMO IFC donné, l'ensemble d_k étant connu. Méme si nous n'avons pas encore de preuve concrète, nous croyons que l'algorithme récursif que nous présentons dans ce chapitre constitue des conditions suffisantes pour l'existence de solutions IA. Dans cette partie de la thèse, nous prétendons donc aux contributions suivantes:

- De nouvelles perspectives pour l'existence de solutions d'alignement des interférences réalisables, pour les MIMO IFC;
- Un algorithme récursif pour évaluer analytiquement l'existence de solutions d'alignement de brouillage pour un MIMO IFC donné.

Les résultats présentés dans ce chapitre ont été publiés dans:
Francesco Negro, Shakti Prasad Shenoy, Irfan Ghauri and Dirk T. M. Slock, "Interference Alignment Feasibility in Constant Coefficient MIMO Interference Channels", *11th IEEE International Workshop on Signal Processing Advances in Wireless Communications (SPAWC 2010), June 20-23, Marrakech, Morocco*

Part I

Equalization

Chapter 3

Equalization for HSDPA in frequency selective channels

3.1 HSDPA review

The High Speed Downlink Packet Access (HSDPA) standard is a downlink packet data transfer scheme designed to significantly increase the throughput in existing 3GPP systems. HSDPA is designed to capitalize on the asymmetry in data transfer in the uplink and downlink in typical packet data traffic like Internet and streaming audio/video applications to provide enhanced throughput and spectral efficiency in existing 3G systems. The first true 3G standard from the 3GPP standards body was called Release 99 whose maximum data rate per user was typically 384kbps. With the introduction of HSDPA and its MIMO variants, the theoretical peak data rate for a single user in currently deployed networks is now 14 Mbps [7], making mobile broadband a commercially viable reality [8].

The efficacy of HSDPA is based in no small part to the enabling technologies like fast hybrid-automatic repeat request (HARQ) and adaptive modulation and coding (AMC). HSDPA supports QPSK, 16 QAM and 64-QAM modulation formats and introduces three new channel types of which two are control channels and one is a data channel. The HSDPA data channel (HS-PDSCH) is shared between all active HSDPA users in the cell. This channel is multiplexed both in time and code. The standard 10 ms frame is divided into subframes of 2 ms each in HSDPA. The resource allocation at the transmitter can be changed in each sub-frame. Furthermore, in each sub-frame 16 users can be simultaneously active since each is allocated at least one spreading code of SF=16. AMC allows the shared channel transport format (i.e., the modulation scheme and the code rate) to depend on the channel quality seen by the receiver. This is fed back periodically and used to change the transport format dynamically in every frame. If the radio channel between the transmitter and receiver is good, the network can use higher-order modulation and less redundancy in the channel codes. More robust modulation and coding schemes can be employed in poor channel conditions. This enhances the throughput of the network and a significant increase in spectral efficiency is achieved.

3.1.1 MIMO in HSDPA

Any wireless communication system that leverages the use of multiple antennas both at the transmitter and the receiver qualifies as a multiple-input-multiple-output (MIMO) wireless system. Multiple antennas at the transmitter and receiver add an additional spatial dimension to the communica-

tion channel. By taking advantage of this fact and by exploiting the spatial properties of the MIMO channel, it is possible to provide the following features to the communication system.

1. Make the communication link resilient/robust to channel fades: Diversity techniques have for long been considered as effective means to combat channel fading. In simple terms, diversity is achieved by combining multiple copies of the same transmit signal. If the fading characteristics of each copy is statistically independent from the rest, the combined signal is more robust to channel fading. In the context of MIMO systems, using the concept of *spatial diversity*, it is possible to show that the probability of losing the signal due to deep fades reduces exponentially with the number of decorrelated transmit-receive antenna pairs (spatial links) between the transmitter and receiver [9].

2. Increase the link capacity: Instead of using the multiple spatial channels to provide diversity, it is possible to use these channels for multiplexing in the spatial domain. A high-data rate stream is first split into multiple sub-streams of lower data rates. Subject to certain channel conditions [10], $\min(N_{tx}, N_{rx})$ streams can be transmitted over the MIMO channel. Here N_{tx}, N_{rx} refer to the number of antennas at the transmitter and receiver respectively. Since this requires no extra spectral resources, the total data rate (bits/s) transmitted over the communication link is increased.

3. Increased coverage area: Transmit beamforming is a technique in which signals transmitted from multiple antennas are multiplied by a complex weighting factor (different for each antenna) such that the transmitted signal power is concentrated in certain spatial directions (or spatial signatures). The resultant signal can now travel over a larger distance in that direction thus increasing the coverage area of the base-station. A similar type of processing can be employed at the receiver whereby the received signal power is increased by combining the signals at each receive antenna after application of suitable weights (receive beamforming).

4. Improved spectral efficiency: By reusing the multiple access resources (for instance, spreading codes in CDMA) over the spatial dimension, MIMO systems can increase spectral efficiency (bits/s/Hz) of the communication system.

However, not all of these features can be provided simultaneously. For instance, there exists a tradeoff between the coverage range and the link quality in any MIMO system [11]. Similarly using multiple transmit antennas for spatial multiplexing reduces the available spatial degrees of freedom for spatial reuse. MIMO systems first attracted attention due mainly to the tremendous increase in channel capacity that is promised [12] [9]. While there has been sustained academic interest in MIMO over the decade as witnessed by the huge number of research publications in this topic, true MIMO systems are only recently being standardized. This has been mainly due to the increased system complexity of MIMO systems. While MIMO can potentially provide huge gains at no extra cost in terms of spectral resources, these gains can only be realized at the cost of increased system and hardware complexity. Moreover, until recently, multiple antennas at the user equipment (UE) were not considered to be desirable due to space, battery and cost constraints of mobile terminals. As a result, standardization bodies have till date concentrated more on the sub-class of MIMO systems (MISO/SIMO) whereby some kind of antenna diversity at the base station is used to exploit transmit and/or receive diversity in the interest of enhancing link quality or increasing the total system capacity. With the emergence of Internet-centric applications and an increased demand of high-data-rate applications in cellular systems this trend is changing very quickly. The present generation of smart phones and Internet enabled devices have both the form factor as well as the computational powers that can support multiple antennas at the receiver. Foreseeing these developments 2×2 MIMO has been standardized in [13] standards. In fact, the worlds first HSPA+ or evolved HSPA network with support for 2×2 MIMO was launched in early 2009 [14]. Along with enabling technologies and user feedback based scheduling, MIMO in HSDPA can lead to peak data rates of 42Mbps in downlink. However, in the present form, MIMO in HSDPA can support only single user (SU) scenarios in DL. While shifting from single user to multiuser paradigm mandates a whole new level of increased system complexity [15], the associated gains are significant. For instance, MU-MIMO opens up the possibility of code-multiplexing which can lead to increased system capacity. MIMO in HSDPA is a variant of Per-Antenna Rate-Control (PARC), namely D-TxAA for Dual-stream Transmit Diversity for Multi-Input Multi-Output (MIMO) transmissions [13] in UMTS WCDMA. Code reuse is made across the two streams and the scrambling sequence is also common to both transmit (TX) streams. All (15) spreading codes are allocated to the same user in the HSDPA MIMO context. In general, all UEs served by a BS feed a Channel Quality Indicator

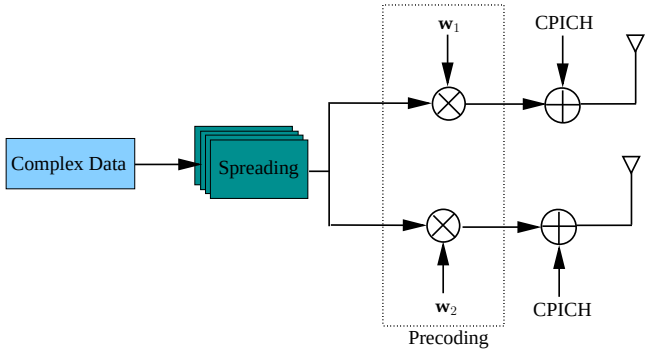

Figure 3.1: Simplified block diagram of processing at transmitter for TxAA.

(CQI) back to the BS. In addition, the UE also computes (and feeds back) the weighting vector(s) that would ideally provide the best instantaneous rate for the next time slot. Together, these feedbacks translate into a specific transport block size and a specific Modulation and Coding Scheme (MCS) for each UE. Based on this information, the BS is capable of maximizing the downlink throughput for each transmission time-interval.

Both transmit diversity and spatial multiplexing has been incorporated by 3GPP as standard in the form of TxAA and its dual stream counterpart D-TxAA for MIMO HSDPA. HSDPA supports a closed loop transmit diversity technique called transmit adaptive array (TxAA). In the 2 transmit-1 receive (2×1) antenna configuration of TxAA, the UE feeds back optimum beamforming weights that the BS uses while transmitting data to UE. D-TxAA is an extension of TxAA when UEs are configured in MIMO mode. Here two separately encoded, interleaved and spread transport blocks are transmitted in parallel. In this case, the UE decides the precoding matrix that the BS has to use when transmitting data to the UE. Let us now look at beamforming/ precoding aspect in more detail.

Precoding and CQI Feedback

In HSDPA, the UE is required to submit regular channel quality indicator (CQI) and precoding control indicator (PCI) reports to the BS. The CQI can be mapped to a particular modulation and coding scheme (MCS). The data packet size associated with a particular MCS can then be mapped to obtain the supported throughput for each stream for a certain predefined Packet-Error Rate (PER). The mapping strategy has been subject to significant simulation study (see e.g., [16]) and SINR $\rightarrow$ CQI $\leftrightarrow$ PER $\leftrightarrow$ throughput rela-

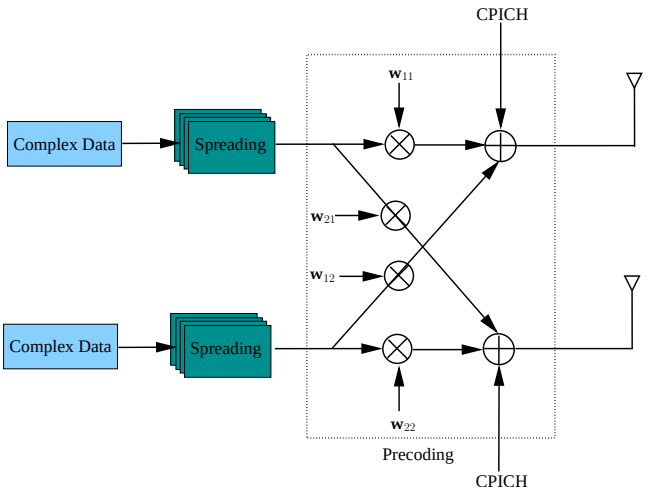

Figure 3.2: Simplified block diagram of processing at transmitter for D-TxAA.

tionship has been agreed to, appearing as CQI to MCS tables in the 3GPP standard document [13]. In addition to this, for each TTI over which the UE computes the CQI, PCI is computed using the CPICH(s) transmitted from both transmit antennas. The PCI encodes information of the beamforming vector/matrix to be applied by the BS to maximize the aggregate transport block size that the UE can support in the present channel conditions. To this end, when UE is not configured in MIMO mode, or when it requests transmission of a single transport block, the UE is required to choose one of 4 beamforming weights that control the antenna phase at BS. The UE indicates the number of transport blocks to be transmitted to it as part the CQI report. The BS fixes the phase of its primary (reference) antenna and alters the phase of the secondary antenna accordingly. Since the precoding weight applied to the reference antenna is a constant $(1/\sqrt{2})$, the feedback consists of the weight for antenna-2 and is one of the following weights $w \in \left\{ \frac{1+\sqrt{-1}}{2}, \frac{1-\sqrt{-1}}{2}, \frac{-1+\sqrt{-1}}{2}, \frac{-1-\sqrt{-1}}{2} \right\}$. One choice of beamforming weight vector, let us call it $\mathbf{w}$, might be one that maximizes the received signal power (or equivalently the receive SNR). For frequency-flat channels, this corresponds to the beamforming vector that is “closest" to the maximum right singular eigenvector of the 2×2 channel matrix $\mathbf{H}$. However, for frequency selective channel with a delay spread L, there are L such MIMO channel taps. In general it is not possible to chose $\mathbf{w}$ to match all channel taps, precoding gains in such conditions is in practice very low.

When the UE is configured in MIMO mode and requests 2 transport blocks to be transmitted, a precoding matrix has to be used in place of a single beamforming weight vector. 2×2 unitary precoding based on receiver feedback is applied alongside spatial multiplexing at the base station in HSDPA [13] in D-TxAA. In order to keep feedback overhead low, both columns of the precoding matrix have exactly the same structure as the beamforming weight vector in TxAA. Moreover, the second column of this matrix is a unique function of the first. This severely restricts possible gains due to precoding. In fact, out of the 4 precoding matrices, 2 matrices are related to the remaining as follows. Let $w_1 = \beta$, then by design $w_3 = \beta$ and $w_4 = -w_2$ and

$$w_2 \in \left\{ \frac{1+\sqrt{-1}}{2}, \frac{1-\sqrt{-1}}{2}, \frac{-1+\sqrt{-1}}{2}, \frac{-1-\sqrt{-1}}{2} \right\} \rightarrow \in \{\gamma, \theta, -\theta, -\gamma\} \tag{3.1}$$

Therefore,

$$\mathbf{W} = \begin{bmatrix} w_1 & w_3 \\ w_2 & w_4 \end{bmatrix},$$

$$\mathbf{W}_1 = \begin{bmatrix} \beta & \beta \\ \gamma & -\gamma \end{bmatrix}, \mathbf{W}_2 = \begin{bmatrix} \beta & \beta \\ \theta & -\theta \end{bmatrix},$$

The other two matrices are formed by interchanging the first and second columns of $\mathbf{W}_1$ and $\mathbf{W}_2$. Since the 2 transmitted streams interfere with each other and thereby influence CQI as well as PCI choice, the precoding matrix has to be computed after joint equalization of both streams.

3.2 Research on equalization for HSDPA

The air-interface of the 3G UMTS standard is based on the principles of CDMA. However, the uniqueness of the problems associated with HSDPA is due mostly to the low spread factor (SF=16) for the codes associated with the high-speed downlink shared data channel. While the classical RAKE receivers perform well in voice bearing channels which have a higher spread factor (typically 128 to 256), and perform reasonably well in low delay spread channels, these receivers fail miserably when the channel delay spread is large. In fact, the error floor introduced by the RAKE receivers is such that even powerful FECs such as turbo-codes used in HSDPA fail to provide adequate error correction. This lead to the use of the chip-level equalizer based max-SINR receivers [17] as a standard receiver for

HSDPA. Needless to say this provided a tremendous fillip to research on chip-equalizers. [18] provides an excellent overview of the huge body of research associated with chip-level equalizers and its adaptive variants for the WCDMA downlink. Link/system level performance results were reported (among other places) in [19]. Optimal linear receivers for HSDPA are symbol level (deterministic) time-varying multiuser receivers that are known to be prohibitively complex. One class of such receivers is based on symbol-level multiuser detection (MUD) where linear or non-linear transformations can be applied to the output of the channel matched filter (RAKE). Linear methods in this category are decorrelating and MMSE MUD both requiring inverses of large time-varying code cross-correlation matrices across symbols thus leading to impractical computational complexities. Non-linear MUD methods focus on estimating, reconstructing and subtracting signals of interfering codes and in general called interference canceling (IC) receivers. A less complex alternative is *dimensionality reducing* linear chip equalization followed by further linear or nonlinear interference canceling or joint detection stages to improve symbol estimates [20]. The spatial separation effected by LMMSE chip equalizer in this context is not perfect and therefore mandates additional processing that can be performed at chip or symbol level. This type of processing can be intuitively treated as a dimensionality reduction stage in MUD. It may take for example, the form of a general chip-level filter carrying out functions of channel *sparsifier* or indeed a more specific spatio-temporal $\rightarrow$ spatial channel-shortener (e.g., $2N \times 2$ to 2×2 in MIMO HSDPA) [21] [22]. This stage precedes either per-code joint detection of data streams at symbol level [23] or can be followed-up by one of the several possible decision-feedback approaches [21] and [24]. Symbol level, time-varying equalization for HSDPA was studied recently in [**?**] by the same authors who first looked at issues pertaining to combined chip-level and symbol level processing earlier in [25] though this was limited to SISO HSDPA. MIMO equalization in literature has largely been discussed in the context of frequency non-selective (OFDM) case, where optimal joint-stream maximum a-posteriori (MAP) detection can be employed. Spatio-temporal receivers based on ordered successive interference cancellation (OSIC) in frequency-selective environments were considered in [26] while [27] proposed a class of maximum likelihood (ML) receivers for multipath channels. For MIMO WCDMA transmission in frequency selective channels, where the multipath mixes signals up in space and time, proposals for receiver solutions include chip-level equalization and despreading followed by joint detection of the data streams at symbol level [23] [21].

Chapter 4

Equalization for SISO HSDPA

In this chapter, we study the HSDPA downlink receivers based on linear Minimum Mean-Square Error (LMMSE) chip-equalizer front-end followed by a Walsh code correlator for Single-Input-Single -Output (SISO) channels with the purpose of highlighting the non-trivial question of bias at the output of the equalizer. In a linear time-invariant channel this bias is constant at chip-equalizer output, but evolves over time at code correlator output impacting Signal-to-Interference-plus-Noise Ratio (SINR) and thus achievable rates in such receivers. In principle, this bias must be taken into account in further receiver/decoding stages. These results will be extended to the Multi-Input-Multi-Output (MIMO) case of UMTS HSDPA in the following chapter.

A typical receiver structure for HSDPA (and also for its MIMO extension) is the classical LMMSE chip-level equalizer followed by a per-Walsh code correlator. This receiver is one of the commonly accepted SISO/SIMO/MIMO receiver structures (see e.g., [23] and references therein). A Successive Decoding/Interference Canceling (SIC) receiver based on this LMMSE feedforward filter was shown to be mutual-information maximizing in [21] when operating at the chip-level (feeding back chip-sequence decisions). The authors of [21] translate chip-level SINR and symbol-level SINR through the spreading gain ($\mathcal{G}$). Such an approach assumes treatment of scrambler as a random (white) sequence, and under this assumption, asymptotic analysis of the equalizer-correlator cascade (in number of codes and spreading

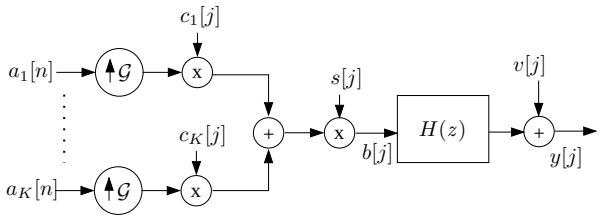

Figure 4.1: SISO FIR downlink signal model.

factor as the ratio remains constant) indeed leads to the well-known SINR expressions [17].

Here we expose a different point of view which ensues from a deterministic treatment of the scrambler and in which the desired signal contribution at the correlator output is not only concentrated in one tap of the channel-equalizer cascade but also contains a scrambler dependent time-varying component (thus not only a mean but also a variance). We describe the relationship linking LMMSE chip-equalizer output bias and correlator output (time-varying) bias. We subsequently derive the somewhat complicated analytical expression for the bias term and evaluate SINR including explicit contribution of this quantity.

4.1 Signal Model

Fig. 4.1 shows a Finite-Impulse Response (FIR) SISO model of the CDMA downlink signal at the receiver. The received signal vector (chip-rate) at the receiver can be modeled as

$$y[j] = H(z)b[j] + v[j].. \tag{4.1}$$

In doing so, we use here the q operator, where q represents a unit sample delay operation, $q^{-l}b[j] = b[j-l]$. Thus the q operator represents the convolution equation and therefore the input output relationship of the channel in a compact fashion as:

$$y[j] = H(q)b[j] + v[j],$$

where

$$H(q) = \sum_{l=0}^{\lceil L/\mathcal{G} \rceil - 1} H(l)q^{-l}.$$

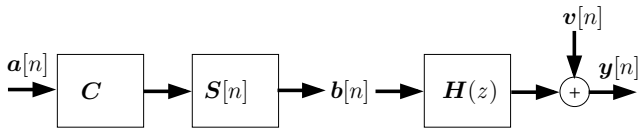

Figure 4.2: Simplified TX signal model.

The z-transform of the channel is obtained by replacing q by z. The received signal vector at the receiver is thus given by

$$y[j] = H(z)b[j] + v[j]. \tag{4.2}$$

In this model, j is the chip index, L is the length of the channel impulse response (in chips) and $v[j]$ represents the vector of noise samples that are zero-mean circular Gaussian random variables. The sequence $b[j]$ introduced into the channel is expressed as

$$b[j] = \sum_{k=1}^{K} s[j]c_k[j \mod \mathcal{G}]a_k[n] \tag{4.3}$$

where k is the code index, n is the index of the symbol, $a_k[n]$ represents the symbol on k^{th} code with $n = \left\lfloor \frac{j}{\mathcal{G}} \right\rfloor$, $\mathcal{G}$ is the spreading factor ($\mathcal{G} = 16$), c_k is a unit-norm spreading code, and $s[j]$ the scrambling sequence element at chip time j, which is zero-mean *i.i.d.* with elements from $\frac{1}{\sqrt{2}}\{\pm 1 \pm j\}$. The chip rate is $1/T_c$.

4.2 MMSE CE and bias

Fig. 4.2 represents a simplified vector signal model of the transmit signal. In this model, we allow a chip-oversampling factor of p. That is, at the receiver, each chip may be oversampled by a factor of p. In Fig. 4.2, $\boldsymbol{b}[n]$ is the $\mathcal{G} \times 1$ chip vector defined as $\boldsymbol{b}[n] = [b_0^T[n] \cdots b_{\mathcal{G}-1}^T[n]]^T$, where $b_m[n]$ is the m^{th} multi-code (K codes) chip corresponding to the n^{th} symbol vector, $\boldsymbol{a}[n]$ of size $K \times 1$ and is given by $\boldsymbol{a}[n] = [a_1^T[n] \cdots a_K^T[n]]^T$. $\boldsymbol{C}$ represents the $\mathcal{G} \times \mathcal{G}$ spreading matrix $\boldsymbol{C} = [\boldsymbol{c}_1 \ \ldots \ \boldsymbol{c}_K]$ with $\boldsymbol{c}_k = [c_k[0] \ \ldots \ c_k[\mathcal{G}-1]]^T$ being the kth user's unit-norm spreading code: $\boldsymbol{c}_j^T \cdot \boldsymbol{c}_k = \delta_{jk}$. The diagonal matrix $\boldsymbol{S}[n]$ of the same dimension represents multiplication of the scrambling sequence for the n^{th} symbol instant. Assuming the aforementioned oversampling factor of p, the symbol level channel $\boldsymbol{H}(z) = \sum_m z^{-m}\boldsymbol{H}[m]$ consists of $p\mathcal{G} \times \mathcal{G}$ matrix taps. Given that the delay spread is L chips, there

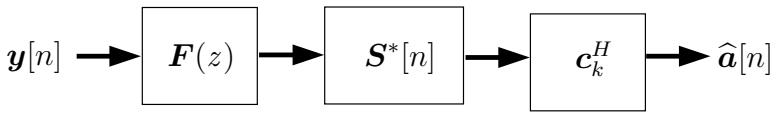

Figure 4.3: SISO RX model.

are $\lceil L/\mathcal{G} \rceil$ *pseudo-circulant* matrices that fully represent the channel. These matrices are defined as

$$\boldsymbol{H}[m] = \begin{bmatrix} \boldsymbol{h}[m\mathcal{G}] & \boldsymbol{h}[m\mathcal{G}+1] & \dots & \boldsymbol{h}[(m+1)\mathcal{G}-1] \\ \boldsymbol{h}[m\mathcal{G}-1] & & & \vdots \\ \vdots & & \ddots & \\ \boldsymbol{h}[(m-1)\mathcal{G}+1] & \dots & \dots & \boldsymbol{h}[m\mathcal{G}] \end{bmatrix}$$

with $\boldsymbol{h}[.]$ being the $p \times 1$ vector of the oversampled channel coefficients. The corresponding vectorized model of the receiver is shown in Fig. 4.3. The LMMSE equalizer $\boldsymbol{F}(z)$ in Fig. 4.3 can be represented in a similar fashion and visualized to be composed of $\boldsymbol{f}[.]$ which would be the $1 \times p$ equalizer coefficients defined at the chip-level. The channel equalizer cascade is then given by

$$\begin{aligned} \boldsymbol{G}(z) &= \boldsymbol{F}(z)\boldsymbol{H}(z), \\ &= \sum_{\kappa=0}^{N-1} \boldsymbol{F}[\kappa] z^{-\kappa} \sum_{m=0}^{M-1} \boldsymbol{H}[m] z^{-m}, \\ &= \sum_{\nu=0}^{N+M-2} \boldsymbol{G}[\nu] z^{-\nu}, \end{aligned} \tag{4.4}$$

where, assuming the chip-equalizer length to be E chips, we have $M = \lceil L/\mathcal{G} \rceil$ and $N = \lceil E/\mathcal{G} \rceil$. The channel-equalizer cascade at symbol level can therefore be defined similarly to be composed of chip-level matrix-coefficients $g[k] = \sum_{l=0}^{L-1} \boldsymbol{f}[k-l]\boldsymbol{h}[l]$. Let the equalizer delay be d. Define

the corresponding channel-equalizer cascade matrix at d as

$$G[0] = \boldsymbol{F}(z)\boldsymbol{H}(z)|_{[0]} = \begin{bmatrix} g[d+0] & g[d+1] & \dots & g[d+\mathcal{G}-1] \\ g[d-1] & & & \vdots \\ \vdots & & \ddots & \\ g[d-\mathcal{G}+1] & \dots & \dots & g[d+0] \end{bmatrix} \tag{4.5}$$

Henceforth, we consider $G[0]$ as the $\mathcal{G} \times \mathcal{G}$ zeroth matrix-tap of the channel-equalizer cascade. Risking a slight abuse of notation we also use $g[0]$ to mean $g[d]$ in the interest of notational consistency and $\boldsymbol{g}[0] = [g[d - \mathcal{G}/2 + 1, \dots, g[d], \dots, g[d + \mathcal{G}/2]]$. We use the notation $\overline{\boldsymbol{g}}[0]$ to represent the vector $\boldsymbol{g}$ with $g[d] = 0$. $\overline{G}(z) = \sum_{m \neq 0} z^{-m} G[m]$ thus represents the inter-symbol interference (ISI). We can now write

$$\widehat{a}_k[n] = \boldsymbol{c}_k^H \boldsymbol{S}^*[n] \left\{ G(z)\boldsymbol{S}[n]\boldsymbol{C}\boldsymbol{a}[n] + \boldsymbol{F}(z)\boldsymbol{v}[n] \right\}.$$

Defining

$$G_{n,k}(z) = \boldsymbol{c}_k^H \boldsymbol{S}^*[n] G(z) \boldsymbol{S}[n] \boldsymbol{C}$$

as the symbol-rate channel at time instant n (also a $\overline{G}_{n,k}(z)$ corresponding to $\overline{G}(z)$) , we can write the correlator output as

$$z_k[n] = \overbrace{G_{n,k}[0]a_k[n]}^{kth\ code} + \overbrace{G'_{n,k}[0]\overline{a}[n]}^{other\ codes} + \underbrace{\sum_m G_{n,k}[m]a[n+m]}_{all\ codes\ other\ symbols} + \underbrace{\boldsymbol{F}(z)\boldsymbol{v}[n]}_{noise}. \tag{4.6}$$

In this expression, $G_{n,k}[0]$ is the desired user channel at symbol-time n (time-varying channel), which one can split into a time invariant part $\mathbb{E}_n[G_{n,k}[0]] = G[0] = g[0] \cdot I_{\mathcal{G}}$ (assuming the scrambler to be white), and a time-varying part (if scrambler is treated as deterministic). Treating the scrambler as white has the effect of capturing the mean signal energy (corresponding to the $g[0]$ contribution) at the output of the per code channel while consigning the variance (off-diagonal part in $G[0]$) definitively and irrecoverably to the interference term. Taking expectation over the scrambler, we can express the output energy of the receiver as

$$\mathcal{R}_{zz} = \mathcal{R}_{des} + \underbrace{\mathcal{R}_{MUI} + \sum_m \mathcal{R}_{m,ISI} + \boldsymbol{f}\mathcal{R}_{vv}\boldsymbol{f}^H}_{\mathcal{R}_{\tilde{z}\tilde{z}}} \tag{4.7}$$

where,

$$\mathcal{R}_{des} = \sigma_{a_k}^2 \left(|g[0]|^2 + \frac{1}{\mathcal{G}^2} \operatorname{tr}\left(\overline{G}[0]\overline{G}^H[0] \right) \right)$$
$$\mathcal{R}_{\widetilde{z}\widetilde{z}} = \sigma_{a_k}^2 \left(\frac{1}{\mathcal{G}} \|\overline{\boldsymbol{g}}[0]\|^2 - \frac{1}{\mathcal{G}^2} \operatorname{tr}\left(\overline{G}[0]\overline{G}^H[0] \right) \right) + \frac{1}{\mathcal{G}} \overline{\sigma}_{tot}^2 \|\overline{\boldsymbol{g}}[0]\|^2 + \sigma_v^2 \|\boldsymbol{f}\|^2$$

where $\overline{\sigma}_{tot}^2 = \sum_{m \neq k} \sigma_m^2$ and σ_m^2 corresponds to the power allocated to the m-th code. From the above equations, it can be seen that while treating the scrambler as deterministic, the desired signal contributions at the output of the LMMSE chip equalizer and correlator cannot simply be related through $\mathcal{G}$ (see e.g., [21]). Furthermore in (4.7), the first term is the mean value of the desired signal energy, while the second (set of terms) is the variance. The SINR at the chip level is

$$\mathsf{SINR}_{chip-eq} = \frac{\sigma_k^2 |g[0]|^2}{\sigma_{tot}^2 \|\overline{\boldsymbol{g}}[0]\|^2 + \boldsymbol{f}\mathcal{R}_{vv}\boldsymbol{f}^H},$$

and by treating the scrambler as random, only this mean value is captured and the symbol-level SINR appears to be simply the scaled version of the chip-level SINR. In treating the scrambler to be deterministic[1], the expression for the time-varying symbol level SINR becomes

$$\mathsf{SINR}_{symb} = \frac{\sigma_{a_k}^2 \left(|g[0]|^2 + \frac{1}{\mathcal{G}^2} \operatorname{tr}\left(\overline{G}[0]\overline{G}^H[0] \right) \right)}{\sigma_{a_k}^2 \left(\frac{1}{\mathcal{G}} \|\overline{\boldsymbol{g}}[0]\|^2 - \frac{1}{\mathcal{G}^2} \operatorname{tr}\left(\overline{G}[0]\overline{G}^H[0] \right) \right) + \frac{1}{\mathcal{G}} \overline{\sigma}_{tot}^2 \|\overline{\boldsymbol{g}}[0]\|^2 + \sigma_v^2 \|\boldsymbol{f}\|^2}.$$

4.3 Chip sparsification and symbol equalization in SISO HSDPA

In this section we take the approach of optimally combining chip-level and symbol-level processing and investigate receivers based on channel sparsification. The chip-level channel is conditioned using a pre-equalizer in order to tradeoff achievable gains at the symbol level equalizer with the associated complexity. The idea itself is not new and dates as far back as early 70's [28] [29] [30] where combined equalization and maximum-likelihood sequence estimation (MLSE) was considered in order to achieve higher data-rates. More recently, Al-Dhahir et.al [31] proposed a unified approach for design of finite length *channel shortening* MMSE equalizers as

[1] only at the target tap d

pre-filters for reduced-order MLSE. In all these contributions, the design goal was to find optimal pre-equalizers that *shorten* the channel impulse response (CIR) to a desired target impulse response (TIR) of specified length. The pre-filters are based on different optimization and design constraints. For instance [28] minimizes the error variance at the output of the pre-filter subject to energy constraints on the TIR, [29] attempts the same while imposing a monocity constraint on the TIR and [30] proposes to render the error white so as to obtain optimal performance for the ML stage. On the other hand, we do not interest ourselves in shortening the CIR, instead we impose a structured sparsity criterion on the resultant sparse impulse response (SIR). We focus on a class of HSDPA receivers based on *channel sparsifying* linear pre-processing, and introduce a time-varying model of the resulting reduced-dimensional (symbol-rate) temporal channel. The sparsification is controlled by an appropriate design criterion for the chip-level channel sparsifier and the time-variant model is a consequence of treating the scrambler as deterministic. The cascade, as for the case of classical chip-equalizer front-end, results in a reduced-parameter problem the dimensionality of which can be controlled through sparsifier design. While the classical MMSE chip-equalizer is highly effective in mitigating the effects of temporal dispersion of the channel and restoring orthogonality of codes, it works on the principle of optimally combining the channel power in a single tap corresponding to the target equalizer delay thereby excluding the possibility of any "Viterbi-like" post processing at later stages. We show here that improved receivers for HSDPA downlink can be designed benefiting from a combination of generalized (and controlled) channel sparsification, deterministic treatment of scrambler and reduced-parameter nonlinear detection.

Consider estimation of the symbol sequence, $a_k[n]$, of the k^{th} code in Fig. 4.2. If the delay spread is L chips, and the sparsifier length in chips is E, assuming an oversampling factor of p, the time domain channel at the chip level can be represented by the block-Toeplitz (FIR) channel convolution matrix $\mathcal{T}(\boldsymbol{H})$ which is a $pE \times L + E - 1$ with $[\boldsymbol{h}[L-1] \dots \boldsymbol{h}[0] \ \mathbf{0}_{p\times E}]$ as its first block row. The channel-sparsifier cascade results in a equivalent sparse impulse response that we denote by $\boldsymbol{g}$. By design, $\boldsymbol{g}$ has dominant tap gains at chip offsets $d + \nu\mathcal{G}$ where $\nu \in \{0, 1, \dots N_f - 1\}$ and arbitrary non-zero values in all other taps. We can now define $\boldsymbol{G}_\nu$ the $\mathcal{G} \times \mathcal{G}$ matrix with $[g[d+\nu\mathcal{G}], g[d+\nu\mathcal{G}+1], \dots, g[d+(\nu+1)\mathcal{G}-1]$ as the first row and $[g[d+\nu\mathcal{G}], g[d+\nu\mathcal{G}-1], \dots, g[d+(\nu-1)\mathcal{G}+1]^T$ as the first column. The

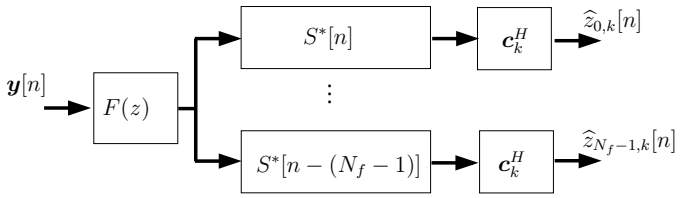

Figure 4.4: SISO receiver model.

matrices $\boldsymbol{G}_{\nu,s}$ and $\overline{\boldsymbol{G}}_\nu$ are defined as

$$\boldsymbol{G}_{\nu,s} = \boldsymbol{G}_\nu - \overline{\boldsymbol{G}}_\nu \tag{4.8}$$

where $\boldsymbol{G}_{\nu,s}$ is a diagonal matrix with $g[d+\nu\mathcal{G}]$ on the diagonal and $\overline{\boldsymbol{G}}_\nu$ is $\boldsymbol{G}_\nu$ with the diagonal set to zero. As shown in Fig. 4.4, the channel sparsifier output serves as input to the descrambler-correlator bank (after an appropriate delay not depicted in the figure in the interest of simplicity). The dependence of the output $\widehat{z}_{r,k}[n]$, $r \in \{0, 1, \ldots N_f - 1\}$ of each descrambler-correlator pair in the bank on the scrambler vector at n results in a time-varying symbol level channel. The expression for $\widehat{z}_{r,k}[n]$ can be derived as in (4.9) where we denote by $g[\nu]$ the tap-values of $\boldsymbol{g}$ at $d + \nu\mathcal{G}$.

$$\begin{aligned}
\widehat{z}_{r,k}[n] &= g[r]a_k[n-r] + \sum_{\nu\neq r} g[\nu]\boldsymbol{c}_k^H S_n^H S_{n-\nu}\boldsymbol{c}_k a_k[n-\nu] \\
&+ \sum_{j\neq k}\sum_{\nu\neq r} g[\nu]\boldsymbol{c}_k^H S_n^H S_{n-\nu}\boldsymbol{c}_j a_j[n-\nu] \\
&+ \sum_{j\in K} \boldsymbol{c}_k^H S_n^H \overline{\boldsymbol{G}}_r S_n \boldsymbol{c}_j a_k[n-r] \\
&+ \sum_{j\in K}\sum_{\nu\neq r} \boldsymbol{c}_k^H S_n^H \overline{\boldsymbol{G}}_\nu S_{n-\nu}\boldsymbol{c}_j a_j[n-\nu] + \boldsymbol{f}^H\boldsymbol{v}[n].
\end{aligned} \tag{4.9}$$

4.3.1 Generalized Channel Sparsification

As discussed earlier, the chip-level sparsifier conditions the channel to have an approximately sparse structure. We say that it is approximately sparse because the resultant channel has N_f dominant taps and all other taps have arbitrary small non-zero tap gains. While we do not constrain the position of first dominant tap, we do constrain the remaining taps to be regularly spaced $\mathcal{G}$ chips apart, where $\mathcal{G}$ denotes the downlink spread factor. Furthermore, the channel sparsifier should be a solution to an appropriately cho-

sen optimization criterion which in our case is the post-processing SINR. The channel sparsifying filter is thus chosen so as to maximize the SINR at the output of symbol-level equalizer. The optimum chip-level channel sparsifying filter is therefore a function of symbol level equalizer. Let $\widetilde{\boldsymbol{H}}$, be the matrix whose columns are formed by the $\mathcal{G}$-spaced N_f columns of $\mathcal{T}(\boldsymbol{H})$ and are the columns of the channel convolution matrix at precisely the chip-position offsets at which the resultant sparse impulse response will have dominant taps and let $\overline{\mathcal{T}}(\boldsymbol{H})$ denote the matrix formed by setting these columns to zero in $\mathcal{T}(\boldsymbol{H})$. For the specific case of $N_f = 2$, $\widetilde{\boldsymbol{H}}$ has 2 columns at equalizer/sparsifier delay d and $d + \mathcal{G}$ that we shall denote henceforth by $\boldsymbol{h}_0$ and $\boldsymbol{h}_1$. We also define the positive definite matrix $\boldsymbol{B}$ as

$$\boldsymbol{B} = \sigma_{tot}^2 \overline{\mathcal{T}}(\boldsymbol{H})\overline{\mathcal{T}}(\boldsymbol{H})^H + \boldsymbol{R}_{vv}. \tag{4.10}$$

Here σ_{tot}^2 corresponds to the total chip variance. These two matrices are of special significance to us. We shall see later that these matrices are the common link to all the different channel-sparsifier and symbol-equalizer pairs. In fact, the channel sparsifier for all three receivers lives in the column span of the product matrix $\boldsymbol{B}^{-1}\widetilde{\boldsymbol{H}}$. A fact that we shall exploit in computing the optimum channel sparsifier. The philosophy behind the proposed receiver structures can be summed up as follows. The channel is rendered sparse by chip-level processing so that this chip-level sparse channel can be exploited by reduced complexity non-linear equalization that operates at symbol level. It is the presence of the aperiodic scrambler that adds to the complexity of the receiver. This type of combined chip and symbol level equalization can provide gains only if the scrambler is treated as deterministic, otherwise, the random scrambler assumption will compel us to treat the time varying signal contribution as noise. For a specific symbol-level equalizer, the post-processing SINR is derived. In the sequel, we will see that this leads to an optimization problem with a quadratic constraint and a quadratic cost function and takes the general form

$$\max_{\boldsymbol{f}} \frac{\boldsymbol{f}^H \boldsymbol{A} \boldsymbol{f}}{\boldsymbol{f}^H \boldsymbol{R} \boldsymbol{f}} \text{ subject to } \boldsymbol{f}^H \boldsymbol{A} \boldsymbol{f} = \text{constant}, \tag{4.11}$$

The solution to this maximization problem is known to be the maximum generalized eigenvector of the matrix pair $(\boldsymbol{A}, \boldsymbol{R})$.

4.3.2 PIC + ML equalization post sparsification

For the rest of the receiver structures we consider deterministic treatment of the scrambler. In section 4.3.1 we introduced channel sparsification that

will remain the common pre-processing stage for all the following receiver structures though the criteria for channel sparsifier design might differ. At each of the descrambler-correlator pairs, $N_f - 1$ dominant taps are not aligned to the de-scrambler in question and hence experience inter-code interference. For ML equalization of the N_f-tap sparsified channel for the code of interest k, the inter-code interference (MUI) present on $N_f - 1$ mis-aligned taps can be canceled by an iterative MUI cancellation algorithm say, PIC. With such a processing stage preceding ML equalization, the ML processing will now be strictly on a per-code basis. Furthermore, we make the following assumptions at the output of the deterministic descrambler; the signal and interference terms are uncorrelated, the interference plus noise components are uncorrelated across $\widehat{z}_{0,k}[n]$ and $\widehat{z}_{1,k}[n]$, $g[1]\boldsymbol{c}_k^H S_n^H S_{n-1} c_k a_k[n-1]$ and $g[0]\boldsymbol{c}_k^H S_{n-1}^H S_n c_k a_k[n]$ are independent for all pairs of n and $n-1$ and the interference plus noise components are themselves uncorrelated across symbol durations. If we then define a matrix $\boldsymbol{A}$ as

$$\boldsymbol{A} = \sigma_k^2 \left(1 + \frac{1}{\mathcal{G}}\right) \widetilde{\boldsymbol{H}} \widetilde{\boldsymbol{H}}^H, \tag{4.12}$$

with σ_k^2 being the power allocated to the k-th code and $\boldsymbol{B}$ as in (4.10) the per-code SINR is given by

$$\mathsf{SINR}_k = \frac{\boldsymbol{f}^H \boldsymbol{A} \boldsymbol{f}}{\boldsymbol{f}^H \boldsymbol{B} \boldsymbol{f}}, \tag{4.13}$$

Clearly, the filter $\boldsymbol{f}$ that maximizes (4.13) is the eigenvector corresponding to the maximum generalized eigenvalue $\lambda_{max}(\boldsymbol{A}, \boldsymbol{B})$.

Indeed, if the inverse of $\boldsymbol{B}$ exists, $\boldsymbol{f}$ is also an eigenvector of $\boldsymbol{B}^{-1}\boldsymbol{A}$. In general, due to the particular structure of $\boldsymbol{A}$, the filter $\boldsymbol{f}$ is of the form

$$\boldsymbol{f} = \alpha \boldsymbol{B}^{-1} \boldsymbol{h}_0 + \beta \boldsymbol{B}^{-1} \boldsymbol{h}_1, \tag{4.14}$$

That $\boldsymbol{f}$ should completely live in the space spanned by $\boldsymbol{h}_0$ and $\boldsymbol{h}_1$ is not surprising, since it is obvious from the expression for per-code SINR that, any other $\boldsymbol{f}$ will increase the value of the denominator in (4.13) thus reducing the SINR.

4.3.3 ML equalization post sparsification

Considering the computational complexity involved in an additional PIC stage in the receiver above, one is tempted to investigate the performance of

ML equalization of the sparse channel without inter-code interference cancellation. Without the PIC pre-processing, however, the channel sparsifier design has to account for inter-code interference on the $N_f - 1$ mis-aligned taps in the descrambler-correlator bank. With the same assumptions on correlation and independence of interference and noise terms as before, the SINR_k for code of interest k for the case of $N_f = 2$ is given by (4.15)

$$\mathsf{SINR}_k = \sigma_k^2 \sum_{i=0,1} \frac{\boldsymbol{f}^H \widetilde{H} \begin{bmatrix} \bar{i} + i/\mathcal{G} & 0 \\ 0 & i + \bar{i}/\mathcal{G} \end{bmatrix} \widetilde{H}^H \boldsymbol{f}}{\boldsymbol{f}^H \left\{ \boldsymbol{B} + \left(\sigma_{tot}^2 - \frac{\sigma_k^2}{\mathcal{G}} \right) \boldsymbol{h}_{\bar{i}} \boldsymbol{h}_{\bar{i}}^H \right\} \boldsymbol{f}} \tag{4.15}$$

We choose $N_f = 2$ here with the intention of simplifying the SINR expression. The extension to $N_f > 2$ is straightforward. The optimum filter $\boldsymbol{f}$ that maximizes (4.15) in this case can be computed based on a 2-D search. Recall that the optimum filter lives in $span\{\boldsymbol{h}_0, \boldsymbol{h}_1\}$ and can be decomposed as (4.14). We also note that SINR is insensitive to any scale factor of $\boldsymbol{f}$, this allows us to set α (or for that matter β) to 1. The problem of finding the optimum filter thus reduces to finding the optimum β which can be a complex co-efficient and whose phase also influences the SINR. We therefore carry out a 2-D search for the optimum β over an appropriate search grid and compute the optimum sparsifying filter using (4.14).

4.3.4 Post sparsification MRC

In this particular receiver we do away with ML processing, however, we retain the stage that cancels the inter-code interference. Let $N_f = 2$ then in (4.9) if code-k is our code of interest, we see that as a consequence of controlled ISI present in the sparse channel, scaled versions of the n^{th} symbol on code-k is present at $\widehat{z}_{0,k}$ at time n and at $\widehat{z}_{1,k}$ at time $n+1$. Since there inter-code interference has been canceled, if all other components of $\widehat{z}_{r,k}$ except the symbol of interest $a_k[n]$ are considered as noise, the matrix $\boldsymbol{A}$ in the optimization problem is given by

$$\boldsymbol{A} = \sigma_k^2 \widetilde{\boldsymbol{H}} \widetilde{\boldsymbol{H}}^H, \tag{4.16}$$

and $\boldsymbol{B}$ can be shown to be as in (4.17) and we arrive at the simplified SINR expression at the output of the maximum ratio combiner that is given by (4.18)

$$\boldsymbol{B} = \sigma_{tot}^2 \sum_{i=0}^{1} \frac{|\boldsymbol{f}^H \boldsymbol{h}_i|^2}{|\boldsymbol{f}^H \boldsymbol{h}_0|^2 + |\boldsymbol{f}^H \boldsymbol{h}_1|^2} \overline{\mathcal{T}}_i(\boldsymbol{H}) \overline{\mathcal{T}}_i^H(\boldsymbol{H}) + \boldsymbol{R}_{vv} \tag{4.17}$$

$$\mathsf{SINR}_k = \frac{\sigma_k^2 \left(\boldsymbol{f}^H \widetilde{\boldsymbol{H}} \widetilde{\boldsymbol{H}}^H \boldsymbol{f} \right)^2}{\sum_{i=0}^{1} |\boldsymbol{f}^H \boldsymbol{h}_i|^2 \boldsymbol{f}^H \left(\sigma_{tot}^2 \overline{\mathcal{T}}_i(\boldsymbol{H}) \overline{\mathcal{T}}_i^H(\boldsymbol{H}) + \boldsymbol{R}_{vv} \right) \boldsymbol{f}} \tag{4.18}$$

Where $\overline{\mathcal{T}}_i(\boldsymbol{H})$ is defined as the channel convolution matrix $\mathcal{T}(\boldsymbol{H})$ with the $d+iL$ column set to zero. Since the SINR is itself a function of channel sparsifier, the optimum channel sparsifying filter is computed in an iterative fashion. The iteration is initialized by using $\boldsymbol{f}$ that maximizes (4.13) to compute $\boldsymbol{B}$. The optimum filter $\boldsymbol{f}_{opt}$ is then computed by alternatively plugging in the maximum generalized eigenvector of the matrix pair $(\boldsymbol{A}, \boldsymbol{B})$ and recomputing the matrix $\boldsymbol{B}$ until convergence.

4.4 Simulation results

We show here simulation results and compare the performance of the different receiver structures. In the first instance, for a fixed value of SNR and over several realizations of a frequency selective FIR channel, we compute the SINRs at the output of the receivers and compare the distribution of SINRs for various receivers. The channel coefficients are complex valued zero-mean Gaussian of length 16 chips. The length of the channel sparsifying filter is the same as that of chip-equalizer. The per-user SINR is used as a performance measure for all receivers. We refer to the classical MMSE-CE/Correlator receiver as RX-1, the receiver that performs PIC+MLE after sparsification as RX-2, RX-3 refers to the receiver that performs MLE after sparsification and finally we refer to the equalizer that performs simple MRC post sparsification as RX-4. In Fig. 4.5 we plot the SINR for receivers 1, 2 and 3. The SINR at the output of chip-equalizer correlator receiver is computed by treating the scrambler as random and compared with the distribution of SINR at the output of the other two receivers where the scrambler is treated as deterministic. In reality, deterministic treatment will imply that the channel is time-varying at the symbol level, nevertheless, we use the averaged value of the time-varying channel gain to plot the SINR. We see here that receiver-2 performs significantly better than the classical chip-equalizer correlator receiver. The complexity of the receiver-3 is significantly reduced due to the absence of inter-code interference canceling stage that is assumed present in receiver-2 but receiver-3 still outperforms receiver-1.

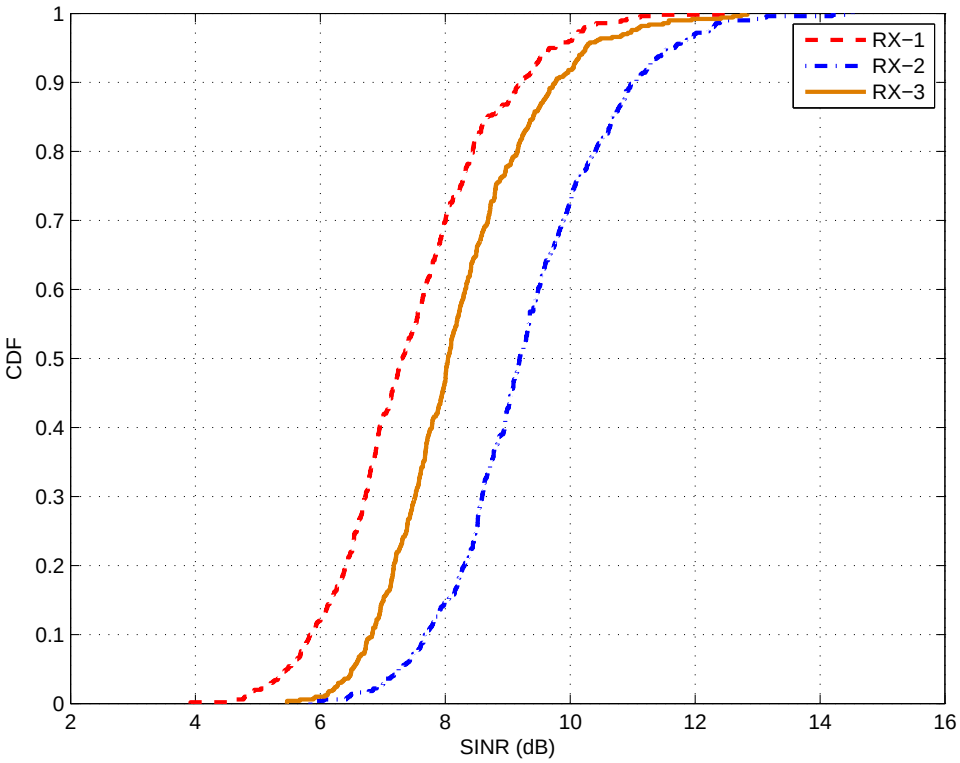

Figure 4.5: SINR comparison of RX 1, RX 2 and RX 3.

In Fig. 4.6 we compare the performance of the MRC receiver with our reference receiver. Here too we find that a receiver that first renders the channel sparse and treats the scrambler as deterministic outperforms the reference receiver. Finally in Fig. 4.7 we compare the performance of all receivers in terms of their average SINRs for various SNR values.

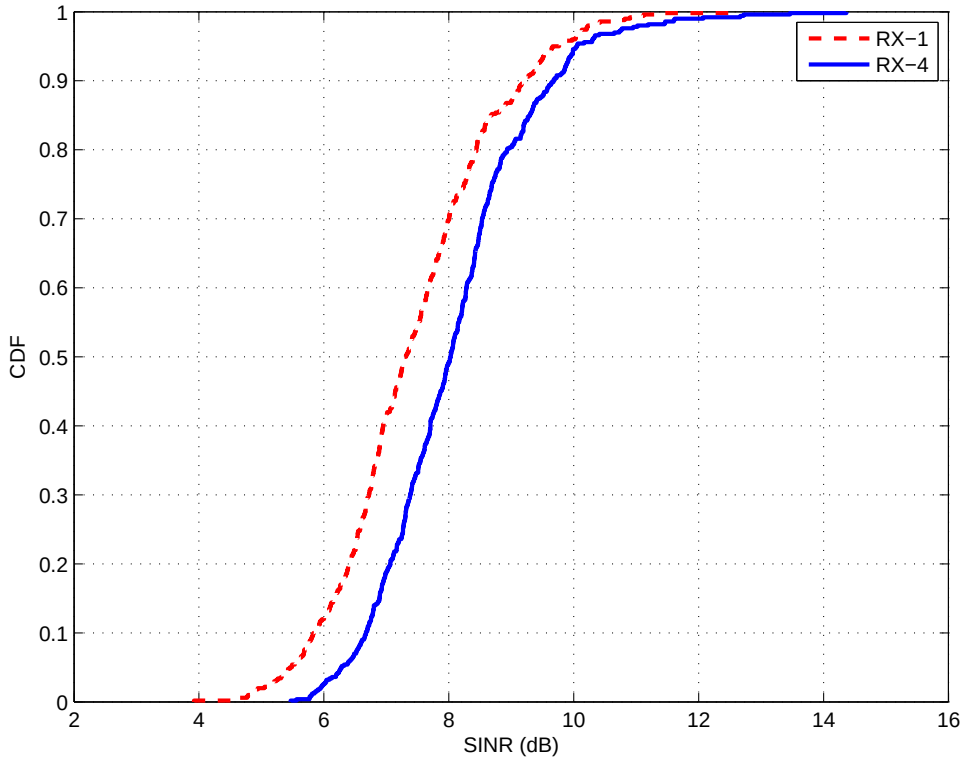

Figure 4.6: SINR comparison of RX 1 and RX 4.

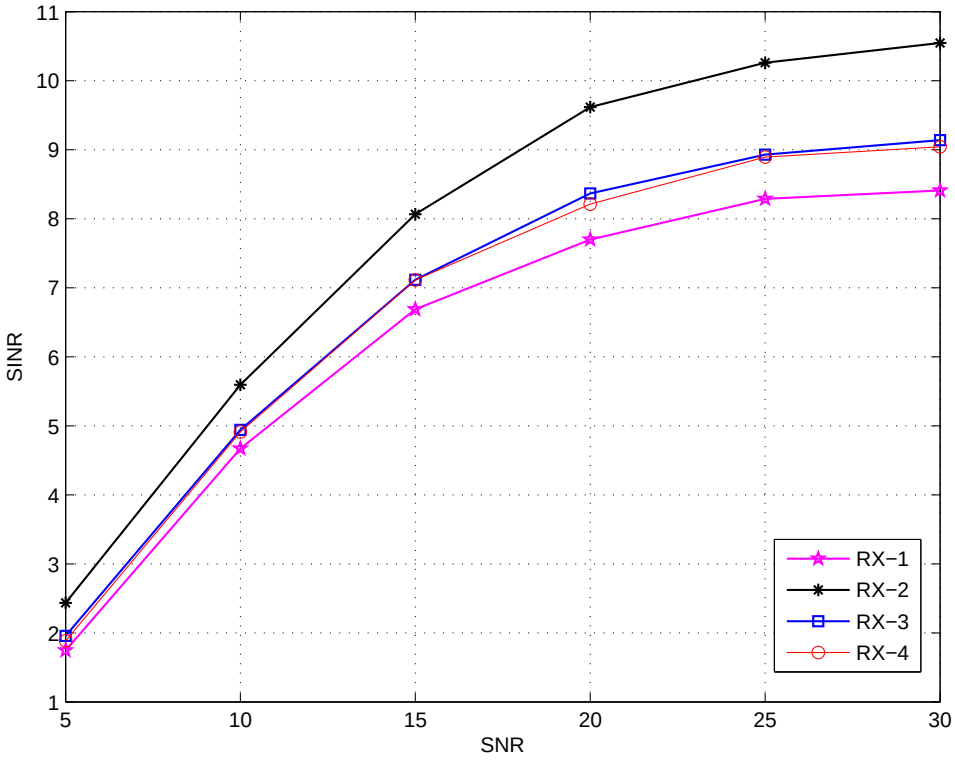

Figure 4.7: SNR vs. average SINR comparison of all receivers.

Chapter 5

Equalization for MIMO HSDPA

5.1 Introduction

In this chapter we shift our attention to the MIMO HSDPA downlink. We propose and analyze the performance of a variety of receiver designs for unitary precoded D-TxAA MIMO in HSDPA. The receiver structures we propose here are based on combining chip-level and symbol level processing for enhanced performance. For each of these receivers we also derive the per-stream Signal-to-Interference-plus-Noise Ratio (SINR) expressions. We will use the SINR to compute the sum-capacity which can be interpreted as upper bound for achievable rates. This will form the basis for comparing the performance of the proposed receivers. The precoding matrix in D-TxAA will influence the achievable sum-rate of the MIMO channel through its influence on the (SINR) of streams at the receiver (RX) output. Therefore, for D-TxAA with unitary precoding, there exists an optimal choice of the precoding matrix that would maximize the sum rate across the two streams. We will show that precoding choice and the extent of its impact depends on the MIMO receiver.

For the spatial multiplexing case in MIMO HSDPA, Fig. 5.1 illustrates the equivalent baseband downlink signal model. In this model, j is the chip index, $\mathbf{H}(z)$ is the frequency selective MIMO channel the output of which

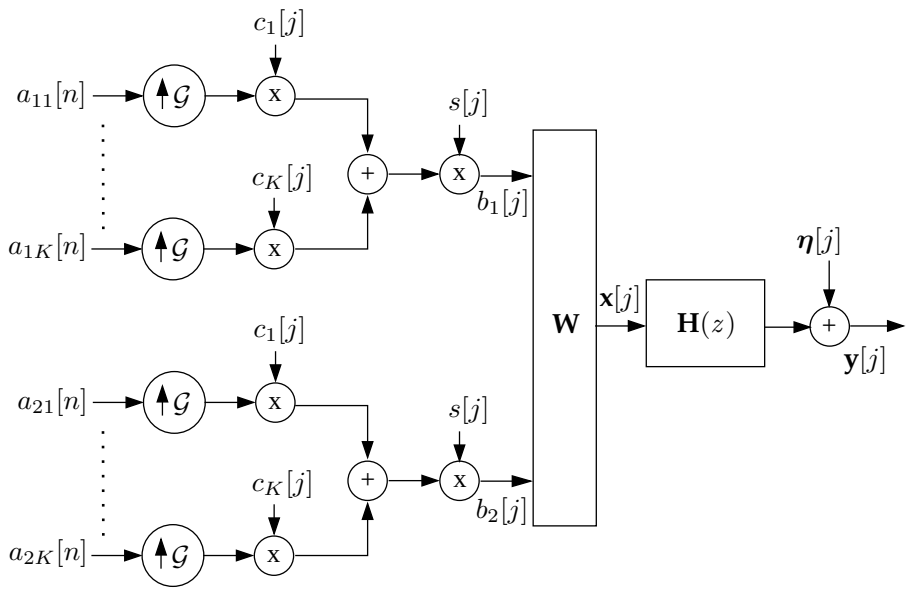

Figure 5.1: MIMO signal model with precoding.

is sampled p times per chip and $\boldsymbol{\eta}[j]$ represents the vector of noise samples that are zero-mean circular Gaussian random variables. The sequence $\mathbf{x}[j]$ introduced into the channel is itself a linear combination (D-TxAA see [13]) of the two steams and is expressed as

$$\mathbf{x}[j] = \underbrace{\mathbf{W}}_{2\times 2}\mathbf{b}[j] = \mathbf{W}\cdot\sum_{k=1}^{K}\underbrace{s[j]c_k[j \mod \mathcal{G}]\mathbf{a}_k[n]}_{\mathbf{b}_k[j]} \tag{5.1}$$

k is the code index, $n = \left\lfloor \frac{j}{\mathcal{G}} \right\rfloor$ is the symbol index, $\mathcal{G}$ is the spreading factor ($\mathcal{G} = 16$ for HSDPA), $\mathbf{W} = [\mathbf{w}_1\, \mathbf{w}_2]$ is the 2×2 precoding matrix with $\mathbf{w}_1 = [\frac{1}{\sqrt{2}}\ w]^T$ and $\mathbf{w}_2 = [\frac{1}{\sqrt{2}}\ -w]^T$. The symbol vector $\mathbf{a}_k[n] = [a_{1k}[n]\ a_{2k}[n]]^T$ represents two independent symbol streams, the unit-norm spreading codes are common to the two streams, and so is the scrambling sequence.

5.2 MMSE CE and optimal precoding

The classical MMSE chip equalizer-correlator receiver is an SINR maximizing chip equalizer followed by code correlation and soft symbol estimate

generation at the output of the correlator.

Consider LMMSE FIR estimation of the 2×1 chip sequence. In the spatial multiplexing context, the LMMSE equalization tries not only to suppress all Inter-Chip Interference (IChI) but also all Inter-Stream Interference (IStI). In Fig. 5.1, $\mathbf{b}[j]$ is the input chip vector defined as $\mathbf{b}[j] = [b_1[j]\ b_2[j]]^T$, where $b_i[j]$ is the jth chip of the ith input stream. Each chip stream is the sum of K spread and scrambled CDMA sub-streams. Thus $b_i[j] = \sum_{k=1}^{K} b_{ik}[j]$. The 2×2 matrix $\mathbf{H}[j]$ is the jth MIMO tap of the FIR channel and $\mathbf{W}$ is the precoding matrix. Denoting by L, the maximum delay spread of the frequency-selective channel (in chips) and assuming an arbitrary oversampling factor p at the receiver, the $2p \times 1$ received signal at the jth time instant is given as

$$\mathbf{y}[j] = \sum_{l=0}^{L-1} \mathbf{H}[l]\mathbf{W}\mathbf{b}[j-l] + \boldsymbol{\eta}[j] = \mathbf{H}\mathcal{W}_L\mathbf{b}_L[j] + \boldsymbol{\eta}[j], \tag{5.2}$$

where $\mathbf{H} = [\mathbf{H}_1\, \mathbf{H}_2]$, with $\mathbf{H}_i$ being the $2p \times L$ FIR channel from the ith transmit antenna to the 2 receive antennas. $\mathcal{W}_L = \mathbf{W} \otimes \mathbf{I}_L$ and $\mathbf{b}_L[j] = [\mathbf{b}_{1,L}^T[j]\, \mathbf{b}_{2,L}^T[j]]^T$ where $\mathbf{b}_{i,L}[j] = [b_i[j-L+1] \ldots\ b_i[j]]^T$ is chip sequence vector of the ith stream. Stacking E successive samples of the received signal $\mathbf{y}[j]$, we can express the received signal as

$$\mathbf{Y}[j] = \mathcal{T}_E(\mathbf{H})\mathcal{W}_{L+E-1}\mathbf{b}_{L+E-1}[j] + \boldsymbol{\Xi}[j], \tag{5.3}$$

where $\mathcal{T}_E(\mathbf{H}) = [\mathcal{T}_E(\mathbf{H}_1)\ \mathcal{T}_E(\mathbf{H}_2)]$ and $\mathcal{T}_E(\mathbf{H}_i)$ is a block Toeplitz matrix with $[\mathbf{H}_i\ \mathbf{0}_{2p\times E-1}]$ as the first block row. Let us assume a $2 \times 2pE$ LMMSE equalizer $\mathbf{F} = [\mathbf{f}_1^T\, \mathbf{f}_2^T]^T$. The output of the equalizer is a linear estimate of the chip sequence given by

$$\widehat{\mathbf{x}}[j] = \mathbf{F}\mathbf{Y}[j] = \mathbf{B}\underbrace{\mathbf{W}\mathbf{b}[j]}_{\mathbf{x}[j]} + \underbrace{\overline{\mathbf{B}}\mathcal{W}_{L+E-1}\overline{\mathbf{b}}_{L+E-1}[j] + \mathbf{F}\boldsymbol{\Xi}[j]}_{-\widetilde{\widetilde{\mathbf{x}}}[j]}, \tag{5.4}$$

Defining $\boldsymbol{\alpha}^{(ij)} = \mathbf{f}_i\mathcal{T}_E(\mathbf{H}_j)$, we have

$$\mathbf{B} = \begin{bmatrix} \alpha_d^{(11)} & \alpha_d^{(12)} \\ \alpha_d^{(21)} & \alpha_d^{(22)} \end{bmatrix} \text{ and } \overline{\mathbf{B}} = \begin{bmatrix} \overline{\boldsymbol{\alpha}}^{(11)} & \overline{\boldsymbol{\alpha}}^{(12)} \\ \overline{\boldsymbol{\alpha}}^{(21)} & \overline{\boldsymbol{\alpha}}^{(22)} \end{bmatrix},$$

respectively are the 2×2 matrix that represents the *joint bias* in the equalizer output, and the residual IChI. Bias arises in LMMSE receivers due to the tradeoff made between interference mitigation and noise enhancement

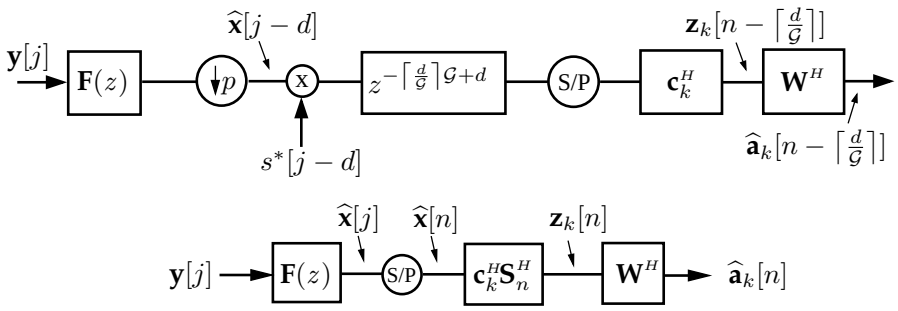

Figure 5.2: LMMSE equalizer and correlator.

by the MMSE design. The $\overline{\boldsymbol{\alpha}}^{(ij)}$ are the same as $\boldsymbol{\alpha}^{(ij)}$ with the $\alpha_d^{(ij)}$ term replaced by 0, and d is the equalization delay associated with $\mathbf{F}$.

We can thus write the equalizer output as the sum of an arbitrarily scaled desired term and an error term

$$\widehat{\mathbf{x}}[j] = \mathbf{B}\mathbf{x}[j] - \widetilde{\widetilde{\mathbf{x}}}[j]. \tag{5.5}$$

In (5.5), an estimate of the chip sequence $\mathbf{b}[j]$ can be obtained after a further stage of processing where the precoding is undone to separate streams. The latter represented by $\mathbf{W}^H$ is a linear operation and can be carried out before or after despreading (the latter case is shown in fig. 5.2 where the second figure is a simplified representation used as chip-equalizer /correlator front-end stage for other receiver structures). The joint-bias can also be interpreted as a spatial mixture at the chip-equalizer correlator output facilitating formulation of the spatial signal model to be treated henceforth. It must be pointed out that the spatial channel $\mathbf{B}$ is so definable assuming the scrambler to be a random sequence. The resulting spatial channel is percode, while still being the same for all codes. The error covariance matrix corresponding to the error term is denoted by $\boldsymbol{\mathcal{R}}_{\widetilde{\widetilde{x}}\widetilde{\widetilde{x}}}$ from which the MMSE can be obtained as below.

$$\boldsymbol{\mathcal{R}}_{\widetilde{\widetilde{x}}\widetilde{\widetilde{x}}} = \begin{bmatrix} r_{11} & r_{12} \\ r_{21} & r_{22} \end{bmatrix}, \tag{5.6}$$

$$\begin{aligned} r_{11} &= \sigma_b^2 \left(\|\overline{\boldsymbol{\alpha}}^{(11)}\|^2 + \|\overline{\boldsymbol{\alpha}}^{(12)}\|^2 \right) + \mathbf{f}_1 \boldsymbol{\mathcal{R}}_{\eta\eta} \mathbf{f}_1^H \\ r_{22} &= \sigma_b^2 \left(\|\overline{\boldsymbol{\alpha}}^{(21)}\|^2 + \|\overline{\boldsymbol{\alpha}}^{(22)}\|^2 \right) + \mathbf{f}_2 \boldsymbol{\mathcal{R}}_{\eta\eta} \mathbf{f}_2^H \\ r_{12} &= r_{21}^* = \sigma_b^2 \left(\overline{\boldsymbol{\alpha}}^{(11)} \cdot \overline{\boldsymbol{\alpha}}^{(21)H} + \overline{\boldsymbol{\alpha}}^{(12)} \cdot \overline{\boldsymbol{\alpha}}^{(22)H} \right) + \mathbf{f}_1 \boldsymbol{\mathcal{R}}_{\eta\eta} \mathbf{f}_2^H \end{aligned} \tag{5.7}$$

where σ_b^2 denotes the chip variance. After despreading (for the kth code) the 2×1 signal at the symbol level is written as

$$\mathbf{z}_k[n] = \mathbf{W}\mathbf{a}_k[n] - \widetilde{\mathbf{z}}_k[n] = \mathbf{B}\mathbf{W}\mathbf{a}_k[n] - \widetilde{\widetilde{\mathbf{z}}}_k[n], \tag{5.8}$$

In this receiver structure we assume $\mathbf{W}^H\mathbf{z}_k[n]$ to be the decision statistic. Considering scrambler as a random sequence and taking expectation over the scrambler as well as input data symbol sequence, one can show that the covariance matrix of the estimation error $\boldsymbol{\mathcal{R}}_{\widetilde{\widetilde{z}}\widetilde{\widetilde{z}}}$ is similar to the chip-equalizer output error covariance matrix $\boldsymbol{\mathcal{R}}_{\widetilde{\widetilde{x}}\widetilde{\widetilde{x}}}$ with scaling of the interference quantities by the number of users (codes). Let σ_a^2 denote the symbol power, then the elements of $\boldsymbol{\mathcal{R}}_{\widetilde{\widetilde{z}}\widetilde{\widetilde{z}}}$ are given by

$$\begin{aligned}
r_{11} = &\quad \sigma_a^2 \tfrac{K}{\mathcal{G}} \left(\|\overline{\boldsymbol{\alpha}}^{(11)}\|^2 + \|\overline{\boldsymbol{\alpha}}^{(12)}\|^2 \right) + \mathbf{f}_1 \boldsymbol{\mathcal{R}}_{\eta\eta} \mathbf{f}_1^H \\
r_{22} = &\quad \sigma_a^2 \tfrac{K}{\mathcal{G}} \left(\|\overline{\boldsymbol{\alpha}}^{(21)}\|^2 + \|\overline{\boldsymbol{\alpha}}^{(22)}\|^2 \right) + \mathbf{f}_2 \boldsymbol{\mathcal{R}}_{\eta\eta} \mathbf{f}_2^H \\
r_{12} = &\quad r_{21}^* = \sigma_a^2 \tfrac{K}{\mathcal{G}} \left(\overline{\boldsymbol{\alpha}}^{(11)} \cdot \overline{\boldsymbol{\alpha}}^{(21)H} + \overline{\boldsymbol{\alpha}}^{(12)} \cdot \overline{\boldsymbol{\alpha}}^{(22)H} \right) + \mathbf{f}_1 \boldsymbol{\mathcal{R}}_{\eta\eta} \mathbf{f}_2^H
\end{aligned}$$

The SINR for the ith stream at the output of the output of the LMMSE chip equalizer/correlator is therefore

$$\mathsf{SINR}_i = \frac{\sigma_a^2}{\left(\mathbf{W}^H \mathbf{B}^{-1} \boldsymbol{\mathcal{R}}_{\widetilde{\widetilde{z}}\widetilde{\widetilde{z}}} \mathbf{B}^{-H} \mathbf{W} \right)_{ii}} - 1, \tag{5.9}$$

Once MIMO joint bias is properly taken into account, the expression for the LMMSE chip equalizer output SINR is exact. We know however, from the analysis in the previous chapter that the situation is different at the symbol-level where the bias, in practice, varies over time.

The corresponding per-code capacity of the ith data stream can now be expressed as

$$\begin{aligned}
\boldsymbol{\mathcal{C}}_i &= \log(1 + \mathsf{SINR}_i) \\
\boldsymbol{\mathcal{C}}_i &= \log\left(\frac{\sigma_a^2}{MMSE_i} \right)
\end{aligned} \tag{5.10}$$

Our objective is to choose the precoding matrix $\mathbf{W}$ to maximize the sum-capacity of two streams. This boils down to the following optimization problem:

$$\mathbf{W}_{opt} = \arg\max_{\mathbf{W}} \left[\log\left(\frac{\sigma_a^4}{MMSE_1 \cdot MMSE_2} \right) \right], \tag{5.11}$$

The optimum precoding matrix can be seen to minimize the product of MMSEs of the streams. By exploiting the structure of the matrices in the unitary codebook specified in the HSDPA standard (3.1) [13], the optimum precoding matrix $\mathbf{W}_{opt}$ maximizes $\Re(|wr_{12}|)$, where r_{12} is the top-right off-diagonal term of the error covariance matrix $\boldsymbol{\mathcal{R}}_{\widetilde{z}\widetilde{z}}$. In other words, the $\mathbf{W}_{opt}$ *attempts to maximize the* SINR *difference between the two streams.*

We observe that the structure of the precoding matrices used in HSDPA is such that two out of the four possible precoding matrices give the same SINR (and thus sum-rate) for the LMMSE/correlator design. The difference between them being that one favors stream 1 by bestowing a higher SINR for stream 1, and the other matrix does just the reverse. This means that one can not only achieve the same sum-rate by choosing any of the two matrices, but one can also choose which stream among the two, contributes a larger fraction of the sum.

5.3 Chip-level and symbol-level equalization

In general, for MIMO, if the scrambler is treated as i.i.d. random, the resulting symbol-rate spatial channel can now be seen as a per-code spatial mixture and is constant. To this mixture simplified (per-code) processing can now be applied. In this section we investigate such class of MIMO HSDPA receivers. To be precise, the chip-level processing stage will always consist of the MIMO LMMSE chip-equalizer which will be followed by the correlator. We then consider various symbol level processing stages that can be employed at the receiver.

5.3.1 LMMSE chip equalizer- symbol level LMMSE

Consider a receiver structure where the output of the chip-equalizer is fed into a symbol level (spatial) LMMSE filter after the descrambler/correlator block. This is shown in Fig. 5.3. The output of the correlator is $\mathbf{z}_k[n]$ given by (5.8). $\mathcal{F}_{sp}$ denotes the spatial MMSE at the output of which we have a linear estimate of the symbol vector as

$$\widehat{\mathbf{a}}_k[n] = \mathbf{a}_k[n] - \widetilde{\mathbf{a}}_k[n]. \tag{5.12}$$

The error covariance matrix for the LMMSE estimate of $\mathbf{a}_k[n]$ is given by

$$\begin{aligned} \boldsymbol{\mathcal{R}}_{\widetilde{a}\widetilde{a}} &= \boldsymbol{\mathcal{R}}_{aa} - \boldsymbol{\mathcal{R}}_{az'}\boldsymbol{\mathcal{R}}^{-1}_{z'z'}\boldsymbol{\mathcal{R}}_{z'a} && (5.13)\\ &= \sigma_a^2\mathbf{I} - \sigma_a^4\mathbf{W}^H\left(\sigma_a^2\mathbf{I} + \mathbf{B}^{-1}\boldsymbol{\mathcal{R}}_{\widetilde{z}\widetilde{z}}\mathbf{B}^{-H}\right)^{-1}\mathbf{W}, && (5.14)\end{aligned}$$

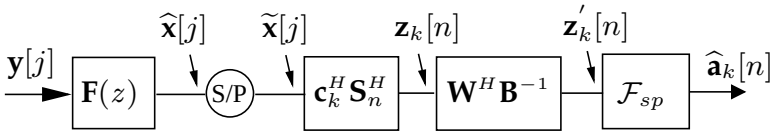

Figure 5.3: Chip LMMSE equalizer and correlator followed by symbol-level (spatial) MMSE.

Expressing the above relation in terms of the correlator output covariances, $\mathbf{B}\boldsymbol{\mathcal{R}}_{\widetilde{z}\widetilde{z}}\mathbf{B}^{-H}$ and using some algebra leads to the expression

$$\boldsymbol{\mathcal{R}}_{\widetilde{a}\widetilde{a}} = \sigma_a^2\mathbf{I} - \sigma_a^4\mathbf{W}^H\left(\sigma_a^2\mathbf{I} + \left(\boldsymbol{\mathcal{R}}_{\widetilde{z}\widetilde{z}}^{-1} - \boldsymbol{\mathcal{R}}_{zz}^{-1}\right)^{-1}\right)^{-1}\mathbf{W}, \tag{5.15}$$

$\boldsymbol{\mathcal{R}}_{\widetilde{z}\widetilde{z}}$ in the above expression is related to the joint-bias $\mathbf{B}$ through

$$\mathbf{B} = \mathbf{I} - \boldsymbol{\mathcal{R}}_{\widetilde{z}\widetilde{z}}\boldsymbol{\mathcal{R}}_{zz}^{-1}, \tag{5.16}$$

Like the LMMSE chip level equalizer/correlator receiver, this translates to a sum-capacity expression similar to the one derived in the previous section.

$$\mathcal{C}_1 + \mathcal{C}_2 = \log\left(\frac{\sigma_a^4}{\det(\mathrm{diag}(\boldsymbol{\mathcal{R}}_{\widetilde{a}\widetilde{a}}))}\right) \tag{5.17}$$

The throughput maximizing precoding matrix can therefore be shown to be the one with element w that maximizes

$$\Re\left(\left|w\left[\left(\sigma_a^2\mathbf{I} + \left(\boldsymbol{\mathcal{R}}_{\widetilde{z}\widetilde{z}}^{-1} - \boldsymbol{\mathcal{R}}_{zz}^{-1}\right)^{-1}\right)^{-1}\right]_{12}\right|\right)$$

We note here that the performance of this receiver is dependent on the strength of the temporal (inter-chip) interference at the correlator output.

5.3.2 LMMSE chip equalizer - predictive DFE

A noise-predictive decision feedback equalizer (DFE) [32] uses past noise estimates to predict the current noise sample. This is readily applied to our spatial-multiplexing problem where once one stream is detected, spatial correlation of noise can be exploited to improve estimation of the stream detected last (second in this case). With some abuse of terminology this can be a branded Successive Interference Cancellation (SIC).

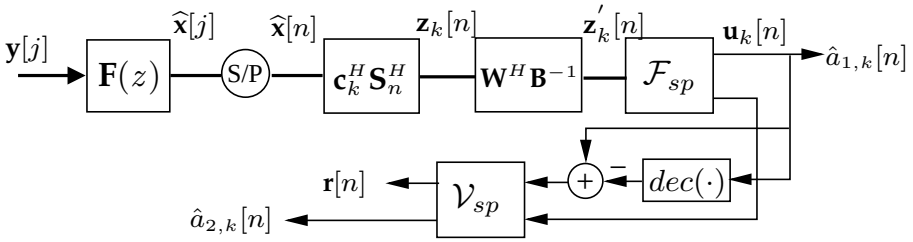

Figure 5.4: Chip LMMSE equalizer/correlator followed by spatial MMSE and symbol-level SIC for stream 2.

The SIC receiver is shown in Fig. 5.4. Denote the output of the correlator as $\mathbf{u}_k[n]$, written as

$$\mathbf{u}_k[n] = \mathbf{W}^H\mathbf{B}^{-1}\mathcal{F}_{sp}\mathbf{z}'_{k,n} = \mathbf{a}_k[n] - \underbrace{\mathcal{F}_{sp}\mathbf{W}^H\mathbf{B}^{-1}\widetilde{\widetilde{\mathbf{z}}}_k[n]}_{\widetilde{\widetilde{\mathbf{u}}}_k[n]} \tag{5.18}$$

The covariance matrix $\boldsymbol{\mathcal{R}}_{\widetilde{\widetilde{u}}\widetilde{\widetilde{u}}}$, the diagonal bias matrix $\mathbf{B}$ and $\boldsymbol{\mathcal{R}}_{\widetilde{\widetilde{z}}\widetilde{\widetilde{z}}}$, the covariance matrix of $\widetilde{\widetilde{\mathbf{z}}}$ can be related as

$$\boldsymbol{\mathcal{R}}_{\widetilde{\widetilde{u}}\widetilde{\widetilde{u}}} = \mathcal{F}_{sp}\mathbf{W}^H\mathbf{B}^{-1}\boldsymbol{\mathcal{R}}_{\widetilde{\widetilde{z}}\widetilde{\widetilde{z}}}\mathbf{B}^{-H}\mathbf{W}\mathcal{F}_{sp}^H \tag{5.19}$$

Assume a 2×2 lower triangular filter $\mathcal{V}_{sp}$ with unit diagonal and the remaining element v_{21} such that $\widetilde{\mathbf{r}}[n] = \mathcal{V}_{sp}\widetilde{\widetilde{\mathbf{u}}}_k[n]$. Then the new error covariance matrix is given as

$$\boldsymbol{\mathcal{R}}_{\widetilde{r}\widetilde{r}} = \mathcal{V}_{sp}\boldsymbol{\mathcal{R}}_{\widetilde{\widetilde{u}}\widetilde{\widetilde{u}}}\mathcal{V}_{sp}^H, \tag{5.20}$$

which is minimized if $\boldsymbol{\mathcal{R}}_{\widetilde{r}\widetilde{r}} = \mathbf{D}$, i.e., a diagonal matrix. Toward this end, consider LDU factorization of $\boldsymbol{\mathcal{R}}_{\widetilde{\widetilde{u}}\widetilde{\widetilde{u}}} = \mathbf{L}\mathbf{D}\mathbf{L}^H$. Then, $\mathcal{V}_{sp} = \mathbf{L}^{-1}$ minimizes (5.20). Denoting elements of $\boldsymbol{\mathcal{R}}_{\widetilde{\widetilde{u}}\widetilde{\widetilde{u}}}$ as r_{ij}, the elements of $\mathbf{D}$ are given as $\sigma^2_{\widetilde{r}_1} = r_{11}$ and

$$\begin{aligned}\sigma^2_{\widetilde{r}_2} &= r_{22} - r_{21}r_{11}^{-1}r_{12} \\ &= \det(\boldsymbol{\mathcal{R}}_{\widetilde{\widetilde{u}}\widetilde{\widetilde{u}}}) \\ &= \det(\mathcal{F}_{sp})\det(\mathbf{B}^{-1}\boldsymbol{\mathcal{R}}_{\widetilde{\widetilde{z}}\widetilde{\widetilde{z}}}\mathbf{B}^{-H})\det(\mathcal{F}_{sp}^H),\end{aligned} \tag{5.21}$$

Thus MMSE for stream 1 is $\sigma^2_{\widetilde{r}_1}$ and that of stream 2 is $\sigma^2_{\widetilde{r}_2}$. As depicted in Fig. 5.4 we see that stream 1 achieves the same performance as that of the chip-level LMMSE/correlator - spatial MMSE receiver, while stream 2 benefits from stripping (and thus achieves the spatial MFB). An inter-

esting observation is that the SINR expression for stream 2 in the symbol-level SIC case is independent of the precoding **W** applied. In this receiver, stream 1 should exhibit better performance than in the case of the chip-equalizer/correlator receiver. An alternative receiver structure proposed in [21] is also possible where stream 1 processing is just limited to the chip equalizer-correlator cascade and stream 2 is subjected to symbol-level SIC as above. However, the receiver discussed above is a better alternative to [21], since in this case, stream 1 should get an additional boost in SINR due to the spatial MMSE processing. This should not only amplify stream 1 rate, but also has the desirable effect of improving stream 1 detection. This improved reliability, although not relevant in this discussion where we assume ideal suppression of stream 1 is important in practical implementations. It reduces the chances of error-propagation during the interference cancellation stage and hence directly impacts detection performance of stream 2. It should however be noted that any low-complexity symbol level processing is hardly comparable to chip-level SIC receiver. While the former exploits noise plus interference correlation between streams to improve SINR of symbol detected last, the latter benefits from stripping of spatio-temporal interference of the entire detected stream, where for stream detected last, all streams can henceforth be considered non-existent (assuming perfect cancellation). Not only do streams see different levels of interference, a new chip-equalizer can be calculated at each stage that benefits from a larger noise-subspace to cancel remaining interference.

5.3.3 Spatial ML receiver

Yet another possible receiver structure is shown in Fig. 5.5 where the chip-equalizer correlator front end is followed up, as before, by the spatial MMSE stage. The resulting spatial mixture

$$\mathbf{u}_k[n] = \mathcal{F}_{sp}\mathbf{z}_k^{'}[n] = \mathbf{a}_k[n] - \widetilde{\widetilde{\mathbf{u}}}_k[n], \tag{5.22}$$

is later processed for joint detection (code-wise ML detection) of the two symbol streams. The ML metric is given as follows.

$$\mathcal{D} = \{\mathbf{u}_k[n] - \mathbf{a}_k[n]\}^H \boldsymbol{\mathcal{R}}_{\widetilde{\widetilde{u}}\widetilde{\widetilde{u}}}^{-1} \{\mathbf{u}_k[n] - \mathbf{a}_k[n]\},$$

This metric can be solved for $\mathbf{a}_k[n]$. It was shown in [21] that joint detection outperforms SIC. However, the SIC structure in [21] addresses a SIC applied directly at the output of the chip equalizer-correlator output. Thus stream 1 gets the same SINR as the chip-equalizer while in our case, stream

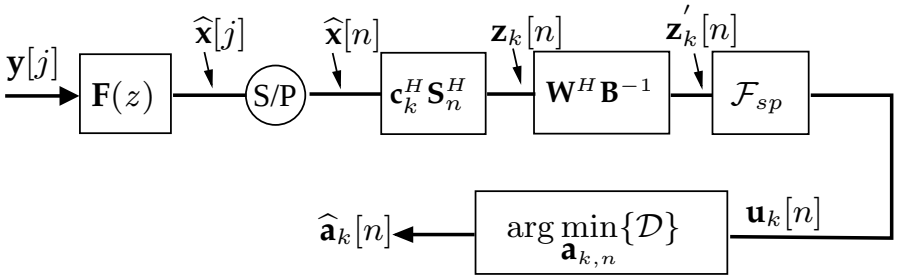

Figure 5.5: Chip LMMSE equalizer/correlator followed by spatial MMSE and joint detection.

1 would also reap the benefits of spatial MMSE processing. For joint detection, the SINR for the ith stream corresponds to the MFB of spatial channel resulting from the cascade of $\mathcal{F}_{sp}$ and $\mathbf{B}$. The MFB can be interpreted as the SNR of ith stream when it is detected assuming that symbols of the other stream(s) are known. $\boldsymbol{\mathcal{R}}_{\tilde{\tilde{u}}\tilde{\tilde{u}}}$ is the noise variance.

5.3.4 Simulation results

We present here some simulation results to compare the performance of the different receiver structures that were discussed in this section. For a fixed, per stream SNR $=$ 10dB, over several realizations of a frequency selective $2p \times 2$ MIMO FIR channel, we compute the optimal precoding matrices and use the corresponding SINRs of both streams at the output of the receivers to calculate an upper bound on the sum capacity. The channel coefficients are complex valued zero-mean Gaussian of length 20 chips. We assume FIR MIMO equalizers of length comparable to the channel. The sum-capacity CDF is thus used as a performance measure for all receivers. Without loss of generality, in all our simulations, we choose the matrix that maximizes the SINR of stream 1. The per stream SNR $=$ 10dB Fig. 5.6 shows distribution of sum-capacity at the output of the MMSE chip-equalizer correlator receiver and that of the spatial MMSE receiver. With an additional processing stage of a very small complexity we are able to see some gain in the achievable rates of the receiver.

In Fig. 5.7 we compare the performance of LMMSE chip equalizer- correlator receiver with the receiver that performs spatial MMSE as well as predictive-DFE and the per-code ML receiver. As before, optimal precoding matrices are used at the base-station. The receiver that performs spatial LMMSE and DFE benefits slightly from the additional spatial processing

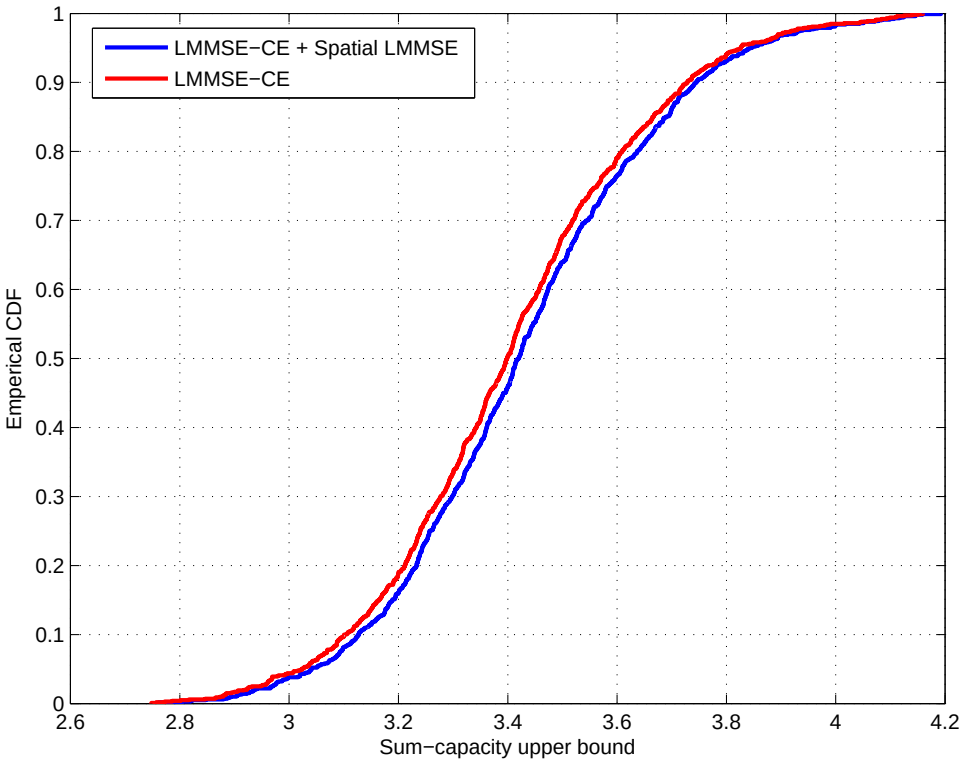

Figure 5.6: Performance of LMMSE chip-equalizer/correlator receiver and LMMSE chip-equalizer and spatial MMSE receiver.

for both streams and a non-linear equalization stage for stream-2. That the gain is not considerable is due to the fact that stream-1 does not benefit from non-linear equalization. Since the performance measure is the sum-capacity of both streams, the performance of this receiver is limited by the performance of stream-1. By performing spatial ML detection one is able to get much better performance. The chip-level SIC, in Fig. 5.8 as can be expected, outperforms all other receivers at the cost of a significant processing delay and architectural complexity at the receiver.

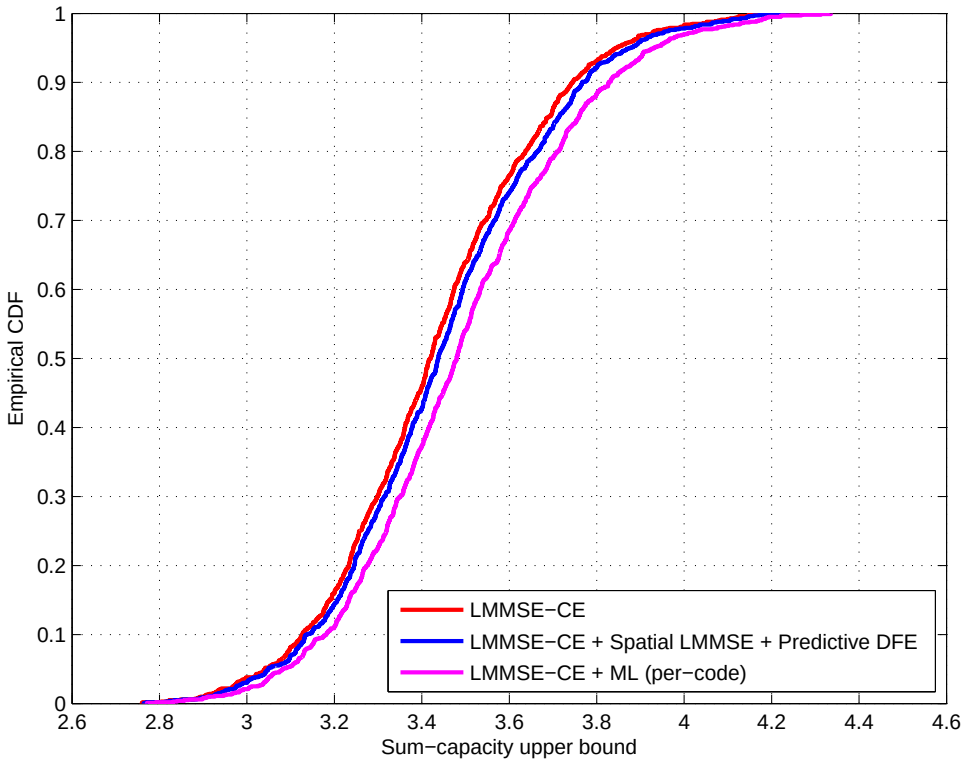

Figure 5.7: Comparison of sum-capacity upper bounds for different receiver structures.

5.4 Chip level and symbol level equalization : Deterministic scrambler

Until now, we discussed various receiver designs that assumed the scrambler to be random i.i.d. Modeling the scrambler as random *i.i.d* leads to a time-invariant spatial signal model which in turn leads to intuitively pleasing and simple receiver designs. However for the second stage of the two-step processing employed in the receivers, it limits their performance. Since the first step in the two-stage approach can be interpreted as a dimensionality reduction step, the limitation on the gain obtained by this design over classical chip-equalization can be linked to the efficacy of the dimensionality reduction achieved at the output of the chip-equalizer and

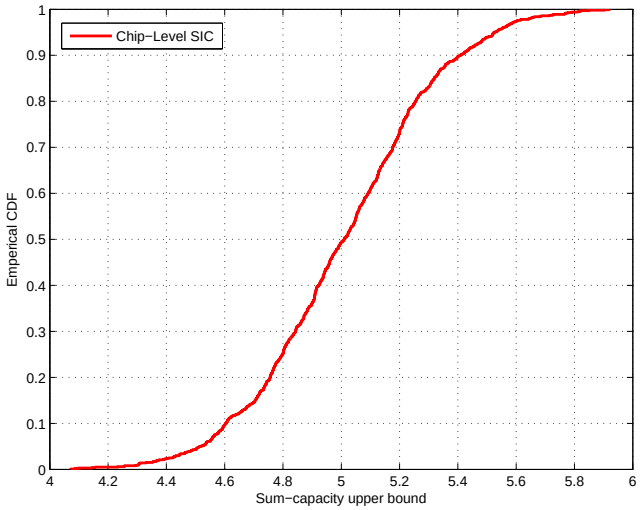

Figure 5.8: Upper bound for sum-capacity for the chip-level SIC receiver.

also the type of processing at symbol level. In the general MIMO case, the resulting symbol-rate spatial channel can now be seen as only a per-code spatial mixture. When the scrambler is treated as random, this mixture becomes time-invariant and therefore simplified (per-code) processing can be applied. For a processing gain $\mathcal{G}$, assuming N_t to be the number of TX streams, N_r the number of RX antennas, and p to be the oversampling factor *w.r.t.* the chip rate, this can be seen as a dimensionality-reduction from $p \cdot \mathcal{G} \cdot N_r$ to N_t. Given this drastic reduction, it is not surprising to see performance falling well short of optimal time-varying symbol-level processing (linear and non-linear MUD solutions). In the previous section, we chose to trade performance off in the interest of reduced complexity symbol level processing in order to point out that despite their shortcomings, their complexity/performance equation encourages use of these solutions. In this section, in an attempt to further increase the performance of our receiver designs, we put forth the idea of deterministic treatment of the scrambler and focus on the resulting spatial channel model. Such a treatment mandates time-varying processing after the equalizer-correlator stage but offsets some of the performance losses of the dimensionality reduction stage and the random scrambler assumption.
We will not consider here, the precoding aspect of downlink transmission. However, we stress that introduction of precoding does not in any way al-

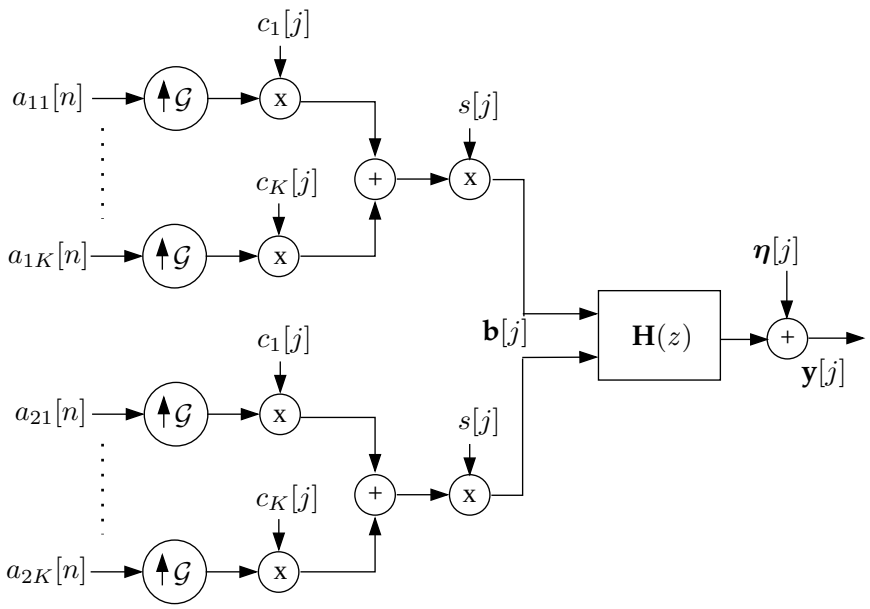

Figure 5.9: MIMO signal model without precoding.

ter the results obtained in this section. The downlink signal model remains exactly the same as before, apart from the absence of linear precoding before transmission and we illustrate it here for convenience.

The received signal vector (chip-rate) at the UE is now modeled as

$$\underbrace{\mathbf{y}[j]}_{2p\times 1} = \underbrace{\mathbf{H}(z)}_{2p\times 2}\underbrace{\mathbf{b}[j]}_{2\times 1} + \underbrace{\boldsymbol{\eta}[j]}_{2\times 1}, \tag{5.23}$$

where

$$\mathbf{b}[j] = \sum_{k=1}^{K} s[j]c_k[j \mod \mathcal{G}]\mathbf{a}_k[n], \tag{5.24}$$

MMSE chip equalizer-correlator revisited

This section is the extension of 4.3 to the MIMO case. As before, we derive the expression for the output energy of this receiver and consider linear MMSE estimation of the 2×1 MIMO symbol sequence $\mathbf{a}_k[n]$ of the k^{th} code among K codes. Fig. 5.10, provides a MIMO version of the vectorized TX signal model introduced in 4.3 where $\mathbf{b}[n]$ is now a $2\mathcal{G} \times 1$ chip vector and $\mathbf{a}[n]$ is of size $2K \times 1$. The symbol level channel $\mathbf{H}(z) = \sum_m z^{-m}\mathbf{H}[m]$ consists of $p\mathcal{G} \times \mathcal{G}$ matrix taps where

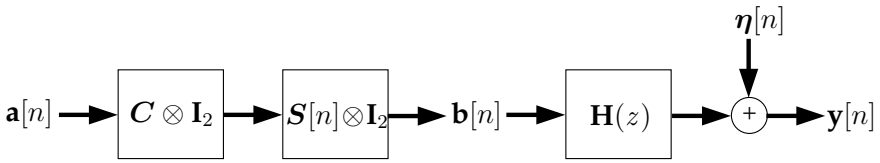

Figure 5.10: MIMO TX signal model.

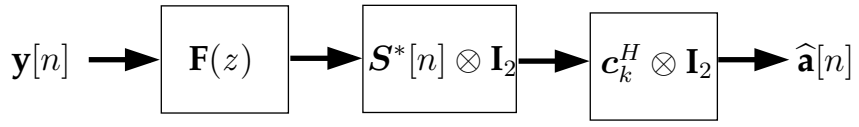

Figure 5.11: MIMO RX model.

$$\mathbf{H}[m] = \begin{bmatrix} \mathbf{h}[m\mathcal{G}] & \mathbf{h}[m\mathcal{G}+1] & \dots & \mathbf{h}[(m+1)\mathcal{G}-1] \\ \mathbf{h}[m\mathcal{G}-1] & & & \vdots \\ \vdots & & \ddots & \\ \mathbf{h}[(m-1)\mathcal{G}+1] & \dots & \dots & \mathbf{h}[m\mathcal{G}] \end{bmatrix}$$

with $\mathbf{h}[.]$ being the $2p \times 2$ chip-level MIMO channel coefficients. The LMMSE equalizer $\mathbf{F}(z)$ in Fig. 5.11 can be represented in a similar fashion. The channel equalizer cascade is then given by

$$\mathbf{G}(z) = \mathbf{F}(z)\mathbf{H}(z), \tag{5.25}$$

$$= \sum_{\nu=0}^{N+M-2} \mathbf{G}[\nu] z^{-\nu}. \tag{5.26}$$

As before, the channel-equalizer cascade at symbol level may be defined similarly to be composed of 2×2 chip-level matrix-coefficients $\mathbf{g}[k] = \sum_{l=0}^{L-1} \mathbf{f}[k-l]\mathbf{h}[l]$ With the equalizer delay set at d. We represent the channel-equalizer cascade matrix at d as

$$\mathbf{G}[0] = \mathbf{F}(z)\mathbf{H}(z)|_{[0]} = \begin{bmatrix} \mathbf{g}[0] & \mathbf{g}[1] & \dots & \mathbf{g}[\mathcal{G}-1] \\ \mathbf{g}[-1] & & & \vdots \\ \vdots & & \ddots & \\ \mathbf{g}[-\mathcal{G}+1] & \dots & \dots & \mathbf{g}[0] \end{bmatrix} \tag{5.27}$$

We can thus write

$$\widehat{\mathbf{a}}_k[n] = (\boldsymbol{c}_k^H \otimes I_2)\,(\boldsymbol{S}^*[n] \otimes \mathbf{I}_2)\,\{\mathbf{G}(z)\,(\boldsymbol{S}[n] \otimes \mathbf{I}_2)\,(\boldsymbol{C} \otimes \mathbf{I}_2)\,\mathbf{a}[n] + \mathbf{F}(z)\boldsymbol{\eta}[n]\}\,.$$

Defining

$$\mathbf{B}_{n,k}(z) = (\boldsymbol{c}_k^H \otimes \mathbf{I}_2)\,(\boldsymbol{S}^*[n] \otimes \mathbf{I}_2)\,\mathbf{G}(z)\,(\boldsymbol{S}[n] \otimes \mathbf{I}_2)\,(\boldsymbol{C} \otimes \mathbf{I}_2)$$

as the symbol-rate channel at time instant n (also a $\overline{\mathbf{B}}_{n,k}(z)$ corresponding to $\overline{\mathbf{G}}(z)$) , we can write the correlator output as

$$\mathbf{z}_k[n] = \underbrace{\mathbf{B}_{n,k}[0]\mathbf{a}_k[n]}^{kth\ code} + \underbrace{\mathbf{B}^{'}_{n,k}[0]\overline{\mathbf{a}}[n]}^{other\ codes} + \underbrace{\sum_m \mathbf{B}_{n,k}[m]\mathbf{a}[n+m]}_{all\ codes\ other\ symbols} + \underbrace{\mathbf{F}(z)\boldsymbol{\eta}[n]}_{noise}, \quad (5.28)$$

In this expression, $\mathbf{B}_{n,k}[0]$ is the desired user channel at symbol-time n. Treating the scrambler as white has the effect of capturing the mean signal energy (corresponding to the $\mathbf{g}[0]$ contribution) at the output of the per code MIMO channel treating the off-diagonal part in $\mathbf{G}[0]$ as the interference term.

It may be noticed that each element of $\mathbf{G}[m]$ is a 2×2 MIMO matrix coefficient. The former can therefore be split into four $\mathcal{G} \times \mathcal{G}$ SISO submatrices $\mathbf{G}_{r\kappa}[m]$, for $r, \kappa \in \{1, 2\}$. A corresponding $\mathcal{G} \times \mathcal{G}$ matrix coefficient $\overline{\mathbf{G}}_{r\kappa}[m] = \mathbf{G}_{r\kappa}[m] - \mathbf{g}_{r\kappa}[m] \cdot I_{\mathcal{G}}$ is also defined and so is $\mathbf{g}_{r\kappa}[m]$, the $r\kappa^{th}$ element of the spatial channel $\mathbf{g}[m]$.

Taking expectation over the scrambler, we can express the output energy of the receiver as

$$\boldsymbol{\mathcal{R}}_{zz} = \boldsymbol{\mathcal{R}}_{des} + \underbrace{\boldsymbol{\mathcal{R}}_{MUI} + \sum_m \boldsymbol{\mathcal{R}}_{m,ISI} + \mathbf{F}\boldsymbol{\mathcal{R}}_{\eta\eta}\mathbf{F}^H}_{\boldsymbol{\mathcal{R}}_{\tilde{z}\tilde{z}}}\,, \quad (5.29)$$

where,

$$\boldsymbol{\mathcal{R}}_{des} = \begin{bmatrix} |g_{11}[0]|^2 + |g_{12}[0]|^2 & \sum_{\kappa=1}^{2} g_{1\kappa}[0]g_{2\kappa}^*[0] \\ \sum_{\kappa=1}^{2} g_{2\kappa}[0]g_{1\kappa}^*[0] & |g_{21}[0]|^2 + |g_{22}[0]|^2 \end{bmatrix} + \frac{1}{\mathcal{G}^2} \cdot \begin{bmatrix} \sum_{\kappa=1}^{2} tr\{\overline{\mathbf{G}}_{1\kappa}[0]\overline{\mathbf{G}}_{1\kappa}^H[0]\} & \sum_{\kappa=1}^{2} tr\{\overline{\mathbf{G}}_{1\kappa}[0]\overline{\mathbf{G}}_{2\kappa}^H[0]\} \\ \sum_{\kappa=1}^{2} tr\{\overline{\mathbf{G}}_{2\kappa}[0]\overline{\mathbf{G}}_{1\kappa}^H[0]\} & \sum_{\kappa=1}^{2} tr\{\overline{\mathbf{G}}_{2\kappa}[0]\overline{\mathbf{G}}_{2\kappa}^H[0]\} \end{bmatrix},$$

$$\boldsymbol{R}_{MUI} = \frac{K-1}{\mathcal{G}^2} \cdot \begin{bmatrix} \sum_{\kappa=1}^{2} tr\{\overline{\mathbf{G}}_{1\kappa}[0]\overline{\mathbf{G}}_{1\kappa}^{H}[0]\} & \sum_{\kappa=1}^{2} tr\{\overline{\mathbf{G}}_{1\kappa}[0]\overline{\mathbf{G}}_{2\kappa}^{H}[0]\} \\ \sum_{\kappa=1}^{2} tr\{\overline{\mathbf{G}}_{2\kappa}[0]\overline{\mathbf{G}}_{1\kappa}^{H}[0]\} & \sum_{\kappa=1}^{2} tr\{\overline{\mathbf{G}}_{2\kappa}[0]\overline{\mathbf{G}}_{2\kappa}^{H}[0]\} \end{bmatrix},$$

where the superscript $*$ represents complex conjugation. The ISI contribution from the m^{th} symbol can be expressed as

$$\boldsymbol{\mathcal{R}}_{m,ISI} = \frac{K}{\mathcal{G}^2} \cdot \begin{bmatrix} \sum_{\kappa=1}^{2} tr\{\overline{\mathbf{G}}_{1\kappa}[m]\overline{\mathbf{G}}_{1\kappa}^{H}[m]\} & \sum_{\kappa=1}^{2} tr\{\overline{\mathbf{G}}_{1\kappa}[m]\overline{\mathbf{G}}_{2\kappa}^{H}[m]\} \\ \sum_{\kappa=1}^{2} tr\{\overline{\mathbf{G}}_{2\kappa}[m]\overline{\mathbf{G}}_{1\kappa}^{H}[m]\} & \sum_{\kappa=1}^{2} tr\{\overline{\mathbf{G}}_{2\kappa}[m]\overline{\mathbf{G}}_{2\kappa}^{H}[m]\} \end{bmatrix},$$

In these relations, the $\boldsymbol{\mathcal{R}}_{des}$ is composed of two contributions shown above as the sum of two 2×2 matrices. When the scrambler is treated as random the term scaled by $1/\mathcal{G}^2$ is the quantity that ceases being a part of the signal energy contribution and is associated instead with the interference.

At the output of the despreader for the k^{th} code, one can therefore express the signal as

$$\mathbf{z}_k[n] = \mathbf{B}_{n,k}[0]\mathbf{a}_k[n] - \widetilde{\widetilde{\mathbf{z}}}_k[n], \tag{5.30}$$

where the time varying MIMO joint-bias $\mathbf{B}_{n,k}[0]$ is no longer constant and varies for each symbol. The per-user SINR of stream i which we denote by $\mathsf{SINR}_{\mathsf{k,i}}$ is given by (5.31).

$$\frac{\sigma_{a_k}^2 \left(|g_{ii}[0]|^2 + \frac{1}{\mathcal{G}^2} \mathrm{tr}\left\{ \overline{\mathbf{G}}_{ii}[0]\overline{\mathbf{G}}_{ii}^{H}[0] \right\} \right)}{\sigma_{a_k}^2 \left(\frac{(K-1)}{\mathcal{G}^2} \sum_{\kappa=1}^{2} \mathrm{tr}\left\{ \overline{\mathbf{G}}_{i\kappa}[0]\overline{\mathbf{G}}_{i\kappa}^{H}[0] \right\} + \frac{K}{\mathcal{G}^2} \sum_{m} \sum_{\kappa=1}^{2} \mathrm{tr}\left\{ \overline{\mathbf{G}}_{i\kappa}[m]\overline{\mathbf{G}}_{i\kappa}^{H}[m] \right\} \right) + \sigma_{\eta}^2 \|\mathbf{f}_i\|^2}, \tag{5.31}$$

We will now briefly discuss the effect of deterministic treatment of scrambler on further linear or non-linear symbol level processing stages when the receiver design is based on combined chip and symbol level equalization. For the spatial MMSE receiver, in order to claim the quantity $\frac{1}{\mathcal{G}^2} \mathrm{tr}\left\{ \overline{\mathbf{G}}_{rr}[0]\overline{\mathbf{G}}_{rr}^{H}[0] \right\}$ in (5.31) as part of signal energy, it suffices to put in place time-varying processing at the correlator output, where the n^{th} symbol vector on the k^{th} code, $z_k[n]$ is given by (5.28). As a result of time-varying symbol level joint-bias, the 2×2 MMSE equalizer will now have to

be computed for each symbol. This will indeed provide higher gains than the spatial MMSE receiver above which treats the time varying signal contribution as noise. In case of the spatial-ML receiver, in treating the scrambler as random the spatial channel (**B**), the ML metrics will deal with a time-invariant channel. A continuous processing matched filter bound can therefore be defined per stream. The i^{th} stream MFB is therefore proportional to the energy in the corresponding SIMO channel. On the contrary, if a deterministic scrambler is assumed, time-variation in the channel must be accounted for in ML metrics. Strictly speaking, the MFB is only defined per symbol as the SINR of the n^{th} symbol considering all other symbols to be known (correctly detected). We can nevertheless argue that deterministic treatment of the scrambler leads to reduced interference variance $\boldsymbol{\mathcal{R}}_{\tilde{z}\tilde{z}}$ and increased recoverable signal power that will lead to performance improvement for the ML solution.

5.4.1 Simulation results

We use the same simulation settings as in the previous section to compare the performance of different receiver structures based on their sum-capacity. We simulate here a single-user situation where 15 codes are assigned to the same user. Furthermore, we assume code-reuse across antennas. In Fig. 5.12 we plot the capacity bounds for two cases. In the first instance, we treat the scrambler as random. The symbol energy for code k is therefore given by the symbol variance for the code scaled by an arbitrary time-invariant scale factor. In the second case, we treat the scrambler as a known sequence. In this case, firstly, the signal power now is time-varying at symbol rate. This time varying signal power can be seen as the sum of a "mean" power contribution equal to the signal power when the scrambler is assumed to be random, and time-varying contribution due to deterministic treatment of the scrambler. Note that the SINR distribution for the deterministic treatment of the scrambler in Fig. 5.13 represents the *average* gains and not the true gain. The actual gain will be higher than that seen in Fig. 5.13. Finally we comment here that the gains observed seem to be small primarily due to the SNR which is comparatively low.

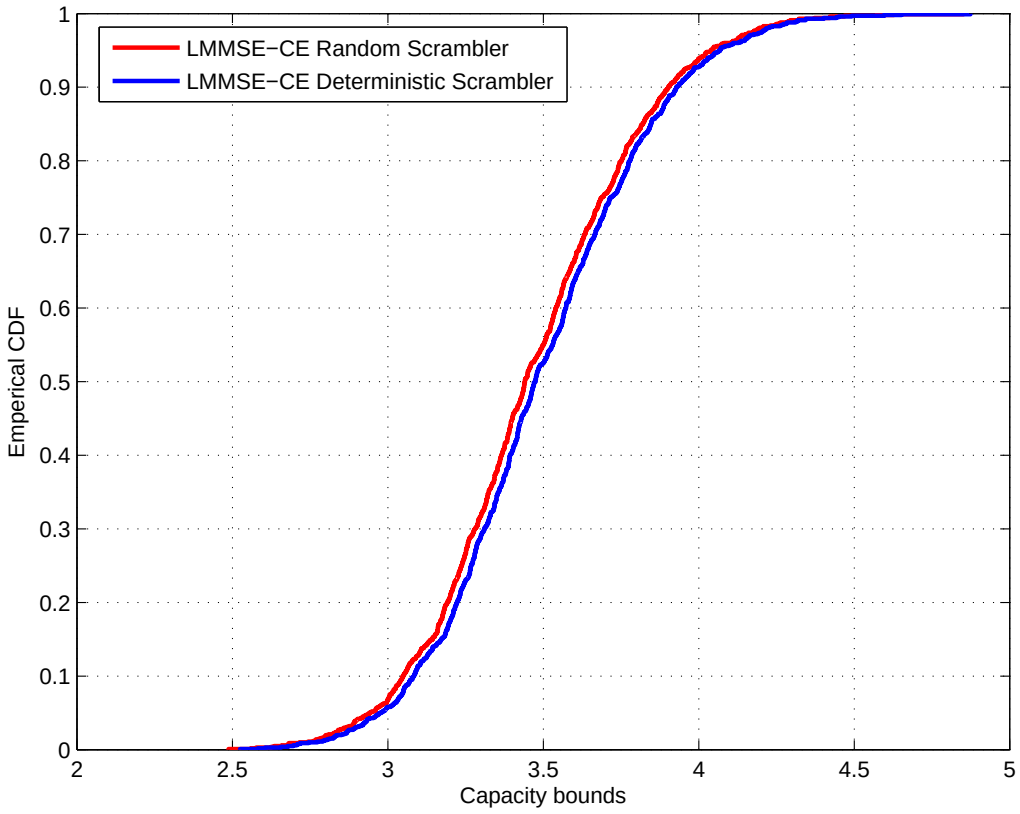

Figure 5.12: Performance of LMMSE chip-equalizer correlator with random and deterministic scrambler.

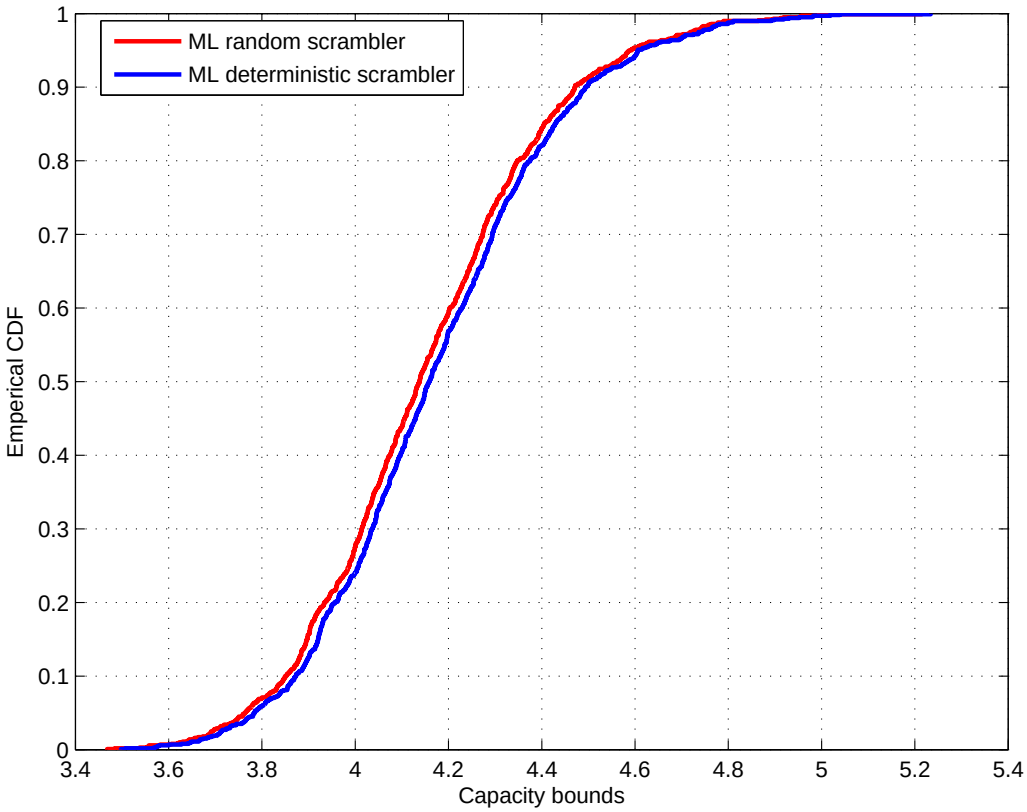

Figure 5.13: Sum-capacity at the output of spatial-ML receiver with deterministic and random scrambler.

Chapter 6

Multiuser extensions to MIMO HSDPA

In this chapter, we shift our focus to extending MIMO in HSDPA to support multiple users in the downlink (MU-MIMO). In its present form, the standard only supports 2×2 SU-MIMO in the downlink (DL) in the form of D-TxAA. It is possible for the BS to employ spatial division multiple access (SDMA) and service multiple UEs in DL instead. In this case, the limitation of 2 transmit antennas implies that a maximum of 2 spatially separated users can be simultaneously served by the BS with the same code. In general, MU extensions for closed loop transmit diversity schemes (both TxAA and D-TxAA) introduce multi-user interference in downlink since there exists the possibility of different users feeding back different beamforming vectors in TxAA or different precoding matrices in D-TxAA.

There is a large amount of literature available for multiuser MIMO communication in the general case. It has been studied previously in [33] and more recently in [15] where multiuser transmission techniques are classified into linear and non-linear transmission algorithms. Non-linear algorithms involving multiuser signal designs that avoid interference generation to other users based on dirty paper coding techniques remain currently impractical due to the requirement of perfect channel state information at the transmitter (CSIT). They also suffer from all the drawbacks associated with outdated CSIT due to scheduling delays at the base station

and/or rapidly changing downlink channels. Linear processing of transmitted signals like multiuser beamforming remain by far the most practical solution for multiuser transmission. Theoretical research in multiuser communications tends to consider frequency-flat channels. In reality most mobile communication channels are frequency selective. There exists some literature on multiuser extension of HSDPA. In [34] the authors propose code reuse in D-TxAA based on a multi-user beamforming (MUB) scheme which schedules users with orthogonal weight vectors to separate them in space. They however limit their analysis to flat-channels. In [35], the authors consider MU-TxAA for frequency selective channels and propose the so-called "interference-aware" receiver which in addition to requiring multiple antennas at the receiver also assumes knowledge of beamforming weight vectors of all the users at the receiver. On the other hand, we look at the problem of maximizing system capacity in the frequency selective MISO/MIMO downlink channels assuming the receivers select weights that maximize receive SINR (and thus increase their individual data rates). In the HSDPA context, the BS is equipped with 2 transmit antennas i.e. $N_{tx} = 2$. In our treatment, we do not assume any explicit knowledge of beamforming weight vectors of other users, for single stream transmission we consider single antenna UE and study different beamforming strategies that can be adopted by the BS and for dual stream transmission we consider UE with two antennas and compare the performance of SDMA against spatial multiplexing to a single user by extending D-TxAA to a MU configuration where at most N_{tx} users can be synchronously served by the BS. Each transmit stream is assigned to a different user. This rules out simultaneously serving any two users that feed back the same beamforming weight vector. Users that request linearly independent weight vectors can however be served simultaneously.

6.1 Multiuser TxAA

We consider a 2-transmit, 1-receive antenna configuration for TxAA. For the rest of the section, whenever we refer to a MU-TxAA system, we consider U separate UEs each having a single receive antenna. The number of codes assigned to each user is denoted by $K_1, K_2, \ldots, K_U$ and $K = \sum_{u=1}^{U} K_u$. Then, for TxAA, from Fig. 6.1 the transmit and beamformed

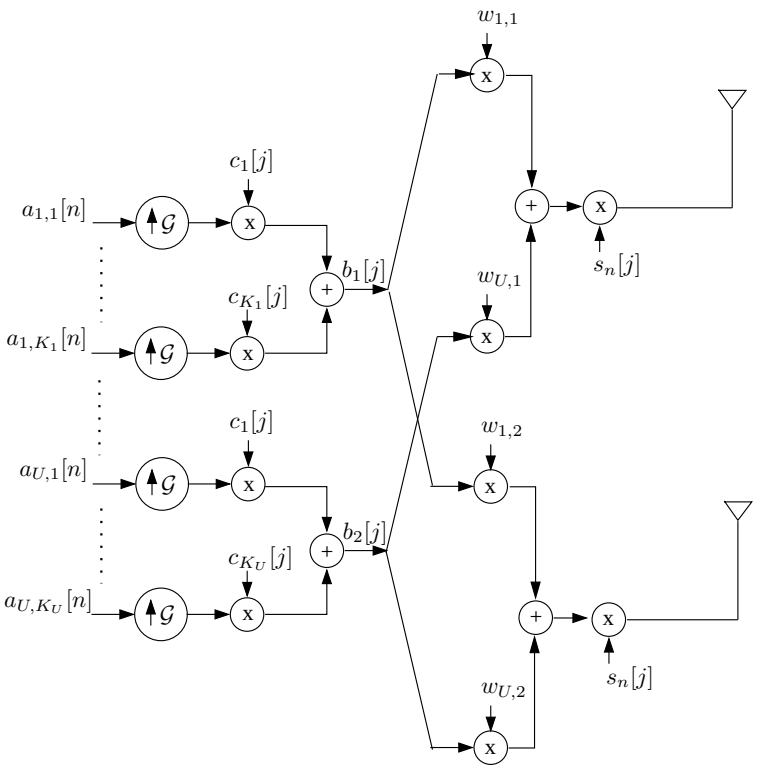

Figure 6.1: Multiuser TxAA transmit signal model.

chip sequence is given by

$$\mathbf{x}[j] = \sum_{u=1}^{U} \mathbf{w}_u \cdot s_n[j \mod \mathcal{G}] \sum_{k \in K_u} c_k[j \mod \mathcal{G}] a_{u,k}[\lfloor \frac{j}{\mathcal{G}} \rfloor n], \qquad (6.1)$$

where j is the chip index, n is the symbol index, u is the user index, k is the code index, $\mathcal{G}$ is the spreading gain, s_n denotes the scrambler for the nth symbol, c_k denotes the kth spreading code, $\mathbf{w}_u = [w_{u,1} w_{u,2}]^T$ is the weight vector corresponding to u^{th} user and finally $a_{u,k}[n]$ is the u^{th} user's symbol on code index k given that $k \in K_u$. The transmitted signal propagates through a multipath channel which we denote here by $\mathcal{H}_u^0, \mathcal{H}_u^1, \ldots, \mathcal{H}_u^{L-1}$. For an oversampling factor of p at the receiver, each $\mathcal{H}_u^l$ matrix is a $p \times 2$ matrix corresponding to the lth tap of the uth user's multipath channel. For simplicity we assume that all UEs see a channel with a maximum delay spread of L chips and employ an equalizer of length E (in chips). The chip-

rate received signal at each UE is given by

$$\mathbf{y}_u = \mathbf{H}_u\mathbf{x} + \boldsymbol{\eta} \tag{6.2}$$

where $\mathbf{H}_u$ is the channel convolution matrix for the uth user given by

$$\mathbf{H}_u = \begin{bmatrix} \mathcal{H}_u^0 & \mathcal{H}_u^1 & \cdots & \mathcal{H}_u^{L-1} & \mathbf{0} & \mathbf{0} \\ \mathbf{0} & \mathcal{H}_u^0 & \cdots & \cdots & \mathcal{H}_u^{L-1} & \vdots \\ \mathbf{0} & \mathbf{0} & \ddots & \ddots & \ddots & \mathbf{0} \\ \mathbf{0} & \mathbf{0} & \ddots & \mathcal{H}_u^0 & \ddots & \mathcal{H}_u^{L-1} \end{bmatrix}, \tag{6.3}$$

$\mathbf{x}$ is the transmit chip-vector formed by stacking $L + E - 1$ vectors and can be expressed as

$$\mathbf{x} = [\mathbf{x}^T[j], \mathbf{x}^T[j-1], \ldots, \mathbf{x}^T[j-L-E+2]], \tag{6.4}$$

and $\boldsymbol{\eta}$ is zero mean, circularly symmetric, Gaussian distributed, additive white noise of variance σ_η^2. In addition, we also define the $p \times 1$ vector $\mathbf{r}_{u,v}^l = \mathcal{H}_u^l\mathbf{w}_v$, $v \in 1, 2, \ldots, U$ and use this to define the l^{th} beamformed channel tap of user u, due to beamforming weight of another synchronous DL user v. We denote this by $\mathbf{R}_{u,v}$ and express this as

$$\mathbf{R}_{u,v} = \begin{bmatrix} \mathbf{r}_{u,v}^0 & \mathbf{r}_{u,v}^1 & \cdots & \mathbf{r}_{u,v}^{L-1} & \mathbf{0} & \mathbf{0} \\ \mathbf{0} & \mathbf{r}_{u,v}^0 & \cdots & \cdots & \mathbf{r}_{u,v}^{L-1} & \vdots \\ \mathbf{0} & \mathbf{0} & \ddots & \ddots & \ddots & \mathbf{0} \\ \mathbf{0} & \mathbf{0} & \ddots & \mathbf{r}_{u,v}^0 & \ddots & \mathbf{r}_{u,v}^{L-1} \end{bmatrix}, \tag{6.5}$$

6.1.1 Beamforming Strategies at Transmitter

Consider the case where the base station serves U simultaneous users in the downlink. We assume standard MMSE chip equalizer-correlator receivers. Let $\mathbf{f}_u$ represent the MMSE filter of length E applied at user u, then the equivalent channel-equalizer cascade at the output of the chip equalizer for user u is given by

$$\boldsymbol{\alpha}^{(u)} = \mathbf{f}_u\mathbf{R}_{u,u} + \mathbf{f}_u\sum_{v\neq u}^{U}\mathbf{R}_{u,v}, \tag{6.6}$$

which can be represented by

$$\boldsymbol{\alpha}^{(u)} = \boldsymbol{\alpha}_{u,u} + \sum_{v \neq u}^{U} \boldsymbol{\alpha}_{u,v}, \tag{6.7}$$

where $\boldsymbol{\alpha}_{u,u}$, is the channel-equalizer cascade for codes assigned to user u and $\boldsymbol{\alpha}_{u,v}$ is the channel-equalizer cascade for codes assigned to user v at user u. $\boldsymbol{\alpha}_{u,u}$ can in turn be split into the desired equalizer response and the residual inter-chip-interference and represented as

$$\boldsymbol{\alpha}_{u,u} = \boldsymbol{\alpha}^{d}_{u,u} + \overline{\boldsymbol{\alpha}}_{u,u} \tag{6.8}$$

$$\boldsymbol{\alpha}^{d}_{u,u} = \left[\overbrace{0 \ldots 0}^{d-1} \; \alpha^{d}_{u,u} \; \overbrace{0 \ldots 0}^{L+E-2-d} \right] \tag{6.9}$$

where d is the equalizer delay. The LMMSE equalizer is considered to be followed by a stacking operation allowing despreading and symbol decision.

Simple multiuser beamforming

To understand the effect of multiple-users with distinct beamforming weights in DL, it is insightful to derive the per-code SINR at the receiver for the case where multiple users are served in the downlink with different beamforming weights. When the BS employs different user-defined beamforming weights in downlink for MU transmission, at each receiver, codes assigned to different users propagate through U distinct *beamformed channels* even though the physical channel through which they propagate is the same. Without explicit knowledge of all beamforming weights used in the downlink, which is the so called interference aware [35] receiver, the receiver will not be able to effectively mitigate the effect of MUI. Since each user is aware only of beamforming weights that will be applied for codes assigned to itself and not of other users, the equalizer at each user is only matched to the beamformed channel seen by the codes assigned to this user. In computing the ideal beamforming weights for itself, a UE has to make some hypothesis on the beamforming weight vectors of other users in DL and choose the weight vector that maximizes the SINR corresponding to that hypothesis. For the general case where there exist U different users, defining K_u as the index set containing code indices of the u^{th} user, the SINR per-code $\mathsf{SINR}_{k \in K_u}$ that is seen by the code assigned to the user is

given by

$$\frac{\sigma_k^2|\alpha_{u,u}^d|^2}{\frac{1}{\mathcal{G}}\sum_{k\in K_u}\sigma_k^2\|\overline{\boldsymbol{\alpha}}_{u,u}\|^2+\sum_{v\neq u}\frac{1}{\mathcal{G}}\sum_{k\in K_v}\sigma_k^2\|\boldsymbol{\alpha}_{u,v}\|^2+\sigma_\eta^2\mathbf{f}_u\mathbf{f}_u^H} \tag{6.10}$$

Where σ_k^2 denotes the chip variance of the k^{th} code. In a simple extension of beamforming with multiple users with different beamforming weight vectors, each UE makes the assumption that all users in DL have the same beamforming weight vectors and computes the ideal beamforming weight vector under this assumption. The BS however makes no attempt to group users with same beamforming weights. As a result, it is expected that the downlink capacity drops significantly.

Weight optimization by average interference criterion

Alternatively UE can anticipate that in reality, any of the four weights may be chosen by the other users in DL. Assuming that other users choose one of four beamforming weights with equal likelihood, it is reasonable to choose that beamforming weight which has the maximum SINR when averaged over all four hypothesis for the other users weights. Each UE therefore computes the ideal beamforming weight by plugging into (6.10), all possible combinations of weight vectors and feeds back the weight vector with the best average SINR over all the hypothesis for all the other users in DL. The idea is that while the true SINR at the receiver may still not be the same as expected SINR, the resulting SINR is higher than obtained by assuming the same beamforming weight is requested by all users scheduled in DL. Thus this beamforming vector must will perform better on average and increase the average data rate per user when compared to the simple multiuser beamforming case.

Cooperative beamforming

If the BS were to have the knowledge of the SINR seen by a particular user for all possible combinations of weight vectors applied at the base station, then, the BS can choose the optimal combination of weights that maximizes the downlink capacity. We call this cooperative beamforming because, in this case, all the users compute all possible SINRs corresponding to the weight vectors in the codebook. From (6.10) we see that for a given weight-vector, the SINR is highest when all other users also have the same beamforming weight-vector. Each user therefore feeds back as many SINRs as the codebook size. Thus it is a form of cooperation between the users and BS to maximize system capacity. In practice, this involves considerable amount of receiver processing and also a lot of feedback to the

BS. Nonetheless, the gains in such a case is worth investigating.

Scheduled beamforming

The practical and indeed the best solution to this problem with least complexity is for the BS to schedule in the DL, only those users that request the same beamforming weights. Each user assumes that same weights are applied to all codes in DL and computes the weight vector that maximizes the per code SINR. For this case, the user can then restore the orthogonality of all codes with the MMSE chip equalizer-correlator receiver. The per-code SINR for the u^{th} user is then given by

$$\frac{\sigma_k^2|\alpha_{u,u}^d|^2}{\frac{K}{\mathcal{G}}\sigma_k^2\|\overline{\boldsymbol{\alpha}}_{u,u}\|^2+\sigma_\eta^2\mathbf{f}_u\mathbf{f}_u^H} \tag{6.11}$$

The combination of scheduling at BS and the choice of weight vector that maximizes the individual SINR at the receiver results in maximization of DL capacity.

6.2 Multiuser D-TxAA

For MU-D-TxAA system, we consider 2 separate UEs with N_{rx} receive antennas each. In a MU-D-TxAA system, the BS transmits 2 transport blocks for as many users scheduled in DL. All codes of a single stream are assigned to one user and re-used across the two streams. From Fig. 6.2, we see that the transmit signal vector in downlink can be modeled as

$$\mathbf{x}[j]=\underbrace{\mathbf{W}}_{2\times 2}\mathbf{b}[j]=\mathbf{W}\cdot\sum_{k=1}^{K}s[j]c_k[j \mod \mathcal{G}]\mathbf{a}_k[n] \tag{6.12}$$

$\mathbf{W}=[\mathbf{w}_1\,\mathbf{w}_2]$ is the 2×2 unitary precoding matrix. The columns of $\mathbf{W}$ are made up of the beamforming weight vectors corresponding to the two downlink users. The symbol vector $\mathbf{a}_k[n]=[a_{1k}[n]\ a_{2k}[n]]^T$ represents two independent symbol streams belonging to two different users. The spreading codes are common to the two streams and so is the scrambling sequence $s[j]$.

6.2.1 Spatial Multiplexing Vs SDMA

In the spatial multiplexing context, there is only a single user in downlink and the precoding matrix corresponds to the weight vectors applied to the

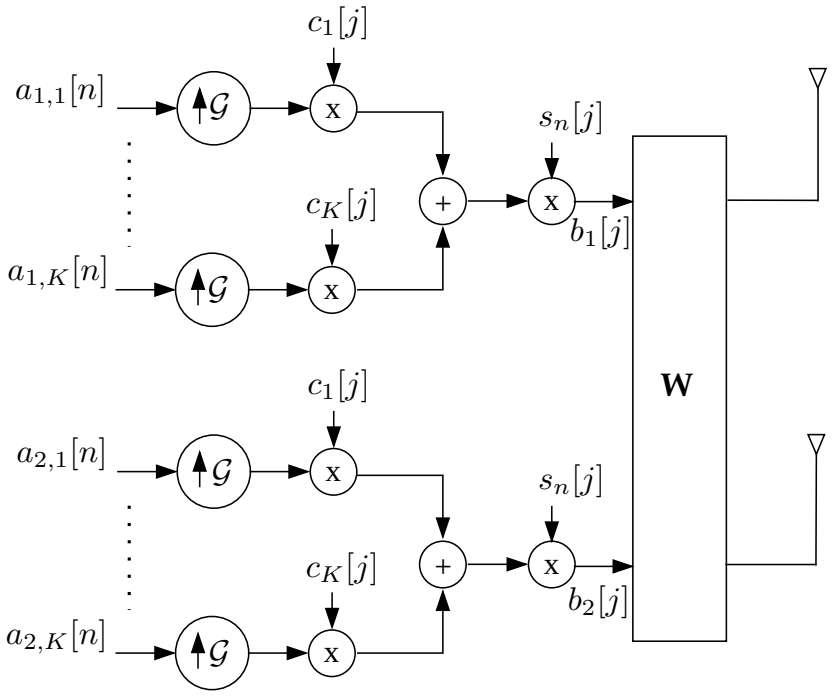

Figure 6.2: Multiuser D-TxAA transmit signal model.

two separate streams transmitted to the same user. For such a case, we can write the equalizer output as the sum of an arbitrarily scaled desired term and an error term

$$\widehat{\mathbf{x}}[j] = \mathbf{x}[j] - \widetilde{\mathbf{x}}[j]. \tag{6.13}$$

The error $\widetilde{\mathbf{x}}[j]$ is a zero-mean complex normal random variable. The error covariance matrix is denoted by $\boldsymbol{\mathcal{R}}_{\widetilde{x}\widetilde{x}}$.

In (6.13), an estimate of the chip sequence can be obtained after a further stage of processing where the precoding is undone to separate streams. The latter represented by $\mathbf{W}^H$ is a linear operation and can be carried out before or after despreading.

Under the assumption of a FIR signal model, the estimation error covariance matrices $\boldsymbol{\mathcal{R}}_{\widetilde{x}\widetilde{x}}$ (chip-level) and $\boldsymbol{\mathcal{R}}_{\widetilde{z}\widetilde{z}}$ (symbol-level) are derived in chapter 5. It can be shown that the SINR for the qth stream at the output of the output of the LMMSE chip equalizer/correlator is given by

$$SINR_q = \frac{\sigma_a^2}{\left(\mathbf{W}^H \boldsymbol{\mathcal{R}}_{\widetilde{z}\widetilde{z}} \mathbf{W}\right)_{qq}} - 1. \tag{6.14}$$

where σ_a^2 corresponds to the symbol variance.

In the SDMA context, the BS transmits a single stream for each of the two downlink users. The BS applies the precoding matrix $\mathbf{W}$ whose columns correspond to the weight vectors fed back by the two users. It is obvious that two users who feedback the same weight-vector cannot be scheduled simultaneously for transmission in the downlink. At the receiver, each UE receives both the streams but processes only the stream assigned to itself. In HSDPA, 2×2 unitary precoding is used, this implies that the two columns of the precoding matrix are orthogonal. Moreover, knowledge of a single column automatically fixes the other column of $\mathbf{W}$. Thus, the BS does not have to explicitly inform one UE of the weight vector applied for the other UE. The SINR for the stream assigned to the user in question is therefore the same as in (6.14)

6.3 Simulation results

In this section, we present Monte-Carlo simulation results and performance comparison of different beamforming strategies proposed in this chapter. We consider a multipath channel with a maximum delay spread L of 10-chips with uniform power in all channel taps. At any given time BS simultaneously serves 2 users. The beamforming weights are calculated to maximize the per-code SINR at the output of the equalizer correlator combination. Simulations were carried out for a fixed SNR at each receive antenna while keeping the total transmit power is normalized to 1. The cumulative distribution function of the sum-capacity upper-bound in DL is then used as a performance metric to compare different strategies. Depending on the number of independent transport blocks at the transmitter the other simulation parameters are given as below

6.3.1 TxAA

Each UE is assumed to have single receive antenna. Normally, each UE feeds back only its preferred weight vector index, only in case of cooperative-operative beamforming, it feeds back SINR values to the BS. For the sake of simplicity we assume that each UE is allocated 7 of the 15 codes in the DL all with the same power.

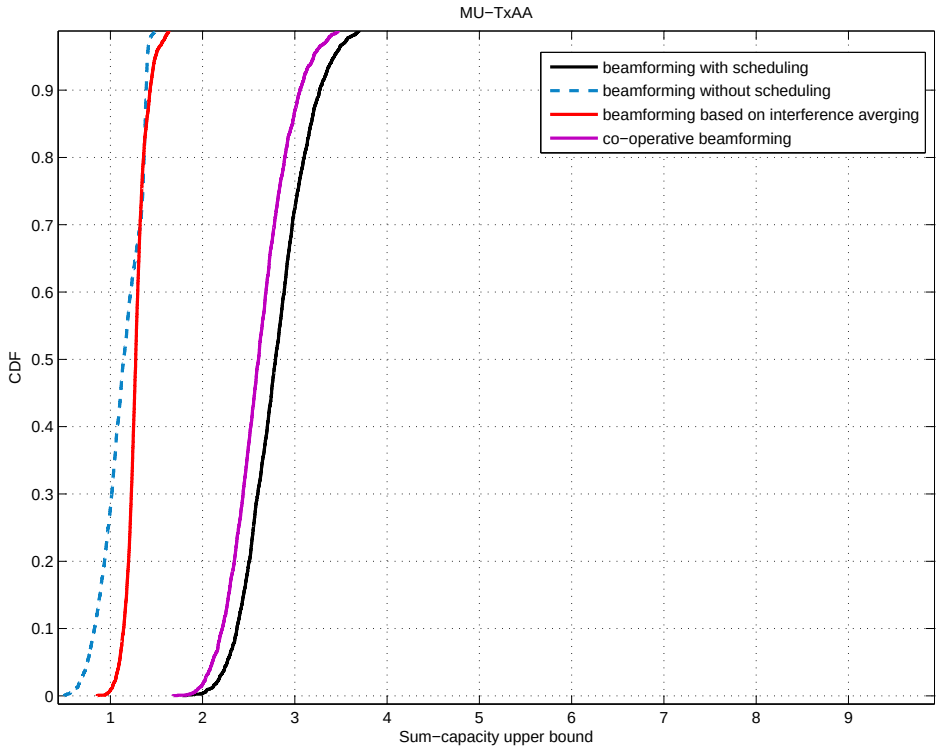

Figure 6.3: Performance of different beamforming schemes for MU-TxAA.

6.3.2 D-TxAA

Each independent transport block is assumed to be allocated to a different user. Thus all codes of a stream are allocated to one user. For SDMA with single antenna receivers, we assume users with orthogonal weights are scheduled together. For SDMA with 2-antenna receivers, users with different beamforming weight vectors are assumed to be scheduled together. In the spatial multiplexing case, a 2×2 MIMO system is assumed with all codes and both streams transmitted to a single user. Fig.6.3 compares the sum-capacity in the DL for the case of TxAA. The DL capacity is worst for the case of beamforming without scheduling. This is because of the inability of the receivers to effectively restore orthogonality for all codes and hence effectively mitigate MUI since they do not know the actual beamforming weight of the other user. When the beamforming weight is optimized by the average interference criterion, the weights are not just chosen based on the channel seen by each user, but also based on the capability of

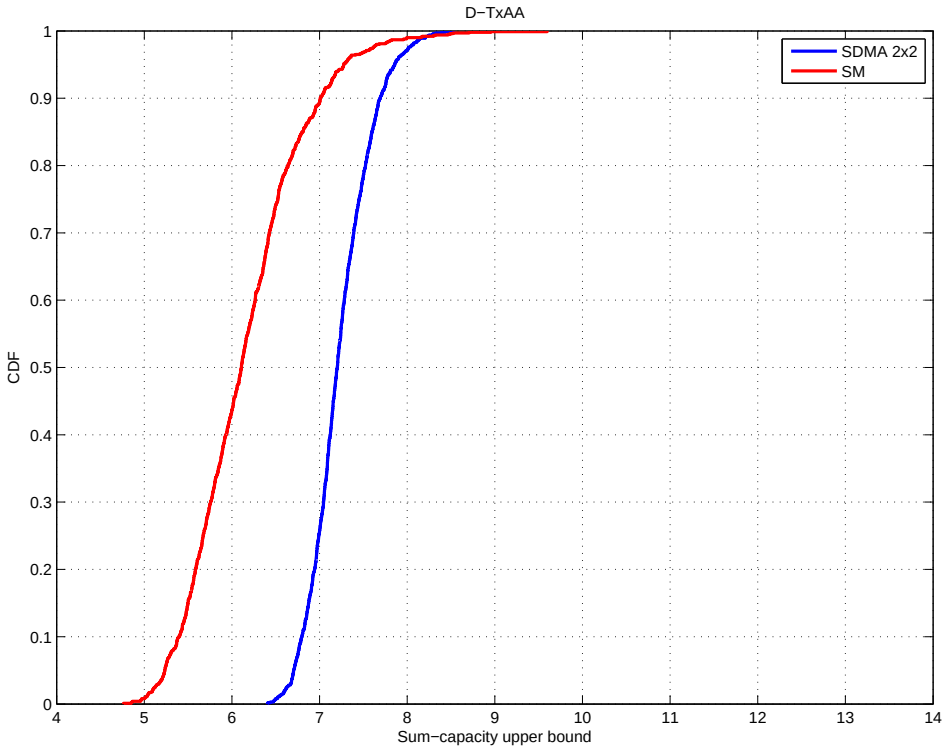

Figure 6.4: DL sum-capacity for MU-D-TxAA.

these weights to reduce the average multi user interference due to different beamforming weights of the other user. The downlink capacity is thus better than that in the case of simple multiuser beamforming. At the cost of an increase in complexity and feedback, cooperative-operative beamforming performs better than that of the earlier schemes, even so, it does not do better than scheduled beamforming because the UEs need not necessarily be assigned the weight vector that maximizes their individual SINR. Scheduled beamforming thus outperforms all the other schemes since in this case each user is able to effectively mitigate MUI due to the same beamformed channel seen by all codes in downlink. It should be noted that for the case where the total number of users in DL far exceed the number of users actually scheduled in the DL, the performance of cooperative-operative beamforming is expected to improve. In Fig.6.4, we compare the performance of D-TxAA in spatial multiplexing mode with that of the multiuser (SDMA) mode. Simulation results show that the DL sum-capacity is greater for the

case of SDMA with single stream transmission to both users.

Part II

Diversity

Chapter 7

Diversity gains in selective channels

7.1 Introduction

Practical wireless communication channels are prone to signal fading due to the presence of multiple signal paths (frequency selective channel) , time-varying nature of the channel (time selective channel) or both (time-and-frequency selective or the so called doubly selective channel). However, it is possible for the receiver to employ equalization techniques that optimally exploit the inherent diversity in these channels as a convenient counter-measure against fading. For instance, the frequency selectivity provides multipath diversity due to the presence of multiple independently fading components (diversity sources) in the channel. In block transmission systems, when the channel coherence time is shorter than the transmit block length, temporal variations of the channel provides Doppler diversity [36] which can be exploited by the receiver. Doubly selective channels offer joint multipath-Doppler diversity. Thus the total diversity in such channels is multiplicative in that, if the time selectivity is due to Q_s diversity sources and frequency selectivity is due to L_s diversity sources, the total diversity in the doubly selective channel is $Q_s L_s$.

The diversity-multiplexing tradeoff was introduced by Zheng and Tse

in [37] for the MIMO frequency-flat fading channel. This was extended in [38] to SISO frequency selective channel and an achievable scheme to achieve the optimal diversity multiplexing tradeoff was proposed when MLE is employed at the receiver. In [2], the authors used the Complex-Exponential Basis Expansion Model (CE-BEM) [39] and showed that for SISO time varying channels that can be modeled by the CE-BEM with $Q+1$ Fourier bases, the maximum achievable diversity is $Q+1$. For doubly selective channels with memory of order L and whose time variation can be similarly captured by $Q+1$ exponentials, the maximum achievable diversity gain is $(Q+1)(L+1)$. Furthermore, they introduced linear precoders that enable maximum likelihood equalization (MLE) to benefit from full channel diversity present in time selective only as well as doubly selective channels. The cost paid to enable full diversity reception is a loss in bandwidth efficiency due to the redundancy introduced by the precoders. However, MLE incurs a significant computational complexity. Motivated by the fact that linear equalizers (LE) are often preferred to non-linear equalizers due to their lower computational complexity (moreover, there is no error propagation as in DFEs) and by the fact that, both LE and DFE, only a limited degree of non-causality (delay) needs to be used (thereby, usually rendering the filters FIR), some initial simulation results on the diversity aspects of FIR LE appeared in an early paper [40]. Some results quantifying the performance of diversity gains of LE in frequency selective channels MMSE DFEs also appeared in [41]. In [42], it was shown that a DFE with unconstrained feedforward filter allows to attain the optimum diversity in the channel. For the MIMO frequency-flat fading channel, similar results were obtained with a linear MIMO prefilter and MMSE MIMO DFE. The analytical proof, for linearly precoded OFDM appeared about a decade later that the first results in [6] closely followed by [43] for single-carrier cyclic prefix (SC-CP) transmission. In [44] it was shown that for SC-CP, LE loses all diversity present in SISO/SIMO frequency selective channels in the classical outage-rate tradeoff, except at constant rate. The concept of *orthogonality defect* $\delta(\mathbf{H})$ [45, p. 140 Sec (5.3.3)] [46] which is a function of the effective channel matrix $\mathbf{H}$ (channel matrix premultiplied by the precoder) can also be used to compare the diversity gain of LE vis-à-vis the MLE. In particular, if $\delta^{-1}(\mathbf{H})$ can be bounded strictly away from 0, LE achieves the same diversity gain as MLE [47]. More recent published results for LE and MLE for the trailing zeros or the zero-padded (ZP) transmission in frequency selective channels appear in [3].

It is well known that the full diversity available in the channel can be

harnessed with appropriate precoders at the transmitters. A well designed precoder acts as a *diversity enabler* thus allowing receivers to benefit from channel diversity. In general, precoders introduce redundancy in the transmit symbols which can then be exploited at the receiver to achieve diversity gains[1]. In this part of the thesis we study diversity gains of non-MLE receivers for ZP-type precoders. One such precoder was proposed in [2] where the authors propose precoders that allow MLE to achieve full channel diversity in time-selective only (TS-only), frequency-selective only (FS-only) as well as time and frequency selective channels (doubly selective (DS) channels). In fact, the precoder in [2] that enables full diversity reception for DS channels can be interpreted as one that introduces a 2-level redundancy. Here, by levels, we actually mean domains. So a 2-level redundancy implies redundancy in 2 domains: time and frequency. This type of design can be seen as a generalization of a precoder that introduces a single-level redundancy in FS-only and TS-only channels (time domain only or frequency domain only for FS-only and TS-only channels respectively) in order to enable full diversity reception. It is obvious that, full diversity reception is also contingent on appropriate equalization strategy employed at the receiver. We broadly classify equalizers under three categories. LE, DFE and MLE. LE are the least complex of the three but their lack of complexity comes at a price of performance degradation as compared to the MLE which makes up the other end of the spectrum of equalizers whose optimality comes at the cost of very large computational complexity. In many aspects, DFE can be seen as a tradeoff between computational complexity and performance. Of course, one can imagine all kinds of *hybrid* equalizers that could be, for instance, part-LE and part-MLE. Indeed, we will propose such equalizers in the context of low-complexity but full diversity equalizers for doubly channels. Since it is known that LE can achieve full diversity in FS-only channels, based on the observation that the precoder for DS channels in [2] can be interpreted as a 2-level generalization of the precoder that introduces single-level redundancy in FS-only channels, it would seem that LE should also be able to exploit full channel diversity in DS channels with appropriate precoders. Based on the redundancy they introduce in the time and frequency domain, we classify the precoders into three categories. Precoders that introduce redundancy in both time and frequency domain are called *tall-tall* precoders, those that introduce redun-

[1] Introduction of redundancy is sufficient but not necessary to exploit channel diversity. For instance, in TS-only channels, constellation rotation precoders can be used to extract time-diversity without incurring any rate loss due to redundancy.

dancy only in time domain are called *square-tall* precoders and those that do not introduce redundancy in either time or frequency domain are called *square-square* precoders. We comment here that the term square-square is a little misleading in that it gives an impression of being a full rate (no precoding overhead) precoder In fact, this is not the case. The square-square precoders have a redundancy of the order of channel delay spread. This redundancy is essential, among other reasons, to null out IBI in the transmit symbol block.

7.1.1 Notations

In this part of the thesis, $\mathbf{F}$ and $\mathbf{F}^H$ are reserved respectively, for the normalized discrete Fourier transform (DFT) and its corresponding inverse discrete Fourier transform (IDFT) matrix. $[\mathbf{F}]_{n_1,n_2} = \sqrt{(1/N_1)}\exp(-j2\pi n_1 n_2/N_1)$. $\mathbf{Z}$ denotes the $P \times K$ matrix $[\mathbf{I}_{K\times K}\ \mathbf{0}_{G\times K}]^T$ and $\mathbf{C}$ the $P \times K$ matrix $[\mathbf{0}_{G\times(K-G)}\ \mathbf{I}_{G\times G};\ \mathbf{I}_{K\times K}]^T$, $P = K + G$. $\otimes$ represents the Kronecker product of matrices and $\oplus$ represents diagonal composition of matrices, for instance $\mathbf{A} = \{\mathbf{A}_1 \oplus \mathbf{A}_2\}$ implies a block diagonal matrix $\mathbf{A}$ with $\mathbf{A}_1$ and $\mathbf{A}_2$ constituting the diagonal blocks.

7.2 Signal model

We introduce here, the signal model that we shall follow throughout this part of the thesis. We first describe the channel model and the assumptions that we make about the behaviour of the channel.

7.2.1 Channel model

We will consider transmission over FS-only, TS-only and the more general case of DS channels. For the case of FS-only (TS-only) channels, we assume that the *effective* delay spread $\tau_{\max}$ (Doppler spread $f_{\max}$) is finite. In other words, the channel is approximately FIR (finite impulse response) in time (frequency) domain. The doubly selective channels that we consider are assumed to be *underspread*. i.e., their dispersion product $\tau_{\max} f_{\max} << 1$. Furthermore, the frequency selectivity of the channel is assumed to be due to a few dominant reflectors and time selectivity is due to changes in the transmission channel as a result of receiver movement. It is well known that the temporal variation of the channel taps in doubly selective channels with a finite Doppler spread can be captured by finite Fourier bases.

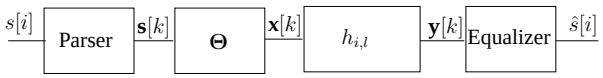

Figure 7.1: Block diagram of transmission model.

We therefore use CE-BEM [39] with $Q+1$ basis functions to model the time variation of each tap in a block duration. The basis coefficients remain constant for the block duration but are allowed to vary with every block. The time-varying channel for each block transmission is thus completely described by the $Q+1$ Fourier bases and $(Q+1)(L+1)$ coefficients. In general, $L = \lceil \tau_{\max}/T_s \rceil$ and Q is chosen such that $Q = \lceil f_{\max} M T_s \rceil$ where T_s is the sampling period. The coefficients themselves are assumed to be (possibly) correlated zero-mean complex Gaussian random variables. Using i as the discrete time (sample) index, we can represent the l-th tap of the channel in the k-th block

$$h_{i,l} = \sum_{q=0}^{Q} h_q(k,l) \exp j2\pi f_q i, \tag{7.1}$$

$l \in [0, L]$, $f_q = q/M$. In Sec. 7.2.2, we will use the doubly selective channel in the description of the transmission model. This is convenient, since the FS-only and the TS-only channels can be viewed as special cases of the channel model when Q and L are respectively set to zero.

7.2.2 Transmission model

In Fig. 7.1 we show the block diagram of the transmission model. The channel state information (CSI) is assumed known at the receiver. The transmitter is required to know only the Doppler/delay spread of the channel. At the transmitter, complex data symbols $s[i]$ are first parsed into N-length blocks.The n-th symbol in the k-th block is given by $[\mathbf{s}[k]]_n = s[kN+n]$ with $n \in [0, 1, ..., N-1]$. The elements of $[\mathbf{s}[k]]_n$ are chosen uniformly and independently across n, from a QAM constellation. Each block $\mathbf{s}[k]$ is precoded by a $M \times N$ matrix $\mathbf{\Theta}$ where $M \geq N$ and the resultant block $\mathbf{x}[k]$ is transmitted over the block fading channel. We consider a channel memory of order L. The corresponding receive signal is formed by collecting M samples at the receiver to form $\mathbf{y}[k] = [y(kM+0), y(kM+1), \ldots, y(kM+M-1)]^T$. When $M \geq L$, this block transmission system can be represented in matrix-vector notation as

$$\mathbf{y}[k] = \mathbf{H}_D[k;0]\mathbf{\Theta}\mathbf{s}[k] + \mathbf{H}_D[k;1]\mathbf{\Theta}\mathbf{s}[k-1] + \mathbf{v}[k], \tag{7.2}$$

where $\mathbf{v}[k]$ is a AWGN vector with $v[k] \sim \mathcal{CN}(0, \sigma_v^2)$ and is defined in the same way as $\mathbf{y}[k]$. Throughout our discussions, we shall assume, without any loss of generality, that $\sigma_v^2 = 1$. The transmit power is therefore the SNR. $\mathbf{H}_D[k;0]$ and $\mathbf{H}_D[k;1]$ are $M \times M$ matrices whose entries are given by $[\mathbf{H}_D[k;t]]_{r,s} = h_{(kM+r,tM+r-s)}$ with $t \in [0,1], r, s \in [0,...,M-1]$. Defining $\mathbf{D}[f_q]$ as a diagonal matrix whose diagonal entries are given by $[\mathbf{D}[f_q]]_{m,m} = e^{j2\pi f_q m}, m \in [0,1,...,M-1]$, and further defining $[\mathbf{H}_q[k;t]]_{r,s} = h_q(k, tM + r - s)$ as Toeplitz matrices formed of BEM coefficients, it is the possible to represent (7.2) as

$$\mathbf{y}[k] = \sum_{t=0}^{1} \sum_{q=0}^{Q} \mathbf{D}[f_q]\mathbf{H}_q[k;t]\mathbf{\Theta}\mathbf{s}[k-t] + \mathbf{v}[k]. \tag{7.3}$$

Throughout our analysis, the linear precoder $\mathbf{\Theta}$ applied at the transmitter is such that all inter-block-interference (IBI) is eliminated. Thus the received signal is simplified further as

$$\mathbf{y}[k] = \sum_{q=0}^{Q} \mathbf{D}[f_q]\mathbf{H}_q[k;0]\mathbf{\Theta}\mathbf{s}[k] + \mathbf{v}[k]. \tag{7.4}$$

Chapter 8

Theoretical analysis of diversity gain

8.1 Diversity analysis of equalizers

Our interest is in investigating diversity aspects of equalizers for precoded transmission in dispersive channels. The linear precoder $\boldsymbol{\Theta}$ eliminates all inter-block-interference (IBI) in the transmit symbol block. Furthermore, we consider block-by-block processing at the receiver. This implies that the error statistics of each block are independent of the previous (or subsequent) blocks. We can therefore drop the block index $[k]$ in the interest of notational simplicity and represent the channel input/output model by the simple equation

$$\boldsymbol{y} = \boldsymbol{H}\boldsymbol{s} + \boldsymbol{v}. \tag{8.1}$$

In (8.1), $\boldsymbol{y},\ \boldsymbol{v} \in \mathbb{C}^M$, $\boldsymbol{s} \in \mathbb{C}^N$ and $\boldsymbol{H} \in \mathbb{C}^{M\times N}$. We will follow the same trend in the rest of the chapter. Block indices will be used insofar as the relationship between the received signal vector and the transmit signal vector through the channel parameters are made unambiguous and clear. Once that is accomplished, the block indices will be dropped.

At the receiver, the symbol vector $\boldsymbol{y}$ serves as the input to the channel

equalizer $\boldsymbol{G}$ which yields the output estimate $\hat{\boldsymbol{y}}$

$$\hat{\boldsymbol{y}} = \boldsymbol{s} + \boldsymbol{n}, \tag{8.2}$$

with $\boldsymbol{n} = \boldsymbol{G}\boldsymbol{v}$ and $\hat{\boldsymbol{y}},\ \boldsymbol{n} \in \mathbb{C}^N$. This is followed by symbol-by-symbol detection on $\hat{\boldsymbol{y}}$ given by

$$\hat{s}_n = \arg\min_{s_n \in \mathcal{S}} \|s_n - \hat{y}_n\|,\ \forall n \in \{0, 1, \ldots, (N-1)\}\,. \tag{8.3}$$

This approach, albeit suboptimal, is preferred in practice to the maximum likelihood (ML) approach

$$\hat{\boldsymbol{s}}_{ML} = \arg\min_{\boldsymbol{s} \in \mathcal{S}^N} \|\boldsymbol{s} - \boldsymbol{y}\|,$$

for large N, due to the fact that the complexity of detection in (8.3) scales linearly with N, whereas that of (8.4) is exponential in N.
In all our analysis, we use the following definition of diversity gain d associated with an equalizer [37].

Definition 8.1.1 *The diversity gain d of an equalizer $\boldsymbol{G}$ is defined as*

$$d \triangleq -\lim_{\mathsf{SNR}\to\infty} \frac{\mathbb{P}_{\mathsf{e}}(\mathsf{SNR})}{\log \mathsf{SNR}}. \tag{8.4}$$

$\mathbb{P}_{\mathsf{e}}(\mathsf{SNR})$ denotes the average probability of error as a function of SNR. Instead of directly dealing with $\mathbb{P}_{\mathsf{e}}(\mathsf{SNR})$, it is more convenient to resort to pairwise error probability (PEP) analysis. Since $\mathbb{P}_{\mathsf{e}}(\mathsf{SNR})$ can be bounded from the above in terms of the PEP, $\mathbb{P}_{\mathsf{e}}(\mathsf{SNR})$ asymptotically ($\mathsf{SNR} \to \infty$) behaves the same as the PEP. In other words, to show that an equalizer $\boldsymbol{G}$ achieves a diversity gain d, it suffices to show that the slope of the PEP curve on a $\log - \log$ scale is $-d$. Moreover, a PEP based analysis is additionally motivated by the fact that it is independent of the symbol constellation. In addition to PEP based analysis, we will also use *outage probability* $\mathbb{P}_{\mathsf{out}}$ based analysis to compute the diversity gain of $\boldsymbol{G}$. $\mathbb{P}_{\mathsf{out}}$ is a particularly important performance criterion in fading channels and is defined as the probability that the instantaneous SNR at the output of the equalizer $\boldsymbol{G}$ is less than a pre-specified reference level $\mathsf{SNR}_{\mathsf{ref}}$ (a design parameter). i.e.,

$$\mathbb{P}_{\mathsf{out}} \triangleq \mathbb{P}(0 \leq \mathsf{SNR}_{\mathsf{dp}} \leq \mathsf{SNR}_{\mathsf{ref}})$$

where $\mathsf{SNR}_{\mathsf{dp}}$ is the *decision point* SNR or the SNR at the output of the equalizer. Please note that we use the term SNR a little loosely here. To be precise, one speaks of the SINR at the output of the equalizer in order to make

allowance for any residual interference left behind by the equalizer (for instance in the MMSE LE). While we will make this distinction when we deal with MMSE designs later in this chapter, we do not make any attempt to do so here since the idea here is to clarify what we mean by $\mathbb{P}_{\text{out}}$.
Our interest in choosing PEP and $\mathbb{P}_{\text{out}}$ based analysis for diversity gains is not without reason. It is known that both the asymptotic behaviour of $\mathbb{P}_{\text{e}}$ and $\mathbb{P}_{\text{out}}$ can be parameterized by the diversity and coding gains of $\boldsymbol{G}$ [48]. Indeed, as as function of SNR, as $\mathsf{SNR} \to \infty$ both can be characterized as

$$\mathbb{P}_{\text{e}} \simeq (c_{\text{e}}\mathsf{SNR})^{d_{\text{e}}} \ , \mathbb{P}_{\text{out}} \simeq (c_{\text{out}}\mathsf{SNR})^{d_{\text{out}}}$$

where d_{e} and d_{out} are the diversity gains associated respectively with the $\mathbb{P}_{\text{e}}$ and $\mathbb{P}_{\text{out}}$ curves and the coding gains.
A common approach to analyze the diversity gain (of an equalizer) consists of following a two-step procedure.
Step 1: Find the exact expression or an approximation (upperbound) of the PEP/$\mathbb{P}_{\text{out}}$ for an instantaneous channel realization $\boldsymbol{H}$. The dependence of the PEP/$\mathbb{P}_{\text{out}}$ on the instantaneous channel realization manifests itself through the equalizer $\boldsymbol{G}$ which itself is a function of $\boldsymbol{H}$. For any two vectors $\boldsymbol{s}_k$ and $\boldsymbol{s}_l \in \mathcal{S}^N$ the pairwise error event that $\boldsymbol{s}_l$ $l \neq k$ is falsely detected given that $\boldsymbol{s}_k$ was transmitted over the instantaneous channel is $\boldsymbol{H}$ is defined as [49]

$$\begin{aligned} E_{lk} &\triangleq (\|\hat{\boldsymbol{y}} - \boldsymbol{s}_l\| \leq \|\hat{\boldsymbol{y}} - \boldsymbol{s}_k\| | \boldsymbol{H}) \\ &= (\Re(\boldsymbol{n}^H \boldsymbol{e}_{lk}) \geq \frac{d_{lk}}{2} \mid \boldsymbol{H}) \\ &= (w \geq \frac{d_{lk}}{2} | \boldsymbol{H}). \end{aligned}$$

Where $d_{lk} = \|\boldsymbol{s}_l - \boldsymbol{s}_k\|$ is the Euclidean distance induced by the inner product and a true mathematical distance metric. $\boldsymbol{e}_{lk} \triangleq (\boldsymbol{s}_l - \boldsymbol{s}_k)/\|\boldsymbol{s}_l - \boldsymbol{s}_k\|$ is the unit vector in the direction of $(\boldsymbol{s}_l - \boldsymbol{s}_k)$. In the last line we substitute the random variable $w = \Re(\boldsymbol{n}^H \boldsymbol{e}_{lk})$. The conditional PEP can therefore be

expressed as

$$\begin{aligned} P(\boldsymbol{s}_k \rightarrow \boldsymbol{s}_l \mid \boldsymbol{H}) &= P(E_{lk}|\boldsymbol{H}) \\ &= P(w \geq \frac{d_{jk}}{2}|\boldsymbol{H}) \\ &= \frac{1}{\sqrt{2\pi\sigma_w^2}} \int_{\frac{d_{lk}}{2}}^{\infty} \exp(-w^2/2\sigma_w^2) dw \\ &= Q\left(\frac{d_{lk}}{4\sigma_w^2}\right) \\ &\leq Q\left(\frac{d_{min}}{4\sigma_w^2}\right) \end{aligned} \tag{8.5}$$

where, in the third line, we have exploited the fact that $\mathbb{E}[w] = 0$ and σ_w^2 corresponds to the variance of w. In the fourth line, $Q(.)$ represents the error function and in the final line we upper bound the PEP by the worst case error probability by taking the minimum distance d_{min} amongst all "codeword" pairs in $\mathcal{S}^N$

Step 2: Average this expression over the channel statistics and use the SNR exponent of this average to compute the diversity gain of the equalizer $\boldsymbol{G}$. If the exact expression for the PEP/$\mathbb{P}_{\text{out}}$ is not available then use appropriate bounds in this step.

We now list some identities and relations that we shall use in most of our analysis.

Identity 1 [I 1]: For a positive definite matrix $\mathbf{M}$ of order N, due to the application of the arithmetic-geometric mean inequality for positive numbers, the trace and the determinant are related as

$$\frac{\mathrm{tr}(\mathbf{M})}{N} \geq \det(\mathbf{M})^{1/N}$$

Identity 2 [I 2]: For any positive definite matrix $\mathbf{M}$ of order N, the determinant is upperbounded as

$$\det(\mathbf{M}) \leq \det(\mathrm{diag}(\mathbf{M}))$$

The above two identities are stated here without proof. However, henceforth proofs of all the lemmas/theorems that are used in this chapter are provided in 8.4 at the end of this chapter. In addition, 8.4 also contains alternate proofs of full diversity gains of LE in selective channels.

Lemma 8.1.2 *Given a $M \times N$ matrix $\boldsymbol{H}$ with $M \geq N$ of full column rank. The square of the Frobenius norm $\|\boldsymbol{G}\|^2$ of the pseudo-inverse $\boldsymbol{G} = (\boldsymbol{H}^H\boldsymbol{H})^{-1}\boldsymbol{H}^H$ is*

upperbounded as

$$(\det(\boldsymbol{H}^H\boldsymbol{H}))^{1/N} \geq \frac{N}{\|\boldsymbol{G}\|^2}$$

Lemma 8.1.3 *When $\boldsymbol{G}$ is an MMSE-ZF equalizer. Assuming the received signal model to be (8.1) and the equalizer output to be given as in (8.2) σ_w^2 conditioned on the channel realization is given by*

$$\sigma_w^2|\boldsymbol{H} = \mathbb{E}[|\Re(\boldsymbol{n}^H\boldsymbol{e}_{lk})|^2 \mid \boldsymbol{H}] = \frac{1}{2\mathsf{SNR}}\|\boldsymbol{G}^H\boldsymbol{e}_{lk}\|^2. \tag{8.6}$$

With this, we proceed to the next section where we study linear equalizers for “tall" or “tall-tall" precoded transmissions.

8.2 Diversity aspects of linear equalization for selective channels

In this section we investigate linear equalization techniques and show that linear equalizers (LE) collect full diversity offered by selective channels. The linear precoder applied at the transmitter introduces redundancy in the transmit block to extract diversity inherent in these channels. For 1-dimensional (1-D) dispersive channels (time selective only or frequency selective only channels), we shall see that redundancy proportional to the *dispersion spread* i.e., the region over which the channel energy experiences dispersion, suffices to allow LE to capture all the diversity present in the channel. Whereas, for the case of doubly selective channels, full diversity with LE comes at a price of a redundancy introduced at the transmitter in both time *and* frequency domains.

8.2.1 Linear MMSE and MMSE-ZF equalizers

Almost all of the analysis in this section is for the MMSE-ZF linear equalizer. We note however that the MMSE-ZF and MMSE processing can be related as follows. Let $\hat{\boldsymbol{y}}_{MMSE}$ and $\hat{\boldsymbol{y}}_{MMSE-ZF}$ represent the output of the MMSE and MMSE-ZF equalizer respectively. Then

$$\begin{aligned}
\hat{\boldsymbol{y}}_{MMSE-ZF} &= (\boldsymbol{H}^H\boldsymbol{H})^{-1}\boldsymbol{H}^H\boldsymbol{y} \\
\hat{\boldsymbol{y}}_{MMSE} &= (\tilde{\boldsymbol{H}}^H\tilde{\boldsymbol{H}})^{-1}\tilde{\boldsymbol{H}}^H\tilde{\boldsymbol{y}},\ \tilde{\boldsymbol{H}} = \begin{bmatrix} \boldsymbol{H} \\ \sigma_v^2\boldsymbol{I}_N \end{bmatrix},\ \tilde{\boldsymbol{y}} = \begin{bmatrix} \boldsymbol{y} \\ \boldsymbol{0}_N \end{bmatrix}
\end{aligned}$$

where $\boldsymbol{I}_N$ is an identity matrix of order N and $\mathbf{0}_N$ is the all zero column vector of length N. Since the MMSE-ZF and MMSE equalizers share the same structure. The analysis for the MMSE-ZF in this section can be extended in a straightforward manner to the MMSE equalizers. The sole exception will be the case of DFE, which we will address in the section that discusses the diversity gain of DFE.

8.2.2 Frequency selective only channel

Consider block transmission over a finite impulse response (FIR) frequency selective (FS) channel. The overall channel (the cascade of the physical channel and pulse shaping filters at the transmitter and receiver) corresponding to the k-th block transmission interval can be modeled in the time domain, with an discrete time channel impulse response vector $\mathbf{h}$ of order L at the baseband level. The coefficients $\mathbf{h} = [h(k,0), h(k,1), \ldots, h(k,L)]^T$, are constant for the duration of the block transmission interval (MT_s) but may vary across blocks.
The precoder $\mathbf{\Theta}_F$ for FS-only channels that we consider here is

$$\mathbf{\Theta}_F = \mathbf{Z}, \tag{8.7}$$

where $\mathbf{Z}$ is $M \times N$ and $M - N \geq L$. Such a transmission system is called the zero padded block transmission (ZP-BT) and is a special case of linearly precoded OFDM (LP-OFDM) [6] $\tilde{\mathbf{\Theta}} = \mathbf{CP}$ where $\mathbf{C}$ is the $M' \times M$ cyclic prefix insertion matrix with $M' - M \geq L$ and $\mathbf{P} = \mathbf{Z}$. Obviously, ZP-BT is a more efficient transmission system compared to LP-OFDM since the minimum redundancy in ZP-BT is L, while that of LP-OFDM is $2L$. For the purpose of diversity analysis of in frequency selective only (FS-only) channels, we look at the ZP-BT system.

The received signal representation for transmission over a frequency selective channel with $\mathbf{\Theta}_F$ applied at the transmitter is obtained by setting $Q = 0$ (and also dropping the q-index) in (7.4) as

$$\mathbf{y}_F[k] = \mathbf{H}_F[k;0]\mathbf{\Theta}_F\mathbf{s}[k] + \mathbf{H}_F[k;1]\mathbf{\Theta}_F\mathbf{s}[k-1] + \mathbf{v}[k] \tag{8.8}$$

The delay spread of the channel introduces inter-block-interference (IBI) at the receiver and is represented by the second term on the RHS of (8.8). $\mathbf{H}_F[k;1]$ is a strictly upper-triangular matrix with non-zero elements in only the last $M - L$ columns of the matrix. However, zero-padding at the transmitter completely eliminates IBI ($\mathbf{H}_F[k;1]\mathbf{\Theta}_F = 0$) and the received signal

can now be expressed as

$$\mathbf{y}_{F}[k] = \mathbf{H}_{F}[k;0]\mathbf{\Theta}_{F}\mathbf{s}[k] + \mathbf{v}[k]. \tag{8.9}$$

The effective channel seen at the receiver due to precoding at the transmitter ($\mathbf{H}_{F}[k;0]\mathbf{\Theta}_{F}$), is a $M \times N$ Toeplitz matrix with $[h(k,0), h(k,1), \ldots, h(k,L), \mathbf{0}_{1\times M-L-1}]^{T}$ as its first column. In the diversity analysis that follows, we shall drop the block index k.

Diversity analysis of LE in FS-only channels

Dropping the block index and absorbing the precoder into the channel matrix we rewrite (8.9) as

$$\boldsymbol{y}_{F} = \boldsymbol{H}_{F}\boldsymbol{s} + \boldsymbol{v}. \tag{8.10}$$

For ZP-BT in frequency selective channels, it is known that the maximal diversity of the channel is $L+1$ when the channel coefficients $h(l)$ (note that here too, we drop the block index) are drawn from a Gaussian distribution and are independent of each other. It is also known [6] that $\mathbf{\Theta}_{F}$ enables a minimum mean squared error zero forcing (MMSE-ZF) LE to achieve this maximal diversity. Denote the MMSE-ZF equalizer by $\boldsymbol{G}_{F}$. Then from (8.10),

$$\boldsymbol{G}_{F} = (\boldsymbol{H}_{F}^{H}\boldsymbol{H}_{F})^{-1}\boldsymbol{H}_{F}^{H}. \tag{8.11}$$

The proof that MMSE-ZF achieves maximum multipath diversity was given in [6]. We provide a brief sketch of the proof here and point the interested reader to [6] for details. First, an upperbound of the PEP conditioned on the channel coefficients $\boldsymbol{h}_{F}^{T} = [h(0), h(1), \ldots, h(L)]$ is derived. This PEP is dependent on $\|\boldsymbol{G}_{F}\|^{-2}$ due to the effect of the MMSE-ZF equalizer on the variance of the noise at the equalizer output. Next, it is shown that if there exists *a* left inverse $\boldsymbol{G}_{\star}$ of $\boldsymbol{H}_{F}$ such that $\|\boldsymbol{G}_{\star}\|^{-2} \geq c\|\boldsymbol{h}_{F}\|^{2}$ for some $c > 0$ and independent of $\boldsymbol{h}$ then the minimum norm property of the pseudo-inverse $\boldsymbol{G}_{F}$ ensures that it achieves the diversity gain $(L+1)$ when the channel coefficients are independent. The final step is then a proof of existence of $\boldsymbol{G}_{\star}$ by construction.

8.2.3 Time selective only channel

We now consider the case of block transmission in time-selective (TS) only channels. The time-selective channel is modeled using BEM by setting $L = 0$. The time-variation of the single channel-tap is captured by $Q+1$ BEM

coefficients $h_q(k)$. Since the channel has no delay-spread, it does not induce IBI. The $M \times N$ precoder $\mathbf{\Theta}_T$ applied at the transmitter, belongs to the class of precoders in (8.7). In particular, $\mathbf{\Theta}_T = \mathbf{F}^H\mathbf{Z}$, where $\mathbf{F}$ is a square matrix of order M. Analogous to the case of the frequency selective channel, $\mathbf{Z}$ is $M \times N$ and $M - N \geq Q$. Consequently, we can express the *frequency domain* representation of the received signal vector as

$$\mathbf{y}_T[k] = \mathbf{F}\sum_{q=0}^{Q} h_q(k)\mathbf{D}[f_q]\mathbf{\Theta}_T\mathbf{s}[k] + \mathbf{F}\mathbf{v}_[k]. \tag{8.12}$$

Let

$$\mathbf{H}_T \triangleq \mathbf{F}\sum_{q=0}^{Q} h_q(k)\mathbf{D}[f_q]\mathbf{\Theta}_T. \tag{8.13}$$

Then, $\mathbf{H}_T$ in (8.13) is the frequency domain dual of the channel-precoder cascade in (8.9) is a $M \times N$ Toeplitz matrix with $[h_0(k), h_1(k), \ldots, h_Q(k), \mathbf{0}_{1\times M-Q-1}]^T$ as its first column. Following the trend of the previous section, we will drop the block index for the diversity analysis.

Diversity analysis of LE in TS-only channels

Given that $\mathbf{H}_T$ is Toeplitz and the frequency domain dual of $\mathbf{H}_F$ with $\boldsymbol{h}_T^T = [h_0, h_1, \ldots, h_Q]$, the proof of full diversity gain of $\boldsymbol{G}_T$ given by

$$\boldsymbol{G}_T = (\boldsymbol{H}_T^H\boldsymbol{H}_T)^{-1}\boldsymbol{H}_T^H$$

is immediate. However, different to the proof method of [6] we provide here a more direct proof that the diversity gain of MMSE-ZF for such a transmission scheme is $(Q+1)$ when the channel coefficients are independent (full Doppler diversity) and that in general, $d = \mathrm{rank}(\mathbb{E}[\boldsymbol{h}_T\boldsymbol{h}_T^H])$. This method also serves to provide an interesting link to concepts from linear prediction theory. For this, we will need the following lemma:

Lemma 8.2.1 *For $\mathbf{H}_T$ defined in (8.13). $\det(\boldsymbol{H}_T^H\boldsymbol{H}_T)^{1/N}$ is lowerbounded by $c_T\|\boldsymbol{h}_T\|^2$ for some $c_T > 0$ independent of $\boldsymbol{h}_T$*

The first step is to express the PEP as a function of $\mathbf{G}_T$. Accordingly, substituting $\mathbf{G}_T$ in (8.6) we have,

$$\sigma_w^2|\boldsymbol{H}_T = \mathbb{E}[|\Re(\boldsymbol{n}^H\boldsymbol{e}_{lk})|^2|\boldsymbol{H}_T] = \frac{1}{2\mathsf{SNR}}\|\boldsymbol{G}_T^H\boldsymbol{e}_{lk}\|^2 \leq \frac{1}{2\mathsf{SNR}}\|\boldsymbol{G}_T\|^2\,\|\boldsymbol{e}_{lk}\|^2.$$

Therefore, (8.5) for the frequency domain dual of ZP-BT for transmission over TS-only channels is given by

$$\begin{aligned} P(\boldsymbol{s}_k \to \boldsymbol{s}_l|\boldsymbol{H}_T) &= Q\left(\frac{d_{lk}}{\sqrt{2\mathsf{SNR}^{-1}\|\boldsymbol{G}_T^H \boldsymbol{e}_{lk}\|^2}}\right) \\ &\leq Q\left(\frac{d_{lk}}{\sqrt{2\mathsf{SNR}^{-1}\|\boldsymbol{G}_T\|^2}}\right) \\ &\leq Q\left(\frac{d_{min}}{\sqrt{2\mathsf{SNR}^{-1}\|\boldsymbol{G}_T\|^2}}\right) \\ &\leq Q\left(d_{min}\sqrt{\frac{\mathsf{SNR}\det(\boldsymbol{H}_T^H\boldsymbol{H}_T)^{1/N}}{2N}}\right) \\ &= Q\left(d_{min}\sqrt{\frac{\mathsf{SNR}c_T\|\boldsymbol{h}_T\|^2}{2N}}\right) \\ &\leq \exp\left(\frac{-d_{min}^2\mathsf{SNR}c_T\|\boldsymbol{h}_T\|^2}{4N}\right) \end{aligned} \tag{8.14}$$

Where we have used the fact that the $Q(.)$ function is a monotonically decreasing function of it's argument to obtain a series of upperbounds for the $Q(.)$ function in the first line. The second line exploits the the fact that e_{lk} is unit-norm. The third line is due to the substitution of the minimum distance and the fourth is due to Lemma 8.1.2. The inequality on the fifth line follows from the result of Lemma 8.2.1 and the final inequality is due to the Chernoff bound.
What remains is to average (8.14) over the channel distribution. To allow for correlated channel coefficients we state the following. Let $\boldsymbol{h}_T$ be given by

$$\boldsymbol{h}_T = \boldsymbol{R}_T^{1/2}\bar{\boldsymbol{h}}_T \ , \bar{\boldsymbol{h}_T}^T = [\bar{h}_1\bar{h}_2\ldots\bar{h}_{Q_s}]$$

Such that $\boldsymbol{R}_T = \mathbb{E}[\boldsymbol{h}_T\boldsymbol{h}_T^H]$ and $Q_s = \operatorname{rank}\boldsymbol{R}_T$ and $\bar{h}_q$ are i.i.d Gaussian. i.e., $\boldsymbol{h}_T$ has Q_s diversity sources. Then averaging (8.14) over the channel

distribution we have

$$\begin{aligned}
\mathbb{E}_{\boldsymbol{H}_T}\left[\exp\left(\frac{-d_{min}^2 \mathsf{SNR}\|\boldsymbol{h}_T\|^2}{4N}\right)\right] &= \mathbb{E}_{\boldsymbol{H}_T}\left[\exp\left(\frac{-d_{min}^2 \mathsf{SNR}\bar{\boldsymbol{h}}_T^H \mathbf{R}_T \bar{\boldsymbol{h}}_T}{4N}\right)\right] \\
&= \mathbb{E}_{\boldsymbol{H}_T}\left[\exp\left(\frac{-d_{min}^2 \mathsf{SNR}(\mathbf{U}^H\bar{\boldsymbol{h}}_T)^H \boldsymbol{\Lambda}\mathbf{U}^H\bar{\boldsymbol{h}}_T}{4N}\right)\right] \\
&= \mathbb{E}_{\boldsymbol{H}_T}\left[\exp\left(-d_{min}^2 \mathsf{SNR}\sum_{q=1}^{Q_s}\lambda_q|\bar{h}_q|^2/4N\right)\right] \\
&= \prod_{q=1}^{Q_s}\left(\frac{1}{1+K\mathsf{SNR}\lambda_q}\right),\ K=\frac{d_{min}^2}{4N} \\
&= (K\mathsf{SNR})^{-Q_s}\prod_{q=1}^{Q_s}\left(\frac{1}{\lambda_q}\right) \qquad (8.15)
\end{aligned}$$

Where, in the second line $\mathbf{U}\boldsymbol{\Lambda}\mathbf{U}^H$ represents the eigen-decomposition of $\mathbf{R}_T$, λ_q are its eigenvalues, and the third line exploits the fact that the distribution of $\bar{\boldsymbol{h}}$ is invariant to a unitary transformation. The fourth line is due to the expression for the moment generating function $\mathbb{E}[\exp(KX)] = (1-K)^{-1}$ for $K < 1$ and a unit mean random variable X. The final line uses the high SNR approximation. The exponent of the SNR then gives us the diversity gain of $\boldsymbol{G}_T$. Note that $d = Q+1$ when coefficients of $\boldsymbol{h}_T$ are independent.

8.2.4 Doubly selective channels

We now look at the case of block transmission in doubly selective channels. The channel is assumed to be of order L and the time-variation of each channel tap within a block is captured by $Q+1$ complex exponential basis functions. The k-th receive block is then represented as in Eq (7.4) which we reproduce here for clarity.

$$\mathbf{y}[k] = \sum_{t=0}^{1}\sum_{q=0}^{Q}\mathbf{D}[f_q]\mathbf{H}_q[k;t]\boldsymbol{\Theta}\mathbf{s}[k-t] + \mathbf{v}[k], \qquad (8.16)$$

The precoder applied at the transmitter is expressed in matrix form by $\boldsymbol{\Theta}$. The precoder for doubly selective channels is related to that of the FS-only and TS-only channels as

$$\boldsymbol{\Theta} = \boldsymbol{\Theta}_T \otimes \boldsymbol{\Theta}_F, \qquad (8.17)$$

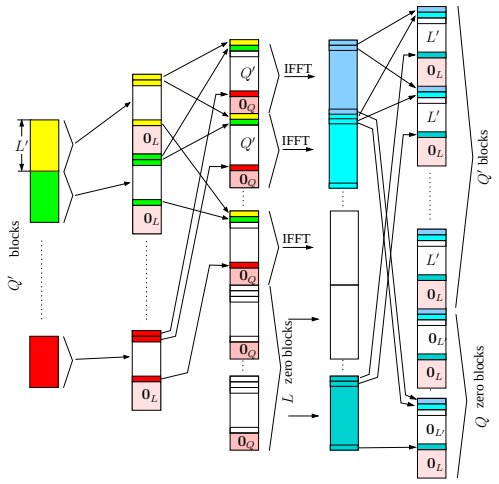

Figure 8.1: Precoding operation.

where $\mathbf{\Theta}_T = \mathbf{F}_{P+Q}\mathbf{Z}_1$, $\mathbf{\Theta}_F = \mathbf{Z}_2$. $\mathbf{Z}_1$ is $(P+Q)\times P$ and $\mathbf{Z}_2$ is $(K+L)\times K$. The block length M is therefore $(P+Q)(K+L)$ and $\mathbf{s}$ is $N\times 1$ with $N = PK$. This precoder was proposed in [2] and was shown to enable diversity order of $(Q+1)(L+1)$ for ML receivers in doubly selective channels. The operation of $\mathbf{\Theta}$ on $\mathbf{s}[k]$ is explained as follows. First, the N-length block is parsed into P blocks of K symbols. Next, L zero-pads are appended to each of these P blocks in an intermediate step to form P blocks of $K+L$ symbols. Next a set of Q zero-blocks of length $K+L$ are appended to this intermediate block vector to form P-length vector $\widetilde{\mathbf{x}}[k]$ consisting of $P+Q$ blocks of length $K+L$. A block IFFT operation is now performed on $\widetilde{\mathbf{x}}[k]$ to form the precoded transmit symbol vector $\mathbf{x}[k]$ which is transmitted over the doubly selective channel. The above series of operations are compactly represented in the following equations

$$\widetilde{\mathbf{x}}[k] = (\mathbf{Z}_1 \otimes \mathbf{Z}_2)\mathbf{s}[k], \tag{8.18}$$

$$\mathbf{x}[k] = (\mathbf{F}_{P+Q}^H \otimes \mathbf{I}_{K+L})\widetilde{\mathbf{x}}[k] = \mathbf{\Theta}\mathbf{s}[k], \tag{8.19}$$

Fig. 8.1 provides more insight into subtleties of the precoding operation. In (8.16), $\mathbf{H}_q[k;1]\mathbf{\Theta}\mathbf{s}[k-1] = 0$ due to $\mathbf{Z}_2$. As a result, the received block can now be represented as

$$\mathbf{y}[k] = \sum_{q=0}^{Q} \mathbf{D}[f_q]\mathbf{H}_q[k;0]\mathbf{\Theta}\mathbf{s}[k] + \mathbf{v}[k], \tag{8.20}$$

Using standard Kronecker product identities, one can show that

$$\mathbf{H}_q[k;0]\mathbf{\Theta} = \mathbf{F}_{P+Q}^H \mathbf{Z}_1 \otimes \widetilde{\mathbf{H}}_q[k;0]\mathbf{Z}_2, \tag{8.21}$$

where $\widetilde{\mathbf{H}}_q[k;0]$ is a $(K+L)\times(K+L)$ Toeplitz matrix formed by the first $(K+L)$ rows and columns of $\mathbf{H}_q[k;0]$. (8.20) can then be re-written as

$$\mathbf{y}[k] = \sum_{q=0}^{Q} \mathbf{D}[f_q]\left(\mathbf{F}_{P+Q}^H \mathbf{Z}_1 \otimes \widetilde{\mathbf{H}}_q[k;0]\mathbf{Z}_2\right)\mathbf{s}[k] + \mathbf{v}[k]. \tag{8.22}$$

Furthermore, we decompose $\mathbf{D}[f_q]$ as

$$\mathbf{D}[f_q] = \mathbf{D}_{P+Q}[f_q(K+L)] \otimes \mathbf{D}_{K+L}[f_q]. \tag{8.23}$$

(8.23) represents $\mathbf{D}[f_q]$ as Kronecker product of time variation over two scales. We interpret it as follows. $\mathbf{D}_{P+Q}[f_q(K+L)]$ is a diagonal matrix of size $(P+Q)$ that represents time variation at a *coarse scale* (complex-exponentials sampled at sub-sampling interval of $(K+L)T_s$) and $\mathbf{D}_{K+L}[f_q]$ is a diagonal matrix of size $(K+L)$ that represents the time variation over a finer grid corresponding to the sampling period T_s. Using (8.23) and standard matrix identities, we can decompose the received signal as

$$\mathbf{y}[k] = \sum_{q=0}^{Q}\left((\mathbf{D}_{P+Q}[f_q(K+L)]\mathbf{F}_{P+Q}^H\mathbf{Z}_1) \otimes (\mathbf{D}_{K+L}[f_q]\widetilde{\mathbf{H}}_q[k;0]\mathbf{Z}_2)\right)\mathbf{s}[k] + \mathbf{v}[k],$$

$$\mathbf{y}[k] = (\mathbf{F}_{P+Q}^H \otimes \mathbf{I}_{K+L})\sum_{q=0}^{Q}\left((\mathbf{J}_{P+Q}[q]\mathbf{Z}_1) \otimes (\mathbf{D}_{K+L}[f_q]\widetilde{\mathbf{H}}_q[k;0]\mathbf{Z}_2)\right)\mathbf{s}[k] + \mathbf{v}[k].$$

$\mathbf{J}[q] = J^q$, J being a circulant matrix with $[0,1,\ \mathbf{0}_{1\times(P+Q-2)}]^T$ as the first column. Since the matrix $(\mathbf{F}_{P+Q}^H \otimes \mathbf{I}_{K+L})$ has no effect on the diversity of the doubly selective channel, for the analysis of the diversity gain of MMSE-ZF receiver, the effective channel matrix can be represented as

$$\mathbf{H}_D[k] = \sum_{q=0}^{Q}(\mathbf{J}_{P+Q}[q]\mathbf{Z}_1) \otimes (\mathbf{D}_{K+L}[f_q]\widetilde{\mathbf{H}}_q[k;0]\mathbf{Z}_2). \tag{8.24}$$

Observe that $\mathbf{H}_D[k]$ is a highly structured matrix. Fig. 8.2 illustrates the structure of this effective channel matrix due to precoding. Here $\bar{\mathbf{H}}_q$ represents the product matrix $\mathbf{D}_{K+L}[f_q]\widetilde{\mathbf{H}}_q[k;0]$ for ease of illustration. In particular, $\mathbf{H}_D[k]$ is a block-Toeplitz matrix with constituent blocks which are in turn formed by the product of a diagonal matrix $\mathbf{D}_{K+L}[f_q]$ and a Toeplitz matrix formed by the BEM coefficients of the q-th basis function.

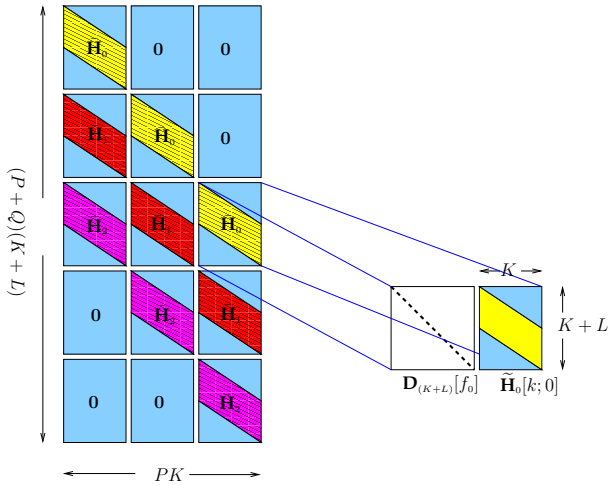

Figure 8.2: Equivalent channel matrix for doubly selective channel.

Diversity analysis of LE in DS channels

As usual, we drop block indices and simplify notations so that the received signal can be represented by the simple relationship in (8.1). Substituting $\bar{\mathbf{H}}_q = \mathbf{D}_{K+L}[f_q]\widetilde{\mathbf{H}}_q[k;0]$ and $\mathbf{J}_q = \mathbf{J}_{P+Q}[q]\mathbf{Z}_1$ in (8.24), we have

$$\boldsymbol{y}_D = \boldsymbol{H}_D\boldsymbol{s} + \boldsymbol{v}, \tag{8.25}$$

$$\boldsymbol{H}_D = \sum_{q=0}^{Q} \mathbf{J}_q \otimes \bar{\mathbf{H}}_q, \tag{8.26}$$

$$\boldsymbol{G}_D = (\boldsymbol{H}_D^H\boldsymbol{H}_D)^{-1}\boldsymbol{H}_D^H, \tag{8.27}$$

To aid the diversity analysis of LE in DS channels, we will need a few additional definitions. Let $\lambda_{\min}(\mathbf{A})$ denote the minimum eigenvalue of the matrix $\mathbf{A}$.

$$\begin{aligned} \boldsymbol{h}_D &= [\boldsymbol{h}^{(0)T}, \boldsymbol{h}^{(1)T}, \ldots, \boldsymbol{h}^{(Q)T}]^T, \\ \boldsymbol{h}^{(q)} &= [h_0^{(q)}, h_1^{(q)}, \ldots, h_L^{(q)}]^T, \forall q \in \{0,1,\ldots,Q\}. \end{aligned}$$

For precoded transmission over doubly selective channels we have the following lemma.

Lemma 8.2.2 *For $\mathbf{G}_D$ defined in (8.27). $\|\mathbf{G}_D\|^{-2}$ is lowerbounded by $c_D\|\boldsymbol{h}_D\|^2$ for some $c_D > 0$ independent of $\boldsymbol{h}_D$*

In order to prove that the maximum diversity gain ν can be achieved by $\mathbf{G}_D$, we use the same 2-step procedure as before. In the first step we express the PEP as a function of $\mathbf{G}_D$. Accordingly, substituting $\mathbf{G}_D$ in (8.6) we have,

$$\sigma_w^2|\boldsymbol{H}_D = \mathbb{E}[|\Re(\boldsymbol{n}^H\boldsymbol{e}_{lk})|^2 \mid \boldsymbol{H}_D] = \frac{1}{2\mathsf{SNR}}\|\boldsymbol{G}_D^H\boldsymbol{e}_{lk}\|.$$

Therefore, (8.5) for transmission over DS channels with the precoder $\boldsymbol{\Theta}$ applied at the transmitter is given by

$$\begin{aligned} P(\boldsymbol{s}_k \to \boldsymbol{s}_l|\boldsymbol{H}_D) &= Q\left(\frac{d_{lk}}{\sqrt{2\mathsf{SNR}^{-1}\|\boldsymbol{G}_D^H\boldsymbol{e}_{lk}\|^2}}\right) \\ &\leq Q\left(\frac{d_{lk}}{\sqrt{2\mathsf{SNR}^{-1}\|\boldsymbol{G}_D\|^2}}\right) \\ &\leq Q\left(\frac{d_{\min}}{\sqrt{2\mathsf{SNR}^{-1}\|\boldsymbol{G}_D\|^2}}\right) \\ &\leq Q\left(d_{\min}\sqrt{\frac{\mathsf{SNR}c_D\|\boldsymbol{h}_T\|^2}{2}}\right) \\ &\leq \exp\left(\frac{-d_{\min}^2\mathsf{SNR}c_D\|\boldsymbol{h}_D\|^2}{4}\right) \end{aligned} \tag{8.28}$$

where we have used the same procedure as in the case of TS-only channels to obtain a series of upperbound of $Q(.)$ to arrive at

$$P(\boldsymbol{s}_k \to \boldsymbol{s}_l|\boldsymbol{H}_D) \leq \exp\left(\frac{-d_{\min}^2\mathsf{SNR}c_D\|\boldsymbol{h}_D\|^2}{4}\right) \tag{8.29}$$

Here too we allow for correlated channel coefficients. However, in order to avoid messy notations, we assume that all $\boldsymbol{h}^{(q)}$ have the same L_s number of diversity sources.

$$\boldsymbol{h}^{(q)} = \boldsymbol{R}_{hh,q}^{1/2}\bar{\boldsymbol{h}}^{(q)} \ , \bar{\boldsymbol{h}}^{(q)T} = [\bar{h}_1^{(q)}\bar{h}_2^{(q)}\dots\bar{h}_{L_s}^{(q)}]$$

where $\bar{h}_l^{(q)}$ are i.i.d Gaussian.

Then averaging (8.29) over the channel distribution we have

$$\begin{aligned}
\mathbb{E}_{\boldsymbol{H}_D}\left[P(\boldsymbol{s}_k \to \boldsymbol{s}_l|\boldsymbol{H}_D)\right] &\leq \mathbb{E}_{\boldsymbol{H}_D}\left[\exp\left(\frac{-d_{\min}^2 \mathsf{SNR} c_D \|\boldsymbol{h}_D\|^2}{4}\right)\right] \\
&= \mathbb{E}_{\boldsymbol{H}_D}\left[\exp\left(\frac{-d_{\min}^2 \mathsf{SNR} c_D \sum_q \bar{\boldsymbol{h}}^{(q)H} \mathbf{R}_{h^{(q)}h^{(q)}} \bar{\boldsymbol{h}}^{(q)}}{4}\right)\right] \\
&= \mathbb{E}_{\boldsymbol{H}_D}\left[\exp\left(\frac{-d_{\min}^2 \mathsf{SNR} c_D \sum_q (\mathbf{U}^{(q)H}\bar{\boldsymbol{h}}^{(q)})^H \boldsymbol{\Lambda}^{(q)} \mathbf{U}^{(q)H} \bar{\boldsymbol{h}}^{(q)}}{4}\right)\right] \\
&= \mathbb{E}_{\boldsymbol{H}_D}\left[\exp\left(\frac{-d_{\min}^2 \mathsf{SNR} c_D \sum_q \sum_l \lambda_{q,l} |\bar{h}_l^{(q)}|^2}{4}\right)\right] \\
&= \prod_{q=0}^{Q+1}\prod_{l=1}^{L_s}\left(\frac{1}{1+K\mathsf{SNR}\lambda_l^{(q)}}\right) \\
&\leq (K\mathsf{SNR})^{-(Q+1)L_s} \prod_{q=1}^{Q+1}\prod_{l=1}^{L_s}\left(\frac{1}{\lambda_l^{(q)}}\right) \qquad (8.30)
\end{aligned}$$

When each $\boldsymbol{h}^{(q)}$ is independent in addition to all the coefficients in it being independent, the SNR exponent will be $-\nu$ which verifies that $\boldsymbol{G}_D$ can achieve the full diversity gain ν offered by the channel.

8.3 Decision feedback equalization for selective channels

In the previous section, the emphasis has been on diversity gains of LE in fading channels. In this section we will show that decision feedback equalizers (DFE) also achieve full channel diversity in these channels. The analysis of diversity gains for DFE is made for doubly selective channels but we point out that it is equally true for FS only and TS only channels addressed earlier.

Consider DFE applied at the receiver when the precoding matrix $\boldsymbol{\Theta}$ is applied at the transmitter and when the channel is doubly selective. The received signal can be represented as (8.24) In principle, the structure of DFE is very similar to that of MMSE-ZF equalizer [32] [50]. Therefore, the fact that MMSE-ZF achieves full diversity gain motivates us to analyze the diversity order of B-DFE in such channels. The goal, in employing B-DFE,

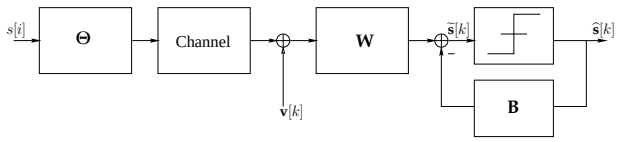

Figure 8.3: Decision Feedback Equalization.

is to minimize $\mathrm{tr}\{\mathbf{R}_{ee}\}$ where $\mathbf{e}[k] = \widetilde{\mathbf{s}}[k] - \mathbf{s}[k]$. In addition we impose the constraint that $\mathbf{B}$ is strictly upper triangular. Again, for the sake of notational convenience, we drop the block indices in our analysis. For the MMSE-ZF-DFE, the feedforward filter $\mathbf{W}_{ZF}$ and the feedback filter $\mathbf{B}_{ZF}$ are then given by

$$\mathbf{W}_{ZF} = (\mathbf{B}_{ZF} + \mathbf{I})(\mathbf{H}_D\mathbf{H}_D^H)^{-1}\mathbf{H}_D^H, \tag{8.31}$$

where $\mathbf{B}_{ZF} = \mathbf{L}^H - \mathbf{I}$ and $\mathbf{L}$ is the result of LDL factorization of $(\mathbf{H}_D^H\mathbf{H}_D)$. A similar analysis for MMSE-DFE yields

$$\mathbf{W}_{MMSE} = (\mathbf{B}_{MMSE} + \mathbf{I})\mathbf{H}_D^H(\mathbf{R}_{vv} + \mathsf{SNR}\mathbf{H}_D\mathbf{H}_D^H)^{-1}, \tag{8.32}$$

where $\mathbf{B}_{MMSE} = \mathbf{L}^H - \mathbf{I}$ and $\mathbf{L}$ is the result of LDL factorization of $(\mathsf{SNR}^{-1}\mathbf{I} + \mathbf{H}_D^H\mathbf{R}_{vv}^{-1}\mathbf{H}_D)$.

8.3.1 Diversity analysis of DFE

We start first with the MMSE-ZF-DFE. One can show that the mean squared error (MSE) of the MMSE-ZE equalizer and the MMSE-DFE are related as

$$MSE_{MMSE-ZF} = \underbrace{\sigma_v^2\,\mathrm{tr}(\mathbf{D}^{-1})}_{MSE_{DFE}} + \sigma_v^2 \sum_{r=1}^{N}\sum_{s=r+1}^{N} [\mathbf{D}^{-1}]_{s,s}|[\mathbf{L}^{-1}]_{s,s}|^2. \tag{8.33}$$

This implies that $\mathsf{SINR}_{\mathsf{dp}}^{(\mathsf{DFE})}(\mathsf{n}) \geq \mathsf{SINR}_{\mathsf{dp}}^{(\mathsf{MMSE-ZF})}(\mathsf{n})$ where $n \in \{0, 1, \ldots, N-1\}$. At the output of the MMSE-ZF equalizer, the $\mathsf{SINR}_{\mathsf{dp}}^{(\mathsf{MMSE-ZF})}(\mathsf{n})$ is given by

$$\begin{aligned} \mathsf{SINR}_{\mathsf{dp}}^{(\mathsf{MMSE-ZF})}(\mathsf{n}) &= \gamma(n)\mathsf{SNR} \\ \gamma(n) &= \frac{1}{[(\boldsymbol{H}_D^H\boldsymbol{H}_D)^{-1}]_{n,n}} \end{aligned} \tag{8.34}$$

To show that the DFE achieves full diversity gains, we depart from the usual approach of PEP analysis and use $\mathbb{P}_{\mathsf{out}}$ analysis instead. In fact, this

can be done by a straightforward extension of the analysis in [3, pp.120] to the present case. To this end we first find a lower bound for γ as follows

$$\begin{aligned}\gamma(n) &= \frac{1}{[(\boldsymbol{H}_D^H \boldsymbol{H}_D)^{-1}]_{n,n}} \\ &\geq \frac{1}{\mathrm{tr}(\boldsymbol{H}_D^H \boldsymbol{H}_D)^{-1}} \\ &\geq \frac{1}{N}\lambda_{\min}(\underline{\boldsymbol{H}}_D^H \underline{\boldsymbol{H}}_D)\|\boldsymbol{h}_D\|^2 \\ &\geq \frac{1}{N}\lambda^\star \|\boldsymbol{h}_D\|^2\end{aligned} \tag{8.35}$$

In other words $\mathsf{SINR}_{\mathsf{dp}}^{(\mathsf{MMSE-ZF})}(\mathsf{n}) \geq \frac{1}{\mathsf{N}}\lambda^\star \|\boldsymbol{h}_{\mathsf{D}}\|^2 \mathsf{SNR}$. Thus for any rate $r > 0$, we have

$$\begin{aligned}\mathbb{P}_{\mathsf{e}}(\mathsf{SNR}) &\doteq \Pr(\gamma \mathsf{SNR} < \mathsf{SNR}^r) \\ &\dot{\leq} \Pr(\|\boldsymbol{h}_D\|^2 < \frac{\mathsf{SNR}^{r-1}}{N\lambda^\star}) \\ &\doteq \frac{\mathsf{SNR}^{-\nu(1-r)}}{\lambda^\star} \\ &\dot{\leq} \mathsf{SNR}^{-\nu(1-r)}\end{aligned} \tag{8.36}$$

It is clear that based on $\mathbb{P}_{\mathsf{out}}$ analysis one can show that MMSE-ZF achieves full diversity gains. Since $\mathsf{SINR}_{\mathsf{dp}}^{(\mathsf{DFE})}(\mathsf{n}) \geq \mathsf{SINR}_{\mathsf{dp}}^{(\mathsf{MMSE-ZF})}(\mathsf{n})$, it follows that so does the MMSE-ZF DFE.

In order to extend the same method to the MMSE case however, we have to first address the fact that the noise variance at the output of the MMSE equalizer is not Gaussian. As opposed to an MMSE feedforward filter, an MMSE-ZF filter makes not attempt to tradeoff between interference cancellation and noise enhancement. Indeed, the goal of the MMSE-ZF filter is one that completely cancels interference with minimal noise enhancement among all ZF filters. Thus, at the output of the MMSE-ZF equalizer, there is no residual interference component (bias) and noise is colored, but Gaussian. This is not the case for MMSE filter. The method above can be extended to the MMSE-DFE if it can be shown that the residual ISI component for the DFE with non-Gaussian distribution does not impact the diversity gain. Indeed, it is possible to do so. Denote the MMSE equalizer

by $\boldsymbol{G}_{MMSE}$ and the output of the equalizer by $\widehat{\mathbf{y}}$. Then the n^{th} component of $\widehat{\mathbf{y}}$ and be expressed as

$$\widehat{y}_n = \underbrace{\sqrt{\mathsf{SNR}}\mathbf{g}_n\mathbf{H}_D\theta_n}_{f_n} s_n + \sqrt{\mathsf{SNR}}\mathbf{g}_n\mathbf{H}_D\boldsymbol{\Theta}\mathbf{s}_{-n} + \mathbf{g}_n\mathbf{v}, \tag{8.37}$$

where θ_n is the n^{th} column of $\boldsymbol{\Theta}$ and $\mathbf{s}_{-n}$ is the transmit vector with the n^{th} symbol set to zero. We also use $\boldsymbol{\Theta}_{-n}$ to denote the precoding matrix without its n^{th} column. Finally, $\mathbf{g}_n$ denotes the n^{th} row of $\boldsymbol{G}_{MMSE}$. The second term on the RHS of the above equation represents residual interference and is not Gaussian. Our intention is to show that this non-Gaussian ISI component in interference plus noise expression is bounded with a bound independent of SNR and therefore its contribution does not have any effect on diversity gain since the diversity gain is computed in the $\mathsf{SNR} \to \infty$ regime.
We do that by introducing a scaling factor for each $\widehat{y}_n$ to be

$$\gamma_n^2 = \mathbf{g}_n\mathbf{g}_n^H + \mathsf{SNR}\mathbf{g}_n\mathbf{H}_D\boldsymbol{\Theta}_{-n}\boldsymbol{\Theta}_{-n}^H\mathbf{H}_D^H\mathbf{g}_n^H \quad 1 \le n \le N \tag{8.38}$$

The scaled vector $\overline{\mathbf{y}}$ then reads

$$\overline{\mathbf{y}} = \boldsymbol{\Gamma}\widehat{\mathbf{y}} = \boldsymbol{\Gamma}\boldsymbol{\mathcal{D}}\mathbf{s} + \widetilde{\mathbf{v}} \tag{8.39}$$

$\boldsymbol{\mathcal{D}} \triangleq \{f_1 \oplus f_2 \oplus \cdots \oplus f_N\}$, $\boldsymbol{\Gamma} = \{\gamma_1 \oplus \gamma_2 \oplus \cdots \oplus \gamma_N\}$ are diagonal matrices and the residual ISI and noise is collected in $\widetilde{\mathbf{v}}$. Following the treatment of noise is [51], we separate the contribution of residual non-Gaussian ISI and Gaussian noise in each component of $\widetilde{\mathbf{v}}$ as

$$\widetilde{v}_n = \frac{1}{\gamma_n}\left(\underbrace{\mathbf{g}_n\mathbf{v}}_{v_n^{(1)}} + \underbrace{\sqrt{\mathsf{SNR}}\mathbf{g}_n\mathbf{H}_D\boldsymbol{\Theta}\mathbf{s}_{-n}}_{v_n^{(2)}}\right) \tag{8.40}$$

Since $E[v_n^{(1)}v_n^{(1)H}] + E[v_n^{(2)}v_n^{(2)H}] = 1$ and the constellation itself is of finite energy, $\|\widetilde{\mathbf{v}}^{(2)}\| \le \beta$, for a constant $\beta > 0$ independent of SNR. The contribution of the non-Gaussian component in the noise is therefore finite. Since an outage event gets situated in the exponentially receding Gaussian tail, the outage probability behaves asymptotically as if the noise was Gaussian. Now from the fact that $\mathsf{SINR}_{\mathsf{dp}}^{(\mathsf{DFE})}(\mathsf{n}) \ge \mathsf{SINR}_{\mathsf{dp}}^{(\mathsf{MMSE})}(\mathsf{n})$, it follows that MMSE-DFE achieves full diversity gains.

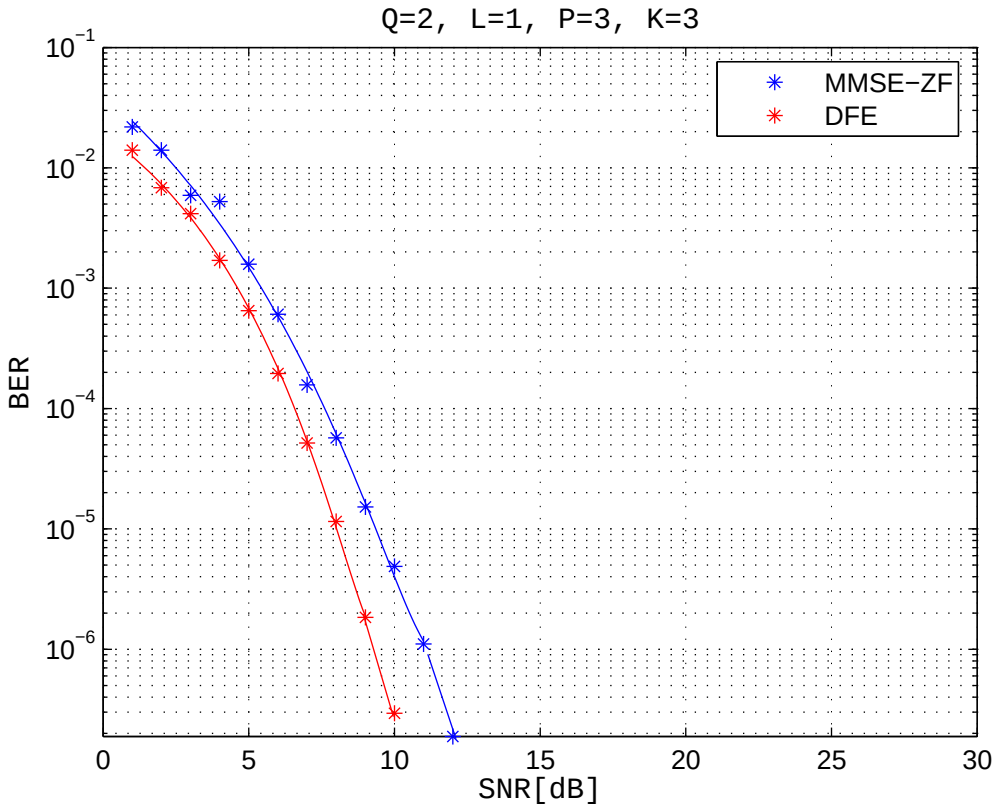

Figure 8.4: Diversity order of LE and DFE.

8.3.2 Simulation results

We provide here simulation results to strengthen the arguments made about the diversity order of DFE with respect to LE. The diversity order of a receiver can be estimated based on the slope of the BER curve at high SNR. In Fig. 8.4 we plot the performance of both the receivers for linearly precoded transmission in a channel parameterized by $Q = 2, L = 1, P = 3, K = 3$. The BER curve has a slope for both LE and DFE have a slope of $(Q+1)(L+1)$ which leads us to conclude that DFE also achieves full diversity in the channel when an appropriate diversity enabling precoder is used at the transmitter. As expected, the BER curve for the DFE has a better coding gain due to the fact that $\mathsf{SINR}_{\mathsf{DFE}} \geq \mathsf{SNR}_{\mathsf{MMSE-ZF}}$

8.4 Appendix

8.4.1 Proof of lemma 8.1.2

We start by using [I 1] on $\boldsymbol{H}^H\boldsymbol{H}$

$$\begin{aligned}
\frac{\mathrm{tr}\left((\boldsymbol{H}^H\boldsymbol{H})^{-1}\right)}{N} &\geq \left(\det(\boldsymbol{H}^H\boldsymbol{H})^{-1}\right)^{1/N} \\
&= \left(\det(\boldsymbol{H}^H\boldsymbol{H})\right)^{-1/N} \\
\det(\boldsymbol{H}^H\boldsymbol{H})^{1/N} &\geq \frac{N}{\mathrm{tr}\left((\boldsymbol{H}^H\boldsymbol{H})^{-1}\right)} \\
&= \frac{N}{\|\boldsymbol{G}\|^2}
\end{aligned}$$

8.4.2 Proof of lemma 8.1.3

$$\begin{aligned}
\sigma_w^2|\boldsymbol{H} &= \mathbb{E}[|\Re(\boldsymbol{n}^H\boldsymbol{e}_{lk})|^2 \mid \boldsymbol{H}] \\
\mathbb{E}[|\boldsymbol{n}^H\boldsymbol{e}_{lk}|^2 \mid \boldsymbol{H}] &= \mathbb{E}[\boldsymbol{e}_{lk}^H\boldsymbol{n}\boldsymbol{n}^H\boldsymbol{e}_{lk}] \\
&= \boldsymbol{e}_{lk}^H\boldsymbol{G}\,\mathbb{E}[\boldsymbol{v}\boldsymbol{v}^H]\boldsymbol{G}^H\boldsymbol{e}_{lk} \\
&= \frac{1}{\mathsf{SNR}}(\boldsymbol{G}^H\boldsymbol{e}_{lk})^H(\boldsymbol{G}^H\boldsymbol{e}_{lk}) \\
&= \frac{1}{\mathsf{SNR}}(\|\boldsymbol{G}^H\boldsymbol{e}_{lk}\|^2 \\
\mathbb{E}[|\Re(\boldsymbol{n}^H\boldsymbol{e}_{lk})|^2 \mid \boldsymbol{H}] &= \frac{1}{2\mathsf{SNR}}(\|\boldsymbol{G}^H\boldsymbol{e}_{lk}\|^2
\end{aligned}$$

8.4.3 Proof of lemma 8.2.1

Consider the linear prediction problem of a stationary process with covariance matrix $(\boldsymbol{H}_T^H\boldsymbol{H}_T)$ *and spectrum* $|H(\xi)|^2$ *given by*

$$H(\xi) = \sum_{q=0}^{Q} h_q e^{-j2\pi\xi q}, \tag{8.41}$$

$$\|\boldsymbol{h}_T\|_2^2 = \int_{-1/2}^{+1/2} |H(\xi)|^2 d\xi. \tag{8.42}$$

Then, $(\boldsymbol{H}_T^H\boldsymbol{H}_T)$ *can be factorized as* $\mathbf{LDL}^H$*, where* $\mathbf{L}$ *is a lower-triangular matrix with unit diagonal and* $\mathbf{D}$ *is a diagonal matrix whose* n^{th} *diagonal element, denoted*

by σ_n^2 corresponds to the $(n-1)^{th}$ order prediction error variance of this process. In the limiting case, we have

$$\lim_{N\to\infty}(\det(\boldsymbol{H}_T^H\boldsymbol{H}_T))^{1/N} = \left(\prod_{n=0}^{N-1}\sigma_n^2\right)^{1/N} \to \sigma_\infty^2, \tag{8.43}$$

where the infinite order prediction error variance σ_∞^2 is related to the spectrum $|H(\xi)|^2$ [52] [53] as

$$\sigma_\infty^2 = \exp\left(\int_{-1/2}^{+1/2}\ln|H(\xi)|^2 d\xi\right) = \frac{|H(\xi)|^2}{|P(\xi)|^2}, \tag{8.44}$$

where $P(\xi)$ is the monic minimum phase equivalent of $H(\xi)$ and is given by

$$P(\xi) = 1 + \sum_{q=1}^{Q} p_l e^{-j2\pi\xi q} = \prod_{q=1}^{Q}(1 - a_q e^{-j2\pi\xi})\ |a_q| < 1, q > 1. \tag{8.45}$$

In the above equation,

$$\begin{aligned} p_q &= \sum_{1\le i_1<i_2<\ldots<i_q\le Q} (-1)^q a_{i_1}a_{i_2}\ldots a_{i_q} \\ &\le \sum_{1\le i_1<i_2<\ldots<i_q\le Q} |a_{i_1}||a_{i_2}|\ldots|a_{i_q}| \\ &< \sum_{1\le i_1<i_2<\ldots<i_q\le Q} 1 \\ &= \binom{q}{Q} \end{aligned}$$

Which implies,

$$\|\mathbf{p}\|_2^2 = \int_{-1/2}^{+1/2}|P(\xi)|^2 d\xi = (1 + \sum_{q=1}^{Q} p_q^2) \le c_Q = \sum_{q=0}^{Q}\binom{q}{Q}^2. \tag{8.46}$$

From (8.44) and (8.46), we can now lowerbound σ_∞^2 by

$$\sigma_\infty^2 = \frac{\|\boldsymbol{h}_T\|_2^2}{\|\mathbf{p}\|_2^2} \ge \frac{\|\boldsymbol{h}_T\|_2^2}{c_Q}. \tag{8.47}$$

Now from (8.47) and (8.43) it is straightforward that for the limiting case as $N \to \infty$, $\|\boldsymbol{G}_T\|^{-2} \ge c_T\|\boldsymbol{h}_T\|^2$ with $c_T = 1/Nc_Q$ which is independent of $\boldsymbol{h}_T$. Let $c_{stt} = 1/c_Q$. Since $\det(.)$ is a decreasing function in N, for any finite N, we have the lowerbound

$$\det(\boldsymbol{H}_T^H\boldsymbol{H}_T)^{1/N} \ge c_T\|\boldsymbol{h}_T\|^2 \tag{8.48}$$

8.4.4 Proof of lemma 8.2.2

In order to prove that

$$\det(\boldsymbol{H}_D^H \boldsymbol{H}_D)^{1/N} \geq c_D \|\boldsymbol{h}_D\|^2$$

we will first need to prove the following lemma.

Lemma 8.4.1

$$\lambda^\star \triangleq \inf_{\boldsymbol{h}_D \in \mathbb{C}^\nu} \inf_{\boldsymbol{d} \in \boldsymbol{\mathcal{D}}} \lambda_{\min}(\underline{\boldsymbol{H}}_D) > 0 \tag{8.49}$$

Proof:
We define $\nu = (Q+1)(L+1)$. We have already defined the following

$$\begin{aligned} \boldsymbol{h}_D &= [\boldsymbol{h}^{(0)T}, \boldsymbol{h}^{(1)T}, \ldots, \boldsymbol{h}^{(Q)T}]^T, \\ \boldsymbol{h}^{(q)} &= [h_0^{(q)}, h_1^{(q)}, \ldots, h_L^{(q)}]^T, \forall q \in \{0, 1, \ldots, Q\}. \end{aligned}$$

Next, we define the normalized block Toeplitz matrix

$$\underline{\boldsymbol{H}}_D \triangleq \frac{\boldsymbol{H}_D}{\|\boldsymbol{h}_D\|}. \tag{8.50}$$

and the following sets

$$\begin{aligned} \boldsymbol{\mathcal{A}} &\triangleq \{\boldsymbol{a} \in \mathbb{C}^N \mid \|\boldsymbol{a}\| \geq 1\}, \\ \boldsymbol{\mathcal{U}} &\triangleq \{\boldsymbol{u} \in \mathbb{C}^\nu \mid \|\boldsymbol{u}\| = 1\}, \\ \boldsymbol{\mathcal{D}} &\triangleq \{\boldsymbol{d}_q\},\ \boldsymbol{d}_q \triangleq [1, e^{j2\pi f_q}, \ldots, e^{j2\pi(L+L'-1)f_q}]^T,\ \forall q \in \{0, 1, \ldots, Q\}. \end{aligned}$$

Then,

$$\begin{aligned} \lambda^\star &= \inf_{\boldsymbol{h}_D \in \mathbb{C}^\nu} \inf_{\boldsymbol{d} \in \boldsymbol{\mathcal{D}}} \left(\inf_{\boldsymbol{a} \in \mathcal{A}} \|\underline{\boldsymbol{H}}_D \boldsymbol{a}\|^2 \right) \\ &= \inf_{\boldsymbol{a} \in \mathcal{A}} \inf_{\boldsymbol{h}_D \in \mathbb{C}^\nu} \inf_{\boldsymbol{d} \in \boldsymbol{\mathcal{D}}} \frac{\|\boldsymbol{H}_D \boldsymbol{a}\|^2}{\|\boldsymbol{h}_D\|^2} \\ &= \inf_{\boldsymbol{a} \in \mathcal{A}} \inf_{\boldsymbol{h}_D \in \mathbb{C}^\nu} \inf_{\boldsymbol{d} \in \boldsymbol{\mathcal{D}}} \frac{\|\boldsymbol{A}\boldsymbol{h}_D\|^2}{\|\boldsymbol{h}_D\|^2} \\ &= \inf_{\boldsymbol{a} \in \mathcal{A}} \inf_{\boldsymbol{u} \in \boldsymbol{\mathcal{U}}} \inf_{\boldsymbol{d} \in \boldsymbol{\mathcal{D}}} \|\boldsymbol{A}\boldsymbol{u}\|^2 \\ &= \inf_{\boldsymbol{u} \in \boldsymbol{\mathcal{U}}} \inf_{\boldsymbol{d} \in \boldsymbol{\mathcal{D}}} \inf_{\boldsymbol{a} \in \mathcal{A}} \|\boldsymbol{H}_U \boldsymbol{a}\|^2 \\ &= \inf_{\boldsymbol{u} \in \boldsymbol{\mathcal{U}}} \inf_{\boldsymbol{d} \in \boldsymbol{\mathcal{D}}} \lambda_{\min}(\boldsymbol{H}_U) \end{aligned}$$

Where $\boldsymbol{H}_U$ has the same structure as $\boldsymbol{H}_D$ but is composed of $\boldsymbol{u} \in \boldsymbol{\mathcal{U}}$ with $\boldsymbol{u}$ partitioned similarly to $\boldsymbol{h}_D$ as

$$\begin{aligned} \boldsymbol{u} &= [\boldsymbol{u}^{(0)T}, \boldsymbol{u}^{(1)T}, \ldots, \boldsymbol{u}^{(Q)T}]^T, \\ \boldsymbol{u}^{(q)} &= [u_0^{(q)}, u_1^{(q)}, \ldots, u_L^{(q)}]^T, \forall q \in \{0, 1, \ldots, Q\}. \end{aligned}$$

Since $\boldsymbol{H}_U$ is a full rank matrix, $\forall \boldsymbol{u} \in \boldsymbol{\mathcal{U}}$ and $\forall \boldsymbol{d} \in \boldsymbol{\mathcal{D}}$, $\sigma^2_{\min}(\boldsymbol{H}_U) > 0$ for each realization (instance) of $\boldsymbol{H}_U$. Since $\boldsymbol{\mathcal{U}}$ and $\boldsymbol{\mathcal{D}}$ are both compact sets

$$\lambda^\star \in \{\lambda_{\min}(\boldsymbol{H}_U)\},$$

where$\{\lambda_{\min}(\boldsymbol{H}_U)\}$ is the set of minimum eigenvalues of all possible realizations of $\boldsymbol{H}_U$. Since each element in the set is non-zero, it follows that

$$\lambda^\star > 0.$$

We now prove Lemma 8.2.2 as follows

$$\begin{aligned} \|\boldsymbol{G}_D\|^2 &= \operatorname{tr}(\boldsymbol{H}_D^H \boldsymbol{H}_D)^{-1} \\ &= \frac{1}{\|\boldsymbol{h}_D\|^2} \operatorname{tr}(\underline{\boldsymbol{H}}_D^H \underline{\boldsymbol{H}}_D)^{-1} \\ \|\boldsymbol{G}_D\|^{-2} &= \frac{\|\boldsymbol{h}_D\|^2}{\operatorname{tr}(\underline{\boldsymbol{H}}_D^H \underline{\boldsymbol{H}}_D)^{-1}} \\ &= \frac{\|\boldsymbol{h}_D\|^2}{\dfrac{N}{\displaystyle\sum_{i=1}^{} \sigma_i^{-2}}} \\ &\geq \frac{\sigma^2_{\min}}{N} \|\boldsymbol{h}_D\|^2 \\ &\geq \frac{\sigma^\star}{N} \|\boldsymbol{h}_D\|^2 \\ &= c_D \|\boldsymbol{h}_D\|^2 \end{aligned}$$

where $c_D = \sigma^\star/N$. From Lemma 8.4.1 we know that $\sigma^\star$ is independent $\boldsymbol{h}_D$ and therefore, so is c_D.

8.4.5 Alternate proofs of full diversity

In [47], the authors introduce a metric called the *orthogonal deficiency* or (*od*) of a matrix. It is defined thus:

Definition 8.4.2 *The orthogonal deficiency of a matrix $\boldsymbol{H}$ is defined as*

$$od(\boldsymbol{H}) \triangleq 1 - \frac{\det(\boldsymbol{H}^H\boldsymbol{H})}{\det(\ \mathrm{diag}(\boldsymbol{H}^H\boldsymbol{H})\ )}. \tag{8.51}$$

By definition $0 \leq od(\boldsymbol{H}) \leq 1$. If $\boldsymbol{H}$ represents the effective channel matrix seen at the receiver, it was shown that LE can achieve the same diversity gain as that of MLE if $od(\boldsymbol{H}) < 1$ i.e., strictly less than 1.

For the precoders that we consider in our analysis, it is known that MLE provides full diversity for TS-only, FS-only and DS channels. Therefore, in order to prove that LE achieves full diversity gains, it suffices to prove that $od(\boldsymbol{H}_F) < 1$, $od(\boldsymbol{H}_T) < 1$,$od(\boldsymbol{H}_D) < 1$. In this section, we provide alternative proofs for full diversity gains of LE based on this approach. To be precise, in the following, we derive upperbounds for $od()$ for all the three cases and show that, in each case it is bounded below 1

Upperbound for $od(\boldsymbol{H}_T)$

Recall that the determinant of a square matrix is a decreasing function of the order of the matrix. From (8.48) we have

$$\det(\boldsymbol{H}_T^H\boldsymbol{H}_T)^{1/N} \geq c_T\|\boldsymbol{h}_T\|^2$$

Noting that $\det(\ \mathrm{diag}(\boldsymbol{H}_T^H\boldsymbol{H}_T)\ ) = (\|\boldsymbol{h}_T\|^2)^N$ and substituting the above in the definition of $od(.)$ in (8.51) we have

$$\begin{aligned} od(\boldsymbol{H}_T) &= 1 - \frac{\det(\boldsymbol{H}_T^H\boldsymbol{H}_T)}{\det(\ \mathrm{diag}(\boldsymbol{H}_T^H\boldsymbol{H}_T)\ )} \\ \frac{\det(\boldsymbol{H}_T^H\boldsymbol{H}_T)}{\det(\ \mathrm{diag}(\boldsymbol{H}_T^H\boldsymbol{H}_T)\ )} &\geq \left(\frac{c_T\|\boldsymbol{h}_T\|^2}{\|\boldsymbol{h}_T\|^2}\right)^N \\ &\geq \left(\frac{1}{c_Q}\right)^N \\ od(\boldsymbol{H}_T) &\leq 1 - \left(\frac{1}{c_Q}\right)^N \end{aligned}$$

Upperbound for $od(\boldsymbol{H}_F)$

Using exactly the same steps that resulted in (8.48), it can be shown that

$$\det(\boldsymbol{H}_T^H\boldsymbol{H}_F)^{1/N} \geq c_F\|\boldsymbol{h}_F\|^2$$

where $c_F = 1/c_L$, where $c_L = \sum_{l=0}^{L} \binom{l}{L}^2$. Combining this with $\det(\ \mathrm{diag}(\boldsymbol{H}_F^H \boldsymbol{H}_F)\ ) = (\|\boldsymbol{h}_F\|^2)^N$ and substituting the above in the definition of $od(.)$ in (8.51) we have

$$\begin{aligned} od(\boldsymbol{H}_F) &= 1 - \frac{\det(\boldsymbol{H}_T^{FH} \boldsymbol{H}_F)}{\det(\ \mathrm{diag}(\boldsymbol{H}_F^H \boldsymbol{H}_F)\ )} \\ \frac{\det(\boldsymbol{H}_F^H \boldsymbol{H}_F)}{\det(\ \mathrm{diag}(\boldsymbol{H}_F^H \boldsymbol{H}_F)\ )} &\geq \left(\frac{c_F \|\boldsymbol{h}_F\|^2}{\|\boldsymbol{h}_F\|^2} \right)^N \\ &\geq \left(\frac{1}{c_L} \right)^N \\ od(\boldsymbol{H}_F) &\leq 1 - \left(\frac{1}{c_L} \right)^N \end{aligned}$$

Chapter 9

Low complexity implementation of full diversity receivers

9.1 Introduction

In this chapter, we address the issue of low complexity implementation of full diversity equalizers for block transmission in selective channels. In fact, we present here, low complexity implementations for all the receivers discussed in the previous chapter with the exception of the B-DFE receiver. In addition we also present a hybrid equalizer for doubly selective channel that benefits from full diversity with reduced precoder overhead. Since we model TS-only channels using CE-BEM and since we have seen in the previous chapter that for the precoders that we consider (namely the zero-padding precoders) the effective channel in this case has the same structure in the frequency domain as that of the time-domain representation of the frequency selective channel, we present here the equalizers for FS-only channels. In the context of FS-only channels, we know that cyclic-prefix (CP) block transmission (CP-BT) systems do not exploit frequency diversity offered by multipath fading but the use of appropriate redundant linear precoding in addition to the cyclic prefix as well as ZP block transmission (ZP-BT) permits a linear equalizer (LE) to benefit from full diversity

in the FS-only channel [6]. In over dimensioned CP-BT systems, by which we mean systems where the CP length is greater than the channel delay spread, the *excess time* in the CP may be exploited in order to increase the efficiency of the LE. We see that by exploiting this excess time the coding gain of LE can be increased whereas the diversity gain for un-precoded CP-BT systems remain unchanged regardless of the excess time. However, if the knowledge of the channel length is exploited at the transmitter to insert trailing zeros in the over dimensioned CP, it is possible to obtain additional diversity gains with LE.

For DS channels, we have seen in the previous chapter that MMSE-ZF equalization can achieve full joint multipath-Doppler diversity gains offered by these channels. In order to reduce the computational complexity involved in implementing this receiver, first an iterative implementation of MMSE-ZF equalizer based on polynomial expansion (PE) approximation is proposed. Then, the structure of a matrix involved in this approximation is exploited to reduce the computational complexity of the PE approximation. Simulation results are provided to show that this approach reduces the computational complexity compared to the brute-force implementation of the MMSE-ZF equalizer and does not effect the diversity gain. Finally, we present a hybrid-equalization scheme that also benefits from full diversity when a precoder with higher bandwidth efficiency is used. This precoder precludes the possibility of LE benefiting from full channel diversity. However, by using a hybrid equalizer that limits non-linear (ML) processing only to derive Doppler diversity and employs LE to harvest time-diversity present in the channel it is possible to benefit from full channel diversity at a complexity less than that of a full blown MLE.

9.2 Low complexity linear equalization for frequency selective channels

In this section we discuss linear equalizers for frequency selective channels. Its application for time-selective only channels when the time-variation can be modeled by the CE-BEM is straightforward.

9.2.1 Zero-padded block transmission (ZP-BT)

Consider the ZP-BT where the transmitter applies precoder $\mathbf{\Theta}_F$ given by (8.7). The received signal is then given by (8.8) (8.9). The effective channel seen

at the receiver due to precoding at the transmitter ($\mathbf{H}_F[k;0]\mathbf{\Theta}_F$), is a $M \times N$ Toeplitz matrix with $[h(k,0), h(k,1), \ldots, h(k,L), \mathbf{0}_{1\times M-L-1}]^T$ as its first column. Henceforth, we omit the block index k since processing is on a block-by-block basis. To differentiate between the different types of precoders that we shall study here, we will suffix the equivalent channel matrix with the precoder type. For instance, in the case of ZP-BT we have $\mathbf{H}_{zp} = \mathbf{H}_F\mathbf{\Theta}_F$. At first glance, the MMSE-ZF equalizer $(\mathbf{H}_{zp}^H\mathbf{H}_{zp})^{-1}\mathbf{H}_{zp}^H$ that achieves full diversity for ZP-BT seems to have a rather large computational complexity due to the large matrix inversion problem. However, we observe that the $\mathbf{H}_{zp}$ matrix is related to its cyclic prefixed counter-part $\mathbf{H}_{cp}$; the effective channel matrix for CP-BT and that this relationship can be exploited to reduce the complexity of the implementation of MMSE-ZF equalizer for ZP-BT. Compare the channel matrix of CP-BT with M subcarriers and a cyclic prefix of length L, with that of a ZP-BT system. Let $P = M + L$, denote the $M \times P$ matrix that represents the cyclic removal operation by $\overline{\mathbf{C}} = [\mathbf{0}_{M\times L}\ \mathbf{I}_M]$ After CP removal the equivalent channel matrix for CP-BT is a $M \times M$ circulant matrix $\mathbf{H}_{cp}$ with the $M \times N$ banded Toeplitz matrix $\mathbf{H}_{zp}$ representing the equivalent channel matrix of the ZP-BT embedded in it. In other words we can partition $\mathbf{H}_{cp}$ as $\mathbf{H}_{cp} = [\mathbf{H}_{zp}\ \mathbf{H}_0]$. We illustrate this with a toy example. Let $P = 9, M = 7, L+1 = 3, N = 5$. Then denoting the effective channel matrix at the receiver for a CP-BT system before and after CP removal as $\mathbf{H}_t$ and $\mathbf{H}_{cp}$, these matrices have the following structure.

$$\mathbf{H}_t = \begin{bmatrix} 0 & 0 & 0 & 0 & 0 & h_0 & 0 \\ 0 & 0 & 0 & 0 & 0 & h_1 & h_0 \\ h_0 & 0 & 0 & 0 & 0 & h_2 & h_1 \\ h_1 & h_0 & 0 & 0 & 0 & 0 & h_2 \\ h_2 & h_1 & 0 & 0 & 0 & 0 & 0 \\ 0 & h_2 & h_1 & h_0 & 0 & 0 & 0 \\ 0 & 0 & h_2 & h_1 & h_0 & 0 & 0 \\ 0 & 0 & 0 & h_2 & h_1 & h_0 & 0 \\ 0 & 0 & 0 & 0 & h_2 & h_1 & h_0 \end{bmatrix}$$

$$\mathbf{H}_{cp} = \left[\begin{array}{ccccc|cc} h_0 & 0 & 0 & 0 & 0 & h_2 & h_1 \\ h_1 & h_0 & 0 & 0 & 0 & 0 & h_2 \\ h_2 & h_1 & 0 & 0 & 0 & 0 & 0 \\ 0 & h_2 & h_1 & h_0 & 0 & 0 & 0 \\ 0 & 0 & h_2 & h_1 & h_0 & 0 & 0 \\ 0 & 0 & 0 & h_2 & h_1 & h_0 & 0 \\ 0 & 0 & 0 & 0 & h_2 & h_1 & h_0 \end{array}\right] = [\mathbf{H}_{zp} \mid \mathbf{H}_0]$$

We know that $\mathbf{F}_M \mathbf{H}_{cp} \mathbf{F}^H = \mathbf{\Lambda}$ is a diagonal matrix.$\mathbf{F}$ is the associated normalized M-DFT matrix. From the above relation, we have

$$\mathbf{F}_M^H (\mathbf{\Lambda}^H \mathbf{\Lambda})^{-1} \mathbf{F}_M = (\mathbf{H}_{cp}^H \mathbf{H}_{cp})^{-1} \tag{9.1}$$

$$\left[\begin{array}{cc} \boldsymbol{\mathcal{A}} & \boldsymbol{\mathcal{B}} \\ \boldsymbol{\mathcal{B}}^H & \boldsymbol{\mathcal{C}} \end{array}\right]^{-1} = \left[\begin{array}{cc} \mathbf{H}_{zp}^H \mathbf{H}_{zp} & \mathbf{H}_{zp}^H \mathbf{H}_0 \\ \mathbf{H}_0^H \mathbf{H}_{zp} & \mathbf{H}_0^H \mathbf{H}_0 \end{array}\right]^{-1} \tag{9.2}$$

The block matrix of the RHS of the equation can be inverted using the following identity [54]

$$\left[\begin{array}{cc} \boldsymbol{\mathcal{A}}^{-1} + \boldsymbol{\mathcal{E}} \boldsymbol{\Delta}^{-1} \boldsymbol{\mathcal{E}}^H & -\boldsymbol{\mathcal{E}} \boldsymbol{\Delta}^{-1} \\ -\boldsymbol{\Delta}^{-1} \boldsymbol{\mathcal{E}}^H & \boldsymbol{\Delta}^{-1} \end{array}\right], \tag{9.3}$$

where $\boldsymbol{\Delta} = \boldsymbol{\mathcal{C}} - \boldsymbol{\mathcal{B}}^H \boldsymbol{\mathcal{A}}^{-1} \boldsymbol{\mathcal{B}}$ and $\boldsymbol{\mathcal{E}} = \boldsymbol{\mathcal{A}}^{-1} \boldsymbol{\mathcal{B}}$. By first constructing $\mathbf{F}_M^H (\mathbf{\Lambda}^H \mathbf{\Lambda})^{-1} \mathbf{F}_M$ and extracting the appropriate matrix blocks corresponding to $\boldsymbol{\mathcal{Q}} = \boldsymbol{\mathcal{A}}^{-1} + \boldsymbol{\mathcal{E}} \boldsymbol{\Delta}^{-1} \boldsymbol{\mathcal{E}}^H$, $-\boldsymbol{\mathcal{E}} \boldsymbol{\Delta}^{-1}$, $\boldsymbol{\Delta}^{-1}$ and $\boldsymbol{\Delta} \boldsymbol{\mathcal{E}}^H$ the MMSE-ZF equalizer can be reconstructed as

$$(\mathbf{H}_{zp}^H \mathbf{H}_{zp})^{-1} \mathbf{H}_{zp}^H = (\boldsymbol{\mathcal{Q}} - \boldsymbol{\mathcal{E}} \boldsymbol{\Delta}^{-1} . \boldsymbol{\Delta} . \boldsymbol{\Delta}^{-1} \boldsymbol{\mathcal{E}}^H) \mathbf{H}_{zp}^H, \tag{9.4}$$

The total effort required for matrix inversion is thus reduced to inversion of the diagonal matrix $(\mathbf{\Lambda}^H \mathbf{\Lambda})$ and the $L \times L$ matrix $\boldsymbol{\Delta}^{-1}$ thereby reducing the complexity of MMSE-ZF equalizer.

9.2.2 Cyclic prefixed-block transmission

It is known that the unprecoded CP-BT systems tradeoff equalization complexity with diversity benefits and that for these systems, the diversity gain is unity. What we consider here (and in the next section) are systems where the CP is over dimensioned. That is the length G of the CP is such that $G > L$. In such cases, it is normal to ask if the excess samples in the CP can

be exploited in some manner at the receiver. Let $\mathbf{C}_{cp}$ represent this operation at the transmitter, then the transmit signal representation is

$$\mathbf{x} = \mathbf{C}_{cp}\mathbf{F}_N^H\mathbf{s}, \tag{9.5}$$

At the receiver, instead of discarding the entire CP, only the first L samples of the received signal $\mathbf{y}$ are discarded. These are in any case corrupted by IBI. Then, denoting the excess samples in the CP by $e_t = G - L$, the $N + e_t$-length input $\tilde{\mathbf{y}}$ to the equalizer can then be represented as

$$\widetilde{\mathbf{y}} = \overline{\mathbf{C}}_{cp}\mathbf{H}_t\mathbf{C}_{cp}\mathbf{F}_N^H\mathbf{s} + \tilde{\mathbf{v}}, \tag{9.6}$$

where $\overline{\mathbf{C}}_{cp}$ represents the removal of L-samples from CP. The resultant equivalent channel can be represented as a block matrix $\mathbf{H}_{cp} = [\mathbf{H}_e\ \mathbf{H}_s]^T$. $\mathbf{H}_s$ is a square circulant matrix with N rows and corresponds to the equivalent matrix for full CP-removal. $\mathbf{H}_e$ is the time-domain channel matrix corresponding to the excess time (e_t) present in CP. $\widetilde{\mathbf{y}}$ can equivalently be represented as

$$\widetilde{\mathbf{y}} = \begin{bmatrix} \mathbf{y}_e \\ \widetilde{\widetilde{\mathbf{y}}} \end{bmatrix} = \begin{bmatrix} \mathbf{H}_e \\ \mathbf{H}_s \end{bmatrix} \mathbf{F}_N^H\mathbf{s} + \begin{bmatrix} \widetilde{\mathbf{v}}_e \\ \widetilde{\widetilde{\mathbf{v}}} \end{bmatrix}, \tag{9.7}$$

We then process $\widetilde{\widetilde{\mathbf{y}}}$ with a N-point DFT while retaining $\mathbf{y}_e$ as is. We thus arrive at

$$\mathbf{y} = \begin{bmatrix} \mathbf{H}_e\mathbf{F}_N^H \\ \mathbf{F}_N\mathbf{H}_s\mathbf{F}_N^H \end{bmatrix} \mathbf{s} + \mathbf{v} \tag{9.8}$$

$$= \boldsymbol{\mathcal{H}}_c\mathbf{s} + \mathbf{v} \tag{9.9}$$

The MMSE estimator for the transmit signal $\mathbf{s}$ given $\mathbf{y}$ is then given by $\mathbf{R}_{sy}\mathbf{R}_{yy}^{-1}$ and the equalizer can be expressed as $\mathbf{G}_c = (\boldsymbol{\mathcal{H}}_c^H\boldsymbol{\mathcal{H}}_c + \sigma_v^2/\sigma_a^2\mathbf{I})^{-1}\boldsymbol{\mathcal{H}}_c^H$ As in the case of cyclic-prefixed ZP-BT, here too, the equalizer can be implemented with low complexity by exploiting the structure of $\boldsymbol{\mathcal{H}}_c$. By using excess time in CP, the resultant equalizer is able to show a better BER performance. The equalizer however, has diversity order-1 in frequency selective channels due to the fact that $\mathbf{H}_e$ in this case loses rank if *any* fading coefficient of the multipath is zero.

9.2.3 Cyclic prefixed zero padded -block transmission

We now introduce a new variation of ZP-BT with the goal of achieving diversity gains in over dimensioned CP-BT systems while retaining the low

complexity associated with linear equalization at the receiver. The scheme exploits knowledge of channel length at the transmitter to split the available guard interval into a cyclic prefixed-interval and a zero-padded postfix instead of using the entire guard (CP) interval for cyclic prefix or trailing zeros. Consider a guard interval $G > L$ available at the transmitter, a L-length cyclic prefix is first added to the transmit symbol vector $\mathbf{s}$. The resultant $N + L$ length vector is then extended to M by appending $G - L$ zeros. We will see later in the section that this operation allows the receiver to achieve additional diversity gains with low equalization complexity. The transmit processing can then be represented by the block matrix $\mathbf{C}_{zc}\mathbf{F}_N^H$ where $\mathbf{C}_{zc} = [\mathbf{C}\ \mathbf{0}]^T$. Where $\mathbf{C}$ is the L-length CP insertion matrix $[\mathbf{0}_{L\times(N-L)}\ \mathbf{I}_{L\times L};\ \mathbf{I}_{N\times N}]^T$, and $\mathbf{0}$ is an all zero matrix with $e_t = G - L$ rows. This leads us to the transmit signal representation

$$\mathbf{x} = \mathbf{C}_{zc}\mathbf{F}_N^H\mathbf{s}, \tag{9.10}$$

At the receiver, after discarding the L-length CP of the received signal $\mathbf{y}$, the $N + e_t$-length input $\tilde{\mathbf{y}}$ to the equalizer can be represented as

$$\widetilde{\mathbf{y}} = \overline{\mathbf{C}}_{zc}\mathbf{H}_F\mathbf{C}_{zc}\mathbf{F}_N^H\mathbf{s} + \tilde{\mathbf{v}}, \tag{9.11}$$

where $\overline{\mathbf{C}}_{zc}$ represents the CP removal operation. The resultant equivalent channel is given by

$$\mathbf{H}_{zc}=\begin{bmatrix} h_0 & 0 & \cdots & h_{L-1} & \cdots & h_1 \\ h_1 & h_0 & \cdots & \cdots & \cdots & h_2 \\ \vdots & \vdots & \cdots & \cdots & \cdots & \cdots \\ \vdots & \vdots & \vdots & \cdots & \cdots & h_{L-1} \\ h_{L-1} & h_{L-2} & \cdots & 0 & \cdots & 0 \\ 0 & \ddots & \ddots & \ddots & \ddots & 0 \\ 0 & \ddots & h_{L-1} & \ddots & \ddots & h_0 \\ 0 & \ddots & \ddots & \ddots & \ddots & \ddots \\ 0 & 0 & 0 & 0 & 0 & h_{N+e_t-1} \end{bmatrix} \tag{9.12}$$

and can be represented as a block matrix $\mathbf{H}_{zc} = [\mathbf{H}_c\ \mathbf{H}_e]^T$. $\mathbf{H}_c$ is a square circulant matrix with N rows and $\mathbf{H}_e$ is a sparse upper-triangular Toeplitz

time-domain channel matrix of dimension $e_t \times N$. $\widetilde{\mathbf{y}}$ can equivalently be represented as

$$\widetilde{\mathbf{y}} = \begin{bmatrix} \widetilde{\widetilde{\mathbf{y}}} \\ \mathbf{y}_e \end{bmatrix} = \begin{bmatrix} \mathbf{H}_c \\ \mathbf{H}_e \end{bmatrix} \mathbf{F}^H \mathbf{s} + \begin{bmatrix} \widetilde{\widetilde{\mathbf{v}}} \\ \widetilde{\mathbf{v}}_e \end{bmatrix}, \tag{9.13}$$

Note that $\mathbf{H}_c$ is diagonalizable by an IDFT operation. The reason for diagonalization is that equalization at this stage involves, among other things, inversion of $\mathbf{H}_{zc}^H \mathbf{H}_{zc}$. Transformation of $\mathbf{H}_c$ with DFT lends a desirable structure to the channel matrix making it a *predominantly diagonal* matrix. Using standard linear algebra we can then reduce the computational complexity of the resultant matrix inversion. With this in mind, we process $\widetilde{\widetilde{\mathbf{y}}}$ with a DFT while retaining $\mathbf{y}_e$ as is. This is expressed mathematically in the following equations

$$\mathbf{y} = \begin{bmatrix} \mathbf{F}_N \mathbf{H}_c \mathbf{F}_N^H \\ \mathbf{H}_e \mathbf{F}_N^H \end{bmatrix} \mathbf{s} + \mathbf{v} \tag{9.14}$$

$$= \begin{bmatrix} \boldsymbol{\mathcal{D}} \\ \boldsymbol{\mathcal{H}}_e \end{bmatrix} \mathbf{s} + \mathbf{v} = \boldsymbol{\mathcal{H}} \mathbf{s} + \mathbf{v} \tag{9.15}$$

The MMSE-ZF equalizer in this case is given by $\mathbf{G}_{zc} = (\boldsymbol{\mathcal{H}}^H \boldsymbol{\mathcal{H}})^{-1} \boldsymbol{\mathcal{H}}^H$. $\boldsymbol{\mathcal{H}}$ is a rank-e_t modification to a diagonal matrix $\boldsymbol{\mathcal{D}}$. The inversion effort of this matrix can therefore be reduced by expressing it in the form

$$(\boldsymbol{\mathcal{H}}^H \boldsymbol{\mathcal{H}})^{-1} = (\boldsymbol{\mathcal{H}}_e^H \boldsymbol{\mathcal{H}}_e + \boldsymbol{\mathcal{D}}^H \boldsymbol{\mathcal{D}})^{-1}, \tag{9.16}$$

Let $A = \boldsymbol{\mathcal{D}}^H \boldsymbol{\mathcal{D}}$, $B = \boldsymbol{\mathcal{H}}_e^H$, $C = \mathbf{I}_{e_t}$ and $D = \boldsymbol{\mathcal{H}}_e$. Now, applying the *Matrix Inversion Lemma*[1], the matrix inversion effort is reduced to that of inverting an $e_t \times e_t$ matrix $(C^{-1} + DA^{-1}B)^{-1}$. Though this involves an inversion of A, this inversion is also of low complexity since it is a diagonal matrix. The fact that linear equalization in this case achieves additional diversity gains is explained by the "triangular" structure of $\mathbf{H}_e$ which ensures, that e_t constraints need to be satisfied for the channel matrix to lose rank. For the case of $G > 2L^2$ LE attains full channel diversity. This leads to the observation that this type of transmission can be interpreted as a type of linear precoding for CP-BT systems. In the simulation section we show that the diversity gains of LE are proportional to the amount of e_t available

[1] $(A + BCD)^{-1} = A^{-1} - A^{-1}B(C^{-1} + DA^{-1}B)^{-1}DA^{-1}$

[2] a rather large overhead in practice

at the transmitter. Assuming input symbols are white with variance σ_a^2, one can also do a similar treatment for the MMSE estimator. The MMSE estimator for the transmit signal $\mathbf{s}$ given $\mathbf{y}$ is then given by $\mathbf{R}_{sy}\mathbf{R}_{yy}^{-1}$ and the equalizer can be expressed as $\mathbf{G}_{MMSE} = (\boldsymbol{\mathcal{H}}^H\boldsymbol{\mathcal{H}} + \sigma_v^2/\sigma_a^2\mathbf{I})^{-1}\boldsymbol{\mathcal{H}}^H$.

9.3 Polynomial expansion approximation for LE in doubly selective channels

We now focus on reduced complexity implementation of the MMSE-ZF equalizer for doubly selective channels. We start with an alternative representation of the received signal in Eq. (8.20)

$$\mathbf{y} = \mathbf{H}_{tv}\boldsymbol{\Theta}\mathbf{s} + \mathbf{v},$$

where $\mathbf{H}_{tv}$ represents the channel matrix in the time-domain and can in turn be represented as the sum of two matrices

$$\begin{aligned}
\mathbf{H}_{tv} &= \mathbf{H}_{\kappa} + \mathbf{H}_{\nu}, \\
\mathbf{H}_{\kappa} &= \sum_{q=0}^{Q} (\mathbf{D}_{P+Q}[f_q(K+L)] \otimes e^{j\bar{\omega}_q}\widetilde{\mathbf{H}}_q), \\
\mathbf{H}_{\nu} &= (\mathbf{D}_{P+Q}[f_q(K+L)] \otimes (\mathbf{D}_{K+L}[f_q] - e^{j\bar{\omega}_q}\mathbf{I}_{K+L})\widetilde{\mathbf{H}}_q).
\end{aligned}$$

$\bar{\omega}_q = \omega_q(K+L-1)/2$. Representing the received signal in this form allows us to iteratively estimate the transmit symbol vector $\mathbf{s}$. The symbol estimate after the m-th iteration is given by

$$\widehat{\mathbf{s}}^{(m)} = (\mathbf{H}_{\kappa}\boldsymbol{\Theta})^{\dagger}(\mathbf{y} - \mathbf{H}_{\nu}\boldsymbol{\Theta}\widehat{\mathbf{s}}^{(m-1)}), \tag{9.17}$$

where the superscript † represents the Moore-Penrose pseudo-inverse. From (9.17), we can derive the signal to interference noise ratio (SINR) expression for the n-th symbol of the symbol estimate $\widehat{\mathbf{s}}^{(m)}$ as

$$\mathsf{SINR}_n = \frac{\mathsf{SNR}[\mathbf{G}_s\mathbf{G}_s^H]_{n,n}}{\mathsf{SNR}\bar{\mathbf{g}}\bar{\mathbf{g}}^H + [\mathbf{G}_v\mathbf{G}_v^H]_{n,n}}, \tag{9.18}$$

where $\bar{\mathbf{g}}$ is the n-th row of $\mathbf{G}_s$ without the element $[\mathbf{G}]_{n,n}$ and

$$\begin{aligned}
\mathbf{G}_s &= \mathbf{I} + (-1)^m((\mathbf{H}_{\kappa}\boldsymbol{\Theta})^{\dagger}\mathbf{H}_{\nu}\boldsymbol{\Theta})^{m+1}, \\
\mathbf{G}_v &= (\sum_{k=0}^{m}(-1)^k((\mathbf{H}_{\kappa}\boldsymbol{\Theta})^{\dagger}\mathbf{H}_{\nu}\boldsymbol{\Theta})^k)(\mathbf{H}_{\kappa}\boldsymbol{\Theta})^{\dagger}.
\end{aligned}$$

Alternatively, it is possible to envisage a polynomial expansion approximation for the MMSE-ZF receiver that minimizes the mean squared error at the receiver. In this case, the symbol vector estimate after m iterations is given by

$$\widehat{\widehat{\mathbf{s}}}^{(m)} = \sum_{k=0}^{m} \mathbf{\Lambda}_k \mathbf{R}^k \mathbf{z}. \tag{9.19}$$

where

$$\mathbf{R} = -(\mathbf{H}_\kappa \mathbf{\Theta})^\dagger \mathbf{H}_\nu \mathbf{\Theta}, \qquad \mathbf{z} = (\mathbf{H}_\kappa \mathbf{\Theta})^\dagger \mathbf{y},$$

and the diagonal scale factor matrices $\mathbf{\Lambda}_k$ of order N are estimated by plugging in the expression for $\widehat{\widehat{\mathbf{s}}}^{(m)}$ in (9.19) in the LMMSE criterion

$$\mathbf{\Lambda}_k^{opt} = \arg \min_{\mathbf{\Lambda}_k : k \in \{0,1,m\}} \mathbb{E} \, \|\mathbf{s} - \widehat{\widehat{\mathbf{s}}}^{(m)}\|^2. \tag{9.20}$$

Note that (9.17) corresponds to the special case of (9.20) where the diagonal elements of all $\mathbf{\Lambda}_k$ are unity. Another special case of (9.20) where the diagonal matrices $\mathbf{\Lambda}_k$ are reduced to scalar weighting coefficients λ_k are addressed before (for instance in [55]). Let $\boldsymbol{\lambda}_{n,k} = [\mathbf{\Lambda}_k]_{n,n}$ and $\boldsymbol{\lambda}_n = [\lambda_{n,0}, \cdots, \lambda_{n,m}]$ then (9.20) can be solved by finding the optimum $\boldsymbol{\lambda}_n^{opt}$ separately for each transmit symbol $n \in \{0, 1, \cdots, N-1\}$ in the symbol vector $\mathbf{s}$ as

$$\boldsymbol{\lambda}_n^{opt} = \arg \min_{\boldsymbol{\lambda}} \mathbb{E} \, |s[n] - \boldsymbol{\lambda}_n \mathbf{q}[n]|^2. \tag{9.21}$$

$\mathbf{q}[n] = [w_0[n] \; w_1[n] \; \cdots \; w_m[n]]^T$ and $w_m[n]$ are elements of $\mathbf{w}_m = \mathbf{R}^m \mathbf{z}$. Once the N vectors corresponding to $\boldsymbol{\lambda}_n^{opt}$ are obtained the diagonal matrices $\mathbf{\Lambda}_k$ are formed and substituted in (9.19) to get the symbol estimate. The SINR at the output of this equalizer is given by

$$\mathsf{SINR}_n^{MMSE-PE} = \frac{\mathsf{SNR}[\boldsymbol{\mathcal{G}}_s \boldsymbol{\mathcal{G}}_s^H]_{n,n}}{\mathsf{SNR}\bar{\boldsymbol{g}}\bar{\boldsymbol{g}}^H + [\boldsymbol{\mathcal{G}}_v \boldsymbol{\mathcal{G}}_v^H]_{n,n}}, \tag{9.22}$$

where $\bar{\boldsymbol{g}}$ is now the n-th row of $\boldsymbol{\mathcal{G}}_s$ without the element $[\boldsymbol{\mathcal{G}}]_{n,n}$ and

$$\begin{aligned} \boldsymbol{\mathcal{G}}_s &= \sum_{k=0}^{m} \mathbf{\Lambda}_k \mathbf{R}^k (\mathbf{I} + (\mathbf{H}_\kappa \mathbf{\Theta})^\dagger \mathbf{H}_\nu \mathbf{\Theta}), \\ \boldsymbol{\mathcal{G}}_v &= \sum_{k=0}^{m} \mathbf{\Lambda}_k \mathbf{R}^k (\mathbf{H}_\kappa \mathbf{\Theta})^\dagger. \end{aligned}$$

Since both (9.19) and (9.17) require the calculation of the pseudo-inverse $(\mathbf{H}_\kappa \mathbf{\Theta})^\dagger$ we now focus our attention to reducing the complexity of the matrix inversion that needs to be performed in order to obtain $(\mathbf{H}_\kappa \mathbf{\Theta})^\dagger$. Notice that $\mathbf{H}_\kappa \mathbf{\Theta}$ can be factored as shown in (9.24) where we replace the

$$\mathbf{H}_{\kappa}\mathbf{\Theta} = (\mathbf{F}_{P+Q}^{H} \otimes \mathbf{I}_{K+L}) \sum_{q=0}^{Q} (\mathbf{J}_{P+Q}[q] \otimes e^{j\bar{\omega}_q}\mathbf{H}_q)(\mathbf{T}_1 \otimes \mathbf{T}_2), \quad (9.23)$$

$$\mathbf{H}_{\kappa}\mathbf{\Theta} = (\mathbf{F}_{P+Q}^{H} \otimes \mathbf{I}_{K+L}) \sum_{q=0}^{Q} (\mathbf{J}_{P+Q}[q] \otimes e^{j\bar{\omega}_q}\mathbf{H}_q^{c})(\mathbf{T}_1 \otimes \mathbf{T}_2). \quad (9.24)$$

block-circulant-with-Toeplitz-blocks (BCTB) matrix in (9.23) with a block-circulant-with-circulant-blocks matrix (BCCB). i.e.,

$$\mathbf{H}_{BCCB} = \sum_{q=0}^{Q} (\mathbf{J}_{P+Q}[q] \otimes e^{j\bar{\omega}_q}\mathbf{H}_q^{c}).$$

where $\mathbf{H}_q^{c}$ is a circulant matrix whose first column is the same as the first column of $\widetilde{\mathbf{H}}_q$, This allows us to take advantage of the fact that $\mathbf{H}_{BCCB}$ is diagonalizable as

$$\boldsymbol{\mathcal{D}} = (\mathbf{F}_{P+Q}^{H} \otimes \mathbf{F}_{K+L}^{H})\mathbf{H}_{BCCB}(\mathbf{F}_{P+Q} \otimes \mathbf{F}_{K+L}),$$

Now plugging this into (9.24) we have

$$\mathbf{H}_{\kappa}\mathbf{\Theta} = (\mathbf{I}_{P+Q} \otimes \mathbf{F}_{K+L})\boldsymbol{\mathcal{D}}\mathbf{\Theta}_{F}.$$

where $\mathbf{\Theta}_{F} = (\mathbf{I}_{P+Q} \otimes \mathbf{F}_{K+L}^{H})\mathbf{\Theta}$ which in turn leads us to

$$(\mathbf{H}_{\kappa}\mathbf{\Theta})^{\dagger} = (\boldsymbol{\mathcal{D}}\mathbf{\Theta}_{F})^{\dagger}(\mathbf{I}_{P+Q} \otimes \mathbf{F}_{K+L})^{H}. \quad (9.25)$$

The problem of computing $(\mathbf{H}_{\kappa}\mathbf{\Theta})^{\dagger}$ is thus reduced to the problem of computing $(\boldsymbol{\mathcal{D}}\mathbf{\Theta}_{F})^{\dagger}$. This can be accomplished by formulating the problem of computing the pseudo-inverse as that of finding the $N \times (M-N)$ matrix Ξ that corresponds to the solution of the minimization problem [56]

$$\arg\min_{\Xi} \ \mathrm{Tr}\{(\mathbf{\Theta}_{F}^{\dagger}\boldsymbol{\mathcal{D}}^{-1} + \Xi\mathbf{\Theta}_{\mathcal{N},F}\boldsymbol{\mathcal{D}}^{-1})^{H}(\mathbf{\Theta}_{F}^{\dagger}\boldsymbol{\mathcal{D}}^{-1} + \Xi\mathbf{\Theta}_{\mathcal{N},F}\boldsymbol{\mathcal{D}}^{-1})\} \quad (9.26)$$

where $\mathbf{\Theta}_{\mathcal{N},F} = \boldsymbol{\mathcal{N}}(\mathbf{\Theta}^{H})$, and $\boldsymbol{\mathcal{N}}(.)$ denotes the null space of a matrix. The solution to (9.26) allows us to compute $(\boldsymbol{\mathcal{D}}\mathbf{\Theta}_{F})^{\dagger}$ as

$$\mathbf{\Theta}_{F}^{\dagger}\boldsymbol{\mathcal{D}}^{-1}[\mathbf{I} - \boldsymbol{\mathcal{D}}^{-H}\mathbf{\Theta}_{\mathcal{N},F}(\mathbf{\Theta}_{\mathcal{N},F}^{H}\boldsymbol{\mathcal{D}}^{-1}\boldsymbol{\mathcal{D}}^{-H}\mathbf{\Theta}_{\mathcal{N},F})^{-1}\mathbf{\Theta}_{\mathcal{N},F}^{H}\boldsymbol{\mathcal{D}}^{-1}] \quad (9.27)$$

which involves inversion of a matrix of dimension $M-N$ in place of inversion of matrix of dimension M in the brute-force approach. Moreover, $\mathbf{\Theta}_{F}^{\dagger}$ is only dependent on the precoding matrix hence it can also be precomputed and used across blocks.

9.4 Full diversity hybrid equalizers for DS channels

The tall-tall precoder succeeds in enabling full diversity reception with LE, DFE as well as MLE. However, this comes at a significant cost. This being the loss of bandwidth efficiency. In order to increase the bandwidth efficiency, the so-called square precoders were introduced in [2]. The basic idea is to embed a constellation-rotation precoder [57] in $\mathbf{\Theta}$. Such a class of precoders is given by $\mathbf{\Theta} = \mathbf{C}_P \otimes \mathbf{Z}_2$ where $\mathbf{C}$ can be any square constellation-rotation precoder. Note that this precoder introduces redundancy of the order of channel delay spread in each *block* of the transmit signal vector (*super-block*). However, no redundancy is introduced in the Doppler domain. We therefore call the precoder a "square-tall" precoder. It is obvious that LE will not benefit from full channel diversity with this precoder. In [2], MLE was employed at the receiver to benefit from full channel diversity. However, there exists a possibility of combining the lower computational complexity of the LE with the full diversity benefits of MLE in a hybrid equalizer that limits ML processing only to extract Doppler diversity while employing a MMSE stage to benefit from multipath diversity. The idea of hybrid equalization (MMSE and MLE) is as follows. The received signal for the case of square-tall precoders is given by (dropping the block index k)

$$\begin{aligned} \mathbf{y} &= \sum_{q=0}^{Q} \mathbf{D}[f_q]\mathbf{H}_q\mathbf{\Theta}\mathbf{s} + \mathbf{v} && (9.28)\\ &= \boldsymbol{\mathcal{H}}(\mathbf{C}_P \otimes \mathbf{I}_K)\mathbf{s} + \mathbf{v} && (9.29)\\ \boldsymbol{\mathcal{H}} &= \sum_{q=0}^{Q} (\mathbf{D}_P[f_q(K+L)] \otimes \mathbf{D}_{K+L}[f_q])(\mathbf{I}_P \otimes \widetilde{\mathbf{H}}_q\mathbf{Z}_2) && (9.30) \end{aligned}$$

where $\widetilde{\mathbf{H}}_q$ is a $K+L \times K+L$ Toeplitz matrix formed by the first $K+L$ rows and columns of $\mathbf{H}_q[k;0]$ described in signal model. $\boldsymbol{\mathcal{H}}$ is a block banded matrix given by $\boldsymbol{\mathcal{H}} = \{\mathcal{H}_0 \oplus \mathcal{H}_1 \oplus ... \oplus \mathcal{H}_{P-1}\}$ with each $\mathcal{H}_p \quad p \in \{0, P-1\}$ given by

$$\mathcal{H}_p = \sum_{q=0}^{Q} [\mathbf{D}_P[f_q(K+L)]]_{p,p}\mathbf{D}_{K+L}[f_q]\widetilde{\mathbf{H}}_q\mathbf{Z}_2 \qquad (9.31)$$

At the receiver, MMSE equalization is first performed separately for each of the P $(K+L)$-length blocks in the received super-block to yield P sets of K input estimates. Denote this MMSE equalizer by $\boldsymbol{\mathcal{F}} = \{\mathcal{F}_0 \oplus \mathcal{F}_1 \oplus ... \oplus \mathcal{F}_{P-1}\}$

and the *partially equalized* signal vector at the output of the MMSE equalization stage by $\widetilde{\mathbf{y}} = [\widetilde{y}_0, \widetilde{y}_1 ..., \widetilde{y}_{PK}]^T$. ML detection on $\widetilde{\mathbf{y}}$ to extract the symbol vector $\mathbf{s}$ will now benefit from full channel diversity. Note that, since the noise at the output of $\boldsymbol{\mathcal{F}}$ is no longer white, the covariance of the colored noise in $\widetilde{\mathbf{y}}$ should be taken into account in the ML metric. We do so by weighting the ML metric according to the weighted least squares (WLS) criterion. Denote this covariance matrix by $\mathbf{R}_{\mathcal{F}\mathcal{F}}$. The ML weight factor is then given by the diagonal matrix $\boldsymbol{\Phi}$ formed by the diagonal elements of $\mathbf{R}_{\mathcal{F}\mathcal{F}}^{-1}$. The symbol estimates are obtained by using the $\boldsymbol{\Phi}$ thus formed in the weighted MLE and the transmit symbols are the solution to

$$\arg\min_{\mathbf{s}\in\mathcal{S}} (\widetilde{\mathbf{y}} - \boldsymbol{\mathcal{F}}\,\boldsymbol{\mathcal{H}}\,\boldsymbol{\Theta}\,\mathbf{s})^H \boldsymbol{\Phi} (\widetilde{\mathbf{y}} - \boldsymbol{\mathcal{F}}\,\boldsymbol{\mathcal{H}}\,\boldsymbol{\Theta}\,\mathbf{s}), \tag{9.32}$$

This is accomplished by setting up K parallel Viterbi equalizers for the K $P \times P$ mixtures. To this end $\widetilde{\mathbf{y}}$ is re-ordered into K sets of P symbols which we denote here by $\mathbf{z}_i$ $i \in 0, K-1$ and $\mathbf{z}_i = [\widetilde{y}_i, \widetilde{y}_{i+K}, ..., \widetilde{y}_{i+(P-1)(K-1)}]^T$. Now, by appropriately re-ordering the channel matrix, ML detection is performed on the $P \times P$ mixture in each block. We comment here that for the detection of symbols in each of the $P \times P$ mixture $\mathbf{z}_i$, the noise covariance matrix is indeed diagonal, however there is non-zero correlation between each of the K $P \times P$ mixtures. In the interest of simplicity, we ignore the correlation across blocks in the weight matrix.

9.4.1 Square-square precoders and MLE

It turns out that for MLE, it is not required to introduce the order L redundancy in each block in the super-block as in the case of the square-tall precoders. A precoder given by $\boldsymbol{\Theta}_{min} = \mathbf{T}(\mathbf{C}_P \otimes \mathbf{I}_K)$ where $\mathbf{C}$ is a square constellation-rotation precoder and $\mathbf{T} = [\mathbf{I}_{PK},\ \mathbf{0}_{PK\times L}]^T$ $P \geq Q+1$ suffices to extract full channel diversity with MLE. The zero-padding matrix $\mathbf{T}$ ensures that the inter-super-block interference is nulled. The cost here is an increase in the complexity of MLE and the payoff is increased bandwidth efficiency. For MLE the Viterbi algorithm may be applied with additional termination constraints. Currently we are able show through simulations that brute force MLE does indeed benefit from full channel diversity with redundancy of the order of the channel delay spread. We present these results in the next section

9.5 Simulation results

In this section we provide numerical results to show the diversity gains of the equalizers presented in this chapter. These results are based on outage probability or BER curves. To get the outage probability plots, Monte-Carlo simulations are carried out for a fixed transmission rate over either a frequency selective or doubly selective channel based on the equalizer being studied. For each channel realization, the resulting SINR for an arbitrary, fixed symbol is computed (in practice we use the symbol in the center of the transmit block as it experiences the maximum interference). When this SINR is not able to support transmission at the predefined rate, channel is declared to be in outage. For the polynomial expansion equalizers, the post-equalization SINR was computed as given by (9.18) and (9.22). The slope of the outage probability curve is then used to estimate the diversity gain of the receiver. In Fig. 9.1, we plot the outage probability for these three cases with the above simulation setup. We note that the slope of the outage probability for ZP-OFDM is greater than that of CP-OFDM system which is not surprising since CP-OFDM system, in the absence of any redundant precoding is not able to exploit multipath diversity present in the channel. The performance of cyclic prefixed ZP-OFDM with low complexity linear equalization for 3 different values of e_t clearly indicates that as e_t approaches L, the diversity of the system also approaches L. In other words, the system is able exploit the available excess time to provide additional diversity gains with linear equalization. In Fig. 9.2 we compare the performance of conventional MMSE equalization in CP-OFDM that does not exploit excess time present in the CP with that of the equalizer that exploits this excess time. The BER is seen to improve, however, as mentioned earlier, the diversity order of the equalizer is 1. Fig. 9.3 illustrates the evolution of the diversity order slope achieved against the order of approximation in the polynomial expansion equalizer in (9.17). It is seen that the slope flattens out understandably at lower order approximations due to large approximation errors but starts to stabilize at about second order approximation of the equalizer.

Fig. 9.4 shows the comparison of the diversity order of brute-force implementation of the MMSE-ZF equalizer for doubly selective channels for the case of $Q = 2$ and $L = 1$. Observe that the slope of the outage probability curves for both the implementations are the same. The polynomial expansion equalizer has an SNR offset when compared to the brute force implementation which is to be expected since the equalizer is an approximation of the MMSE-ZF receiver however, it succeeds in collecting full

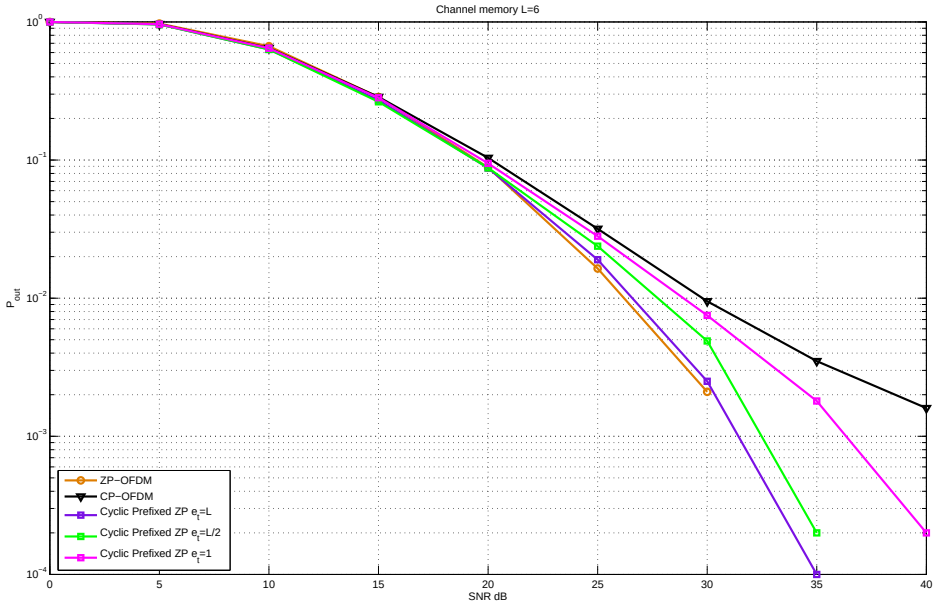

Figure 9.1: Outage Probability results for frequency selective channels.

diversity offered by the doubly selective channel at relatively low order of approximation. The performance of PE approximation that minimizes the MSE at the receiver (9.19) is shown in Fig. 9.5. We see a significant enhancement in performance for the first order approximation when compared to the PE approximation in (9.17). The effect of PE is a saturation floor of the outage probability. This floor gets lower with higher PE order. However, for lower SNR, before the floor is reached, the outage probability enjoys the full diversity gains and the only effect of the PE approximation is a SNR offset loss. For a given PE order, the use of MMSE diagonal combination coefficients in the PE leads to significant lowering of the floor compared to straight ZF PE. From the simulations, it appears that the sub-optimality of first order PE with MMSE diagonal combination coefficients is negligible compared to the brute force MMSE-ZF linear receiver, over any outage probability range of practical interest.
In Fig. 9.6 we compare the performance of the hybrid equalizer for square-tall precoders. Note that MMSE-ZF receiver does not collect full diversity whereas the diversity order of the hybrid equalizer is the same as that of full blown MLE which has a much higher computational complexity com-

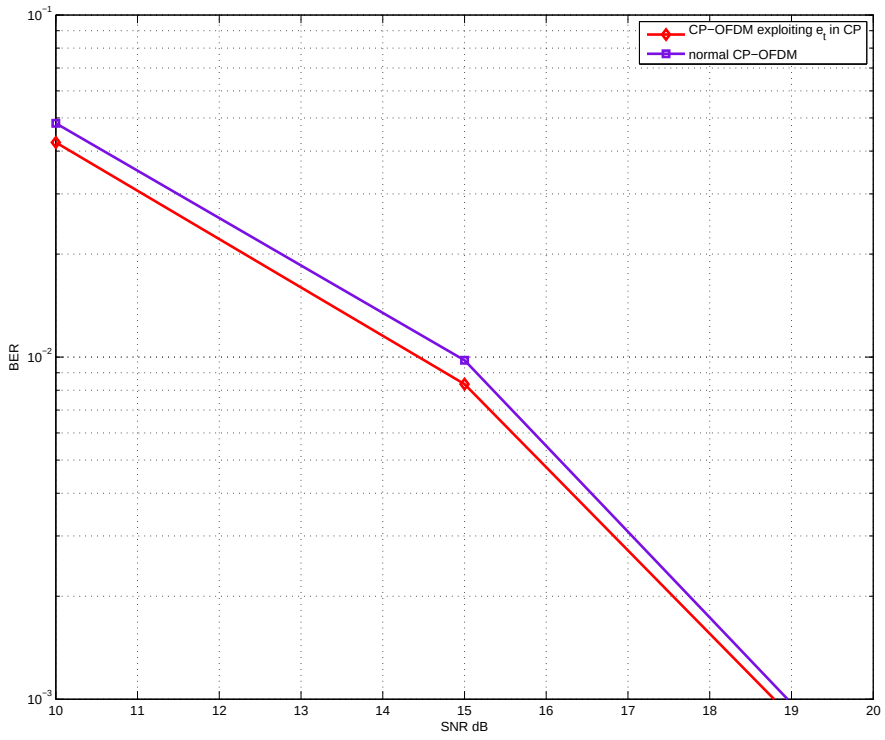

Figure 9.2: BER comparison of CP-OFDM exploiting excess time in CP.

pared to the hybrid equalizer. Finally in Fig. 9.7 we compare the diversity order with square-tall precoders with that of the square-square precoders when MLE is applied at the receiver. We see that both the precoders enable MLE to exploit full channel diversity. However, the square-square precoders have a higher bandwidth efficiency while the square-tall precoders have better coding gain.

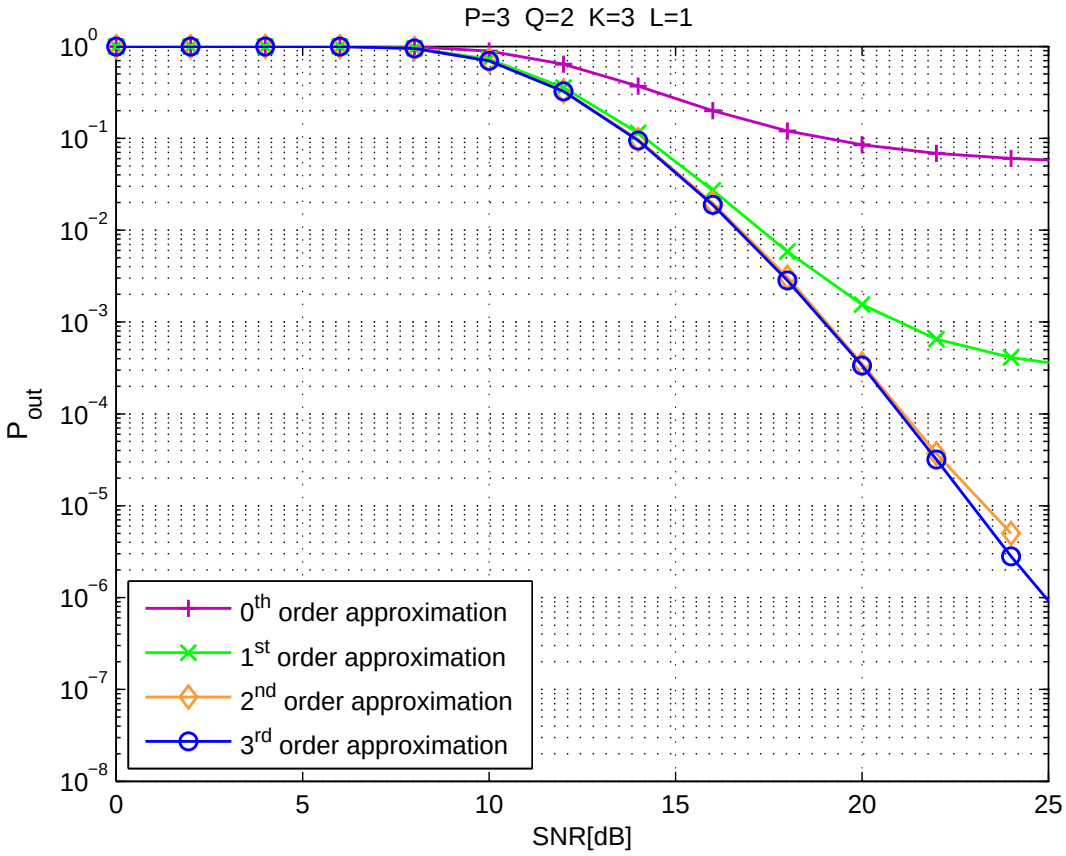

Figure 9.3: Evolution of diversity order for different iterations.

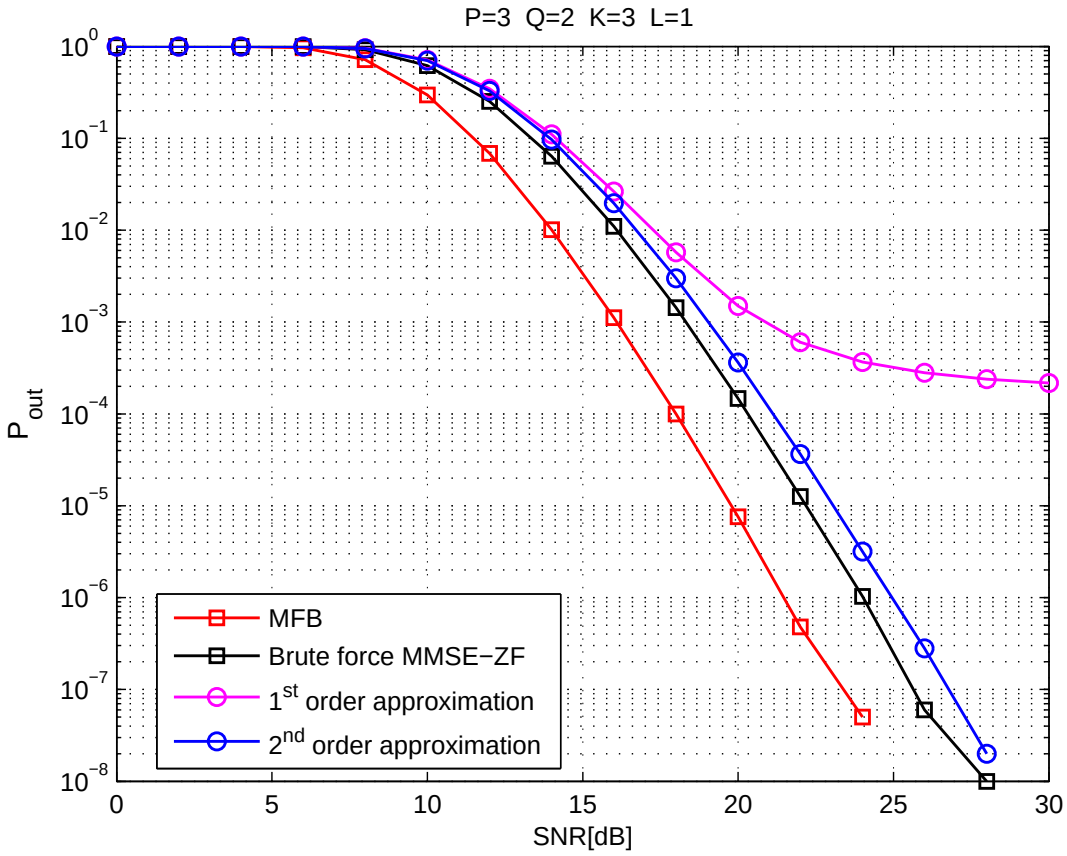

Figure 9.4: Diversity order of LE approximated by PE.

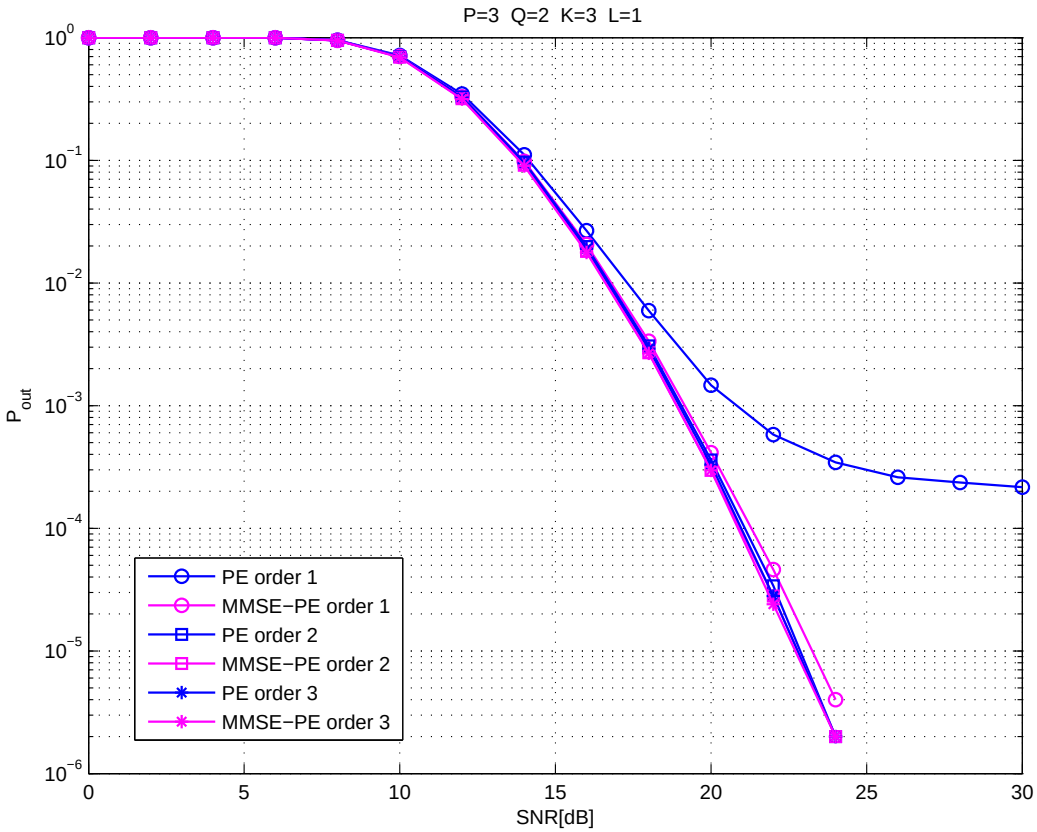

Figure 9.5: Comparison of performance of the two PE approximations.

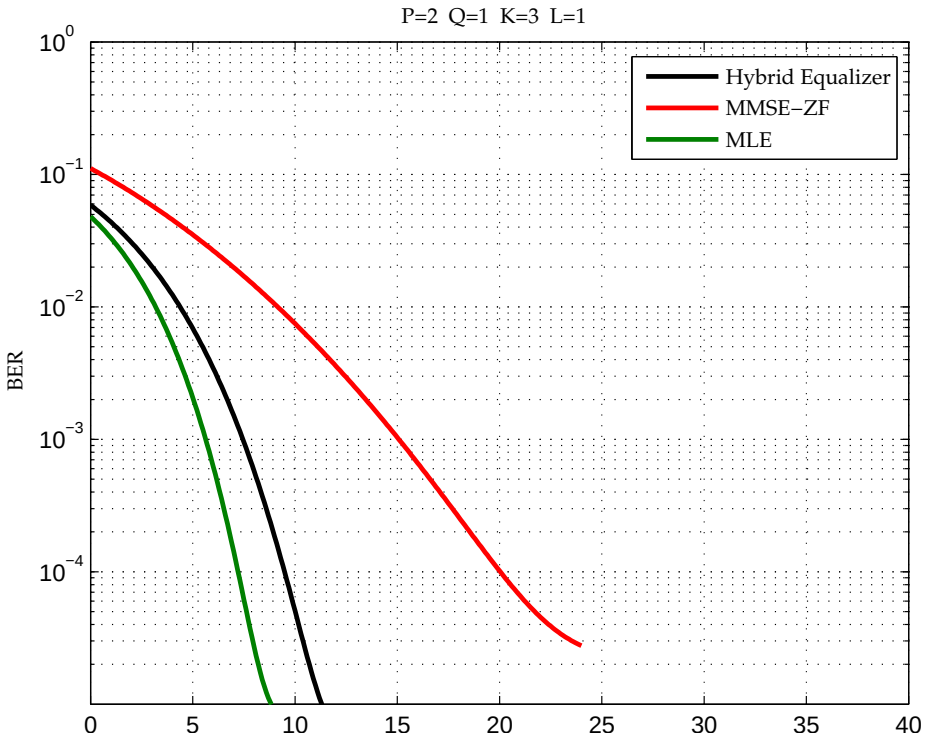

Figure 9.6: Performance of hybrid equalizer with square-tall precoder.

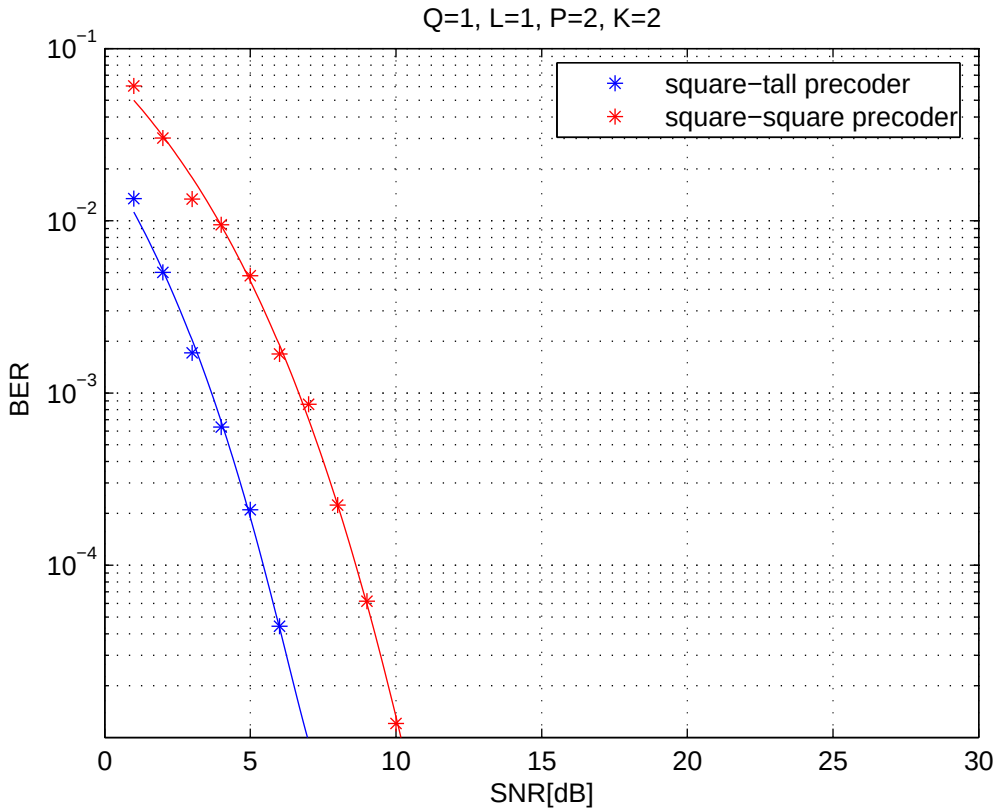

Figure 9.7: Comparison of diversity order with square-tall and square-square precoders.

Part III

Interference alignment

Chapter 10

Interference alignment in constant coefficient MIMO channels

10.1 Introduction

Interference is being increasingly accepted as the major bottleneck limiting the throughput in wireless communication networks. Recent research [1] has however shown that at least in the high signal to noise ratio (SNR) regime the per-user capacity of an interference channel (IFC) with arbitrary number of users scales at half the rate of each user's interference-free capacity. Such a scaling was obtained in [1] using the concept of interference alignment (IA). The key idea behind IA is to process the transmit signal (data streams) at each TX so as to align all the undesired signals at each receiver (RX) in a subspace of suitable dimension. This alignment allows each RX to suppress more interfering streams than it could otherwise cancel. In fact, in the high SNR regime, simple zero-forcing (ZF) receivers suffice to separate the desired signal from the interferers. In a constant coefficient MIMO IFC (channel coefficients are constant over the transmit duration), the total number of streams contributing to the input signal at each RX are typically greater than the number of antennas available at the RX. Aligning the streams at the TX allows each RX to cancel more steams than the

number of “spare antennas" at its disposal. Thus underscoring the importance of IA in the high-SNR regime since IA maximizes the sum-capacity pre-log factor, the so called total *degrees of freedom* (DoF) for a given antenna distribution in the K-link Noisy IFC (inter-link interference is treated as Gaussian noise) when the processing at the TX and RX is constrained to be linear.

The capacity of an IFC in general has been an open problem for long. Till date, the best result is [58] for the 2-user Gaussian IFC. For $K > 2$, the problem is even more complicated. This has lead to an alternative line of attack; that of characterizing the capacity region in terms of the total DoF in the high SNR regime. Such a characterization, assuming time-varying channels was provided in [59] with linear precoders and in [60] where non-linear precoders were considered for the constant coefficient channel. However, the DoF characterization for the K-user constant coefficient MIMO IFC with linear processing is still an open problem.

In a K-link MIMO IFC where the k-th link is characterized by a TX with M_k antennas, a RX with N_k antennas and a requirement of d_k independent streams to be communicated over the k-th link, the existence of an IA solution is not known. Numerical solutions in [61] [5] can be used to evaluate their existence through simulations. The feasibility of IA solutions for a constant coefficient MIMO IFC was studied in [62] [4]. In [4], when $d_k = 1 \ \forall k$, a MIMO IFC with a given distribution of TX/RX antennas is classified as *proper* or *improper*. All proper systems are almost surely (a.s) feasible. For a system to be proper, it is required that, for *every subset* of equations that arise due to the IA constraints, the number of variables be at least equal to the number of equations in that subset. This condition (that the system be proper) is sufficient but may not be necessary. Moreover, such a classification can be computationally expensive even for systems with relatively small number of transmit and receive antennas. Furthermore, for an arbitrary DoF allocation amongst users (d_k not constrained to be 1), additional outerbounds need to be satisfied for a system to be feasible. It turns out however, that for multi-stream transmission, conformance with the outerbounds do not necessarily provide insight into the feasibility of an IA solution. In other words, an IA solution is not guaranteed if the outerbounds are satisfied. An example follows: For a $K = 3$ user MIMO IFC where $d_k = 2 \ \forall k$, $M_1 = N_1 = 4$, $M_2 = 5$, $N_2 = 3$, and $M_3 = 6$, $N_3 = 2$, the outerbounds (cf. (21) in [4]) are satisfied. However, the system does not admit an IA solution.

In this part of the thesis we propose a systematic method to check the feasibility of IA solutions for a given K-link Noisy MIMO IFC and an arbitrary

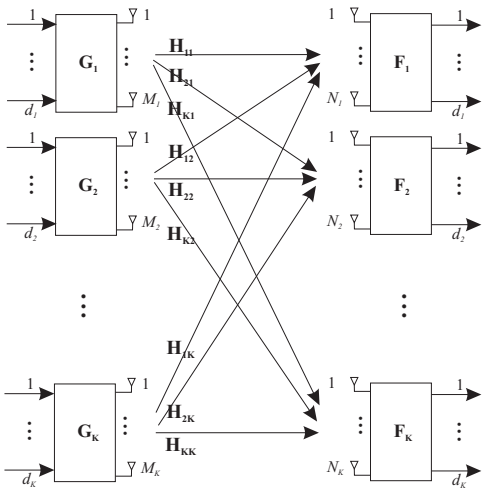

Figure 10.1: MIMO Interference Channel

DoF allocation. Throughout this part, when we refer to a K-link MIMO IFC, we mean the K-link constant coefficient Noisy MIMO IFC.

10.2 System model

Fig. 10.1 depicts a typical K-link MIMO IFC with K TX-RX pairs. The k-th TX and the k-th RX are equipped with M_k and N_k antennas respectively. The k-th TX generates interference at all $l \neq k$ receivers. Assuming a constant coefficient channel, the $\mathbb{C}^{N_k \times 1}$ received signal $\mathbf{y}_k$ at the k-th RX can be represented as

$$\mathbf{y}_k = \mathbf{H}_{kk}\mathbf{x}_k + \sum_{\substack{l=1 \\ l \neq k}}^{K} \mathbf{H}_{kl}\mathbf{x}_l + \mathbf{n}_k,$$

where $\mathbf{H}_{kl} \in \mathbb{C}^{N_k \times M_l}$ represents the channel matrix between the l-th TX and k-th RX, $\mathbf{x}_k$ the $\mathbb{C}^{M_k \times 1}$ transmit signal vector corresponding to the k-th TX and the $\mathbb{C}^{N_k \times 1}$ vector $\mathbf{n}_k$ represents the additive white Gaussian noise with zero mean and covariance matrix $\mathbf{R}_{n_k}$. Each entry of the channel matrix is a complex random variable drawn from a continuous distribution without any deterministic relation between channel coefficients. We assume centralized processing with complete knowledge of all direct-link and cross-link channel matrices on the transmit side.
Let $\mathbf{G}_k$ denote the $\mathbb{C}^{M_k \times d_k}$ beamforming matrix of the k-th TX. Then $\mathbf{x}_k =$

$\mathbf{G}_k\mathbf{s}_k$, where the $d_k \times 1$ vector $\mathbf{s}_k$ represents the transmitted symbols and d_k the number of independent streams transmitted to its RX. We assume $\mathbf{s}_k$ to have a Gaussian distribution with $\mathcal{N}(0, \mathbf{I}_{d_k})$. At the k-th RX, $\mathbf{F}_k \in \mathbb{C}^{d_k \times N_k}$ is applied to suppress interference and retrieve the d_k desired streams. Applying the interference suppressing filter $\mathbf{F}_k$ to $\mathbf{y}_k$, we obtain the following $d_k \times 1$ vector $\mathbf{r}_k$

$$\mathbf{r}_k = \mathbf{F}_k\mathbf{H}_{kk}\mathbf{G}_k\mathbf{s}_k + \sum_{\substack{l=1 \\ l\neq k}}^{K} \mathbf{F}_k\mathbf{H}_{kl}\mathbf{G}_l\mathbf{s}_l + \mathbf{F}_k\mathbf{n}_k.$$

Chapter 11

Interference alignment feasibility

11.1 Interference alignment feasibility

The objective in IA is to design aligning matrices to be applied at the transmitters such that, the interference caused by all transmitters at each non-intended RX lies in a common *interference subspace*. Moreover, the interference subspace and the *desired signal subspace* of each RX should be non-overlapping (linearly independent). If alignment is complete, simple ZF can be applied to suppress the interference and extract the desired signal in the high-SNR regime. Thus, the following conditions need to be satisfied for IA:

$$\mathbf{F}_k \mathbf{H}_{kl} \mathbf{G}_l = \mathbf{0} \quad \forall l \neq k \tag{11.1}$$

$$\mathrm{rank}(\mathbf{F}_k \mathbf{H}_{kk} \mathbf{G}_k) = d_k \quad \forall k \in \{1, 2, \ldots, K\} \tag{11.2}$$

In addition, the traditional single user MIMO constraint $d_k \leq \min(M_k, N_k)$ also needs to be satisfied for d_k streams to be able to pass over the k-th link. The first step toward analytical evaluation of the existence of an IA solution for a given DoF allocation in a K-link MIMO IFC is the translation of the above equations into a set of conditions that need to be satisfied to admit an IA solution. To this end, the approach we adopt here is of formulating the given IA problem as finding a solution to a (bilinear) system of equa-

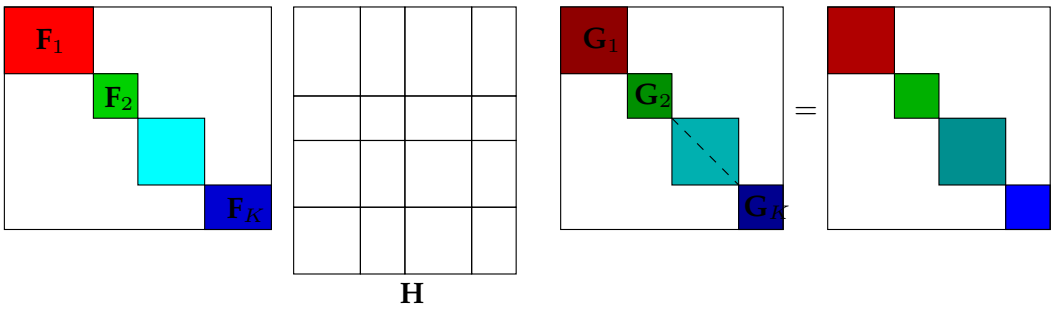

Figure 11.1: Block matrix representation of the interference alignment problem.

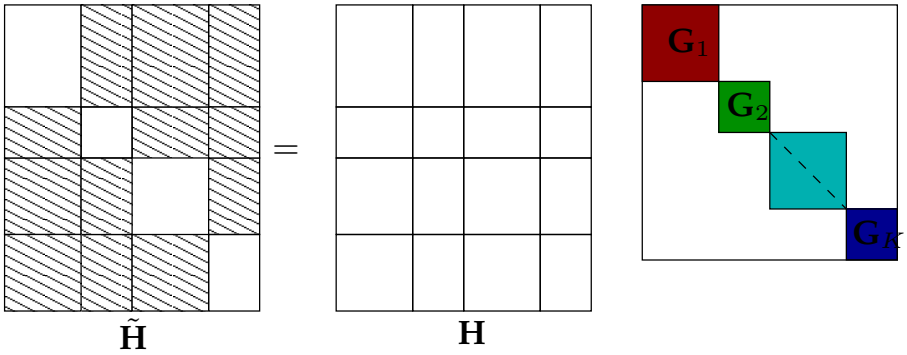

Figure 11.2: Interference alignment at all receivers .

tions with limited number of variables dictated by the dimensions of the overall system (the M_ks, N_ks and d_ks of the MIMO IFC). Fig. 11.1 presents a pictorial representation of such a system of equations where the block matrices **F**, **H** and **G** on the left hand side (LHS) of the equality represent respectively, the ZF RX, overall channel matrix and beamformers. The block diagonal matrix to the right hand side (RHS) of the equality represents the total constraints in the system that need to be satisfied for an IA solution to exist. The block matrices on the diagonal of **H** represent the direct-links and the off diagonal blocks in any corresponding block row k represent the cross channels of the k-th link. The interference aligning beamformer matrix $\mathbf{G}_k$ (the diagonal blocks in **G**) aligns the transmit signal of the k-th user to the interference subspace at all $l \neq k$ users while ensuring the rank of the equivalent channel matrix $\mathbf{F}_k\mathbf{H}_{kk}\mathbf{G}_k$ is d_k. In other words, in Fig. 11.2, the $\mathbf{G}_k$ matrices are designed such that pre-multiplication of the

overall beamformer matrix $\mathbf{G}$ with the overall channel matrix $\mathbf{H}$ results in a block matrix $\widetilde{\mathbf{H}}$ in which, all the off-diagonal blocks in any block row k (the shaded blocks of each block row) share a common column space whose dimension is at most $(N_k - d_k)$. With this accomplished, $\mathbf{F}_k$ simply projects the received signal into a subspace orthogonal to the interference subspace to retrieve the desired signal at the k-th RX resulting in a $(d_k \times d_k)$ matrix (the rank d_k equivalent channel) for its desired streams and $(K-1)$ block-zero matrices in the k-th block row of the matrix to the right.

The only requirement on the $(d_k \times d_k)$ matrix that mixes up the desired streams is that it be of full rank. The beamforming matrix therefore, is determined up to an arbitrary $(d_k \times d_k)$ square matrix. Thus, of the total number of $(M_k \times d_k)$ variables available for the design of $\mathbf{G}_k$ matrix, transmission of d_k independent streams results in an immediate loss of d_k^2 variables thus reducing the total number of variables available for the design of an interference aligning beamformer at each TX to $d_k(M_k - d_k)$. The reason for evaluating the number of variables available at the TX is the nature of the IA problem. The IA scheme essentially requires that all alignment be done at the TX. Therefore every TX imposes a set of constraints on the entire system (as a consequence of alignment conditions at each non intended RX) whenever it transmits a stream to its RX. Thus, an IA solution will be feasible only if the total number of variables available in the system is greater than or equal to the total number of constraints to be satisfied. Moreover, the variables should be distributed appropriately at each of the TX. In the sequel, we provide a systematic method of counting the number of variables available for the design of an interference aligning beamformer at each TX and comparing them with the constraints imposed on the system by each TX. This method can be seen as arriving at the K-link MIMO IFC for which the existence of an IA solution is to be analyzed, by successively adding a single TX and computing the total number of variables available for the joint design of the interference aligning beamformers at the transmitters and comparing it against the total number of alignment constraints imposed by the TX (due to its d_k streams) at each step of this build-up.

The main idea of our approach is to convert the alignment requirements at each RX into a rank condition of an associated interference matrix. At RX k, the interference due to all other $(K-1)$ transmitters is grouped into a $(N_k \times \sum_{l=1;l\neq k}^{K} d_l)$ matrix

$$\mathbf{H}_I^{[k]} = [\mathbf{H}_{k1}\mathbf{G}_1, ...\mathbf{H}_{k(k-1)}\mathbf{G}_{(k-1)}, \mathbf{H}_{k(k+1)}\mathbf{G}_{(k+1)}, ...\mathbf{H}_{kk}\mathbf{G}_K],$$

that spans the interference subspace at the k-th RX. We call this the interference matrix at user k. The total signal-space dimension at RX k is given by the total number of receive antennas N_k, of which d_k interference-free signaling dimensions are to be reserved for the signal from the k-th TX. This is achieved when the interference from all other transmitters lies in an independent subspace whose dimension can be at most $(N_k - d_k)$. Thus the dimension of the subspace spanned by the matrix $\mathbf{H}_I^{[k]}$ must satisfy

$$\mathrm{rank}(\mathbf{H}_I^{[k]}) = r_I^{[k]} \leq N_k - d_k \tag{11.3}$$

While the above equation prescribes an upper bound for the rank of the interference matrix, the nature of the channel matrix (full rank property) combined with the rank requirement of the beamformer at each TX $(\mathrm{rank}(\mathbf{G}_k) = d_k)$ specifies the following lower bound on $r_I^{[k]}$

$$r_I^{[k]} \geq \max_{l \neq k}(d_l - [M_l - N_k]_+) \tag{11.4}$$

where $[x]_+ = \max(0, x)$ and $[M_l - N_k]_+$ discounts the possibility of the columns of $\mathbf{G}_l$ belonging to the orthogonal complement of $\mathbf{H}_{kl}$. Forcing the rank of $n \times m$ matrix $\mathbf{A}$ to some $r \leq \min(m, n)$ implies imposing $(n - r)(m - r)$ constraints. We explain this briefly as follows. Without loss of generality, assume that the columns of this $n \times m$ matrix are partitioned into $\mathbf{A} = [\mathbf{A}_1 | \mathbf{A}_2]$ where $\mathbf{A}_1$ is $n \times r$ and is of full column rank. Then imposing a rank r on $\mathbf{A}$ implies that $\mathbf{A}_2$ shares the same column space as $\mathbf{A}_1$ which in turn implies that $\mathbf{A}_1^{\perp T}\mathbf{A}_2 = \mathbf{0}$. Since $\mathbf{A}_1^{\perp}$ is $n \times (n - r)$, it follows that $(n - r)(m - r)$ constraints need to be satisfied for $\mathbf{A}$ to be of rank r. Thus imposing a rank $r_I^{[k]}$ on $\mathbf{H}_I^{[k]}$ implies imposing

$$(N_k - r_I^{[k]})(\sum_{\substack{l=1 \\ l \neq k}}^{K} d_l - r_I^{[k]})$$

constraints at RX k. $r_I^{[k]}$ is maximum when the interference contribution of each interferer spans an independent subspace. Which leads us to the upper bound $r_I^{[k]} \leq \sum_{l=1; l \neq k}^{K} d_l$. However, accounting for the inequality in (11.3) we have

$$r_I^{[k]} \leq \min(d_{tot}, N_k) - d_k \tag{11.5}$$

where $d_{tot} = \sum_{k=1}^{K} d_k$, and $\min(.)$ operation appears in the above equation due to the fact that the rank of $\mathbf{H}_I^{[k]}$ cannot exceed its dimensions.

11.2 Recursive procedure to evaluate feasibility

In this section we detail a recursive method of evaluating the feasibility of an IA solution for a MIMO IFC and a corresponding DoF distribution. As mentioned earlier, the main idea here is to interpret the interference alignment requirement at each RX as forcing a certain rank on the associated interference channel $\mathbf{H}_I^{[k]}$ which in turn imposes a certain number of constraints on the IA problem. In the earlier section we show that this rank is bounded above and below by the system parameters. The first step therefore is to ensure that the range of each r_i is non-empty. From (11.3) and (11.4), this amounts to checking if

$$(\min(d_{tot}, N_k) - d_k) - \max_{j \in \mathcal{K}-\{k\}} (d_j - [M_j - N_k]_+) \geq 0 \quad \forall k \in \mathcal{K} \qquad (11.6)$$

where $\mathcal{K} = \{1, 2, ...K\}$. Indeed, an IA solution is immediately ruled out if (11.6) is not true. This is due to the fact that the full rank nature of the cross channel $\mathbf{H}_{kj}$ will ensure that the minimum rank of $\mathbf{H}_I^{[k]}$ due to $j \neq k$ will be d_j unless it possesses a null space of non zero dimension in which case it can shrink the rank by a maximum of $[M_j - N_k]_+$. (11.6) can be interpreted as check for the minimum values of M_k and N_k $\forall k$ for a given DoF allocation.

Proposition: Let $\boldsymbol{\mathcal{M}}_K = \{\{M_k\}, \{N_k\}, \{d_k\}\}$ represent a K-link MIMO IFC where $\{M_k\}$ and $\{N_k\}$ represent the ordered set of transmit and receive antennas of each user in the system and $\{d_k\}$ is the ordered set of the associated DoF desired for each user (ordering is by user index). Denote by $\mathcal{K}_o$ the ordered set of users with decreasing d_k such that users with equal d_ks are ordered according to increasing M_k. Similarly, define $\boldsymbol{\mathcal{M}}_K^{'}$ to be the MIMO IFC and the associated set $\mathcal{K}_o^{'}$ obtained by interchanging $\{M_k\}$ and $\{N_k\}$. Then an IA solution exists if both of the following conditions are satisfied:

1. (11.6) holds true for $\boldsymbol{\mathcal{M}}_K$ and $\boldsymbol{\mathcal{M}}_K^{'}$

2. Starting from a system consisting only of the K receivers, if the complete system $\boldsymbol{\mathcal{M}}_K$ (respectively $\boldsymbol{\mathcal{M}}_K^{'}$) is "built" by successively adding one TX at a time from $\mathcal{K}_o$ (respectively $\mathcal{K}_o^{'}$) and (11.7) is valid (satisfied) at each step of this "build-up".

$$\begin{aligned}\sum_{i=1}^{k} d_i(M_i - d_i) &\geq \sum_{i=1}^{k}(N_i - \overline{r}_I^{[i]})(\ \underline{d} - d_i - \min(\underline{d} - d_i, (N_i - d_i))\ ) \\ &\quad + \sum_{i=k+1}^{K}(N_i - \overline{r}_I^{[i]})(\ \underline{d} - \min(\underline{d}, (N_i - d_i))\ ) \qquad (11.7) \\ \overline{r}_I^{[i]} &= \min(\underline{d} - d_i, (N_i - d_i))\ i \in \{1, \ldots k\} \\ &= \min(\underline{d}, (N_i - d_i))\ i \in \{k+1, \ldots K\}\end{aligned}$$

The need to satisfy both the above conditions for $\boldsymbol{\mathcal{M}}_K$ *and* $\boldsymbol{\mathcal{M}}_K^{'}$ arises due to the alignment duality. From the IA conditions in (11.1) (11.2), it is clear that taking the transpose of these equations results in IA conditions for the *dual* MIMO IFC and the same existence conditions should be satisfied for this dual MIMO IFC as well.

At each step k of the recursion, (11.7) accumulates the total number of variables available for designing an IA solution in an associated sub-problem comprising of a k-link MIMO IFC where only k transmitters are transmitting non-zero streams and aligning their streams into some interference subspace of all non-intended receivers in the LHS of (11.7). The RHS accumulates the total number of constraints at all receivers that arise due to these transmitters. That the number of variables contributed by the i-th TX is given by $d_i(M_i - d_i)$ is obvious from the discussion in the previous section. We now elaborate on the method of obtaining the constraints on the RHS of (11.7). Forcing a rank on $\mathbf{H}_I^{[k]}$ amounts to satisfying a number of constraints that is a function of the rank and the dimensions of $\mathbf{H}_I^{[k]}$. While we do not have knowledge of the exact rank of $\mathbf{H}_I^{[k]}$ at each k (since that will be the result of the IA design whose feasibility we are evaluating in the first place) we do know the numerical *range* of $r_I^{[k]}$ for each k. Therefore, instead of using the actual rank it is useful to use its upper bound (denoted by $\overline{r}_I^{[k]}$, as specified in (11.6). On the RHS of (11.7) the first summation reflects the total number of constraints to be satisfied for an IA solution to exist in a k-link MIMO IFC with k-links transmitting a total of $\underline{d} = \sum_{i=1}^{k} d_i$ streams. For each user i accounted for in this summation, we have to ensure that at RX-i, $r_I^{[i]} \leq (N_i - d_i)$. The column dimension of $\mathbf{H}_I^{[i]}$ is $(\underline{d} - d_i)$. In order to minimize the total number of constraints that we impose of the system (due to the act of forcing a particular $r_I^{[i]}$ at the i-th RX), we choose the maximum possible rank of $r_I^{[i]}$, which we know to be $\min(\text{column dimensions}, N_i - d_i)$

i.e., $\overline{r}_I^{[i]} = \min(\underline{d} - d_i, N_i - d_i)$. The second summation consists of all "unpaired" receivers in the sub-problem i.e., those receivers whose corresponding transmitters are presently not transmitting any streams but still need $\underline{d}$ streams to be aligned in their interference subspace. Therefore, the maximum allowable rank of the interference matrices for all these receivers is $\overline{r}_I^{[i]} = \min(\underline{d}, N_i - d_i)$. Thus, (11.7) when true at each step, verifies that the number of variables available for the design of IA beamformers at all k transmitters is greater than the number of constraints that are imposed by an IA solution. In fact, it verifies that its is possible to align all the interference not just in the associated k-link MIMO IFC but also in the interference subspace of all un-intended receivers that are not in the k-link MIMO IFC (the un-paired receivers accounted for in the second summation). Finally, the ordering of the users in terms of increasing d_k in $\mathcal{K}_o$ ($\mathcal{K}_o^{'}$ for $\boldsymbol{\mathcal{M}}_K^{'}$) ensures early identification of in-feasibility of an IA solution since a larger dof requirement typically results in smaller number of variables available at the TX in order to meet the rank constraints.
In the next section we present numerical examples to show that our approach is able to check the feasibility (or in-feasibility) of an IA solution for a given MIMO IFC. For a $\boldsymbol{\mathcal{M}}_K$ which conforms to both the conditions of our approach, we are able cross validate that an IA solution exists using an iterative algorithm proposed in [5]. Indeed, it can be shown that the algorithm in [5] will always converge to an optimum solution when our conditions are met since convergence to an optimum solution implies that the d_k minimum eigenvalues of $\sum_{i \neq k} \mathbf{H}_{ki}\mathbf{G}_i\mathbf{G}_i^H\mathbf{H}_{ki}^H$ are zero which will be true if $\mathrm{rank}(H_I^{[k]}) \leq \min(d_{tot}, N_k) - d_k$ which is a part by our systematic approach.

11.3 Numerical examples

We provide here some numerical examples to validate the conditions derived in the previous section. In all the examples given in this section, when the MIMO IFC that satisfied the conditions in Sec. 11.2, the numerical algorithm in [5] was able to find an IA solution whereas it failed to find one when these conditions were not satisfied[1].
Example 1: Consider a 2-link MIMO system with $M = 2, N = 4, d = 2$. This system satisfies the 2 conditions in Sec. 11.2 and IA solutions do exist for

[1] In addition to these, we tested our conditions extensively with varied antenna and stream distributions. We do not provide these examples here due to space constraints. In particular, all the examples in [4] we also tested.

this system.
Example 2: Similarly, the 6 user case where $M_k = 3, N_k = 4, d_k = 1 \forall k$, both conditions in Sec. 11.2 are satisfied and an IA solution is possible for this case.
Example 3: There exists an IA solution for $\boldsymbol{\mathcal{M}}_3$ where $\{M_k\} = \{3, 1, 10\}, \{N_k\} = \{4, 3, 4\}, \{d_k\} = \{2, 1, 2\}$ and it can be shown that indeed, it satisfies the conditions in the previous section.
Example 4: We now look at another 2-link MIMO system with $M_1 = 4, N_1 = 7, d_1 = 3, M_2 = 10, N_2 = 4, d_2 = 2$. For this system, the rank conditions are not satisfied and indeed, there is no IA solution for this case.
Example 5: In the 4-link case characterized by $M_k = 2, N_k = 3 \; k = 1, 2, 3$ and $M_4 = N_4 = 2 \; d_k = 1 \forall k$. The rank conditions are satisfied but (11.7) is not satisfied. Therefore we conclude that there cannot be an interference alignment solution for this system.

11.4 Alternative zero forcing approach to IA

Another possible approach to determine if a K-link MIMO interference channel has an IA solution can be obtained interpreting interference alignment as joint transmit-receive linear zero forcing. The idea is that a stream transmitted from TX k and causes interference to the non intended RX j can be suppressed at either the TX or at the RX. Denoting with t_{kj} the size of the subset of streams d_k, that are received at RX j that the k-th TX suppresses, and with r_{kj} the size of the subset of streams d_k, that are received at RX j, that the j-th RX suppresses, the sum of these two quantities should be: $t_{kj} + r_{kj} \geq d_k$. The total number of streams that TX k can suppress is at most $M_k - d_k$ and the total number of streams that the j-th RX can suppress is not greater than $N_j - d_j$. Therefore, to check the feasibility of an interference alignment solution, the following conditions should be satisfied:

$$\begin{array}{ll} \sum_{j \neq k} t_{kj} & \leq M_k - d_k \\ \sum_{k \neq j} r_{kj} & \leq N_j - d_j \end{array} \tag{11.8}$$

$$\forall t_{kj}, r_{kj} \in \{0, 1 \ldots, d_k\}, \text{ and } t_{kj} + r_{kj} = d_k$$

$$\max_{k \neq j}(d_j - [M_k - N_j]) \leq (N_j - d_j) \forall j \in \{1, \ldots, K\}$$

As before, due to alignment duality, (11.8) must be true when M_k and N_k values are interchanged (the dual channel case). One possible way to verify if all this inequalities are satisfied or not is to check all the possible

$\prod_{k=1}^{K}(d_k+1)^{K-1}$ combination of t_{kj} and r_{kj}. If there is at least one combination that satisfies the constraints, then an interference alignment solution is bound to exist.Such an alternate approach has some interesting implications.

Example 6: Consider $\boldsymbol{\mathcal{M}}_3 = \{\{M_k\} = \{N_k\} = \{1,3,6\}, \{d_k\} = \{1,2,3\}\}$. w.l.o.g., order the users in terms of increasing d_k, then, the first user pair is in no position to do anything. However, $\mathbf{G}_2$ can be designed to suppress interference caused at the RX of user-1 and $\mathbf{G}_3$ can be designed to suppress interference caused at the receivers of users 1 and 2. Similarly, $\mathbf{F}_2$ can suppress interference generated by user-1 while $\mathbf{F}_3$ can be designed to suppress interference from transmitters of user-1 and user-2. Thereby enabling reception of d_k interference free streams $\forall k$ user pairs. More interestingly, based on the structure of the above problem, we have the following conjecture that draws attention to the benefits of systems with unequal stream distributions.

Conjecture: There exists a MIMO IFC $\boldsymbol{\mathcal{M}}_K^{(u)}$ with unequal antenna and stream distribution for any given network dof d_{tot}, such that the total number of antennas in $\boldsymbol{\mathcal{M}}_K^{(u)}$, $\mathcal{A}_{tot}^{(u)} = \sum_k (M_k + N_k)$, required to achieve d_{tot} is less than the total number of antennas in $\boldsymbol{\mathcal{M}}_K^{(e)}$ where $M_k = M, N_k = N, d_k = d_{tot}/K\ \forall k$. $\boldsymbol{\mathcal{M}}_K^{(e)}$ is the so-called identical stream and antenna configuration (ISAC) [62] or symmetric [4] system.

The conjecture is motivated by the generalization of *Example 6* to any K-link system. Consider a K-link MIMO IFC with user pairs indexed in the order of increasing d_k. Let the following relationship hold.

$$d_{(k+1)} = d_k + 1,\ k \in 2, \ldots, K.$$

Then it can be shown that an IA solution exists if each user pair has the following antenna distribution:

$$M_k = N_k = \sum_{i=1}^{k} d_i,\ k \in \{1, \ldots, K\}.$$

Let $\mathcal{A}_{tot}^{(e)}$ represent the total number of antennas in an ISAC system $\boldsymbol{\mathcal{M}}_K^{(e)}$. We know from [62] [4] that, for $\boldsymbol{\mathcal{M}}_K^{(e)}$ the minimum number of antennas per-user needs to satisfy

$$M + N \geq (K+1)\frac{d_{tot}}{K}.$$

It is easily verified that, for $K \geq 2$, $\mathcal{A}_{tot}^{(u)} \leq \mathcal{A}_{tot}^{(e)}$.

It is also possible to prove this starting from a given $\boldsymbol{\mathcal{M}}_K^{(e)}$ and splitting the d_{tot} into a DoF allocation where not all users have the same DoF.

Chapter 12

Concluding remarks

In this PhD dissertation we investigated various methods to achieve efficient communications over wireless channels. In the first part where we concentrated on equalizer designs for HSDPA, we introduced a class of receivers for SISO HSDPA downlink based on the novel concept of chip-level sparsification and symbol level equalization. Due to channel sparsification, the resultant channel presents itself as a symbol-level ISI channel at the output of the correlator. By treating the scrambler as deterministic, we showed that the receiver can benefit from reduced parameter time-varying non-linear equalization at symbol-level. We presented solutions for obtaining the optimum channel-sparsifying filter depending on the non-linear processing stages that exploit the resultant sparse channel. We derived SINR expressions for these receivers and compared their performance against the classical MMSE chip-equalizer correlator receiver. We showed that such receivers can outperform the best chip-level linear equalization solution. For the MIMO case, we proposed equalizers based on the concept of combined chip-level and symbol level processing. In particular, the chip-level processing stage was the SINR maximizing LMMSE chip-equalizer which in addition to restoring the orthogonality of the codes also achieves spatial separation to a certain degree. Further processing stages at symbol level was introduced to enhance the performance of the receivers. When MIMO HSDPA receivers are based on MMSE designs, we showed that there exists an optimal choice of precoding matrix to be

employed at the transmitter that maximizes the sum-capacity of these receivers and derived analytical expressions for the choice of the optimal precoding matrix. We found that receivers that treat the scrambler as a deterministic sequence can resort to time-varying symbol level processing after the equalizer-correlator stage in order to re-gain the time varying signal contribution which would otherwise be treated as noise leading to additional gains in SINR which ultimately effects achievable capacity of the receivers. Finally we discussed multi-user extensions to closed loop transmit diversity techniques that have been standardized in [13] and proposed multi-user beamforming strategies that can be employed at the BS in order to maximize the downlink capacity. Simulation results show that for MIMO HSDPA, downlink capacity is maximized by using the MIMO channel to service multiple single stream users (SDMA) instead of single user spatial multiplexing which is currently supported in the standards.

The main contributions of the second part of the thesis can be itemized as follows

- For time-selective channels, LE can achieve full Doppler diversity when appropriate guard-bands are inserted into the transmit symbol in much the same way as zero-symbols are padded in ZP-only transmission to enable LE to achieve full multipath diversity.
- LE and DFE achieve maximal diversity offered by doubly selective channels with a 2-level precoder that enables MLE to achieve multiplicative multipath-Doppler diversity.
- With a 1-level precoder that introduces redundancy only in the time-domain, it is possible to achieve full diversity gains with a hybrid equalization technique whose complexity is less than that of a full blown MLE.

We also presented some results that suggest that a the large amount of redundancy introduced by the 2-D precoders is not required for MLE and that redundancy of the order of channel delay spread is sufficient to enable full diversity reception with MLE in DS channels. The following tables 11.1 and 11.2 serve as a quick reference to the contributions and the cases addressed in this thesis. Other than these main contributions, we also studied in some detail the issue of implementing such full diversity receivers with low computational complexity. A couple of interesting by products of our study are the observations that precoding at the transmitter can aid the reduction in complexity of receiver equalization while enabling full diversity.

	η	Known Results	This Thesis
tall	$\frac{N}{M}$	ML [MG] BLE (MMSE) [CT]* BLE (MMSE-ZF) [CT]*	BLE (MMSE) BLE (MMSE-ZF) BDFE (MMSE) BDFE (MMSE-ZF)

Table 12.1: Overview of full diversity combinations and bandwidth efficiency η for TS-only/FS-only channels as a function of precoder type, and for various receivers.
LEGEND: [MG]:- [2] [CT]:- [6]
BDFE:- Block DFE, BLE:- Block Linear Equalizer, MMSE-ZF:- Minimum Mean Squared Error-Zero Forcing
* [6] shows these results only for the case of FS-only channels

	η	[MG]	This Thesis
tall-tall	$\frac{Q'L'}{(Q'+Q)(L'+L)}$	ML	ML-BLE BDFE (MMSE) BDFE (MMSE-ZF) BLE (MMSE) BLE (MMSE-ZF)
square-tall	$\frac{L'}{L'+L}$	ML	ML-BLE

Table 12.2: Overview of full diversity combinations and bandwidth efficiency η for DS channels as a function of precoder type, and for various receivers.
LEGEND: [MG]:- [2]
BDFE:- Block DFE, BLE:- Block Linear Equalizer, MMSE-ZF:- Minimum Mean Squared Error-Zero Forcing

We showed this for the case of frequency selective channels. Another interesting observation is that from simulation results for doubly selective channels, it appears that the sub-optimality of an approximated receiver, namely a first order polynomial expansion (PE) equalizer with MMSE diagonal combination coefficients is negligible compared to the brute force MMSE-ZF linear receiver over any outage probability range of practical interest.

In the final part of the thesis, we considered the problem of analytically evaluating the feasibility of an interference alignment (IA) solution for a given degrees of freedom (DoF) allocation in a general K-link MIMO IFC. We derived a set of conditions and presented a systematic method to check if these conditions are satisfied for a given MIMO IFC. We showed that, when an IA solution exists, these conditions are satisfied at every step of this systematic approach.We also show that an IA solution does not exist when these conditions are not satisfied.

Bibliography

[1] V. Cadambe and S. Jafar, "Interference alignment and degrees of freedom of the K-user interference channel," *IEEE Trans. Inform. Theory*, vol. 54, no. 8, pp. 3425–3441, Aug. 2008.

[2] X. Ma and G. Giannakis, "Maximum-diversity transmissions over doubly selective wireless channels," , *IEEE Trans. Info. Theory*, vol. 49, no. 7, pp. 1832–1840, July 2003.

[3] L. Grokop and D. Tse, "Diversity-multiplexing tradeoff in isi channels," *IEEE Trans. Info. Theory*, vol. 55, no. 1, pp. 109 –135, jan. 2009.

[4] C. M. Yetis, T. Gou, S. A. Jafar, and A. H. Kayran, "On feasibility of interference alignment in MIMO interference networks," *http://arxiv.org/abs/0911.4507*, vol. abs/0911.4507, 2009.

[5] S. W. Peters and R. W. Heath, "Interference alignment via alternating minimization," in *Proc. IEEE Conf. on Acoustics, Speech and Signal Processing (ICASSP)*, April 2009, pp. 2445–2448.

[6] C. Tepedelenlioglu, "Maximum multipath diversity with linear equalization in precoded OFDM systems," *IEEE Trans. Info. Theory*, vol. 50, no. 1, pp. 232–235, Jan. 2004.

[7] M. Harteneck, M. Boloorian, S. Georgoulis, and R. Tanner, "Throughput measurements of HSDPA 14 Mbit/s terminal," *Electronics Letters*, vol. 41, no. 7, pp. 425 – 427, 31 2005.

[8] J. Gozalvez, "Hsdpa goes commercial," *IEEE Vehicular Technology Magazine*, vol. 1, no. 1, pp. 43 –53, march 2006.

[9] I. E. Telatar, "Capacity of multi-antenna gaussian channels," *European Transactions on Telecommunications*, vol. 10, pp. 585–595, 1999.

[10] G. J. Foschini, "Layered space-time architecture for wireless communication in a fading environment when using multielement antennas," Bell Labs, Tech. Rep., Autumn 1996.

[11] A. J. Paulraj and C. B. Papadias, "Space-time processing for wireless communications," *IEEE Signal Processing Magazine*, pp. 49–83, November 1997.

[12] G. J. Foschini and M. J. Gans, "On limits of wireless communications in a fading environment when using multiple antennas," *Wirel. Pers. Commun.*, vol. 6, no. 3, pp. 311–335, 2009.

[13] 3GPP, *TS 25.214 Physical layer procedures (FDD) (Release 7)*, May 2007, version 7.5.0.

[14] Global Mobile Suppliers Association, "3G/WCDMA-HSPA Fact Sheet," GSA, Tech. Rep., March 2009.

[15] D. Gesbert, M. Kountouris, R. Heath, C.-B. W;Chae, and T. Sälzer, "Shifting the MIMO paradigm," *IEEE Signal Processing Magazine*, vol. 24, no. 5, pp. 36–46, September 2007.

[16] K. Ko, D. Lee, M. Lee, and H. Lee, "Novel sir to channel-quality indicator (CQI) mapping method for HSDPA system," in *Proc. IEEE Vehicular Technology Conference*, Montreal, Canada, September 2006.

[17] M. Lenardi and D. T. M. Slock, "A RAKE structured SINR maximizing mobile receiver for the WCDMA downlink," in *Asilomar 2001, 35th IEEE Annual Asilomar Conference on Signals, Systems & Computers, 4-7 Nov. 2001 - Pacific Grove, USA*, Nov 2001.

[18] K. Hooli, M. Juntti, M. J. Heikkilä, P. Komulainen, M. Latva-aho, and J. Lilleberg, "Chip-level channel equalization in WCDMA downlink," *EURASIP Journal on Applied Signal Processing*, vol. 8, 2002.

[19] R. Love, K. Stewart, R. Bachu, and A. Ghosh, "Mmse equalization for umts hsdpa," in *Vehicular Technology Conference, 2003. VTC 2003-Fall. 2003 IEEE 58th*, vol. 4, 6-9 2003, pp. 2416 – 2420 Vol.4.

[20] A. Baştuğ and D. T. M. Slock, "Downlink WCDMA receivers based on combined chip and symbol level equalization," *European Transactions on Telecommunications*, vol. 10, Feb 2005.

[21] J. C. Zhang, B. Raghothaman, Y. Wang, and G. Mandyam, "Receivers and CQI measures for MIMO-CDMA systems in frequency-selective channels," *EURASIP Journal on Applied Signal Processing*, no. 11, pp. 1668–1679, November 2005.

[22] M. Juntti, K. Hooli, K. Kiiskila, and J. Ylioinas, "Space-time equalizers for MIMO high speed WCDMA downlinks," *IEEE Trans. Wireless Commun.*, vol. 6, no. 7, pp. 2582 –2592, july 2007.

[23] L. Mailaender, "Linear MIMO equalization for CDMA downlink signals with code reuse," *IEEE Transactions on Wireless Communications*, vol. 4, no. 5, pp. 2423–2434, September 2005.

[24] J. Choi, S.-R. Kim, Y. Wang, and C.-C. Lim, "Receivers for chip-level decision feedback equalizer for CDMA downlink channels," *IEEE Transactions on Wireless Communications*, vol. 3, no. 1, pp. 300–313, January 2004.

[25] A. Bastug and D. Slock, "Optimization issues in combined chip and symbol level equalization for downlink wcdma receivers," in *Signals, Systems and Computers, 2004. Conference Record of the Thirty-Eighth Asilomar Conference on*, vol. 1, 7-10 2004, pp. 893 – 897 Vol.1.

[26] A. Lozano and C. Papadias, "Layered space-time receivers for frequency-selective wireless channels," *Communications, IEEE Transactions on*, vol. 50, no. 1, pp. 65–73, Jan 2002.

[27] D. So and R. Cheng, "Detection techniques for v-blast in frequency selective fading channels," vol. 1, Mar 2002, pp. 487–491 vol.1.

[28] D. D. Falconer and F. R. Magee, "Adaptive channel memory truncation for maximum likelihood sequence estimation," *Bell System Technical Journal*, vol. 52, no. 9, Nov. 1973.

[29] D. Messerscmitt, "Design of a finite impulse response for the Viterbi algorithm and decision-feedback equalizer," in *IEEE International Conference on Communications*, Minneapolis, MN, June 1974, pp. 37D.1–37D.5.

[30] C. Beare, "The choice of the desired impulse response in combined linear-Viterbi algorithm equalizers," *IEEE Trans. Communications*, vol. 26, no. 8, Aug. 1978.

[31] N. Al-Dhahir and J. M. Cioffi, "Efficiently computed reduced-parameter input-aided MMSE equalizers for ML Detection: A unified approach," *IEEE Trans. Information Theory*, vol. 42, no. 3, May 1996.

[32] J. M. Cioffi, G. P. Dudevoir, M. V. Eyuboglu, and G. D. Forney, "MMSE Decision-Feedback Equalizers and Coding. Part 1: Equalization Results," *IEEE Trans. Communications*, vol. 43, no. 10, Oct. 1995.

[33] Q. Spencer, C. Peel, A. Swindlehurst, and M. Haardt, "An introduction to multi-user MIMO downlink," *IEEE Communications Magazine*, October 2004.

[34] V. Haikola, M. Lampinen, and M. Kuusela, "Practical multiuser beamforming in WCDMA," in *Proc. IEEE Vehicular Technology Conference*, Fall 2006.

[35] M. Wrulich, C. Mehlfuhrer, and M. Rupp, "Interference Aware MMSE Equalization for MIMO TxAA," in *Proc. 2008 3rd International Symposium on Communications, Control and Signal Processing (ISCCSP2008)*, March 2008, st.Julians, Malta.

[36] A. Sayeed and B. Aazhang, "Joint multipath-doppler diversity in mobile wireless communications," *Communications, IEEE Transactions on*, vol. 47, no. 1, pp. 123–132, Jan 1999.

[37] L. Zheng and D. Tse, "Diversity and multiplexing: A fundamental tradeoff in multiple-antenna channels," *IEEE Trans. Info. Theory*, vol. 49, no. 5, pp. 1073 – 1096, may 2003.

[38] L. Grokop and D. Tse, "Diversity/multiplexing tradeoff in ISI channels," in *Proc. Int'l Symp. Info.Theory (ISIT)*, june-2 july 2004, p. 97.

[39] G. Giannakis and C. Tepedelenlioglu, "Basis expansion models and diversity techniques for blind identification and equalization of time-varying channels," *Proceedings of the IEEE*, vol. 86, no. 10, pp. 1969–1986, Oct 1998.

[40] M. Hebley, W. Kennedy, and D. Taylor, "The performance of a space diversity receiver with finite-length fractionally-spaced equalisers with frequency selective rayleigh fading and co-channel interference," in *Proc. IEEE Conf. Global Communications (GLOBECOM)*, nov-2 dec 1994.

[41] N. Al-Dhahir and J. Cioffi, "MMSE decision-feedback equalizers: Finite-length results," *IEEE Trans. Info. Theory*, vol. 41, no. 4, pp. 961 –975, jul 1995.

[42] A. Medles and D. Slock, "Decision-feedback equalization achieves full diversity for finite delay spread channels," in *Proc. IEEE Int'l Symp.Info.Theory (ISIT)*, June-2 July 2004, pp. 99–.

[43] A. Hedayat, A. Nosratinia, and N. Al-Dhahir, "Outage probability and diversity order of linear equalizers in frequency-selective fading channels," in *Proc. 38th Asilomar Conf. on Signals, Systems and Computers*, vol. 2, Pacific Grove, CA, USA, Nov. 2004.

[44] D. T. M. Slock, "Diversity aspects of linear and decision-feedback equalizers for frequency-selective multi-antenna channels," in *Proc. 40th Asilomar Conf. on Signals, Systems and Computers*, Pacific Grove, CA, USA, 29 2006-nov. 1 2006.

[45] M. Grötschel, L. Lovász, and A. Schrijver, *Geometric Algorithms and Combinatorial Optimization*, ser. Algorithms and Combinatorics. Springer, 1988, vol. 2.

[46] M. Taherzadeh, A. Mobasher, and A. Khandani, "LLL reduction achieves the receive diversity in MIMO decoding," *IEEE Trans. Info. Theory*, vol. 53, no. 12, pp. 4801 –4805, dec. 2007.

[47] X. Ma and W. Zhang, "Fundamental limits of linear equalizers: Diversity, capacity, and complexity," *IEEE Trans. Info. Theory*, vol. 54, no. 8, pp. 3442–3456, Aug. 2008.

[48] Z. Wang and G. Giannakis, "A simple and general parameterization quantifying performance in fading channels," *IEEE Trans. Communications*, vol. 51, no. 8, pp. 1389 – 1398, aug. 2003.

[49] G. Caire and R. Knopp, "Signal detection in AWGN," in *Introduction to Digital Communications*, 2008.

[50] A. Stamoulis, G. Giannakis, and A. Scaglione, "Block fir decision-feedback equalizers for filterbank precoded transmissions with blind channel estimation capabilities," *Communications, IEEE Transactions on*, vol. 49, no. 1, pp. 69–83, Jan 2001.

[51] A. Medles and D. Slock, "Achieving the optimal diversity-versus-multiplexing tradeoff for MIMO flat channels with qam space-time spreading and DFE equalization," *IEEE Trans. Info. Theory*, vol. 52, no. 12, pp. 5312–5323, Dec. 2006.

[52] J. Makhoul, "Linear prediction: A tutorial review," *Proceedings of the IEEE*, vol. 63, no. 4, pp. 561–580, April 1975.

[53] A. Medles, "Coding and advanced signal processing for MIMO systems," Ph.D. dissertation, Ph.D Thesis, 04 2004.

[54] T. Kailath, *Linear Systems (Prentice-Hall Information and System Science Series)*. Prentice Hall, November 1979.

[55] S. Moshavi, E. G. Kanterakis, and D. L. Schilling, "Multistage linear receivers for DS-CDMA systems," *International Journal of Wireless Information Networks*, vol. 3, pp. 1–17, October 1996.

[56] C. Tepedelenlioglu and Q. Ma, "On the performance of linear equalizers for block transmission systems," *IEEE Conf. on Global Communications (GLOBECOM)*, vol. 6, pp. 5 pp.–, Nov.-2 Dec. 2005.

[57] J. Boutros and E. Viterbo, "Signal space diversity: a power- and bandwidth-efficient diversity technique for the rayleigh fading channel," *Information Theory, IEEE Transactions on*, vol. 44, no. 4, pp. 1453–1467, Jul 1998.

[58] R. H. Etkin, D. N. C. Tse, and H. Wang, "Gaussian interference channel capacity to within one bit," *IEEE Trans. Inform. Theory*, vol. 54, no. 12, pp. 5534–5562, 2008.

[59] T. Gou and S. A. Jafar, "Degrees of freedom of the K user M x N MIMO interference channel," *http://arxiv.org/abs/0809.0099*, vol. abs/0809.0099, 2008.

[60] A. Ghasemi, A. S. Motahari, and A. K. Khandani, "Interference alignment for the K user MIMO interference channel," *http://arxiv.org/abs/0909.4604*, vol. abs/0909.4604, 2009.

[61] K. Gomadam, V. Cadambe, and S. Jafar, "Approaching the capacity of wireless networks through distributed interference alignment," in *Proc. IEEE Global Telecomm. Conf. (GLOBECOM)*, Dec. 2008.

[62] F. Negro, S. P. Shenoy, D. T. M. Slock, and I. Ghauri, "Interference alignment limits for K-user frequency-flat MIMO interference channels," in *Proc. 17th European Signal Proc. Conf., (Eusipco)*, Glasgow, Scotland, Aug. 2009.